

**STUDIES OF GAS-PHASE FRAGMENTATION
MECHANISMS OF PEPTIDE *b* IONS BY MASS
SPECTROMETRY**

**A Thesis Submitted to
the Graduate School of Engineering and Sciences of
İzmir Institute of Technology
in Partial Fulfillment of the Requirements of the Degree of**

DOCTOR OF PHILOSOPHY

in Chemistry

**by
Ahmet Emin ATİK**

**December 2013
İZMİR**

We approve the thesis of **Ahmet Emin ATİK**

Examining Committee Members:

Prof. Dr. Şefik SÜZER
Department of Chemistry, Bilkent University

Prof. Dr. Bekir SALİH
Department of Chemistry, Hacettepe University

Prof. Dr. Levent ARTOK
Department of Chemistry, İzmir Institute of Technology

Prof. Dr. Nuran ELMACI IRMAK
Department of Chemistry, İzmir Institute of Technology

Prof. Dr. Talat YALÇIN
Department of Chemistry, İzmir Institute of Technology

20 December 2013

Prof. Dr. Talat YALÇIN
Supervisor, Department of Chemistry
İzmir Institute of Technology

Prof. Dr. Ahmet Emin EROĞLU
Head of the Department of Chemistry

Prof. Dr. R. Tuğrul SENGER
Dean of the Graduate School of
Engineering and Sciences

ACKNOWLEDGEMENTS

It is a great pleasure to thank all the people who helped me during my Ph.D. studies at the İzmir Institute of Technology. First and foremost, I would like to thank my research advisor Prof. Dr. Talat YALÇIN for past wonderful eight years in mass spectrometry community. This thesis will not come into life without his guidance, encouragement, immense knowledge, and patience. He thought me how to be the best scientist in academic area. It was an honor for me being his first MSc. and Ph.D student. Besides to all these scientific points, his fatherly behaviors will not be forgotten.

I would like to express my sincere appreciation to my thesis progressing committee members, Prof. Dr. Şefik SÜZER and Prof. Dr. Levent ARTOK, for their numerous productive discussions and constructive advices in each progress seminars which were held in every six months. I am also sincerely grateful to my thesis examining committee members, Prof. Dr. Bekir SALİH and Prof. Dr. Nuran ELMACI IRMAK, for their valuable criticism and constructive comments along the dissertation.

Special thanks are extended to Prof. Dr. Philippe MAÎTRE from University of Paris-Sud for his fruitful and pleasant collaboration. I greatly appreciate his sincere help and kindness during my stay in Orsay. *Merci de votre aide.*

For financial support, I am pleased to acknowledge the Scientific and Technological Research Council of Turkey, TÜBİTAK, with a project no109T430.

Furthermore, I am deeply grateful to my dear friends Dr. Betül ÖZTÜRK, Melda Zeynep GÜRAY, Sıla KARACA, İbrahim KARAMAN, Deniz BÖLEK, Esen DÖNERTAŞ, Özge TUNUSOĞLU, Burcu YILDIRIM ÜREM, Nevin TEVRÜZ and Zehra Özden KEÇECİ for standing by me throughout challenging times. Their honest friendships are very important for me, thank you!

Last but not least, I owe my endless thanks to my lovely mother, Ümran ATİK, who is always beside to me with her great motivation. In addition, I remember my father, Halim ATİK, with a great longing and reminisce the times when we were together. I believed that he still supports me. I would like to extend my appreciation to my brother, İsa Doğan ATİK and his little cute daughter Eylül Duru ATİK for not missing their smiles from me. Finally, my dearest thanks are addressed to Canan ŞEN for her endless love, understanding, tolerance, and patience since 2008. She makes my life meaningful by loving me, thank you!

ABSTRACT

STUDIES OF GAS-PHASE FRAGMENTATION MECHANISMS OF PEPTIDE *b* IONS BY MASS SPECTROMETRY

This dissertation presents detailed studies of gas-phase fragmentation mechanism of peptide *b* ions under low-energy collision-induced dissociation (CID). Understanding the gas-phase structures and fragmentation mechanisms of the *b* ions is especially important for interpretation of peptide mass spectra.

Recently, larger b_n ($n = 5, 6, 7\dots$) ions are shown to form macrocyclic structures which can lead to erroneous in sequencing of unknown peptides. Therefore, in the first part of thesis, the effect of acidic amino acid residues (glutamic or aspartic acid) on the formation of macrocyclic structure is probed using various model hepta- and octapeptides. The results indicate that neither the presence nor the positions of acidic residues in peptides prevents macrocyclization of *b* ions. In addition, the dependence of preferential cleavage of acidic residues on applied collision energy is investigated for macrocyclic *b* ions.

In the second part, the effect of ϵ -amine group of lysine residue is examined for the macrocyclization of *b* ions even if the N-terminal of the peptide is acetylated. The obtained results reveal that the macrocyclization is accomplished between ϵ -amine group of lysine and the oxazolone structure in the N-terminal acetylated peptide. Moreover, the lysine position is important parameter for the macrocyclization of *b* ions for N-terminal acetylated peptide.

In the third and fourth parts of the thesis, the novel rearranged fragment ions are detected in the CID mass spectra of *b* ion series of acetylated lysine and side chain hydroxyl group containing model peptides, respectively. The gas-phase structures and fragmentation mechanisms of these novel fragment ions are investigated via multi-stage tandem mass spectrometry (MS^4) experiments.

In conclusions, the results presented in this dissertation can be used to elucidate the correct and reliable peptide sequences, and this improve protein identification strategies which is required for high-throughput proteomic studies.

ÖZET

PEPTİT *b* İYONLARININ GAZ-FAZI PARÇALANMA MEKANİZMALARININ KÜTLE SPEKTROMETRESİ İLE ÇALIŞILMASI

Bu tez düşük-enerjili çarpışmayla-indüklenmiş ayrışma (CID) altında peptit *b* iyonlarının gaz-fazı parçalanma mekanizmalarının detaylı çalışmalarını göstermektedir. *b* iyonlarının gaz-fazı yapılarının ve parçalanma mekanizmalarının anlaşılması özellikle peptit kütle spektrumlarının yorumlanması için önemlidir.

Son zamanlarda, büyük b_n ($n = 5, 6, 7...$) iyonlarının makrohalkalı yapı oluşturduğu ve bu yapının bilinmeyen peptitlerin sekanslanmasında hataya yol açabileceği gösterilmiştir. Bu nedenle, tezin ilk bölümünde çeşitli hepta- ve oktapeptitler kullanılarak asidik amino asitin (glutamik veya aspartik asit) makrohalkalı yapının oluşmasına olan etkisi araştırılmıştır. Sonuçlar göstermiştir ki, peptitlerdeki ne asidik amino asitlerin varlığı ne de pozisyonları *b* iyonlarının makrohalkalaşmasını engellemiştir. Buna ek olarak, asidik amino asitlerin tercihli bölünmesinin uygulanan çarpışma enerjisine olan bağlılığı makrohalkalı *b* iyonları için incelenmiştir.

İkinci bölümde, peptinin N-ucu asetillenmiş olsa bile lizin amino asitinin yan zincirindeki ϵ -amin grubun *b* iyonlarının makrohalkalaşmasına olan etkisi incelenmiştir. Elde edilen sonuçlar, makrohalkalaşmanın N-ucu asetillenmiş olan peptitteki lizinin ϵ -amin grubu ile okzazon yapısı arasında gerçekleştiği ortaya koymuştur. Diğer taraftan, N-ucu asetillenmiş peptitlerdeki lizinin pozisyonu *b* iyonlarının makrohalkalaşma için önemli bir parametredir.

Tezin üçüncü ve dördüncü bölümlerinde ise, asetillenmiş lizin veya yan zincirlerinde hidroksil grubu içeren model peptitlerden elde edilen *b* iyon serilerinin CID kütle spektrumlarında yeni parçalanma iyonlarının varlığı saptanmıştır. Bu yeni oluşan iyonların gaz-fazı yapıları ve parçalanma mekanizmaları çok-aşamalı ikili kütle spektrometresi (MS^4) deneyleri ile çalışılmıştır.

Sonuç olarak, bu çalışmalarda gösterilen sonuçlar peptit sekanslarının doğru ve güvenilir bir şekilde açıklamak için kullanılabilir ve bu durum proteomik çalışmalar için gerekli olan protein tanımlama stratejilerini geliştirebilir.

*Dedicated to;
my lovely mother Ümran ATİK
and
the memory of my father Halim ATİK*

TABLE OF CONTENTS

LIST OF FIGURES	x
LIST OF TABLES	xii
LIST OF ABBREVIATIONS	xii
CHAPTER 1. MASS SPECTROMETRY	1
1.1. What is a Mass Spectrometer?	1
1.2. Ionization Techniques	3
1.2.1. Electrospray Ionization (ESI).....	4
1.2.2. Matrix-Assisted Laser Desorption/Ionization (MALDI)	7
1.3. Mass Analyzers	10
1.3.1. Quadrupole (Q)	11
1.3.2. Ion-Trap (IT)	13
1.3.3. Time-of-Flight (TOF).....	15
1.3.4. Fourier Transform-Ion Cyclotron Resonance (FT-ICR).....	18
1.3.5. Hybrid Mass Analyzers	19
1.4. Detectors	20
1.4.1. Faraday Cup	20
1.4.2. Electron Multiplier	20
1.4.3. Microchannel Plate.....	21
CHAPTER 2. FRAGMENTATION MECHANISMS OF PROTONATED PEPTIDES IN THE GAS-PHASE.....	22
2.1. Peptides and Proteins	22
2.2. Sequence Analysis by Tandem Mass Spectrometry (MS/MS).....	25
2.2.1. Collision-Induced Dissociation (CID)	26
2.2.2. Other Ionization Techniques	27
2.3. Peptide Fragmentation Chemistry.....	28
2.3.1. Mobile Proton Model	28
2.3.2. Peptide Fragmentation Nomenclature.....	29

2.3.3. Formation and Structures of <i>b</i> Ions	33
2.4. Literature Review	35
2.5. Overview of the Thesis	38

CHAPTER 3. A SYSTEMATIC STUDY OF ACIDIC PEPTIDES FOR *b*-TYPE

SEQUENCE SCRAMBLING	39
3.1. Introduction	39
3.2. Experimental	41
3.3. Results and Discussion	42
3.3.1. Effect of <i>b</i> -Type Sequence Scrambling on $[M + H]^+$ Product Ion Mass Spectra	42
3.3.2. <i>b</i> -Type Sequence Scrambling of Glutamic or Aspartic Acid Containing Heptapeptides	46
3.3.2.1. Alanine Series	46
3.3.2.2. YAGFLV Series	49
3.3.3. <i>b</i> -Type Sequence Scrambling of Two Adjacent Glutamic or Aspartic Acid Containing Octapeptides	52
3.3.4. Effect of Acidic Residue Position in the Peptide on the Macrocyclization of b_n ($n = 7$ or 8) Ions	57
3.3.5. Collision Energy Dependence of the Preferential Cleavage of Glutamic or Aspartic Acid Residue(s) from the Macrocylic Structure	58
3.3.6. Effect of Amino Acid Composition for Preferential Cleavage of Acidic Residue	59

CHAPTER 4. THE ROLE OF LYSINE ϵ -AMINE GROUP ON THE

MACROCYCLIZATION OF <i>b</i> IONS	61
4.1. Introduction	61
4.2. Experimental	62
4.3. Results and Discussion	63
4.3.1. Effect of Lysine, Glutamine, and Asparagine Side Chain Amine Groups on the Side-to-Tail Cyclization of b_7 Ions	63

4.3.2. Formation and Structure of m/z 651 in the b_7 Ion CID Mass Spectra of N-Terminal Acetylated Lysine, Glutamine, and Asparagine Containing Peptides	67
4.3.3. Positional Effect of Lysine Residue on the Side-to-Tail Cyclization of b_7 Ions in the N-Terminal Acetylated Octapeptides.....	69
4.3.3.1. Ac-KYAGFLVG	70
4.3.3.2. Ac-YKAGFLVG	72
4.3.3.3. Ac-YAKGFLVG	73
4.3.3.4. Ac-YAGKFLVG	75
4.3.3.5. Ac-YAGFKLVG	76
4.3.3.6. Ac-YAGFLKVG	76

CHAPTER 5. A REARRANGMENT REACTION OF ACETYLATED LYSINE

CONTAINING PEPTIDE b_n ($n = 4-7$) ION SERIES.....	77
5.1. Introduction.....	77
5.2. Experimental	78
5.3. Results and Discussion	79
5.3.1. Fragmentation Reactions of b_n ($n = 4-7$) Ions Originated from $K_{Ac}YAGFLVG$ and Ac-KYAGFLVG.....	79
5.3.2. Fragmentation Reactions of b_n ($n = 4-7$) Ions Originated from Ac- $K_{Ac}YAGFLVG$ and KYAGFLV-NH ₂	84
5.3.3. Positional Effect of Acetylated Lysine Residue for the Formation of Novel Fragment Ions	85

CHAPTER 6. PROTONATED DIPEPTIDE LOSSES FROM b_5 AND b_4 IONS OF SIDE CHAIN HYDROXYL GROUP CONTAINING

PENTAPEPTIDES	90
6.1. Introduction.....	90
6.2. Experimental	91
6.3. Results and Discussion	92
6.3.1. The Formation of m/z 279 Fragment Ion in the b_5 Ion Mass Spectra of XGGFL-NH ₂ (where X is S, T, E, D, or Y)	92

6.3.2. The Formation of m/z 223 Fragment Ion in the b_4 Ion Mass Spectra of XGGFL-NH ₂ (where X is S, T, E, D, or Y)	97
6.3.3. The Formation of m/z 295 Fragment Ion in the b_5 Ion Mass Spectra of AXVYI-NH ₂ (where X is S, T, E, D, or Y).....	101
6.3.4. The Formation of m/z 281 Fragment Ion in the b_4 Ion Mass Spectra of AXVYI-NH ₂ (where X is S, T, E, D, or Y).....	104
CHAPTER 7. CONCLUSION	107
REFERENCES	111
APPENDICES	
APPENDIX A. BREAKDOWN GRAPHS FOR [M + H] ⁺ IONS OF ACIDIC PEPTIDES	133
APPENDIX B. MS/MS SPECTRA OF [M + H] ⁺ IONS OF N-TERMINAL ACETYLATED PEPTIDES.....	142
APPENDIX C. MS/MS SPECTRA OF [M + H] ⁺ IONS OF DIPEPTIDES AND MS ³ SPECTRA OF b_5 IONS OF XGGFL-NH ₂ AND AXVYI-NH ₂	143

LIST OF FIGURES

<u>Figure</u>	<u>Page</u>
Figure 1.1. Basic components of a mass spectrometer	2
Figure 1.2. Schematic representation of the ESI ion source	4
Figure 1.3. Formation of ions in MALDI process	7
Figure 1.4. Common matrices used in MALDI-MS experiments	9
Figure 1.5. Schematic diagram of a quadrupole mass analyzer.....	11
Figure 1.6. Stability diagram for ions in a quadrupole	12
Figure 1.7. Schematic view of a 3D ion trap	13
Figure 1.8. Schematic representation of MS/MS in ion trap	14
Figure 1.9. Schematic view of linear TOF mass analyzer	16
Figure 1.10. Schematic view of FT-ICR mass analyzer	18
Figure 1.11. Schematic view of electron multiplier.....	20
Figure 1.12. Schematic views of microchannel plate	21
Figure 2.1. General structure of an amino acid.....	23
Figure 2.2. The nomenclature of peptide fragment ions.....	30
Figure 2.3. Proposed mechanism for the formation of b_3 and y_2 ions via b_n - y_m pathway.....	32
Figure 2.4. Possible structures for b ions.....	33
Figure 2.5. Proposed mechanism for the formation of macrocyclic b_5 ion	36
Figure 3.1. Product ion mass spectrum of $[M + H]^+$ derived from EAAAAAA-NH ₂	42
Figure 3.2. Comparison of $[M + H]^+$ ion breakdown graphs of EAAAAAA-NH ₂ and DAAAAAA-NH ₂	44
Figure 3.3. Comparison of $[M + H]^+$ ion breakdown graphs of EEAAAAAA-NH ₂ and DDAAAAAA-NH ₂	45
Figure 3.4. Comparison of the CID mass spectra of b_7 ions of EAAAAAA-NH ₂ , AAAEAAA-NH ₂ , and AAAAAAE-NH ₂	46
Figure 3.5. Comparison of the CID mass spectra of b_7 ions of DAAAAAA-NH ₂ , AAADAAA-NH ₂ , and AAAAAAD-NH ₂	47
Figure 3.6. Precursor ion mass spectra of the m/z 467 ion from EAAAAAA-NH ₂	48
Figure 3.7. Sources of the elimination of A + H ₂ O from the b_7 ion of EAAAAAA-NH ₂	49

Figure 3.8. Comparison of the CID mass spectra of b_7 ions of	
(a) EYAGFLV-NH ₂ , YAGEFLV-NH ₂ , and YAGFLVE-NH ₂ ,	
(b) DYAGFLV-NH ₂ , YAGDFLV-NH ₂ , and YAGFLVD-NH ₂	50
Figure 3.9. Comparison of b_7 ion breakdown graphs of EYAGFLV-NH ₂ ,	
YAGEFLV-NH ₂ , YAGFLVE-NH ₂ , DYAGFLV-NH ₂ ,	
YAGDFLV-NH ₂ , and YAGFLVD-NH ₂	51
Figure 3.10. Comparison of the CID mass spectra of b_8 ions of EEAAAAAA-NH ₂ ,	
AAEEAAAA-NH ₂ , AAAAEEAA-NH ₂ , and AAAAAAEE-NH ₂	52
Figure 3.11. Comparison of the CID mass spectra of b_8 ions of DDAAAAAA-NH ₂ ,	
AADDAAAA-NH ₂ , AAAADDAA-NH ₂ , and AAAAAADD-NH ₂	54
Figure 3.12. Proposed mechanism for the elimination of water molecules from	
the side chains of glutamic acid residues	55
Figure 3.13. Proposed mechanism for the formation of b_8 macrocyclic ion	
from linear oxazolone AAEEAAAA _{oxa} and eight possible	
ring-opening pathways	56
Figure 3.14. Comparison of the preferential cleavages of acidic residue(s) from	
macrocyclic b_7 or b_8 ions	59
Figure 3.15. Comparison of the preferential cleavages of glutamic or aspartic acid	
from macrocyclic b_7 ions of alanine and YAGFLV series	60
Figure 4.1. Schematic representation of lysine, glutamine, and asparagine	
amino acids	62
Figure 4.2. Comparison of the MS ³ mass spectra of b_7 ions of protonated	
Ac-KYAGFLVG, Ac-QYAGFLV-NH ₂ , and Ac-NYAGFLV-NH ₂	64
Figure 4.3. Proposed macrocyclization mechanism for b_7 ion of Ac-KYAGFLVG.....	65
Figure 4.4. Seven possible ring opening pathways of macrocyclic b_7 ions.....	66
Figure 4.5. The MS ³ mass spectrum of b_7 ion from protonated Ac-K _{Ac} YAGFLVG	66
Figure 4.6. Comparison of the MS ⁴ mass spectra of m/z 651 ions from protonated	
Ac-KYAGFLVG, Ac-QYAGFLV-NH ₂ , Ac-NYAGFLV-NH ₂ with	
MS ³ mass spectrum of b_6 ion derived from YAGFLV-NH ₂	68
Figure 4.7. Proposed fragmentation pathway leading to the formation of	
neutral Ac-X (X = K, Q, or N) and protonated YAGFLV _{oxa} from	
Ac-KYAGFLVG, Ac-QYAGFLV-NH ₂ , and Ac-NYAGFLV-NH ₂ ,	
respectively	69

Figure 4.8. Comparison of the MS ³ mass spectra of <i>b</i> ₇ ions from protonated (a) Ac-KYAGFLVG, (b) Ac-YKAGFLVG, (c) Ac-YAKGFLVG, (d) Ac-YAGKFLVG, (e) Ac-YAGFKLVG and (f) Ac-YAGFLKVG.....	70
Figure 4.9. Proposed fragmentation pathway for the formation of neutral Ac-K and protonated YAGFLV _{oxa} from YAGFLV-Ac-K _{oxa} <i>b</i> ₇ isomer	71
Figure 4.10. Proposed fragmentation pathways leading to neutral Ac-Y and protonated KAGFLV _{oxa} from Ac-YKAGFLVG.....	72
Figure 4.11. Comparison of the MS ⁴ mass spectrum of <i>m/z</i> 616 ion from Ac-YKAGFLVG with the MS ³ mass spectrum of <i>b</i> ₆ ion of KAGFLVG peptide.....	73
Figure 4.12. Comparison of the MS ⁴ mass spectrum of <i>m/z</i> 616 ion from Ac-YAKGFLVG with the MS ³ mass spectrum of <i>b</i> ₆ ion of AKGFLVG peptide.....	74
Figure 4.13. Proposed fragmentation pathway leading to formation of <i>m/z</i> 545 and <i>m/z</i> 417 ions from <i>b</i> ₇ ion of Ac-YAKGFLVG	74
Figure 4.14. Breakdown graph of fragment ions at <i>m/z</i> 821, 616, 545, and 417 originated from Ac-YAKGFLVG.....	75
Figure 4.15. Breakdown graph of fragment ions at <i>m/z</i> 821, 616, 545, and 488 originated from Ac-YAGKFLVG.....	76
Figure 5.1. Comparison of the MS ³ mass spectra of <i>b</i> ₇ , <i>b</i> ₆ , <i>b</i> ₅ , and <i>b</i> ₄ ions originated from (a) K _{Ac} YAGFLVG and (b) Ac-KYAGFLVG, respectively	80
Figure 5.2. Comparison of MS ⁴ mass spectrum of <i>m/z</i> 668, 569, 456, and 309 ions with MS/MS mass spectrum of [M + H] ⁺ ion of protonated YAGFLV-NH ₂ , YAGFL-NH ₂ , YAGF-NH ₂ , and YAG-NH ₂ , respectively .	81
Figure 5.3. Proposed macrocyclization reaction mechanism for <i>b</i> ₇ ion of K _{Ac} YAGFLVG	82
Figure 5.4. Proposed fragmentation pathway for the formation of protonated YAGFLV-NH ₂ (<i>m/z</i> 668) from newly formed <i>b</i> ₇ isomer, YAGFLVK _{Ac-oxa}	83
Figure 5.5. MS ³ mass spectra of <i>b</i> ₃ ion originated from KAcYAGFLVG	83
Figure 5.6. Comparison of the MS ³ mass spectra of <i>b</i> ₇ , <i>b</i> ₆ , <i>b</i> ₅ , and <i>b</i> ₄ ions originated from (a) Ac-K _{Ac} YAGFLVG and (b) KYAGFLV-NH ₂ , respectively.....	85
Figure 5.7. Comparison of the MS ³ mass spectra of <i>b</i> ₇ , <i>b</i> ₆ , <i>b</i> ₅ , and <i>b</i> ₄ ions originated from YAK _{Ac} GFLVG.....	86

Figure 5.8. Comparison of MS ⁴ mass spectrum of <i>m/z</i> 668, 569, 456, and 309 ions with MS/MS mass spectrum of [M + H] ⁺ ion of protonated GFLVYA-NH ₂ , GFLYA-NH ₂ , GFYA-NH ₂ , and GYA-NH ₂ , respectively .	87
Figure 5.9. (a) MS ³ mass spectrum of <i>b</i> ₃ ion from protonated YAK _{Ac} GFLVG, (b) MS ⁴ mass spectrum of <i>m/z</i> 252 ion from <i>b</i> ₃ ion of protonated YAK _{Ac} GFLVG, (c) MS/MS mass spectrum of [M + H] ⁺ ion from protonated YA-NH ₂	88
Figure 5.10. Comparison of the MS ³ mass spectra of <i>b</i> ₇ , <i>b</i> ₆ , <i>b</i> ₅ , and <i>b</i> ₄ ions originated from (a) Ac-YAKGFLVG and (b) Ac-YAK _{Ac} GFLVG, respectively	89
Figure 6.1. (a) MS ³ mass spectrum of <i>b</i> ₅ ion from protonated SGGFL-NH ₂ , (b) MS ⁴ mass spectrum of <i>m/z</i> 279 ion from <i>b</i> ₅ ion of protonated SGGFL-NH ₂ , (c) MS ² mass spectrum of [M + H] ⁺ ion from protonated FL-OH	93
Figure 6.2. Comparison of the MS ⁴ mass spectra of <i>m/z</i> 279 fragment ions originated from protonated TGGFL-NH ₂ , EGGFL-NH ₂ , DGGFL-NH ₂ , and YGGFL-NH ₂ , respectively	95
Figure 6.3. The possible mechanism for the formation of either <i>m/z</i> 279 or 184 fragment ions from the <i>b</i> ₅ ion of SGGFL-NH ₂	96
Figure 6.4. The MS ³ mass spectrum of <i>b</i> ₅ ion from protonated S _{Me} GGFL-NH ₂	97
Figure 6.5. (a) MS ³ mass spectrum of <i>b</i> ₄ ion from protonated EGGFL-NH ₂ , (b) MS ⁴ mass spectrum of <i>m/z</i> 223 ion from <i>b</i> ₄ ion of protonated EGGFL-NH ₂ , (c) MS ² mass spectrum of [M + H] ⁺ ion from protonated GF-OH.....	98
Figure 6.6. Comparison of the MS ⁴ mass spectra of <i>m/z</i> 223 fragment ions originated from protonated SGGFL-NH ₂ , TGGFL-NH ₂ , and DGGFL-NH ₂ , respectively	99
Figure 6.7. The possible mechanism for the formation of either <i>m/z</i> 223 or 169 fragment ions from the <i>b</i> ₄ ion of EGGFL-NH ₂	100
Figure 6.8. The MS ³ mass spectrum of <i>b</i> ₄ ion from protonated E _{OMe} GGFL-NH ₂	101
Figure 6.9. (a) MS ³ mass spectrum of <i>b</i> ₅ ion from protonated ASVYI-NH ₂ , (b) MS ⁴ mass spectrum of <i>m/z</i> 295 ion from <i>b</i> ₅ ion of protonated ASVYI-NH ₂ , (c) MS ² mass spectrum of [M + H] ⁺ ion from protonated YI-OH.....	102
Figure 6.10. Comparison of the MS ⁴ mass spectra of <i>m/z</i> 295 fragment ions originated from protonated ATVYI-NH ₂ , AEVYI-NH ₂ , ADVYI-NH ₂ , and AYVYI-NH ₂ , respectively	104

Figure 6.11. (a) MS³ mass spectrum of *b*₄ ion from protonated ATVYI-NH₂, (b) MS⁴ mass spectrum of *m/z* 281 ion from *b*₄ ion of protonated ATVYI-NH₂, (c) MS² mass spectrum of [M+H]⁺ ion from protonated VY-OH 105

Figure 6.12. Comparison of the MS⁴ mass spectra of *m/z* 281 fragment ions originated from protonated ASVYI-NH₂, AEVYI-NH₂, and ADVYI-NH₂, respectively 106

LIST OF TABLES

<u>Table</u>	<u>Page</u>
Table 2.1. A list of twenty natural amino acids	23
Table 6.1. Relative intensities of m/z 279 and m/z 223 fragments in the CID mass spectra of b_5 and b_4 ions from XGGFL-NH ₂ model peptides, respectively	92
Table 6.2. Relative intensities of m/z 295 and m/z 281 fragments in the CID mass spectra of b_5 and b_4 ions from AXVYI-NH ₂ model peptides, respectively	101

LIST OF ABBREVIATIONS

2-D PAGE	Two-Dimensional Polyacrylamide Gel Electrophoresis
3D	Three-Dimension
B	Magnetic Field
BIRD	Blackbody Infrared Radiative Dissociation
CAD	Collisional-Activated Dissociation
CI	Chemical Ionization
CID	Collision-Induced Dissociation
CRM	Charge Residue Model
Da	Dalton
DC	Direct Current
DFT	Density Functional Theory
DHB	2,5-Dihydroxybenzoic Acid
e	Elementary Charge
eV	Electronvolt
ECD	Electron Capture Dissociation
EDD	Electron Detachment Dissociation
EI	Electron Ionization
EID	Electron-Induced Dissociation
EM	Electron Multiplier
EPI	Enhanced Product Ion
ETD	Electron Transfer Dissociation
ESI	Electrospray Ionization
FAB	Fast Atom Bombardment
FD	Field Desorption
FI	Field Ionization
FT-ICR	Fourier Transform-Ion Cyclotron Resonance
H/D	Hydrogen-Deuterium
HABA	2-(4'-Hydroxybenzeneazo)Benzoic acid
HPA	3-Hydroxypicolinic acid
HPLC	High Pressure (Performance) Liquid Chromatography
IEM	Ion Emission Model
IRMPD	Infrared Multiphoton Dissociation
IT	Ion-Trap
IT-TOF	Ion Trap/Time-of-Flight
kDa	KiloDalton
keV	Kilo Electronvolt
kV	Kilovolt
L	Length
LC-MS	Liquid Chromatography-Mass Spectrometry
LDI	Laser Desorption Ionization
<i>m/z</i>	mass-to-charge ratio
mg	Milligram
min	Minute
mm	Millimeter
ms	Millisecond
M	Molarity

MALDI	Matrix-Assisted Laser Desorption / Ionization
MCP	Microchannel Plate
MRFA	Met-Arg-Phe-Ala
MS	Mass Spectrometry
MS/MS	Tandem Mass Spectrometry
MS ⁿ	Multi-Stage Tandem Mass Spectrometry
MW	Molecular Weight
nL	Nanoliter
nm	Nanometer
ns	Nanosecond
N ₂	Nitrogen
NA	Nicotinic Acid
Nd-YAG	Neodymium-Yttrium Aluminum Garnet
Ne	Neon
PA	Picolinic Acid
PD	Plasma Desorption
PIC	Pathways in Competition
PITC	Phenylisothiocyanate
PMF	Peptide Mass Fingerprint
ppm	parts-per million
ps	Picosecond
PSD	Post-Source Decay
PTM	Post-Translational Modification
Q	Quadrupole
Q-TOF	Quadrupole / Time-of-Flight
QqQ	Triple Quadrupole
QIT	Quadrupole Ion-Trap
r	Radius
RA	Retinoic Acid
RF	Radio Frequency
SA	Sinapinic Acid
SID	Surface-Induced Dissociation
SIMS	Secondary Ion Mass Spectrometry
SORI	Sustained Off-Resonance Irradiation
t	Time
T	Tesla
TS	Thermospray Ionization
TOF	Time-of-Flight
TOF/TOF	Time-of-Flight / Time-of-Flight
u	Atomic Mass Unit
UV	Ultraviolet
v	Volume
α-CHCA	Alpha-Cyano-4-Hydroxycinnamic Acid
μL	Microliter
μm	Micrometer
μM	Micromolar
μs	Microsecond
λ	Wavelength

CHAPTER 1

MASS SPECTROMETRY

1.1. What is a Mass Spectrometer?

A mass spectrometer is an analytical instrument which generates gas-phase ions from an analyte solution followed by subsequent separation and detection of those ions qualitatively and quantitatively based on their individual mass-to-charge ratio (m/z). The idea of mass spectrometer first suggested by Sir Joseph John Thomson in the late 1800s. He studied the conduction of electricity through gases and his works, later, led to the discovery of electrons. In 1906, he was awarded by Nobel Prize in Physics for "*in recognition of the great merits of his theoretical and experimental investigations on the conduction of electricity by gases*". Afterwards, in 1912, Thomson and his students separated non-radioactive stable isotopes of neon, ^{20}Ne and ^{22}Ne , on photographic plate (called as a parabola spectrograph) according to their different parabolic trajectories in the electromagnetic field. This experiment is accepted as an invention of the first mass spectrometer and today, Sir J. J. Thomson is known as the father of mass spectrometer.

Mass spectrometry (MS) has undergone countless technological improvements since its invention. It allows identifying and quantifying of variety of unknown compounds as well as characterization of their chemical structures with their molecular masses due to its high sensitivity and accuracy, ultimate speed, and small sample amount requirements. Its application areas have been spreaded into a wide range such as biotechnology, environmental, clinical, and pharmaceutical.

A mass spectrometer consists of three major components: an ionization source, a mass analyzer, and an ion-detector, as illustrated in Figure 1.1. Once the sample is introduced into the system through a sample inlet, it is ionized by the ionization source. The charged particles (either the loss or gain of a charge) are then electrostatically propelled into a mass analyzer where they are sorted according to their m/z values. Then, the ion energy is converted into electrical signals by the detector and transmitted to a computer. Finally, the signals are displayed as a mass spectrum which is a plot of ion intensity (ordinate) versus the m/z ratios (abscissa). The m/z ratio is dimensionless

quantity where m represents the mass of an ion and z is the number of elementary charge. Additionally, in biological mass spectrometry studies, the Dalton (Da) mass unit is preferably used instead of unified atomic mass unit (u) to express the molecular masses of an analyte.

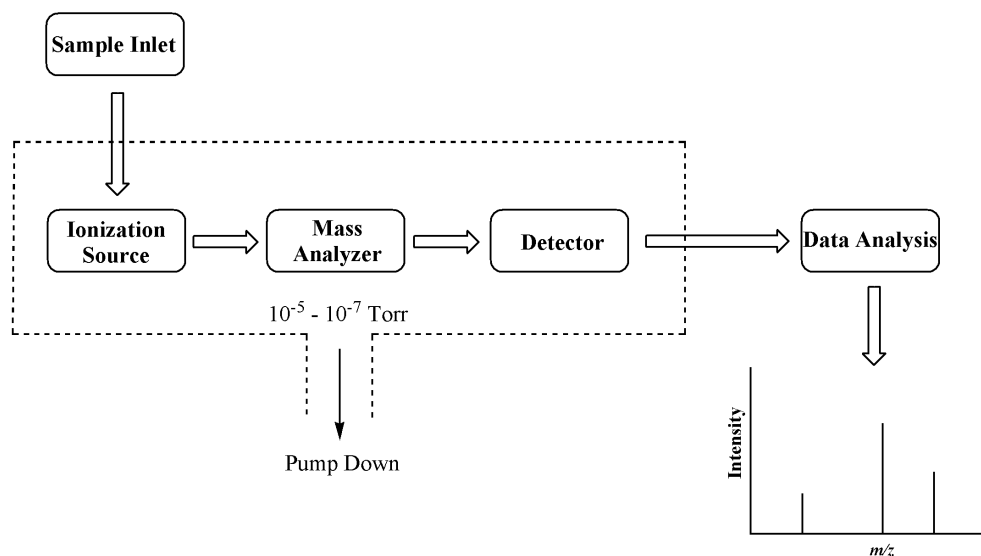


Figure 1.1. Basic components of a mass spectrometer

All the three components are operated under high vacuum conditions. The pressure inside the instrument must be reduced down to the 10^{-5} or 10^{-7} Torr and this vacuum is maintained by two-stage vacuum systems, mainly oiled sealed rotary pumps (rough pumps) and followed by turbomolecular pumps. The movement of the gas-phase ions from the source to the detector needed to be free, or in other words, the collisions between ions and any other gas molecules must be avoided. For that reason, the mean free path (the average distance between the two collisions) of gas molecules must be longer than the distance from the source to the detector. The mean free path is inversely proportional with the pressure, i.e. the lower the pressure, the longer the free path of the ions.

In the subsequent sections of this chapter, the fundamentals and the operation principles of the ionization techniques, the mass analyzers, and the detectors is discussed in detail.

1.2. Ionization Techniques

The neutral analyte is converted to an ion in the ion source by inducing either the loss or gain of a charge (or charges) after introduction into the mass spectrometer via direct insertion, infusion, or liquid/gas chromatographic techniques. Several alternative ionization techniques have been introduced to the literature. These ionization techniques are electron ionization (formerly termed as electron impact, EI) (Dempster 1918, Bleakney 1929, and Nier 1947), chemical ionization (CI) (Munson and Field 1966), secondary ion mass spectrometry (SIMS) (Herzog and Viehboeck 1949, Castaing and Slodzian 1962), laser desorption ionization (LDI) (Fenner and Daly 1966, Vastola and Firone 1968), field ionization/field desorption (FI/FD) (Beckey 1969), plasma desorption (PD) (Macfarlane and Torgerson 1976), fast atom bombardment (FAB) (Barber et al. 1981), thermospray ionization (TS) (Blakley and Vestal 1983), electrospray ionization (ESI) (Yamashita and Fenn 1984, Whitehouse et al. 1985, Mann et al. 1989, and Fenn et al. 1989), and matrix-assisted laser desorption/ionization (MALDI) (Karas et al. 1987, Karas et al. 1988, Tanaka et al. 1987, Tanaka et al. 1988).

The ionization methods are divided into two categories, namely “*soft*” and “*hard*”, according to the extent of fragmentation of analyte molecules in the course of ionization process. The main difference between these two techniques is the ability to keep the molecule intact or not. EI is classified as a hard ionization method due to the subjection of analyte vapor to the highly energetic electron beams (typically 70eV) which results extensive fragmentation by bond breakage of the analyte molecules. The application of EI is limited due to the difficulties in volatility and thermal lability of the molecules with a molecular weight less than 1000 Da.

On the other hand, little or no fragmentation is observed during the soft ionization process because little energy is imparted to the analyte. It generates predominantly stable molecular or quasimolecular ions in the mass spectra. The ionization of large biomolecules (proteins, peptides, polymers, oligosaccharides, lipids, oligonucleotides, etc.) is only achieved by soft ionization methods, particularly via FAB, ESI and MALDI. FAB is less frequently used for the analysis of biomolecules due to the noisy signals caused by matrix clusters. However, ESI and MALDI, which were developed in the late 1980s, are among the most promising ionization methods for analysis of biomolecules. For the revolution of these soft ionization techniques in the

analysis of biological macromolecules, John Bennett Fenn (for ESI) and Koichi Tanaka (for MALDI) shared the Nobel Prize (each 1/4) in Chemistry in 2002.

1.2.1. Electrospray Ionization (ESI)

ESI is known as a liquid-phase ionization method under atmospheric pressure conditions. Dole et al. (1968) and Mack et al. (1970) formerly proposed a possible gas-phase ion formation via spraying of a polystyrene solution (MW \approx 51,000 Da) through a charged capillary needle. However, Fenn et al. (1989) from Virginia Commonwealth University introduced for the first time the electrospray ionization (ESI) coupled with MS for the analysis of large biomolecules in the late 1980s. In this technique, the sample solution (the mixture of analyte and solvent) is directly sprayed from a thin metal capillary needle together with a sheat gas, as shown in Figure 1.2. The needle is maintained at a high voltage, typically \pm 2-5 kV, either positive or negative. The strong electric field is formed between a needle tip and a counter-electrode (orifice) where the sample solution has been dispersed into a fine aerosol to form a Taylor cone (Taylor 1964).

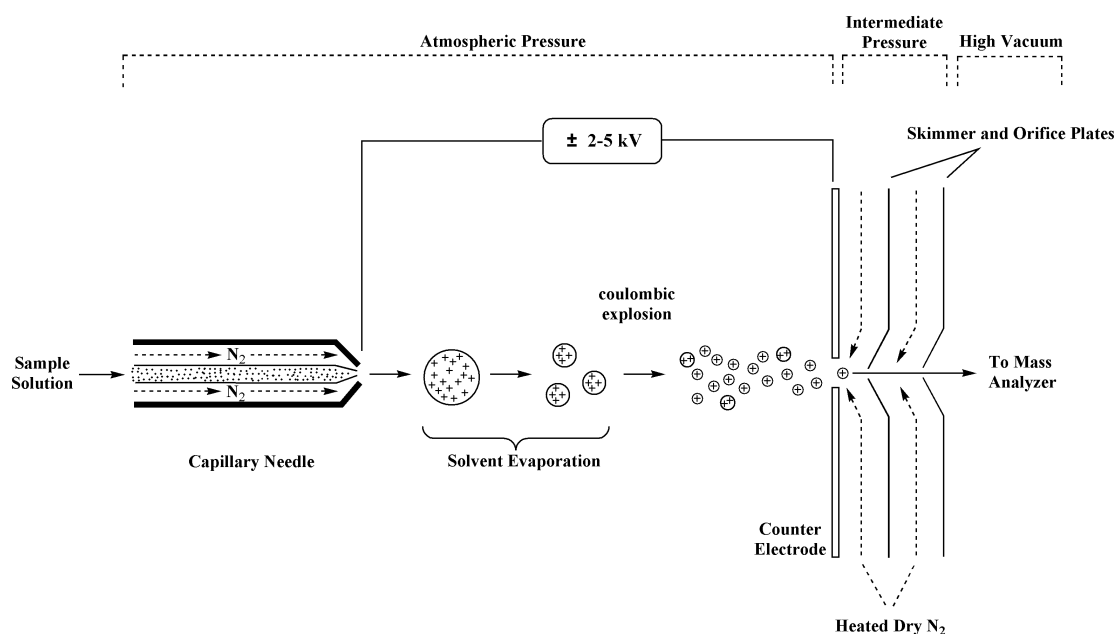


Figure 1.2. Schematic representation of the ESI ion source

The aerosol contains small highly charged droplets of the analyte-solvent mixture. Due to the potential difference, the droplets traverse from the needle to the entrance of the mass spectrometer. Meanwhile, the counter-current flow of heated dry nitrogen (N₂) gas is assisted as a nebulizing gas to evaporate the solvent (desolvation) in the ion source region. The size of the droplets is reduced as the evaporation continues, which tends to increase the charge density of the droplet surface. Afterwards, a coulombic explosion occurs (fission of a droplet) as the droplet surface reaches its Rayleigh instability limit (Rayleigh 1882). Then, the desolvated charged ions are eventually generated. Finally, the charged analyte ions are transferred into the mass analyzer, as illustrated in Figure 1.2.

The ionization of the analyte solution is proposed to occur through two mechanisms namely the “charge residue model (CRM)” and the “ion emission model (IEM)”. The RCM was originally proposed by Dole et al. (1968) and Mack et al. (1970) in the late 1960s and the IEM was subsequently introduced by Iribarne and Thomson (1976 and 1979). The RCM suggests that successive fission cycles lead to the formation of small charged droplets ($r \approx 1$ nm) containing only a single analyte molecule and followed by evaporation of excess solvent molecules (Kearle and Tang 1993). It is demonstrated that the gas-phase ions of globular proteins and polymers are probably formed by this method (Winger et al. 1993, Kearle and Peschke 2000 and Felitsyn et al. 2002). By contrast, IEM assumes that the charged droplets have enough electric field strength on its surface when the radius is equal to the 10 nm or smaller. Then, the droplet instantaneously assists to desorb ions out. This model is experimentally shown that as an appropriate method for the ionization of small molecules, generally below ~ 3000 Da (Cole 2000, de la Mora 2000, Gamero-Castaño and de la Mora 2000, Kearle 2000, and Nguyen and Fenn 2007). Recently, a third method was proposed for the ionization of analyte molecules (Hogan et al. 2009). In their study, the authors combined both mechanisms and named as a “charged residue-field emission model”.

ESI mainly generates a series of multiply charged $[M + nH]^{n+}$ cations or $[M - nH]^{n-}$ anions in the gas-phase. The number of charges on the ions formed by ESI are effected by several parameters, such as solution pH (Chowdhury et al. 1990), solvent identity (Loo et al. 1991, Iavarone et al. 2000, de la Mora 2000, Iavarone et al. 2001), capillary temperature (LeBlanc et al. 1991, Rockwood et al. 1991, and Miraz et al. 1993), presence of salts in the sample solution (Hoyau et al. 1999 and Chapman 2000), size of the biomolecules (Tolic et al. 1997 and de la Mora 2000), and

conformation of the biomolecules (Koneremann and Douglas 1998 and Dobo and Kaltashov 2001). In addition, the instrument parameters can also affect the quality of analyte signal, and these factors can be listed as ion spray voltage (Kebarle and Tang 1993), source and capillary temperature (Gabelica et al. 2004), orifice diameter (Wilm and Mann 1996, and Li and Cole 2003), declustering potential (Thomson 1997), sheath/auxiliary/sweep gas flow rates (Fenn 1993), and position of the ESI probe (Niessen 1999).

The solvent used in ESI is generally mixture of ultra pure water with polar and volatile organic solvents, such as methanol, acetonitrile, or isopropanol. The addition of organic solvents decreases the surface tension of the liquid which facilitates formation of gas-phase ions via ESI. Additionally, for the positive mode analysis, the solvent mixture is acidified with acetic acid or formic acid (0.1-1 %), whereas ammonium hydroxide is generally added (1-2 %) for the negative mode analysis.

Moreover, the inert gases are generally used in order to assist the nebulization of the liquid sample solution through a needle tip. The inert gases are preferred because they are not able to form any covalent bonds with the analyte ions. N₂ gas is more commonly used because it is cheap and it has high purity. Additionally, it is also used as a counter current gas to prevent cluster ion formation (Anacleto et al. 1992) and pushing contaminants away from the entrance of mass analyzers.

In recent years, liquid chromatography-mass spectrometry (LC-MS) systems have become versatile instrument for separation, identification and quantification of analyte in a complex mixture with a high sensitivity (Ardrey 2003). ESI is compatible with LC due to a being continuous flow-based technique of analyte-solvent mixture and can be applied either an online or an offline modes.

On the other hand, Wilm and Mann (1996) introduced the nanospray ionization to the field of ESI. In this technique, the typical flow rate of analyte solution is ranged from 20-50 nL/min. The smaller droplets are formed with nanospray ionization results higher ionization efficiency compared to the conventional ESI. This technique is especially important in clinical applications in which low amount of analyte is obtained from tissue samples.

1.2.2. Matrix-Assisted Laser Desorption/Ionization (MALDI)

Matrix-assisted laser desorption/ionization, referred to as MALDI, was introduced at the same time by Koichi Tanaka (1987 and 1988) at Shimadzu Corporation and Michael Karas & Franz Hillenkamp (1987 and 1988) at the University of Münster in the late 1980s. It is known as a solid-phase ionization method which provides a non-destructive vaporization and ionization of macromolecules. In this technique, the analyte is dissolved in an appropriate volatile solvent and mixed with an ultraviolet (UV) absorbing matrix solution typically at a concentration ratio of 1:100-1:10,000 (analyte:matrix) (Schriemer and Li, 1996). The matrix is a weak organic acid (with an aromatic ring) act as a chromophore that preferentially absorbs the laser energy. Therefore, it serves as a proton donor or acceptor during desorption event. The solution mixture is placed onto a multi-position sample target plate (either stainless steel or gold coated) and allows to analyte molecules dry and co-crystallize with the matrix solution at laboratory conditions, as illustrated in Figure 1.3.

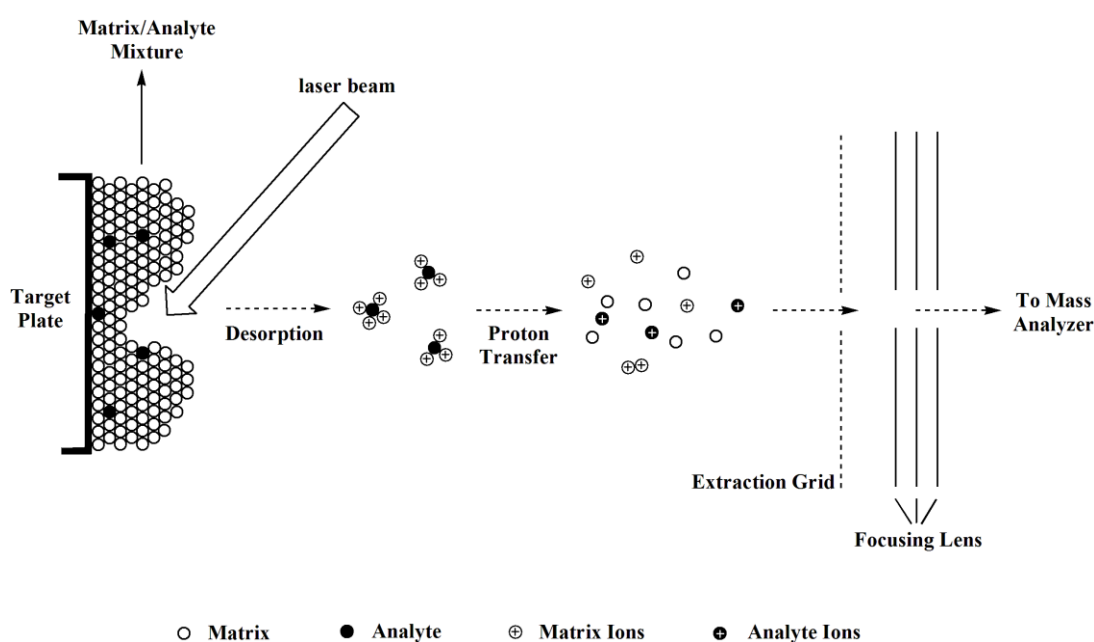


Figure 1.3. Formation of ions in MALDI process

Afterwards, the target plate is placed in the mass spectrometer for analysis where the mixture is irradiated with a pulsed UV-laser, typically nitrogen laser with an operating wavelength of 337 nm. In some cases Nd-YAG ($\lambda = 355$ nm) lasers also used.

The laser pulses supply heat to the matrix which allows the ablation and vaporization of the matrix and analyte together from the solid state into the gas-phase and this process generates a dense gas cloud (plume). This expanding plume contains matrix ions/radicals and neutrals which instantly produce gas-phase analyte ions by proton transfer reactions. Finally, the gas-phase ions are directed by an electric field to the mass analyzer of the mass spectrometer (Figure 1.3). In contrast to ESI, MALDI generally produces mainly singly charged ions.

However, desorption and ionization mechanisms in MALDI are still under debate, and numerous processes, such as gas-phase photo-ionization, disproportionation, ion-molecule reactions, thermal ionization, energy pooling, desorption of preformed ions, and excited-state proton transfer, have been recommended (Zenobi and Knochenmuss 1998 and Dreisewerd 2003).

The choice of the most compatible matrix with the analyte is the crucial step for obtaining the best signal in MALDI experiments. Several different matrices have been recommended in the literature (Beavis et al. 1989 and 1992, Strupat et al. 1991, Wu et al. 1993). The most intrinsic property of the matrix is the ability to absorb readily and resonantly the energy which is emitted by the laser at specific wavelength. Additionally, matrices must be miscible with the analyte, must have vacuum stability, must have a small molecular weight (mass range of 100-350 Da) and must be able to co-crystallize with an analyte at ambient conditions. The most commonly used MALDI matrices are various cinnamic and benzoic acid derivatives and some other aromatic compounds. The chemical structures of some matrices are depicted in Figure 1.4.

In particular, the α -CHCA (α -cyano-4-hydroxycinnamic acid) matrix is used for peptides and small proteins (up to 5 kDa) (Beavis et al. 1992), while SA (sinapinic acid) and NA (nicotinic acid) matrices are suitable for large proteins (Beavis and Chait 1989, Karas and Hillenkamp 1988). Additionally, HABA (2-(4'-hydroxyphenylazo)-benzoic acid) is used for peptides, proteins, and glycopeptides (Juhansz et al. 1993). Wu et al. (1993 and 1994) introduced PA (picolinic acid) and 3-HPA (3-hydroxypicolinic acid) as matrices for oligonucleotides. DHB (2,5-dihydroxybenzoic acid or gentisic acid) is mainly used for the analysis of oligosaccharides and peptides (Strupat et al. 1991). RA (retinoic acid) and dithranol is best suited to polymer analysis (Rader and Schrepp 1998 and Nielen 1999). On the other hand, it has been reported that the combination of two matrices (α -CHCA and DHB) greatly improves shot-to-shot reproducibility and

generates better peptide ion signals rather than obtained from single matrix (Laugesen and Roepstorff 2003).

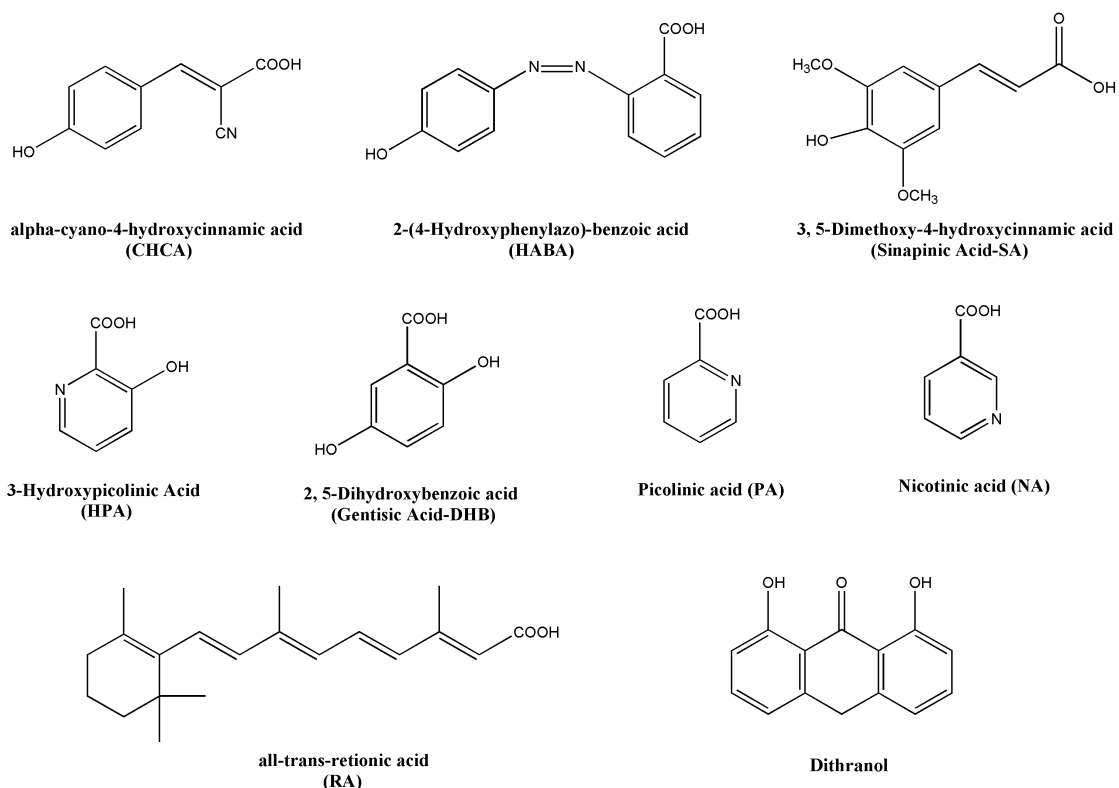


Figure 1.4. Common matrices used in MALDI-MS experiments

The sample preparation (co-crystallization of matrix with analyte) is the key step in order to obtain high shot-to-shot reproducibility and high quality ion signals in MALDI-MS experiments. Several sample preparation methods have been introduced in order to improve the sensitivity and the resolution. These methods can be listed as: dried-droplet (Karas and Hillenkamp 1988 and Thomas et al. 2004), active film (Mock et al. 1992 and Bai et al. 1994), vacuum drying (Weinberger et al. 1993), slow crystal growing (Xiang and Beavis 1993), thin-layer by fast solvent evaporation (Vorm et al. 1994, Gobom et al. 2001), pneumatic spray (Köchling and Biemann 1995), sandwich (Li et al. 1996, Kussman et al. 1997), crushed-crystal (Xiang and Beavis 1994), two-layer (Dai et al. 1999), three-layer (Keller and Li 2006), sample-matrix wash (Zhang et al. 2007), and matrix-layer (Garaguso and Borlak 2008). With the advance of these methods, it is possible to scan the crystallized surface of the mixture with the laser beam in order to obtain the best informative signals of the analyte. The point is called as a

“sweet spot”, where the analyte is well mixed and distributed within the matrix solution and it gives better results than other parts of the crystallized surface.

On the other hand, it was documented that MALDI is more tolerant than ESI to the contaminants (various salts, buffers, surfactants, and organic additives) up to moderate concentration levels (Amini et al. 2000). Moreover, several matrix-related background peaks (i.e. dimmers, trimmers, and their Na⁺ and K⁺ adduct) can highly interfere in the low mass region (MW < 500 Da). Therefore, MALDI gives the best results for the molecules with a molecular weight greater than 500 Da (Lidgard and Duncan 1995, Knochenmuss et al. 1996).

In the analysis of synthetic polymers and carbohydrates, the samples are generally ionized by the formation of metal-ion adduct which is called a cationization process (Knochenmuss et al. 1998, Zhang and Zenobi 2004). The sodium and potassium adduct cluster ions are often detected in the MALDI mass spectrum due to the impurities coming from incompletely deionized water, solvents, matrices, or glasswares (Danis and Karr 1993). These adducts can greatly suppress the analyte signals and make the elucidation of the molecular ion peaks difficult by complicating the mass spectra. However, in some cases, the metal salts (AgNO₃, CuCl₂, ZnCl₂, etc) are added to the matrix/analyte mixture in order to enhance the intensity of analyte signal by improving the ionization efficiency of the molecule.

1.3. Mass Analyzers

Once the gas-phase ions have been generated in the ionization source, they need to pass through to the mass analyzer where they are sorted based on their m/z values. Nowadays, several different types of mass analyzers are commercially available for ion separation. These mass analyzers are quadrupole (Q), ion-trap (IT), time-of-flight (TOF), and Fourier transform-ion cyclotron resonance (FT-ICR). These analyzers use electric and/or magnetic fields to differentiate the masses. The first three analyzers are classified as electric field analyzers; in contrast, FT-ICR uses magnetic field to separate ions. Each analyzer has its own strengths and weaknesses; however, the common features of them are their resolution, mass range, mass accuracy, dynamic range, analysis speed, and ion transmission. The resolution, $m/\Delta m$, is the most important parameter of the mass analyzers which is defined as an ability to separate two adjacent

peaks. In this dissertation, the quadrupole and ion trap technologies are mainly used as mass analyzers.

1.3.1. Quadrupole (Q)

A quadrupole (Q) mass analyzer was firstly described by Paul and Steinwedel (1953) and Paul and Raether (1955). Quadrupoles are also known as mass filters because it only transmits an ion with a specific m/z ratio to the detector. It consists of four perfectly parallel cylindrical or hyperbolic rods (metal or metal-coated ceramic) in a square configuration spaced around a central axis, as shown in Figure 1.5. The cylindrical rods are routinely used rather than hyperbolic ones in today's commercial mass spectrometers due to the easy of manufacture.

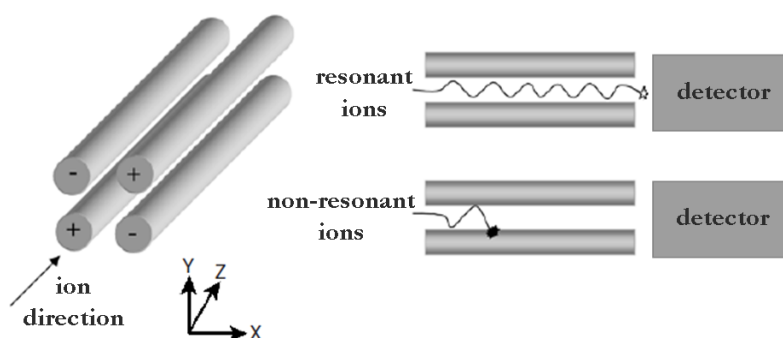


Figure 1.5. Schematic diagram of a quadrupole mass analyzer
(Source: Liebler 2002)

A combination of time dependent radio frequency (RF) and time independent direct current (DC) potentials are applied to opposite pairs of electrodes which are electrically connected to each other. Two opposite rods have the same polarity, either positive or negative. The generated electrical field on the rods represent as $\pm (U + V\cos(\omega t))$ where U is the magnitude of the DC voltage, V and (ωt) stands for the amplitude and frequency of the RF voltage, respectively. The generated ions are introduced continuously to the quadrupoles. The certain RF and DC potentials select and stabilize only a specific m/z ratio and allow the ions to travel perpendicular to the field (x-direction). These resonant ions with stable trajectories can pass through the quadrupoles and are directed to the detector within the oscillating electrical field.

However, non-resonant ions with unstable trajectories are completely thrown out of the quadrupoles or hit one of the rods. On the other hand, all ions can be transmitted to the detector by applying only RF potential to the rods in order to obtain the full spectrum. In this case, quadrupoles are used in the scanning mode rather than filtering mode.

The behavior of ion motion in the quadrupoles can be best understood by plotting a stability diagram which is a function of RF and DC voltages, as illustrated in Figure 1.6. This graphical representation is also known as Mathieu stability diagram and describes ion's stability (McLachan 1951).

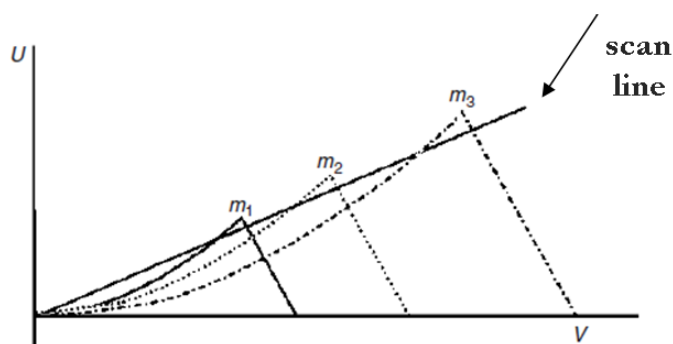


Figure 1.6. Stability diagram for ions in a quadrupole
(Source: Hoffmann and Stroobant 2007)

In the quadrupoles, the trajectories of ions in the x and y directions lead to the construction of stable and unstable regions. The area under the curve indicates that stable trajectory of ion. The straight scan line is drawn at various combinations of potentials while keeping the DC/RF ratio constant. The m_1 , m_2 , and m_3 denote the ions with different masses. It should be mentioned that different ions have different stability regions but the shape of the curve remain the same. The most of the ions are unstable through the scan line; however, when it passes through the stable region, ions become stable and can reach the detector. In other words, ions only above the scan line can pass through the quadrupole.

The benefits of quadrupole mass analyzers are its reproducibility, robustness, relatively low cost, small size, and easy of maintenance. On the other hand, quadrupoles have a limited mass range ($< 4,000$ Da) and low resolution ($\sim 3,000$) which is usually operated at unit mass resolution. The mass accuracy is around 100 ppm. However, it is not suited for pulsed ionization method (i.e. MALDI).

1.3.2. Ion-Trap (IT)

The theory of an ion-trap (IT) was first described for the analysis of isolated ions after the development of quadrupole mass filters (Paul and Steinwedel 1953, Dehmelt 1967 and 1969). Even though it was invented in the late 1950s, the first commercial ion trap mass spectrometer has been available by Finnigan MAT in 1984 (Stafford Jr. et al. 1984). Later, Wolfgang Paul and Hans Georg Dehmelt (each $\frac{1}{4}$) were recognized by the Nobel Prize in Physics in 1989 for their contributions of the development of the ion trap technique.

This analyzer is also called as a quadrupole ion-trap (QIT) because its operation principle is similar to a quadrupole mass filter. The QITs exist in both a linear (Douglas et al. 2005) and three-dimensional (3D) forms (Stafford Jr. et al. 1984). The two configurations have the same operation principles. The linear QIT has a set of quadrupole electrodes which can act both as a filter and a trap. The 3D QIT is composed of three electrodes; two end-cap electrodes and a ring electrode, each of have a hyperbolic internal surface to the central cavity. The ring electrode is squeezed between two end-cap electrodes, as Figure 1.7 displays.

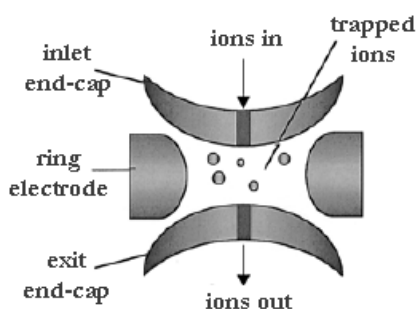


Figure 1.7. Schematic view of a 3D ion trap
(Source: Liebler 2002)

The low amplitude RF voltage is applied only to the ring electrode whereas end-cap electrodes are held nearly at ground potential (Cooks et al. 1991). Once the ions are generated in the ionization source, they are focused toward the center of the QIT where the applied RF voltage creates an electrical field in order to trap the ions within the QIT for a period of time. As a consequence of coulombic interactions among like charged particles, the trapped ions cause distortion of the electric field. This effect is known as

“*space-charge effect*”, which causes the loss of dynamic response range and limits the performance of the instrument. This effect can be diminished by introducing a helium (He) gas (purity > 99.9 %) at a pressure of nearly 10^{-3} Torr to the trapping media. It is generally referred as a bath gas, damping gas or target gas. It dampens the kinetic energy of the ions and also to focus ion trajectories near the center of the ion trap. Additionally, the use of damping gas leads to improve both the mass resolution and the sensitivity. All confined ions are cooled down with the aid of damping gas and they move in a complex motion with an oscillating frequency in the cavity of trap. Finally, the motions of trapped ions can be progressively changed by scanning the amplitude of the RF potential which causes the ions of different m/z ratios sequentially adopts unstable trajectories along the axis of the end caps. This mode of operation is known as mass-selective instability. These ions are then ejected from the ion trap (resonance ejection) one by one and reach the detector to generate full-scan mass spectrum (see Figure 1.8).

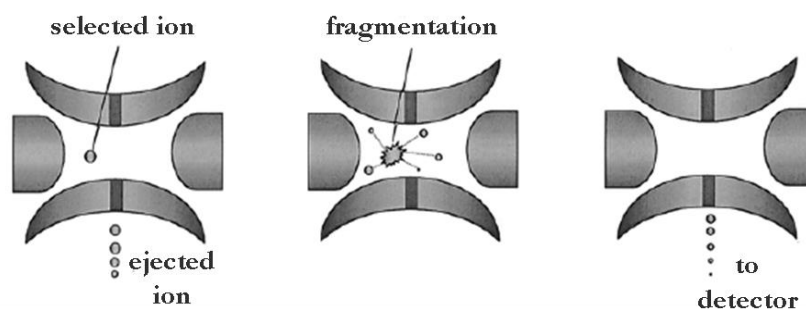


Figure 1.8. Schematic representation of MS/MS in ion trap
(Source: Liebler 2002)

Probably, the most important feature of ion traps is their capability to perform multi-stage tandem mass spectrometry (MS^n) experiments which provide detailed structural information of the analyte. The trap voltage is adjusted to select only one particular ion of interest while all other ions are ejected. Afterwards, the amplitude of applied RF voltage (tickle voltage) is slightly ramped across the end-cap electrodes to increase the kinetic energy of the selected ion. These ions undergo energetic collisions with the existing He gas (damping gas) within the trap region. This process leads to ion fragmentation (dissociation) and the fragment ions are sequentially ejected according to

their m/z ratios from the trap. Consequently, the fragment ions are ultimately transmitted to the detector in a similar manner described above.

For MS^n experiments, this trapping/ejection cycle is repeated n times. It is reported that up to 12 stages of tandem mass spectrometry have been accomplished (Louris et al. 1990). However, the total ion intensity is dramatically decreased in each cycle. In order to improve the resolution, the trap performance and the ion transmission efficiency, the multipole trap (hexapole or octopole) components are generally placed in front of the ion trap and quadrupole systems (McDonnell et al. 2002, Ding et al. 2003, Sudakov and Douglas 2003, Kononkov et al. 2006, and Zhao et al. 2008).

OITs are widely used in mass spectrometers due to its high sensitivity, high specificity, availability of MS^n experiments, relatively small size and mechanical simplicity. It has a mass accuracy about 20 ppm (Wells et al. 1998). On the other hand, the mass range of QIT is below 4000 Da with a unit mass resolution up to 3000. The resolution can be improved by using lower excitation amplitudes of RF voltage (Goeringer et al. 1992). Despite to these advantages, the major drawback of the ion trap technology is the low mass cut-off restriction which results in the loss of fragment ion information. The cut-off mass corresponds to the approximately one-third of the precursor ion mass which is selected for further fragmentation.

The ion traps are divided into two categories: the Paul trap (QIT) and the Penning trap (FT-ICR). The Paul trap uses RF voltage whereas the Penning traps uses static electromagnetic field for resonance excitation of the ions in the trap volume. An Orbitrap, a new version of trap technology, was first described by a Russian scientist Makarov (2000), from the Thermo Electron Corporation. The instrument was then appeared in the mass spectrometry market in 2005 (Hu et al. 2005). It has been developed by the theory based on the Kingdon type ion trap (Kingdon 1923) where static electrostatic fields are used to trap and eject the ions. It provides a high mass accuracy (2-5 ppm) with high mass resolution (up to 150,000). It also has a high dynamic range ($> 10^3$) with a high sensitivity (Makarov et al. 2006).

1.3.3. Time-of-Flight (TOF)

The concept of time-of-flight (TOF) was firstly proposed by Stephens (1946) in American Physical Society Meeting. However, the TOF-MS design was initially

demonstrated by Wiley and McLaren (1955) and the commercial TOF instrument first came out in the market by the Bendix Aviation Corporation in the late 1950s. The principle of TOF is based on the precise measurement of the flight times of ions in a field-free drift tube, from one end to the other. The term field-free basically defines that there is no magnetic or electric field acting on the ions during their flight in TOF tube. MALDI, a laser-pulsed (discontinuous) ionization technique, is typically combined to TOF mass analyzers. Once the ions are formed via MALDI, they are accelerated towards the field-free region receiving an equal kinetic energy which is caused by potential difference (i.e. 20-30 kV) between acceleration electrodes and entry grid. As the ions gain a kinetic energy of several keV, their velocity will vary because of having different masses. In practice, ions travel with different velocities along the field-free region before striking to the detector. The velocities of ions are inversely proportional to their m/z ratios; in other words, the lighter ions reach the detector faster than the heavier ones. Hence, the ions are separated based on their velocity differences. Additionally, all formed ions will reach the detector one by one. An illustration of a linear TOF tube is shown in Figure 1.9.

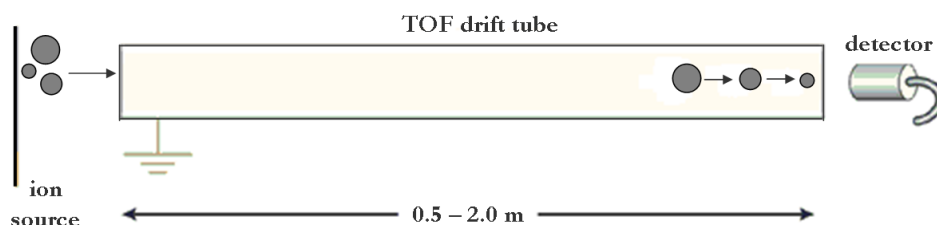


Figure 1.9. Schematic view of linear TOF mass analyzer
(Source: Glish and Vachet 2003)

The m/z ratio of ions can be easily determined by the formula, $2eUt^2/L^2$, where e , U , t , and L represent an elementary charge, an applied voltage, a flight time, and a length of the drift tube, respectively. The U and L kept constant during the analysis and the flight time is directly proportional to the square root of the ion's m/z ratio. In the TOF tube, the flight times of the ions are in microsecond (μs) scale, and the length of the flight tube typically ranges from 0.5 to 2.0 meters.

One of the problems encountered in linear TOF-MS experiments is uneven kinetic energy distribution for identical ions in the course of MALDI process. In this

case, the peaks are expected to be broadened and the mass accuracy and the resolution are ultimately lost. In order to improve the mass accuracy and the resolution, a short time delay (100-500 ns) is introduced between the ion formation and the extraction grid. Thus, ions will have the same kinetic energy before accelerating in the field-free region. This technique is known as delayed extraction (Brown and Lennon 1995). The concept of delay extraction was firstly described by Wiley and McLaren (1955) with the ions generated by electron ionization in a two-stage accelerating region and it is formerly referred as time-lag focusing.

In addition to delay extraction, the reflectron TOF configuration is also used to compensate for initial kinetic energy distribution of ions with the same m/z . The idea of using reflectron in TOF was proposed in order to gain better mass resolution (Alikhanov 1957). The first reflectron TOF-MS instrument was introduced by Mamyrin et al. (1973). In fact, reflectron is an ion optical device consisting of long series of electrodes located at the end of the drift tube and acting as an electrostatic ion mirror. It reverses the direction of flight path of the ions and focuses them towards the reflectron (second) detector. The ions with a higher kinetic energy spend more time in reflectron compared to the less energetic ones. Thus, the ions can travel longer than their normal flight in the linear mode which substantially improves resolution of TOF analyzers. The combination of delayed extraction and reflectron modes greatly improves the resolution ($> 10,000$) and mass accuracy (< 20 ppm) of the instrument.

After the precursor ion leaves the source, it may fragment via post-source decay (PSD) process. The fragmentation occurs in the field-free region via unimolecular decomposition. The reflectron resolves the PSD fragments due to the difference in their kinetic energies but basically they have the same velocities as the precursor ion. The reflectron potential is varied step by step to acquire a mass spectrum in each energy window and a full PSD mass spectrum is obtained by stitching individual spectra together.

The TOF mass analyzers have theoretically unlimited mass range. It has been reported that polystyrene polymer with a molecular weight of approximately 1.5 million was successfully analyzed by MALDI TOF-MS (Schriemer and Li 1996). Additionally, the data acquisition is very rapid with a high sensitivity for ion detection. However, the mass spectrum may be complex due to the transmission of all ions by TOF which may create problems for interpretation of the peaks.

1.3.4. Fourier Transform-Ion Cyclotron Resonance (FT-ICR)

The technique of ion cyclotron resonance (ICR) was introduced by Hipple et al. (1949). However, Comisarow and Marshall (1974) were the first researchers to apply Fourier transform (FT) to ICR. This can be regarded as the birth of the FT-ICR MS instrument (also abbreviated as FTMS). Basically, it applies a strong magnetic field (B) to determine the m/z of ions which is a characteristic of the particular cyclotron frequency. Briefly, as the ions are generated either by ESI or MALDI, they are guided up to the Penning trap (a form of ion trap) under high vacuum where a uniform magnetic field is created previously. The ions subsequently start to move a circular orbit in a plane perpendicular to the field by Lorentz forces. The term Penning trap is used for a cubic cell in here and it consists of three pairs of plates: excitation (transmitter), trapping, and detector (receiver) plates, which they are oppositely located in the cubic structure (see Figure 1.10).

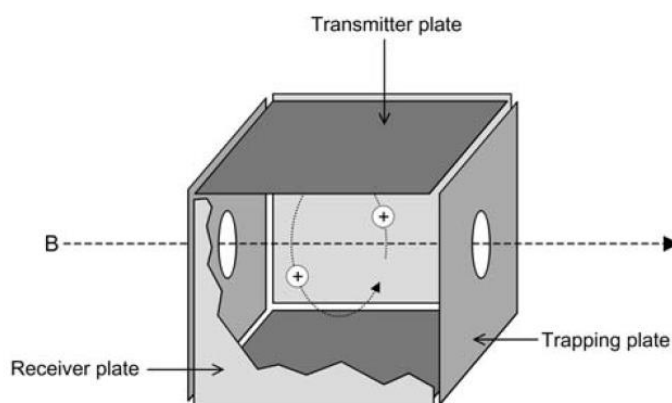


Figure 1.10. Schematic view of FT-ICR mass analyzer
(Source: Lane 2005)

The trapping plates are charged and then used to keep the ions in their orbits, whereas a pulse of RF is applied across the excitation plates to excite the ions coherently to a higher orbit. Then, the detector plates are used to measure the image current of orbiting ions as a time domain signal. The FT methods are used to convert these time dependent signals into frequency domain which then is transformed into the mass spectrum due to the inverse relationship between cyclotron frequency and m/z .

The sustained off-resonance irradiation collision-induced dissociation (SORI-CID) technique is commonly used for ion activation and fragmentation in order to gain structural information of an analyte in FT-MS experiments (Senko et al. 1994).

The strong magnetic field, which is maintained by a superconductive magnet with strengths of 4.7–9.4 Tesla (T), is employed to force the ions in cyclotron motion. The resolving power of the instrument can be improved as the magnetic field of the electromagnets increased (Marshall and Guan 1996). Hence, the superconducting magnets with strengths of 11.5 T and 20 T are also constructed and used in today's commercial instruments (Gorshkov et al. 1998, Hendrickson et al. 1996). These strong magnets must be shielded actively or passively for the protection of users.

FT-ICR has a unique sensitivity (attomole level) compared to the other mass analyzers, because it has a very high mass resolution ($> 1,000,000$) and very high mass accuracy (< 1 ppm) in the analysis of compounds from complex mixtures.

1.3.5. Hybrid Mass Analyzers

In hybrid analyzer systems, two or more mass analyzers are combined into a single instrument. They are constructed in order to obtain higher sensitivity and mass accuracy in one device. In earlier studies, EBE (Russell et al. 1980), EBEB (McLafferty et al. 1980), BEqQ (Schoen et al. 1985 and Harrison et al. 1986) and BEEQ (Winger et al. 1992) hybrid mass spectrometers have been introduced where the shorthand notations of B, E, q, and Q stands for a magnetic sector, an electric sector, a collision cell, and a mass filter, respectively. Nowadays, several different hybrid mass spectrometers have been used, such as a triple quadrupole (QqQ) (Yost and Enke 1978, 1979), a quadrupole/time-of-flight (Q-TOF) (Glish and Goeringer 1984, Morris et al. 1996 and 1997), an ion trap/time-of-flight (IT-TOF) (Fountain et al. 1994 and Campbell et al. 1998), a time-of-flight/time-of-flight (TOF/TOF) (Medzihradzky et al. 2000, Vestal and Campbell 2005), a linear ion trap/FT (Syka et al. 2004), and a linear ion trap/orbitrap (Makarov et al. 2006). In tandem mass spectrometry (MS/MS) experiments, the first mass analyzer is used for mass selection while the fragmentation is done in the collision cell and the scanning of the fragments is achieved in the second mass analyzer.

1.4. Detectors

The final element of the mass spectrometers is a detector. Basically, a detector converts the ion energy into a current signal. The detectors must possess some features, such as large dynamic range, high amplification, high stability, fast response time, low or no noise, low cost, and mass-independent response. Based on the design of the mass spectrometers, several types of detectors exist for ion detection. The most common ones are a Faraday cup, an electron multiplier (EM), and a microchannel plate (MCP).

1.4.1. Faraday Cup

In Faraday cup, the charged ions strike the surface of the dynode. The dynode surface is made of thin metal sheets of GaP, CsSb, or BeO emitting alloys. The striking causes the ejection of the secondary electrons from its surface and the induced current is amplified and recorded. It is robust but does not have very high sensitivity.

1.4.2. Electron Multiplier

The electron multiplier (EM) has a series of dynodes with increasing potentials. The schematic view of discrete electron multiplier is shown in Figure 1.11. Ions hit the emissive surface of the first dynode, which causes an emission of secondary electrons.

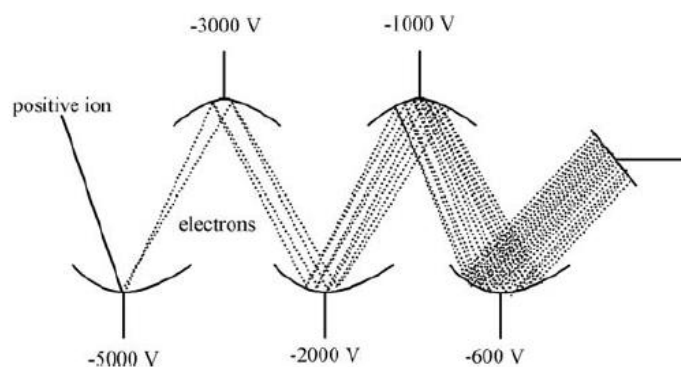


Figure 1.11. Schematic view of electron multiplier
(Source: Hoffmann and Stroobant 2007)

The ejected electrons are accelerated to the next dynode to produce more secondary electrons. These steps are repeated several times to form a cascade emission of electrons on the order of 10^6 or more. It is the most commonly used detector in a quadrupole and ion-trap mass spectrometer systems because of high sensitivity with low level of noises. Moreover, the curved (horn) shape of EM is also designed with a continuous dynode rather than discrete dynodes.

1.4.3. Microchannel Plate

The last detector is microchannel plate (MCP) detector. It comprised of a regular array of 10^4 - 10^7 independent channels on a disk-shaped device, which are electrically connected in parallel to one another, as Figure 1.12 displays. Each channel is considered as a continuous-dynode electron multiplier which provides higher spatial and temporal resolution.

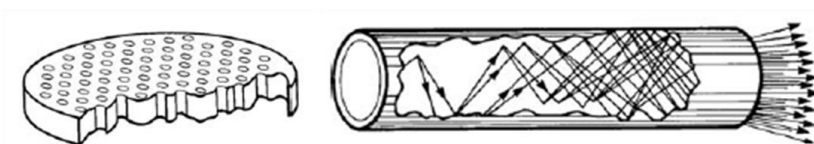


Figure 1.12. Schematic views of microchannel plate
(Source: Hoffmann and Stroobant 2007)

The diameter of microchannels is in the range of 5-15 μm with a length of 0.5-0.8 mm and typically spaced apart by 15 μm . An ion can enter the plates with an angle of $\sim 8^\circ$ to the surface and hits the wall of the microchannel plate, which allows the secondary electrons to be ejected. The ejected electron strikes the surface again and generates more secondary electrons. Thus, the signal is amplified by several orders of magnitude via propagation of electrons down the channel. The response time is very fast; therefore MCP detectors are generally equipped with a TOF mass analyzer. However, they are so expensive and very sensitive to air.

CHAPTER 2

FRAGMENTATION MECHANISMS OF PROTONATED PEPTIDES IN THE GAS-PHASE

Over the past two decades, MS has become the most prominent tool for researches in life sciences with the development of two novel soft ionization techniques, i.e. ESI and MALDI. These methods allow gentle ionization of thermally labile biological macromolecules in the gas-phase without extensive fragmentation and yield protonated or multiply protonated (or in some cases deprotonated) molecular ions. The intact molecular ions, which enable to determine the molecular weight of biomolecules with a high accuracy, are generated. Additionally, the structural information of biomolecules is obtained by tandem mass spectrometry (MS/MS) experiments. The gas-phase fragmentation mechanism studies of peptides via MS are the subject of this thesis. Firstly, brief information of proteins and peptides will be given in the following section, and then the sequence elucidation by mass spectrometric techniques will be covered in detail.

2.1. Peptides and Proteins

Proteins are the biological macromolecules found in every living cell with very large abundances. They have many vital cellular functions, such as transportation and storage of molecules, repair and maintenance, structural support, cellular signaling, energy, movement, and defense mechanism (McKee and McKee 2003). Additionally, enzymes are form of protein that can function as a catalyst in almost every metabolic reaction within living organisms. Peptides and proteins are comprised of small building blocks called amino acids. All amino acids consist of an α -carbon atom (an asymmetric carbon) at the center and are surrounded by a hydrogen atom, a carboxylic acid group, a primary amine group, and a distinctive R group. The general chemical structure of an amino acid is represented in Figure 2.1.

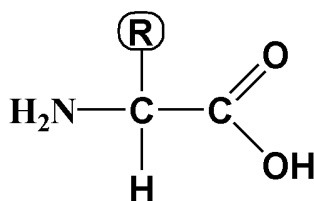


Figure 2.1. General structure of an amino acid

Each R group has different features which characterize the chemical and physical identity, structure and function of the amino acids. There are twenty natural amino acids and they can join together by covalent bonds (peptide bond) to form peptide followed by water elimination. The names of natural amino acids with their abbreviations and monoisotopic residue masses are listed in Table 2.1.

Table 2.1. A list of twenty natural amino acids

Amino acid name	Three-letter code	One-letter code	Residue Mass (Da)
Glycine	Gly	G	57.021
Alanine	Ala	A	71.037
Serine	Ser	S	87.032
Proline	Pro	P	97.053
Valine	Val	V	99.068
Threonine	Thr	T	101.048
Cysteine	Cys	C	103.009
Isoleucine	Ile	I	113.084
Leucine	Leu	L	113.084
Aspartic Acid	Asp	D	114.027
Asparagine	Asn	N	114.043
Glutamine	Gln	Q	128.059
Lysine	Lys	K	128.095
Glutamic Acid	Glu	E	129.043
Methionine	Met	M	131.040
Histidine	His	H	137.059
Phenylalanine	Phe	F	147.068
Arginine	Arg	R	156.101
Tyrosine	Tyr	Y	163.063
Tryptophan	Trp	W	186.079

Amino acids are shown by either one- or three-letter code, as tabulated in the Table 2.1. Except glycine, the central carbon has chiral character, in other words it is not superposable on its mirror image. Amino acids have different physical and chemical

properties based on having various R groups on their side chains. For instance; Gly, Ala, Pro, Val, Leu, Ile, and Met have non-polar aliphatic R groups, while Ser, Thr, Cys, Asn, and Gln have polar uncharged R groups. On the other hand, Lys, His, and Arg are classified as positively charged (basic) amino acids whereas Glu and Asp are negatively charged (acidic) amino acids. Moreover, Phe, Tyr, and Trp include aromatic R groups on their side chains.

The structure of protein can be divided into four categories: primary, secondary, tertiary, and quaternary structure. The amino acid sequence (primary structure) certainly determines three dimensional structures of proteins and its function. In a general view, the proteins contain a free amine group (N-terminal) at the one end while the other end is terminated by a free carboxyl group (C-terminal). The long chains of peptides can be linked to each other to form a protein.

International Human Genome Sequencing Consortium completed the Human Genome Project in 2001 and the researchers in the consortium estimated that the haploid human genome comprises between 20,000 - 25,000 putative protein-encoding genes (Lander et al. 2001 and Venter et al. 2001). However, the number of proteins encoded is dramatically more than the number of genes. It is demonstrated that the number of proteins in human body may vary from 200,000 to 2 millions (Black 2000 and Jensen 2004). This increased diversity can be explained by alternative splicing of mRNA and post-translational modifications (PTMs) of proteins. It has been documented that over 200 different naturally occurring PTMs have been detected on proteins (Walsh 2006), such as phosphorylation, acetylation, methylation, and glycosylation.

The elucidation of the amino acid sequence of proteins has vital importance in system biology, because proteins can be considered as biomarkers in disease diagnosis. For that reason, a new term "*proteome*", which expresses the total protein content of a cell, a tissue, or an organism in a given state of time, was recommended in 1994 (Wilkins et al. 1996). The term *proteome* is the combination of *protein* and *genome*. The proteome of a cell is highly dynamic; in other words, the cell responses to any stress conditions immediately, and the proteome is changed. In contrast to proteome, the genome is static. The proteomic studies mainly cover the identification, quantification, modification, and localization of each individual protein in a given cell or tissue at a specific time.

2.2. Sequence Analysis by Tandem Mass Spectrometry (MS/MS)

Previous studies focused on the determination of amino acid sequence of protein by Edman degradation procedure (Edman 1950). In this method, the cleavage of N-terminal amino acid of the protein is achieved one by one with phenylisothiocyanate (PITC) reagent. The derivatized residue is cleaved from the chain and identified with HPLC analysis. The new N-terminal amino acid residue continues to react with PITC, and the derivatization cycles go on. The peptide length with a maximum 25 amino acid long can be sequenced with the help of this method. However, this technique does not work for N-terminal modified peptides and cyclic peptides; therefore, it is not suited for analysis of complex protein mixtures.

For these reasons, MS has been introduced as an analytical tool to the field of protein chemistry in order to identify proteins as well as PTM sites. For large sample sets, the peptide mass fingerprinting (PMF) strategy is generally used for protein identification (Cleveland et al. 1977, Yates et al. 1993, Mann et al. 1993). This approach is based on the separation of total protein mixture by two-dimensional polyacrylamide gel electrophoresis system (2D-PAGE) (O' Farrell 1975). Each spot on the 2D gel represents only one protein with a specific isoelectric point and molecular weight. Then, the spot can be excised from the gel carefully and digested with a site-specific enzyme (i.e. trypsin) which forms various lengths of polypeptide chains in solution. The formed peptides are removed from the gel and analyzed by MALDI TOF-MS (Henzel et al. 1993). As a final step, protein identification relies on the comparison of observed mass spectrum against calculated ones in *in silico* (computer simulated) which already exist in the database. The automated search algorithms, such as MASCOT (Perkins et al. 1999) and SEQUEST (Eng et al. 1994), enable protein identification through database searches.

Currently, two main strategies have been utilized for MS based proteomic studies, namely “*top-down*” and “*bottom-up*” (Chait 2006). In top-down approach, intact protein is ionized and subsequently undergoes fragmentation within the mass spectrometer. Protein identification entirely relies on the comparison of masses of both the protein and its fragment ions with protein sequence databases (Reid and McLuckey 2002). On the other hand, in the bottom-up approach, the protein is digested with an enzyme (generally trypsin) and the obtained tryptic peptide mixture is analyzed by

MS/MS. The experimental MS/MS spectra are then compared with the predicted MS/MS spectra through sequence databases.

The development of MS/MS technique greatly assists the correct and reliable peptide sequencing for proteomic studies (Biemann and Scoble 1987); therefore, the details of MS/MS technique is explained in the following section.

2.2.1. Collision-Induced Dissociation (CID)

The primary structure of the protein is elucidated via collision-induced dissociation (CID) MS/MS experiments of peptide ions in the gas-phase (McLuckey 1992, Aebersold and Goodlett 2001). The CID-MS/MS technique was first introduced in 1968 for gaining structural information of molecules (Haddon and McLafferty 1968). In some cases, collisional-activated dissociation (CAD) is used instead of CID. In order to conduct CID-MS/MS experiments, the instrument requires at least two mass analyzers within the same instrument. The theory behind the method is to select the precursor peptide ion in the first analyzer followed by subjection to the reaction region (collision cell) for excitation. In the collision cell, several energetic and inelastic collisions occurred between the precursor peptide ion and chemically inert collision gases (like helium, argon, xenon, or nitrogen) (Vachet and Glish 1996) that triggers the dissociation (fragmentation) of the precursor ion. Briefly, a portion of the precursor ion's kinetic energy is converted into internal vibrational energy through repeated collisions, and the energy is well distributed among the all covalent bonds in picosecond (ps) time scale. The precursor peptide ion starts to vibrate at its resonant frequency. When the vibrational energy of the ions exceeds the activation barrier of bond cleavage, the bond eventually fragments prior to leaving the collision cell via unimolecular decomposition. The formed ions are called fragment ions or product ions. Finally, the fragment ions are scanned in the second analyzer and reach the detector (Hunt et al. 1986). The resultant mass spectrum is composed of several complex fragment ions and these ions are then used to derive the amino acid sequence of peptides, which is known as *de novo* sequencing. In some cases, multi-stage (sequential) tandem mass spectrometry (MS^n) is also employed for further elucidation of fragmentation pathways for peptide ions (Busch et al. 1988). The “*n*” represent how many times isolation/fragmentation cycle takes place. The activation time, collision energy, type of

collision gas and the number of the collisions are the important parameters which affect the CID of the precursor ion (Wells and McLuckey 2005).

The CID is categorized into two fragmentation-energy regimes, namely low-energy (Hunt et al. 1986) and high-energy (Biemann et al. 1990). Triple quadrupole and ion trap instruments are mainly operated under low-energy CID and the applied collision energy is in the 0-100 eV range. On the other hand, sector and TOF instruments use the order of keV collision energy in high-energy CID to induce fragmentation of gas-phase peptide ions. The time frames are on the order of a few hundred μ s to ms for former method and a few μ s for latter method, respectively. In low-energy CID, peptide backbone is mainly cleaved; however, the side chain cleavage is generally observed in the high-energy CID. Hence, the formed fragment ions significantly vary in each category. The detailed information for nomenclature of the peptide ions will be given in the section 2.3.2.

2.2.2. Other Ionization Techniques

CID is the most widely used technique to dissociate peptide ions for gaining its sequence information (Jennings 2000, Wells and McLuckey 2005) while other alternative ion activation modes are also reported in the literature, such as electron capture dissociation (ECD) (Zubarev et al. 1998 and Cooper et al. 2005), electron transfer dissociation (ETD) (Syka et al. 2004), surface-induced dissociation (SID) (Mabud et al. 1985, Williams et al. 1990, Dongré et al. 1996), infrared multiphoton dissociation (IRMPD) (Little et al. 1994). In ECD, the protonated (or multiply protonated) peptide/protein ion captures a thermal electron which induces peptide backbone to fragment at the N-C $_{\alpha}$ bond. This technique is widely used in top-down proteomic studies (Ge et al. 2002). ETD can be accomplished by using reagent gas radical anions (typically anthracene and fluoranthene) in the dissociation of protonated peptide ions. The combination of ECD/ETD and CID mass spectra provides complementary sequence information of peptides. Moreover, the SID allows the fragmentation upon energetic collision of peptide ions with a surface of metal plate under high vacuum conditions. Lastly, the IRMPD technique uses a tunable infrared laser at a particular frequency to induce fragmentation of peptide ions upon by absorption multiple photons.

In addition to these ion activation techniques, FT-ICR MS uses blackbody infrared radiative dissociation (BIRD) (Price et al. 1996 and Dunbar 2004), sustained off-resonance irradiation collision-induced dissociation (SORI-CID) (Gauthier et al. 1991 and Senko et al. 1994), on-resonance excitation CID (RE-CID) (Cody et al. 1982), electron detachment dissociation (EDD) (Budnik et al. 2001, Anusiewicz et al. 2005, and Kjeldsen et al. 2005), electron-induced dissociation (EID) (Cody and Freiser 1979, 1987) and UV photo-dissociation (Williams et al. 1990) for ion fragmentation.

In the subsequent sections, the fragmentation pathways of protonated peptides are described in detail upon low-energy CID conditions. Additionally, the gas-phase structures of fragment ions are also discussed.

2.3. Peptide Fragmentation Chemistry

MS/MS coupled to CID has become an invaluable technique in peptide sequencing and protein identification with the advent of soft-ionization techniques (Hunt et al. 1981, Tanaka et al. 1988, Karas and Hillenkamp 1988, Fenn et al. 1989, Medzihradszky 2005). Understanding the structures of fragment ions and their fragmentation mechanisms is especially important in the *de novo* sequencing of peptides/proteins (Aebersold and Goodlett 2001, Medzihradszky 2005). The knowledge of gas-phase fragmentation pathways of peptides is vital in the protein identification. With these facts in mind, it is important to know peptide fragmentation routes and the location of charge(s) in the peptide sequence.

2.3.1. Mobile Proton Model

Under low-energy CID conditions, the fragmentation of protonated peptides is explained by “*mobile proton model*” which was proposed in the early 1990s (Burlet et al. 1992, Tang et al. 1993, Dongré et al. 1996, Cox et al. 1996, Wysocki et al. 2000, Boyd and Somogyi 2000). Based on this model, the gaseous peptide sample easily captures a proton(s) from the gas-phase media during ionization process. Before the activation, the proton is initially located on the most basic sites within the peptide sequence. These sites are N-terminal of the peptide (α -amine group), side chains of basic amino acid residues, *e.g.* Lys (ϵ -amine group), His (imidazole ring), and Arg

(guanidino group), or amide carbonyl oxygen atoms (Rodriquez et al. 2001 and Wu and McMahon, 2007). During the course of collisional activation, the proton freely moves to the thermodynamically less stable sites of the peptide backbone (*e.g.* amide nitrogen). The protonation of amide nitrogen drives to weaken and cleavage of the CO-NH (amide) bond (Somogyi et al. 1994), which results in the formation of sequence-informative fragment ion series in the MS/MS spectra (Paizs and Suhai 2002). This fragmentation is called as a charge-directed pathway in which the mobile proton promotes the cleavage.

In contrast, a mobile proton can be sequestered if the number of protons does not exceed the number of arginine residues. The basic residues (His, Arg, and Lys) can hold the proton on their side chains and more energy is required for the mobilization of proton along the peptide backbone. These specific amino acid residues promote the fragmentation pathways, and it is called charge-remote fragmentation (Gross 1992). Therefore, the resultant mass spectrum can be more complex compared to the obtained one by charge-directed fragmentation and the more energy is required for this type of fragmentation. Moreover, residue-specific fragmentation pathways have been also documented for His, Pro and Asp containing peptides (Schwartz and Bursey 1992, Yu et al. 1993, Tsaprailis et al. 2000, Gu et al. 2000, Brechi et al. 2003, Tsaprailis et al. 2004, and Perkins et al. 2009). The combination of charge-directed and charge-remote pathways is used to describe the fragmentation of protonated peptides in the gas-phase.

The mobile proton model only explains the pre-dissociation event with proton transfer reactions; it does not consider the dissociation and post-dissociation processes. Recently, Paizs and Suhai (2005) proposed a “*pathways in competition*” (PIC) model which provides a detailed framework for explaining all these three events during the peptide fragmentation. The combination of mobile proton and PIC models greatly improves our current understanding of the peptide fragmentation routes.

2.3.2. Peptide Fragmentation Nomenclature

The nomenclature for fragment ions was initially proposed by Roepstorff & Fohlmann (1984) and then modified by Biemann (1988). Upon activation, the C_α-C, C-N, or N-C_α bonds can be cleaved. During these cleavages, if the charge is retained on the N-terminal, *a*-, *b*-, and *c*-ion series are formed. On the other hand *x*-, *y*-, and *z*-ion

series are generated when the charge is resided on the C-terminal of the peptide sequence and the nomenclature of peptide fragments is illustrated in Figure 2.2.

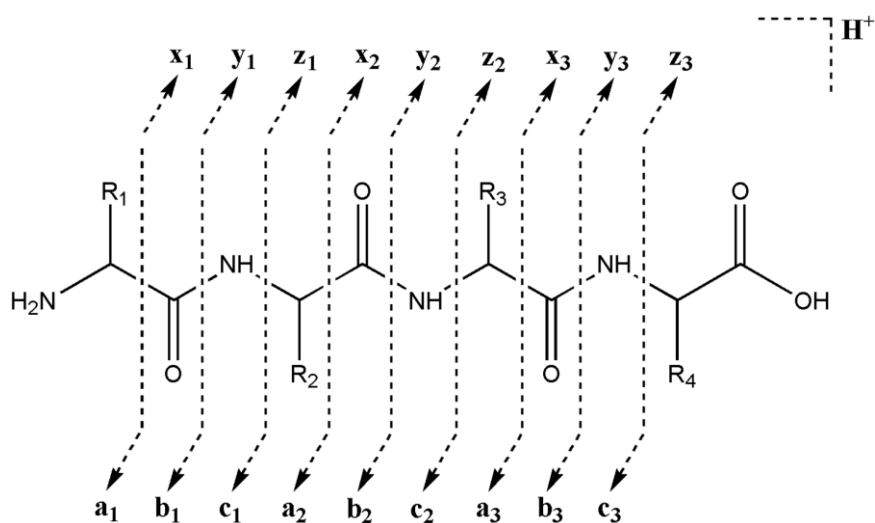


Figure 2.2. The nomenclature of peptide fragment ions

The subscript numbers are generally used to assign how many residues are present in the fragment, for instance the b_2 fragment indicates that it contains two amino acids in its structure. The a - x , b - y , and c - z ions are complementary ions and their formation entirely depends on their gas-phase proton affinities. The most commonly observed fragments are N-terminal b and a ions and/or C-terminal y ions via cleavage of protonated peptides at amide bonds (CO-NH) under low-energy CID (Harrison 2009). On the contrary, ECD and ETD techniques, which are operated under high-energy CID conditions, predominantly produce c and z fragment ions through the cleavage of N-C_α bond (Zubarev et al. 1998 and Cooper et al. 2005). Similarly, a and x fragment ions primarily detected in EDD via C_α-C bond cleavage (Budnik et al. 2001, Anusiewicz et al. 2005, and Kjeldsen et al. 2005).

It is apparent that the mass difference between consecutive fragments of b and/or y ions series provides the residue mass of intervening amino acid which can be used to deduce the peptide sequence. In ideal case, the series of b ions is used to determine the sequence from N-to C-terminal, while the y ion series sequenced the peptide from C-to N-terminal. Beside to b and y ions, the fragments formed by neutral loss of water (-18 Da) and/or ammonia (-17 Da) are also observed (Sun et al. 2008). These fragments are denoted with superscripts “ o ” and “ * ” in order to show water and

ammonia loss, respectively. Similarly, internal fragment ions (Ballard and Gaskell 1991) and immonium ions of amino acids (Ambihapathy et al. 1997) have been also detected in the MS/MS spectra. The immonium ions, which indicate the presence of certain amino acid residues in the peptide sequence, mainly appear in the low-mass region (< 180 Da) of the mass spectrum. However, it does not define the position of residues within the peptide sequence.

As an illustration, the mechanism for the formation of b_3 and y_2 ions derived from $[M + H]^+$ ion of hypothetical pentapeptide is shown in Figure 2.3. The b_n - y_m pathway leads the generation of N-terminal b ions and/or the C-terminal y ions. It has been well defined that y ions are protonated C-terminal amino acids (y_1) or protonated truncated peptides (y_n) (Mueller et al.1988 and Cordero et al.1993), and its structure is shown in Figure 2.3. The mass of y ions is calculated by adding residue masses of amino acids present in the fragment and mass of one hydrogen atom and water molecule. Similarly, the mass of b ion can be calculated by adding the residue masses of all amino acids present in the fragment and mass of one hydrogen atom.

In the last two decades, the structures, reactions, and thermochemistry of gas-phase b ions are under intense scrutiny; hence, the attention is focused to clarify the characteristic pathways of b ions in the CID mass spectra.

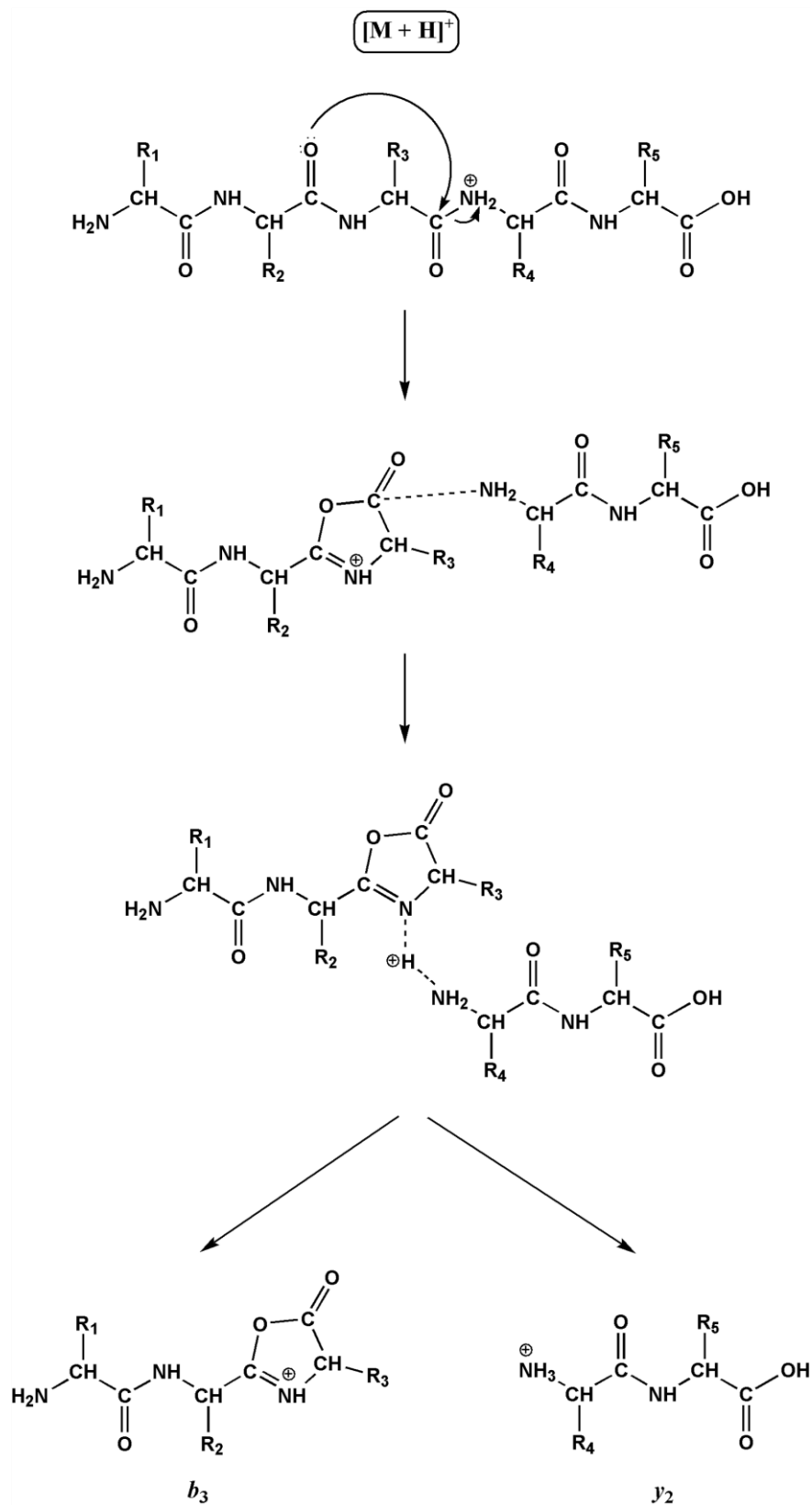


Figure 2.3. Proposed mechanism for the formation of *b*₃ and *y*₂ ions via *b*_{*n*}-*y*_{*m*} pathway

2.3.3. Formation and Structures of *b* Ions

In the numerous peptide fragmentation studies, the most of the interest has been devoted to the structure elucidation and fragmentation mechanism of *b* ions (Yalcin et al. 1995, Yalcin et al. 1996, Paizs et al. 1999, Polce et al. 2000, Paizs and Suhai 2005). It has been demonstrated that *b* ions may have four possible structures, namely an acylium, a diketopiperazine (six-membered ring), an oxazolone (five-membered ring), and a macrocyclic (Harrison 2009) and these four structures are displayed in Figure 2.4. This structural diversity is influenced by the amino acid composition in the peptide sequence, peptide N-terminal amino acid identity and the length of the peptide.

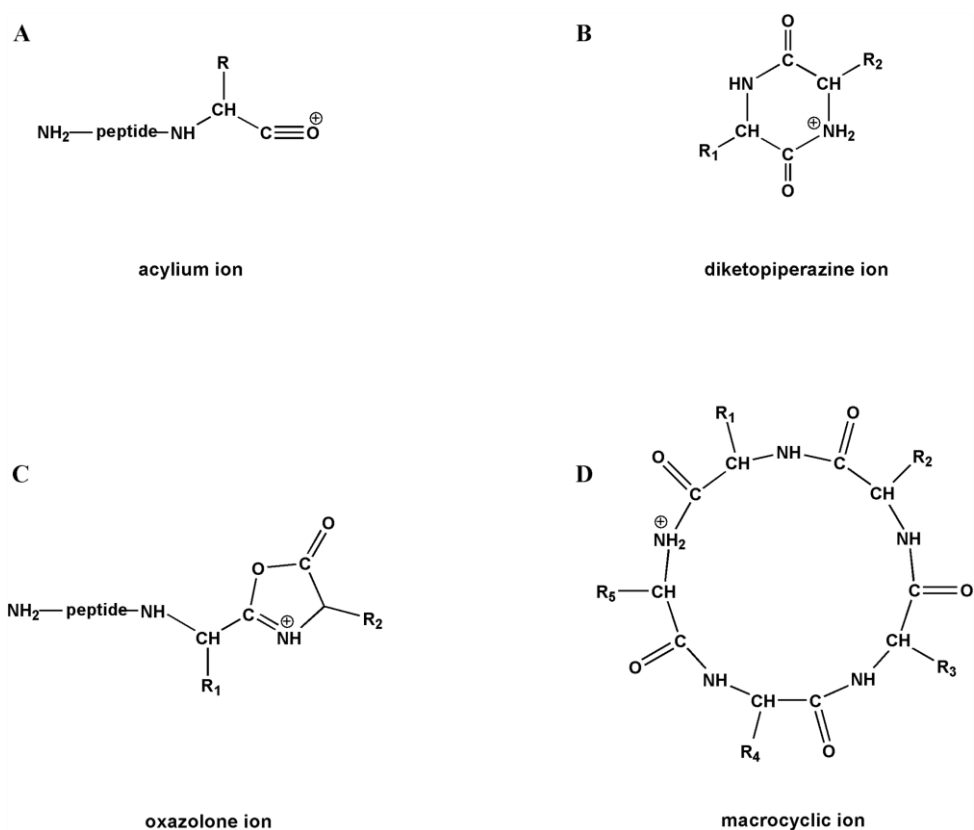


Figure 2.4. Possible structures for *b* ions

An acylium ion structure was proposed for *b* ions in early studies (Roepstorff and Fohlmann, 1984, Biemann 1988). It is known that the acylium ion is thermodynamically unstable species and easily loses CO exothermically to form stable immonium ion ($RCH=NH_2^+$). However, the abundances of *b* ions (except b_1) are dominant in peptide CID mass spectra. This behavior reveals that the structure of *b* ions

must be thermodynamically stable in the gas-phase. To explain this stability, Cordero et al. (1993) reported that the protonated five-membered ring structure might be formed for b ions. Subsequently, Arnott et al. (1994) presented a poster at the 42nd ASMS conference and demonstrated that the larger b ions also favored this cyclic structure in the gas-phase. In 1995, extensive studies (MS/MS experiments, kinetic energy release data, and *ab initio* calculations) by Yalcin et al. (1995, 1996) have shown that the five-membered oxazolone ring as the most stable structure for small b_n ($n = 2-4$) ions. As illustrated in Figure 2.3, the mechanism for the formation of oxazolone structure is initiated by proton migration to the amide nitrogen followed by a nucleophilic attack of the N-terminal neighbor amide oxygen to the next C-terminal carbonyl carbon of the protonated amide bond. The proton-bound dimer is formed and then dissociated to generate either b and/or y ions (by sharing mobile proton) based on their relative gas-phase proton affinities (basicity) (Paizs and Suhai 2004). It should be stated that b_n ions with an oxazolone structure generates its next-lower b_{n-1} ions during the fragmentation, and this fragmentation pathway is known as an “*oxazolone rule*”. That is the reason for observation of the cascade of b ions in the tandem mass spectra for protonated peptides (Yalcin et al. 1996, Harrison and Young 2004). Additionally, a ions are formed with a loss of CO (-28 Da) from its corresponding b ions via dissociation in the gas-phase (Yalcin et al. 1996, Ambihapathy et al. 1997).

As a third structure, a six-membered ring diketopiperazine structure may be formed by a nucleophilic attack at the carbonyl carbon of the protonated amide bond by the N-terminal nitrogen atom (Cordero et al. 1993). The formation of diketopiperazine structure requires a *trans-cis* isomerization which makes the pathway kinetically controlled (Paizs and Suhai, 2001). Many studies were conducted to examine the effects of amino acid identity (His and Pro) on the generation of thermodynamically stable b_2 diketopiperazine structure through the fragmentation of simple di- and tri-peptides (Farrugia et al. 2001, Smith et al. 2006, Gucinski et al. 2012 and 2013). Perkins et al. (2009) showed that the structure of b_2 ion originated from HA dipeptide as a mixture of both diketopiperazine and oxazolone by means of MSⁿ, theoretical calculations, IRMPD, and H/D exchange experiments. Moreover, the b_2 ions derived from lysine and arginine containing peptides may form a cyclic structure with the aid of their side chains, and the formed structure is more stable than oxazolone structure (Farrugia et al. 2001). However, aliphatic amino acid residues (Gly, Ala, etc.) still lead to form an oxazolone structure rather than a diketopiperazine or any other cyclic structures.

Recently, a macrocyclic *b* ion structure has been proposed as a fourth probable structure (Harrison et al. 2006, Bleiholder et al. 2008). In this case, the N-terminal amine group can attack to the carbonyl carbon of the N-protonated oxazolone ring which is located at the C-terminal of the peptide. The interconversion between oxazolone and macrocyclic structure is valid for b_5 or even larger *b* ions (b_6 , b_7 , and so on) (Bleiholder et al. 2008). Herein, it should be mentioned that an oxazolone structure must be formed firstly for the generation of macrocyclic structure. More detailed information about the formation of macrocyclic *b* ions is presented in the following section.

2.4. Literature Review

As emphasized above, *b* ions more likely adopt an oxazolone structure through the gas-phase fragmentation. Therefore, the oxazolone structure and its characteristic fragmentation pathways, which is required for high-throughput peptide/protein identification in proteomic studies, have been used to deduce the peptide sequence. In the last two decades, the oxazolone structure has been confirmed by many studies. The theoretical calculations and gas-phase H/D exchange studies have supported that the simple *b* ion has an oxazolone structure (Paizs et al. 1999, Rodriguez et al. 2000, Chen and Turecek 2005, Bythell et al. 2009, Bythell et al. 2009). Additionally, Polfer et al. (2005, 2007) have presented IRMPD experiments as well as density functional theory (DFT) calculations to support the oxazolone structure for b_4 ions originated from Leu-enkephalin model peptide (YGGFL). Through IRMPD studies, the stretching modes for diagnostic carbonyl group of the oxazolone ring structure is expected to appear in the high-frequency region (1770-1950 cm^{-1}) of the spectrum.

In early low-energy CID studies, it was pointed out that the fragment ions correspond to the internal amino acid losses might be formed due to the intra-molecular rearrangement reactions in trap instruments (Vachet et al. 1997, Yagüe et al. 2003). Upon complex rearrangement, these ions might complicate the interpretation of CID mass spectra. In order to explain the internal amino acid losses, the formation of protonated macrocyclic structure is proposed for larger b_n ($n = 5, 6, 7 \dots$) ions (Harrison et al. 2006, Bleiholder et al. 2008). In the mechanistic point of view, macrocyclic structure is formed by the attack of free N-terminal amine group on the charged

C-terminal oxazolone ring. This reaction is called as “*head-to-tail cyclization*” or “*macrocyclization*”. The mechanism for the formation of macrocyclic b_5 ion is illustrated in Figure 2.5 by using hypothetical pentapeptide ($R_1R_2R_3R_4R_5\text{-oxa}$). The superscript “*oxa*” is used to define that the peptide has an oxazolone structure at the C-terminal end.

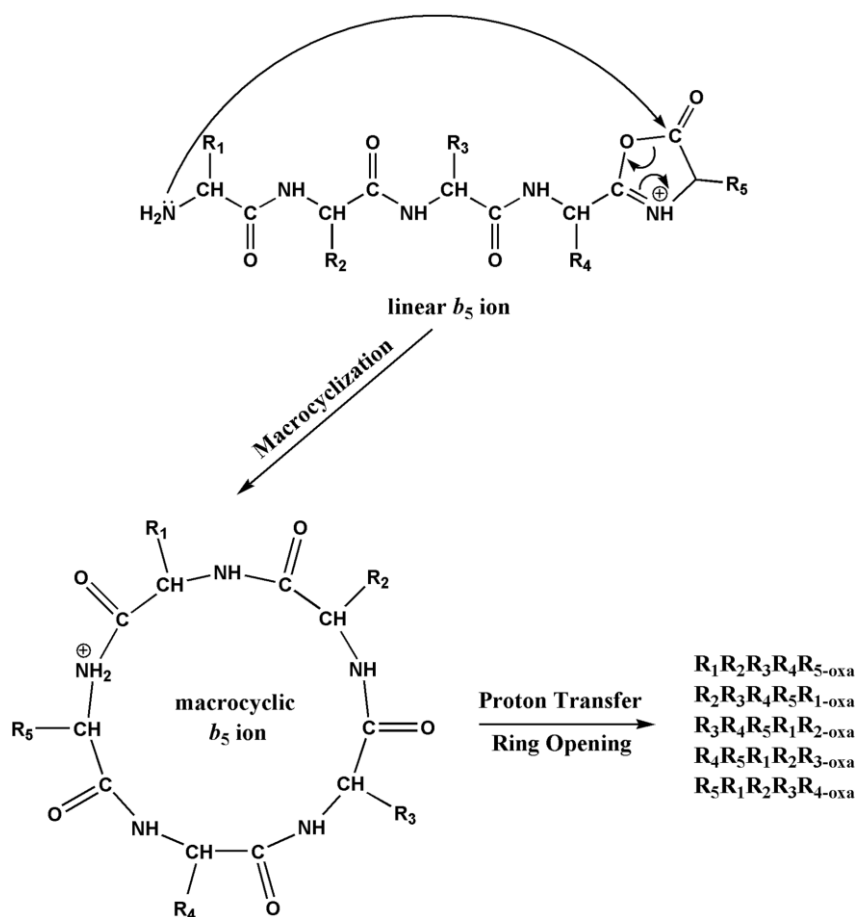


Figure 2.5. Proposed mechanism for the formation of macrocyclic b_5 ion

This macrocyclic structure subsequently undergoes several ring opening pathways at different amide bonds due to the mobile proton and forms various isomeric linear C-terminal oxazolones. This fragmentation model is referred as *b*-type sequence scrambling (Bleiholder et al. 2008). Consequently, the original primary sequence of peptide is scrambled and generates non-direct sequence fragment ions (internal amino acid losses) in MS/MS spectra. For that reason, the resultant CID mass spectra of peptides have become more complex with the presence of direct and non-direct sequence ions together.

To put the explanation in a more simple way, for instance, the elimination of the third amino acid residue, R_3 , is not expected from the original peptide sequence ($R_1R_2R_3R_4R_{5-oxa}$) if the conventional oxazolone rule is considered. However; in the CID mass spectrum, the fragment ion corresponds to the elimination of R_3 from b_5 ion of the original peptide sequence is observed. This behavior is only explained by fully cyclization/reopening process of b_5 ion of original peptide sequence to form $R_4R_5R_1R_1R_{3-oxa}$ isomer in the gas-phase. In this case, the R_3 residue is re-located at the C-terminal of the newly formed isomer and then it follows the loss of last amino acid from its C-terminal (oxazolone rule).

Several methods have been shown to confirm and to support the macrocyclic b ion structure. These methods are IRMPD spectroscopy, DFT calculations, and ion mobility-mass spectrometry (IM-MS) (Polfer et al. 2008, Riba-Garcia et al. 2008, Erlekam et al. 2009). On the other hand, the free N-terminal amine group is required for the formation of the macrocyclic b ion structure, as Figure 2.5 displays (Harrison et al. 2006). To support the proposed mechanism, the N-terminal of the peptide is acetylated and the CID mass spectrum of the b ion is recorded. It has been shown that head-to-tail cyclization reaction is completely blocked by N-terminal acetylation (Yagüe et al. 2003, Jia et al. 2007, and Harrison 2008).

There are two main criteria to decide whether the b ions undergo macrocyclization or not: (1) internal amino acid residues eliminations from b ion and (2) the similarity of non-direct sequence ion abundances originated from permuted peptide b isomers. A more detailed explanation was reported by Bleiholder et al. (2008) using C-terminal amidated pentapeptide sequence, YAGFL-NH₂. The CID mass spectrum of b_5 ion derived from this peptide contains non-direct sequence ions (loss of Y, A, G, and F amino acid residues from b_5 ion) in addition to regular direct sequence ions (b_4 , a_4 , b_3 , etc). Additionally, the b_5 ions obtained from permuted isomeric peptides, namely AGFLY-NH₂, GFLYA-NH₂, FLYAG-NH₂, and LYAGF-NH₂, completely show the identical mass spectra even though these peptides are formally different from each other. The authors also confirmed the formation of macrocyclic structure by comparison of MS/MS spectrum of cyclo-(YAGFL) with the b_5 ions of the mentioned isomeric pentapeptides (Bleiholder et al. 2008).

2.5. Overview of the Thesis

In this dissertation, the structures, reactivities, and formation mechanisms of gas-phase peptide *b* ions have been investigated in detail under low-energy CID conditions in quadrupole and ion-trap mass spectrometer instruments.

Chapter 3 presents a systematic study which examines the effects of acidic amino acid residues (glutamic or aspartic acid) and the position of the acidic groups on the macrocyclization of *b* ions. Additionally, the preferential cleavage of glutamic or aspartic acid residues from macrocyclic *b* structures is also examined under various collision energy conditions by constructing breakdown graphs.

Chapter 4 discusses the effects of amine group (-NH₂) located on the side chains of lysine (K), glutamine (Q), or asparagine (N) residue on the macrocyclization of *b* ions even though the N-terminals of the model peptides are acetylated. In addition, the positional effect of the lysine residue in the N-terminal acetylated peptides is also examined for the *b*-type sequence scrambling chemistry.

Chapter 5 demonstrates the fragmentation reactions of *b_n* (*n* = 4-7) ions derived from side chain acetylated lysine residue containing model peptides. Novel rearranged fragment ions are observed in the side-chain acetylated mass spectra compared to the N-terminal acetylated one, and these novel formed ions can be accepted as diagnostic ions for lysine acetylation.

In chapter 6, the C-terminal protonated dipeptide losses are reported in the dissociation of the *b₅* and *b₄* ions of pentapeptides containing side chain hydroxyl group (-OH) residues. These residues are located at the first or second position counting from N-terminal position.

CHAPTER 3

A SYSTEMATIC STUDY OF ACIDIC PEPTIDES FOR *b*-TYPE SEQUENCE SCRAMBLING¹

3.1. Introduction

As discussed in chapter 2, the macrocyclization reaction generates non-direct sequence ions which may lead to uncertainty in the interpretation of CID mass spectra of unknown peptides (Bleholder et al. 2008). Therefore, *b*-type sequence scrambling chemistry needs to be clarified. Several studies have been carried out up to date to understand the factors affecting the scrambling chemistry upon CID and these factors are listed below.

The influence of varying the size of peptides on *b*-type sequence scrambling was studied (Molesworth et al. 2009). It was reported that the macrocyclization reaction is still occurred for larger peptides, such as hepta-, octa-, and nonapeptides. Later, a detailed study on the macrocyclization of peptide *b*₉ ions was published by Harrison (2009). The author documented that the product ion mass spectra of *b*₉ ions derived from YA₉, A₄YA₅, and A₈YA (where Y is tyrosine and A is alanine residue) are almost identical which is direct evidence of macrocyclization reaction and sequence scrambling of *b*₉ ion before fragmentation.

On the other hand, the effects of the nucleophilic side chain of amino acid residues, e.g. glutamic acid (E), aspartic acid (D), glutamine (Q), asparagine (N), and lysine (K), on the selective opening of macrocyclic *b*₅ ion of the YAXFLG peptides were investigated (Molesworth et al. 2010). Additionally, potential influence of the arginine residue (R) on macrocyclic *b* ion formation from singly charged protonated model peptides of YARFLG and its permuted sequence isomers were also reported (Molesworth and Van Stipdonk 2010). The authors highlighted that macrocyclization reaction is inhibited by the presence of arginine residue.

¹ A part of this chapter is published as: Atik, A. E. and Yalcin, T. "A Systematic Study of Acidic Peptides for *b*-Type Sequence Scrambling" *J. Am. Soc. Mass Spectrom.* **2011**, 22, 38-48.

Recently, effects of the histidine (H) residue on the macrocyclization of *b* ions were studied using HA₅, AHA₄, A₂HA₃, A₃HA₂, A₄HA (where A is alanine residue) model hexapeptides both experimentally and theoretically (Bythell et al. 2010). It was reported that if the H residue is close to the N-terminal position, no clear evidence for macrocyclization is observed; even though theoretical calculations supported that this processes are energetically allowed. However, when the H residue gets closer to the C-terminal position, the formation of non-direct sequence ions has become more evident due to the scrambling chemistry. It was concluded that the position of the H residue is important for the macrocyclization of *b*₅ ions, at least when these model hexapeptides series have been used.

On the other hand, Saminathan et al. (2010) reported that the presence of non-direct sequence ions in the MS/MS spectra does not affect peptide and protein identifications via Mascot search. Similarly, Goloborodko et al. (2011) also documented that the rate of *b*-type macrocyclization is negligible (< 1 %) in shotgun proteomics.

Except the works related with arginine and histidine on the macrocyclization reaction, most of the studies were conducted with neutral amino acid containing peptides, like C-terminal amidated YAGFL-NH₂ peptide sequence motif and its permuted isomers (Bleiholder et al. 2008). There is no detail study on acidic amino acid (either glutamic or aspartic acid) containing peptides to explain their potential effects on sequence scrambling chemistry.

In the current work, a systematic study was carried out to examine the effects of acidic amino acid residues- glutamic acid (E) or aspartic acid (D)- on the macrocyclization of *b* ions. In addition, the effects of the positions of the acidic residues in the model peptide were studied. The study utilized three sets of model peptides. The first set is composed of six alanine residues and one glutamic or aspartic acid residue (heptapeptides), where the position of the acidic residue is varied. The second set is comprised of six alanine residues with two adjacent glutamic or aspartic acid residues (octapeptides), where the position of the acidic amino acid is changed. The third set has a YAGFLV-NH₂ peptide sequence motif where the acidic amino acid was placed before tyrosine (N-terminal), between glycine and phenylalanine, or after valine residues (C-terminal). All hepta- or octapeptides were designed as C-terminal amides rather than free acids in order to get highly abundant *b*₇ or *b*₈ ion signal, respectively.

3.2. Experimental

The C-terminal amidated synthetic model hepta- and octapeptides, namely XAAAAAA-NH₂, AXAAAAA-NH₂, AAXAAAA-NH₂, AAAXAAA-NH₂, AAAAXAA-NH₂, AAAAAXA-NH₂, AAAAAAX-NH₂, XYAGFLV-NH₂, YAGXFLV-NH₂, YAGFLVX-NH₂, XXAAAAAA-NH₂, AAXXAAAA-NH₂, AAAAXXAA-NH₂, and AAAAAAXX-NH₂ where X is a glutamic acid (E) or aspartic acid (D) residue, were purchased from GL Biochem Ltd. (Shanghai, China) and used as received. A 1-2 mg of each solid peptide was dissolved in 1:1 (v/v) mixture of HPLC-grade MeOH and deionized H₂O to make stock solutions with a concentration of 10⁻³ or 10⁻⁴ M.

Two different mass spectrometer systems were used throughout the experiments. An LTQ XL linear ion-trap mass spectrometer (Thermo Finnigan, San Jose, CA, USA) equipped with an ESI source was used for acquiring the product ion mass spectra of *b* ions. Before each experiment, the instrument was calibrated with the company's calibration mixture (Calmix: caffeine, MRFA, and Ultramark). The experimental settings (multipole, lens voltages, etc.) were optimized for maximum [M + H]⁺ signal with the LTQ Tune software. The spray voltage was + 5.0 kV and the N₂ sheath gas flow rate was 10 (arbitrary units). The capillary temperature was maintained at 275 °C and the capillary voltage at 21 V. Helium was used as the collision gas for CID and as a bath/buffer gas to improve trapping efficiency. A 100 μM peptide solution was prepared in 50:50:1 (v/v/v) MeOH/H₂O/HCOOH and introduced into the ion source with an incorporated syringe pump at a flow rate of 5 μL min⁻¹. The CID conditions for peptide fragmentations were as follows. Normalized collision energy was set at between 19-23 % with an activation (*q*) of 0.250, and an activation time of 30 ms was applied at each CID stage. The isolation width (*m/z*) for precursor ions was set at between 1.2 and 1.8 for both MS² and MS³ acquisitions, and at least 500 scans were averaged, with a scan rate of 1 employed.

For the breakdown graphs, a hybrid triple quadrupole/linear ion trap instrument (4000 QTRAP, Applied Biosystems/MDS Sciex, Concord, Canada) equipped with a turbo ion spray source was used. Model peptide solutions at a concentration of 10 μM were introduced into the system with an infusion pump at a flow rate of 5 μL min⁻¹. N₂ gas was used as nebulizer, curtain, and collision gases during the experiments. The ion

spray voltage was set at + 5.5 kV. In Q1 scan mode, the appropriate declustering potential is chosen for best precursor ion selection with highest intensity. Then, MS/MS data for $[M + H]^+$ were acquired in enhanced product ion (EPI) scan mode. The collision energy was varied from 18 to 36 eV in increments of 2 eV, and at least 40 cycles were averaged, with a scan rate of 1000 Da/s employed.

3.3. Results and Discussion

3.3.1. Effect of *b*-Type Sequence Scrambling on $[M + H]^+$ Product Ion Mass Spectra

The formation of non-direct sequence ions as a consequence of macrocyclization reaction is mainly pronounced in the MS/MS spectra of b_5 or even larger *b* ions. In addition to the contributions to *b* ions, we aimed to explore the effects of sequence scrambling chemistry on the product ion mass spectra of $[M + H]^+$ ions derived from model peptides. We selected alanine (A) residue as a spacer amino acid residue in the designing of the model peptide sequences due to having an inert side chain group ($-\text{CH}_3$). The MS/MS spectrum of $[M + H]^+$ ion derived from EAAAAAA-NH₂ is shown in Figure 3.1.

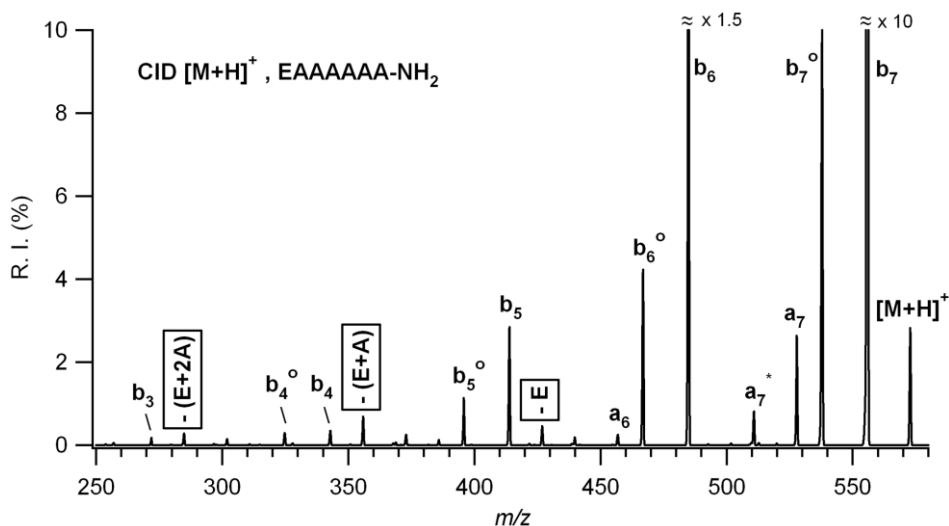


Figure 3.1. Product ion mass spectrum of $[M + H]^+$ derived from EAAAAAA-NH₂

It is clear to see that MS/MS spectrum consist of both direct and non-direct sequence ions during low-energy CID. The direct sequence ions, namely b_7 (m/z 556), $b_7 - \text{H}_2\text{O}$ (b_7° , m/z 538), a_7 (m/z 528), a_7^* (m/z 511), b_6 (m/z 485), b_6° (m/z 467), b_5 (m/z 414), and b_5° (m/z 396) greatly dominate the mass spectrum while the intensities of non-direct sequence ions (shown in box), e.g. $b_7 - \text{E}$ (m/z 427), $b_7 - (\text{E} + \text{A})$ (m/z 356), and $b_7 - (\text{E} + 2\text{A})$ (m/z 285), are below 1 %. It is obvious that non-direct sequence ions do not complicate the mass spectrum of $[\text{M} + \text{H}]^+$ ions, at least for this type of model peptide sequence. We observed the similar fragmentation behavior for other model hepta- and octapeptides series (mass spectra are not shown for simplification).

In order to support these findings, the breakdown graphs have been constructed separately for each model peptide. Breakdown graphs evaluate the relationship between the relative intensities of direct/non-direct sequence ions with the applied collision energy. In theory, the breakdown graph is generated by acquiring the tandem mass spectra of certain ion at different collision energy conditions. Afterwards, the percent ion intensity is calculated by dividing the interested ion's intensity to the total ion intensities at specified collision energy. The evaluation of breakdown graphs provides an information on fragmentation pathways of peptides, such as to determine the stability of the product ions over different collision energy regime, to identify the first/second generation product ions, and to distinguish between competitive/consecutive fragmentation routes.

The comparison of the breakdown graphs for $[\text{M} + \text{H}]^+$ ions originated from EAAAAAA-NH₂ and DAAAAAA-NH₂ is shown in Figure 3.2 (only sequence and non-sequence ions are shown). The collision energy was varied from 18 eV to 36 eV. In a general view, the fragmentation profile for glutamic and aspartic acid containing heptapeptides were similar in terms of direct and non-direct sequence ions under low-energy CID condition. As collision energy increased, the percent intensities of b_7 ions were drastically decreased for two peptide series (upper panels). Additionally, the percent ion intensities of b_6 , b_5 , and b_4 ions were increased as the collision energy increased up to certain eV value, after which it decreased. However, the percent intensity of b_3 ion was increased as the collision energy reaches to 36 eV (middle panels). On the other hand, the percent non-direct sequence ion intensities that belong to the loss of X, (X + A), and (X + 2A) from b_7 ions were increased up to certain eV value, and then decreased; while the percent intensities of $b_7 - (\text{X} + 3\text{A})$ and $b_7 - (\text{X} + 4\text{A})$ (where X is either E or D) fragments were increased as the collision energy increased

(last panels). It is clear to see that the percent intensities of non-direct sequence ions are less (max 3 %) compared to the intensities of direct sequence ions (max 6 %). Hence, it can be concluded that the scrambled b ions do not complicate the $[M + H]^+$ ion mass spectrum very much upon low-energy CID conditions. For simplification, the comparison of other breakdown graphs of $[M + H]^+$ ions obtained from AAAXAAA-NH₂ and AAAAAAX-NH₂ (where X is either E or D) is shown in Appendix A.

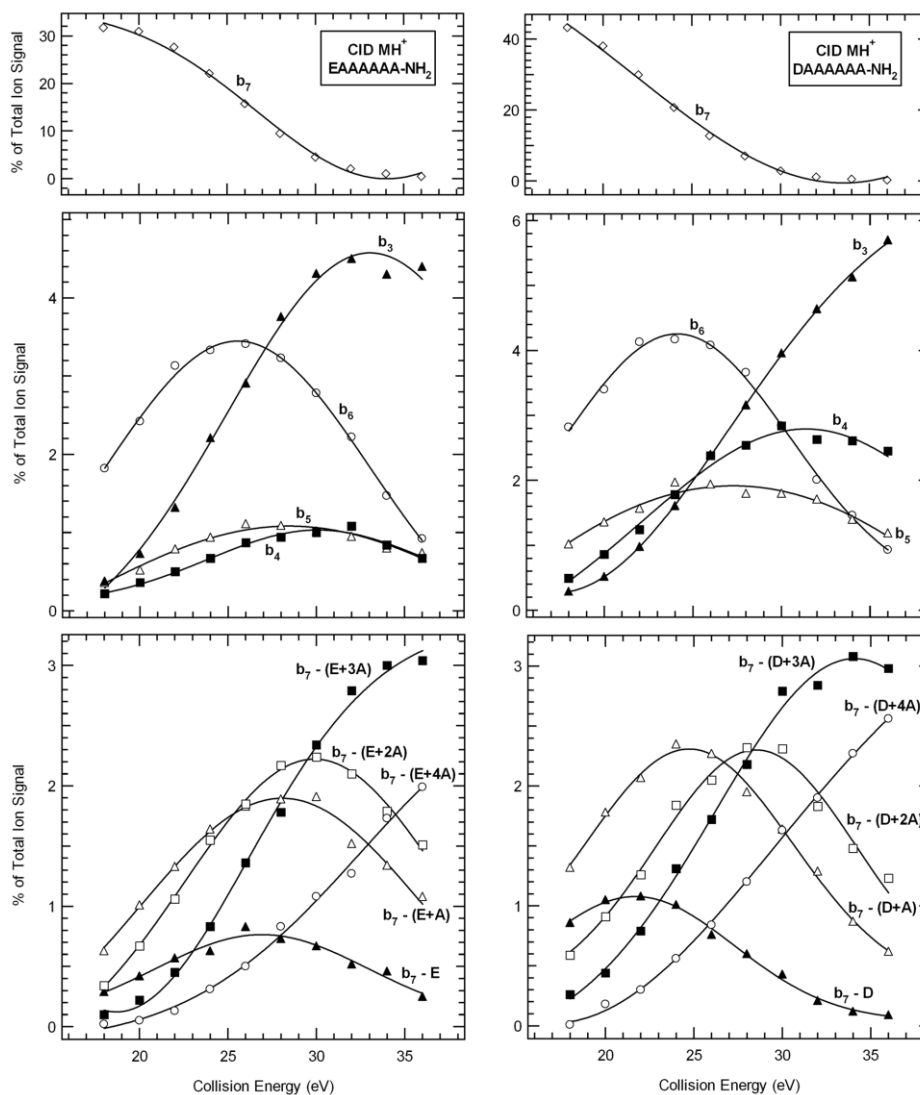


Figure 3.2. Comparison of $[M + H]^+$ ion breakdown graphs of EAAAAAA-NH₂ and DAAAAAA-NH₂

On the other hand, the comparison of breakdown graphs for $[M + H]^+$ ions originated from EEAAAAAA-NH₂ and DDAAAAAA-NH₂ octapeptides is illustrated

in Figure 3.3 (only direct and non-direct sequence ions are shown). It is obvious that nearly identical fragmentation patterns were observed for direct sequence ions at low-energy CID. By contrast, the fragmentation profiles of non-direct sequence ions were completely different from each other. Moreover, the percent intensities of non-direct sequence ions are approximately 2 %, while the relative intensities of direct sequence ions are around 6 %. For that reason, the non-direct sequence ions do not complicate the $[M + H]^+$ ion tandem mass spectrum. For simplification, the comparisons of other breakdown graphs of $[M + H]^+$ ions obtained from AAXXAAAA-NH₂, AAAAXXAA-NH₂, and AAAAAAXX-NH₂ (where X is either E or D) are shown in Appendix A.

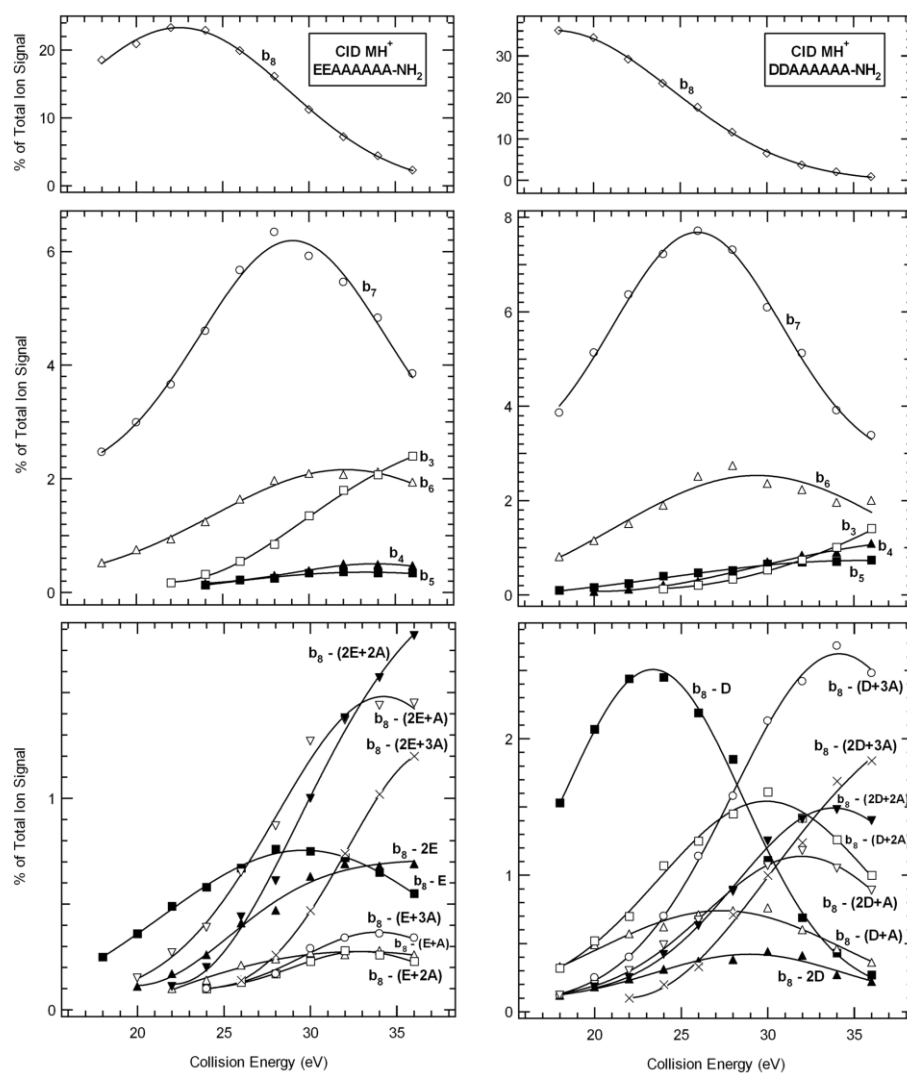


Figure 3.3. Comparison of $[M + H]^+$ ion breakdown graphs of EEA and DDA peptide sequences.

3.3.2. *b*-Type Sequence Scrambling of Glutamic or Aspartic Acid Containing Heptapeptides

3.3.2.1. Alanine Series

The product ion mass spectra of b_7 ions derived from seven isomeric heptapeptides containing glutamic acid residue at various positions are entirely identical and these CID mass spectra are illustrated in Appendix A. For simplification, the CID mass spectra of b_7 ions generated from EAAAAAA-NH₂, AAAEAAA-NH₂, and AAAAAAE-NH₂ are shown in Figure 3.4. The dominant fragment ion is water loss from b_7 ion which is denoted as b_7° (m/z 538) in the CID mass spectra.

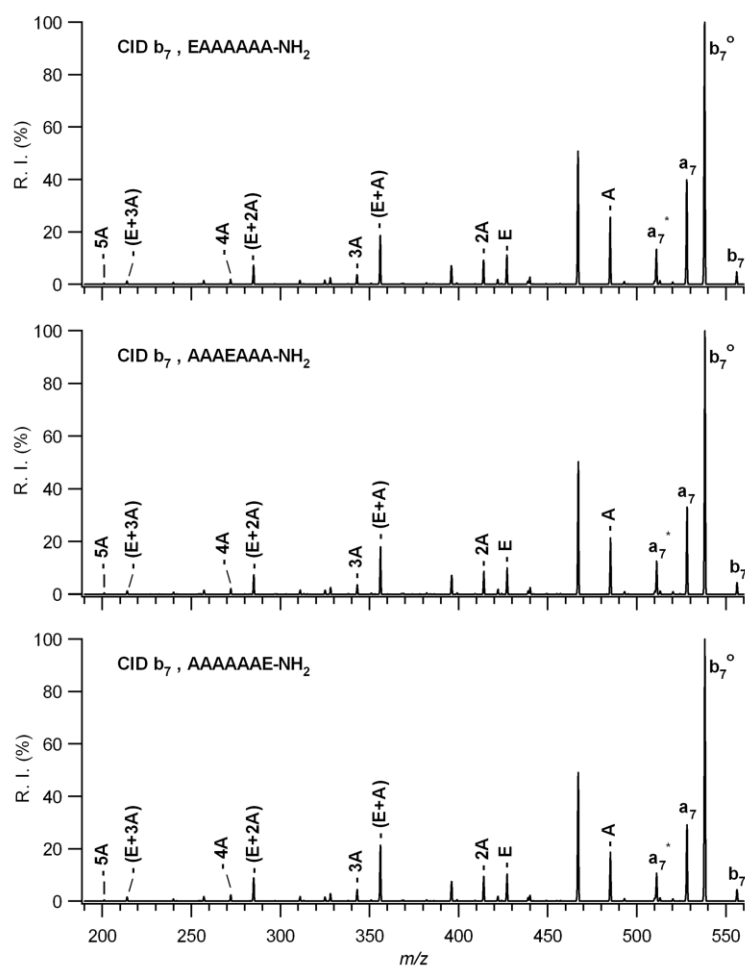


Figure 3.4. Comparison of the CID mass spectra of b_7 ions of EAAAAAA-NH₂, AAAEAAA-NH₂, and AAAAAAE-NH₂

The relative intensity of glutamic acid elimination ($-E$, m/z 427) from the b_7 ion is approximately 10 %. Moreover, the elimination intensities of CO (a_7 , m/z 528), CO + NH₃ (a_7^* , m/z 511), A (m/z 485), 2A (m/z 414), E (m/z 427), E + A (m/z 356), and E + 2A (m/z 285) are significant while the peaks corresponding to the elimination of 3A (m/z 343), 4A (m/z 272), 5A (m/z 201), and E + 3A (m/z 214) have minor intensities in b_7 ion mass spectra. Additionally, A + H₂O (m/z 467) and 2A + H₂O (m/z 396) fragments are also detected in the CID mass spectra.

Similarly, the CID mass spectra of the b_7 ions obtained from DAAAAAA-NH₂, AAADAAA-NH₂, and AAAAAAD-NH₂ are identical, as illustrated in Figure 3.5 (all seven b_7 ion CID mass spectra are illustrated in Appendix A). Again, the b_7° fragment ion (m/z 524) is the most abundant peak in the CID mass spectra of b_7 . In addition, the relative intensity of aspartic acid elimination ($-D$, m/z 427) from b_7 ions is about 35 %.

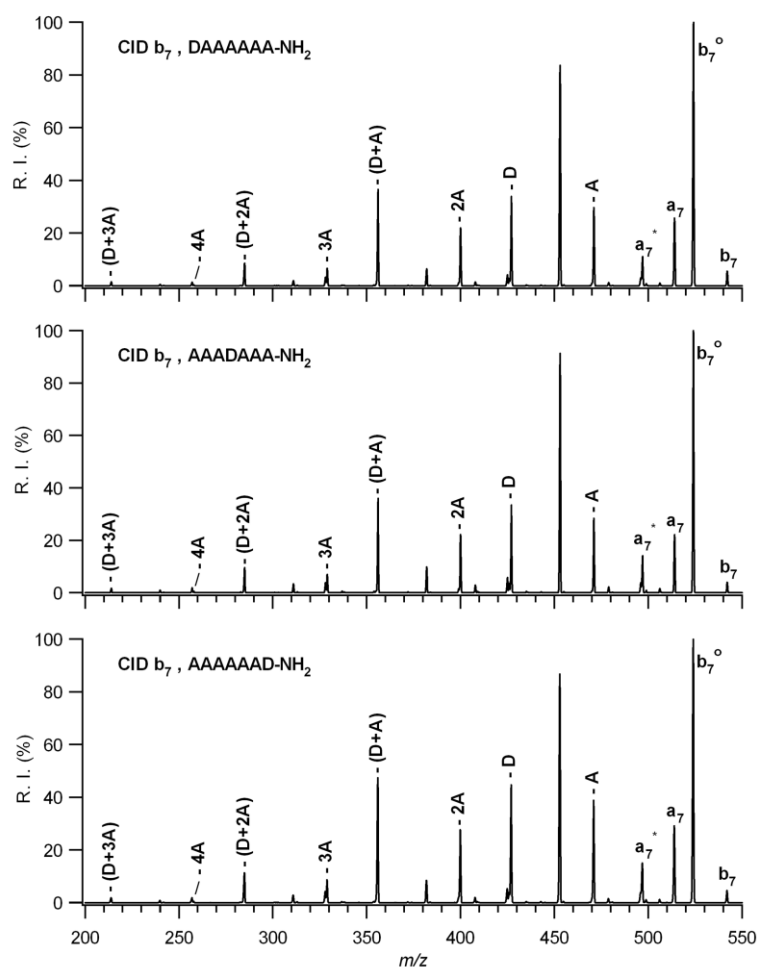


Figure 3.5. Comparison of the CID mass spectra of b_7 ions of DAAAAAA-NH₂, AAADAAA-NH₂, and AAAAAAD-NH₂

Moreover, the elimination intensities of CO (a_7 , m/z 514), CO + NH₃ (a_7^* , m/z 497), A (m/z 471), 2A (m/z 400), D (m/z 427), D + A (m/z 356) and D + 2A (m/z 285) are major whereas the peaks corresponding to the elimination of 3A (m/z 329), 4A (m/z 258), and D + 3A (m/z 214) have minor intensities in b_7 ion CID mass spectra. Moreover, A + H₂O (m/z 453), 2A + H₂O (m/z 382), and 3A + H₂O (m/z 311) fragments also contributed the mass spectra.

The dominant fragment ion is water loss from b_7 ions due to the presence of hydroxyl group (–OH) on the side chains of both glutamic and aspartic acid residues. Detailed studies of water loss from the backbones of protonated peptides have been reported previously by several groups (Ballard and Gaskell 1993, Reid et al. 1999). Surprisingly, the second most intense fragment ion is the loss of one alanine residue and water (A + H₂O) in the MS/MS spectra of b_7 ions for both glutamic and aspartic acid containing model heptapeptides. For instance, the loss of A + H₂O from b_7 ion leads to the generation of m/z 467 fragment ion for EAAAAAA-NH₂. In order to investigate the source of this fragment ion, precursor ion scan analysis was performed using Q-TRAP mass spectrometer. The precursor ion mass spectrum is shown in Figure 3.6.

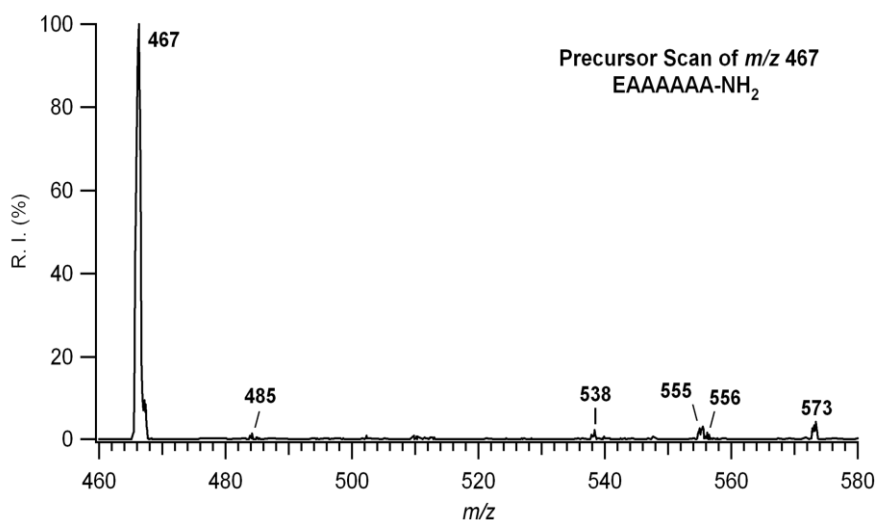


Figure 3.6. Precursor ion mass spectra of the m/z 467 ion from EAAAAAA-NH₂

The precursor ion mass spectrum revealed that there are five possible sources for the formation of m/z 467 ion: it may come directly from $[M + H]^+$ (m/z 573), and/or from b_7 (m/z 556), and/or from $[M + H]^+ - H_2O$ (m/z 555), and/or from b_7° (m/z 538), and/or from $b_7 - A$ (m/z 485). These five pathways are illustrated in Figure 3.7.

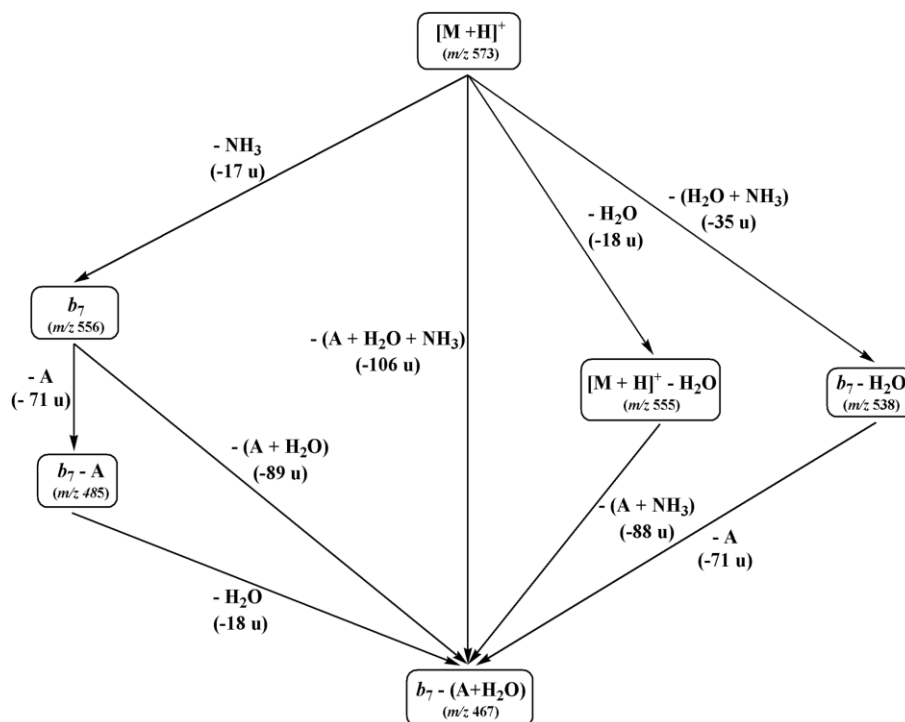


Figure 3.7. Sources of the elimination of $A + H_2O$ from the b_7 ion of EAAAAAA-NH₂

It is apparent from Figure 3.4 and 3.5 that non-direct sequence ions are observed in each b_7 ion's mass spectrum as a result of the sequence scrambling of b ions under applied experimental conditions in the ion trap mass spectrometer. In addition to b_7 , the b_6 ions obtained from XAAAAAA-NH₂, AXAAAAA-NH₂, AAXAAAA-NH₂, AAAXAAA-NH₂, AAAAXAA-NH₂, and AAAAAXA-NH₂ heptapeptides (where X is either E or D) exhibit nearly identical MS/MS spectra (see Appendix A). Hence, we can conclude that the side chains of either glutamic or aspartic acid residue do not prevent the macrocyclization of b ions.

3.3.2.2. YAGFLV Series

The CID mass spectra of b_7 ions of EYAGFLV-NH₂, YAGEFLV-NH₂, and YAGFLVE-NH₂ are shown in Figure 3.8a. For the purpose of comparison, only non-direct sequence ions (internal amino acid losses) are labeled. It is obvious that the product ion mass spectra of b_7 ions where the glutamic acid is located at the first and the last position of the peptide sequence are essentially identical. On the contrary, the CID mass spectra b_7 ion derived from YAGEFLV-NH₂ showed different relative intensities

for internal amino acid losses compared to the other two heptapeptides. The similar fragmentation behavior is observed for aspartic acid containing heptapeptides (DYAGFLV-NH₂, YAGDFLV-NH₂, and YAGFLVD-NH₂, see Figure 3.8b).

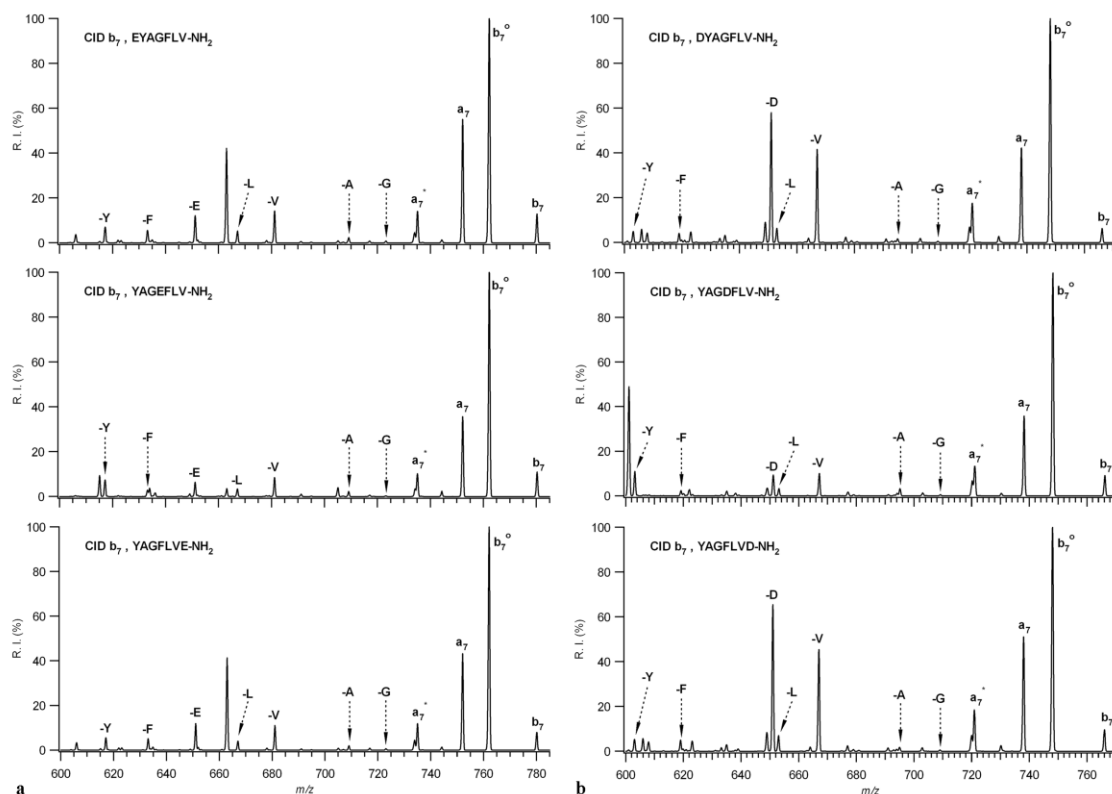


Figure 3.8. Comparison of the CID mass spectra of b_7 ions of (a) EYAGFLV-NH₂, YAGEFLV-NH₂, and YAGFLVE-NH₂, (b) DYAGFLV-NH₂, YAGDFLV-NH₂, and YAGFLVD-NH₂

In XYAGFLV-NH₂ and YAGFLVX-NH₂ (where X is either E or D) peptides, the acidic residues put itself at the C-terminal position after macrocyclization and re-opening process. Thus, we observed completely the same CID mass spectra for their b_7 ions. However, this cyclization/re-opening pathway is not valid for YAGEFLV-NH₂ and YAGDFLV-NH₂. This aspect can be explained by neighboring effects of amino acids of acidic residues in macrocyclization/re-opening reaction of b_7 ions.

In order to evaluate the dependence of non-direct sequence ions over different applied collision energy, the breakdown graphs are constructed for b_7 ions of each heptapeptides (see Figure 3.9). The breakdown graphs reveal that the preferential cleavage profiles of non-direct sequence ions are nearly the same for glutamic acid containing heptapeptides, as illustrated in the left panel of Figure 3.9.

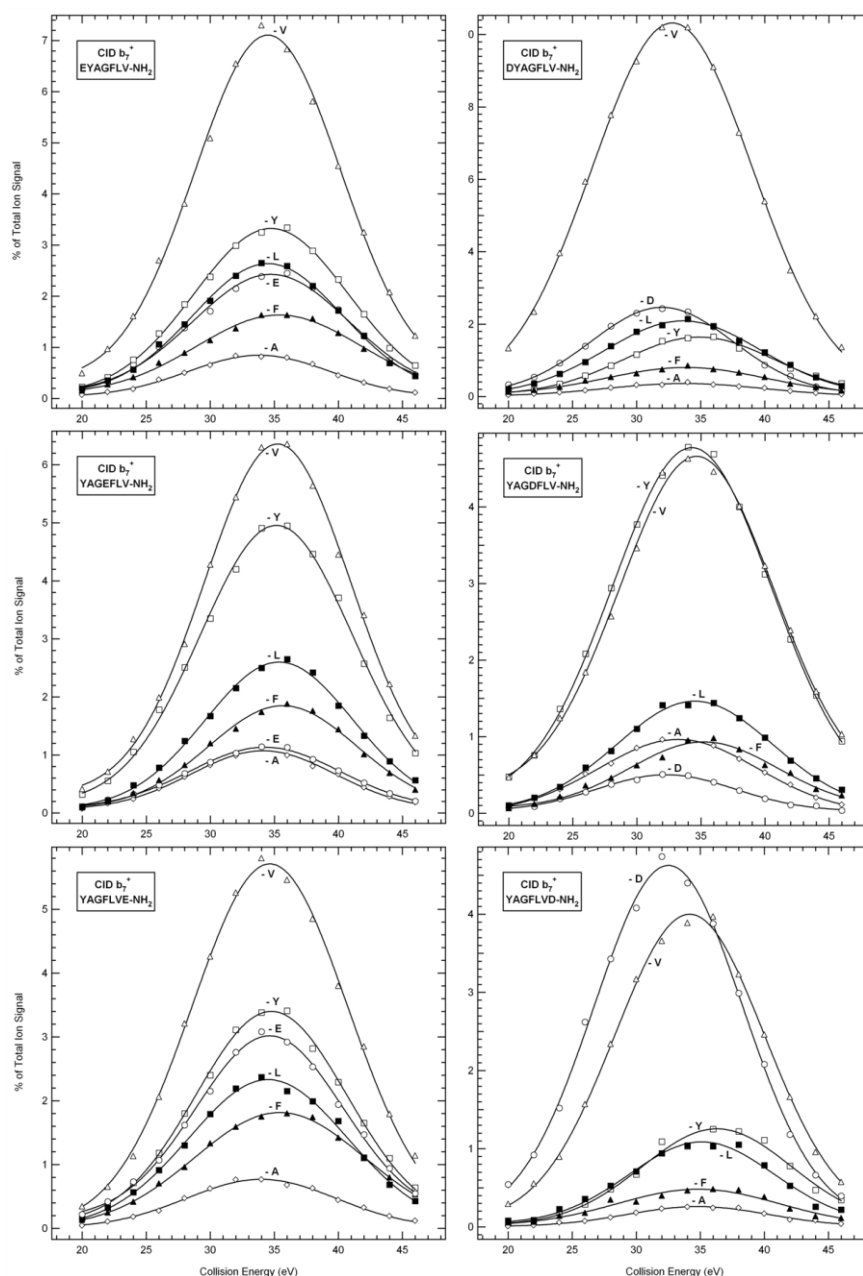


Figure 3.9. Comparison of b_7 ion breakdown graphs of EYAGFLV-NH₂, YAGEFLV-NH₂, YAGFLVE-NH₂, DYAGFLV-NH₂, YAGDFLV-NH₂, and YAGFLVD-NH₂

On the other hand, the valine loss (-V) greatly dominates the breakdown graph of DYAGFLV-NH₂. For YAGDFLV-NH₂, the preferential cleavages of tyrosine (-Y) and valine (-V) have essentially the same percent ion intensities (~ 5 %), while the preferential cleavage of aspartic acid (-D) is dominant for YAGFLVD-NH₂ peptide sequence (right panel of Figure 3.9).

3.3.3. *b*-Type Sequence Scrambling Two Adjacent Glutamic or Aspartic Acid Containing Octapeptides

The second set contained six alanine residues with two adjacent glutamic or aspartic acid residues, and eight model peptides were designed on this basis, namely XXAAAAAA-NH₂, AAXXAAAA-NH₂, AAAAXXAA-NH₂, and AAAAAAXX-NH₂ (where X is either E or D), in order to examine the effects of the presence of two adjacent acidic residues on *b*-type sequence scrambling. The CID mass spectra of the *b*₈ ions originating from octapeptides with two glutamic acid residues are nearly identical, as shown in Figure 3.10.

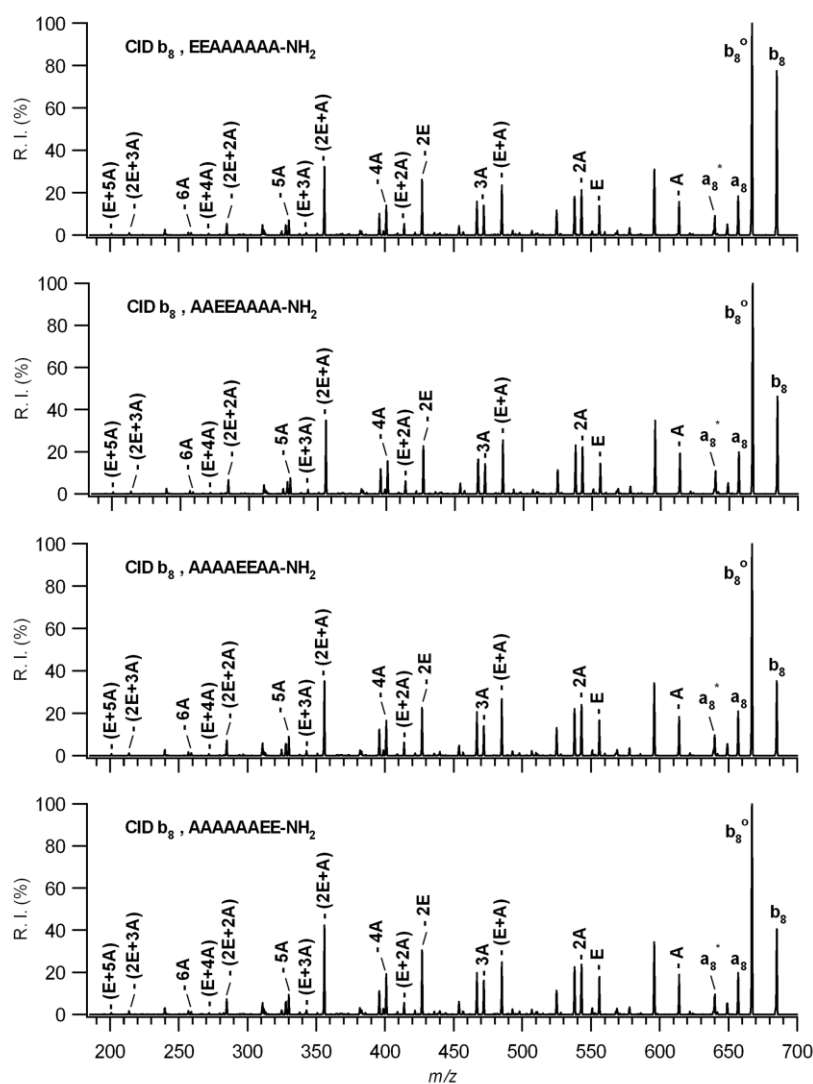


Figure 3.10. Comparison of the CID mass spectra of *b*₈ ions of EEAAAAAA-NH₂, AAEAAAAA-NH₂, AAAAEEAA-NH₂, and AAAAAAEE-NH₂

The strongest peak is water loss from b_8 ion (b_8° , m/z 667) in the CID spectra. In addition, the relative intensity arising from the elimination of one glutamic acid residue is nearly 18 %. The elimination intensities of two glutamic acid residues are all nearly 22 % in the CID spectra of the b_8 ions for the first three octapeptides, while this intensity is higher (30 %) for AAAAAAEE-NH₂. Moreover, major elimination intensities belong to CO (a_8 , m/z 657), A (m/z 614), 2A (m/z 543), 3A (m/z 472), 4A (m/z 401), E (m/z 556), 2E (m/z 427), E + A (m/z 485), and 2E + A (m/z 356). The peaks corresponding to the elimination of CO + NH₃ (a_8^* , m/z 640), 5A (m/z 330), 6A (m/z 259), E + 2A (m/z 414), E + 3A (m/z 343), E + 4A (m/z 272), E + 5A (m/z 201), 2E + 2A (m/z 285), and 2E + 3A (m/z 214) have minor intensity in b_8 ion CID mass spectra. The A + H₂O (m/z 596), 2A + H₂O (m/z 525), 3A + H₂O (m/z 454), 4A + H₂O (m/z 383), E + H₂O (m/z 538), E + A + H₂O (m/z 467), and E + 2A + H₂O (m/z 396) fragments are also detected with different relative intensities in the CID mass spectra of b_8 ions.

In the same vein, the CID mass spectra of the b_8 ions obtained from octapeptides with two adjacent aspartic acid residues are nearly identical, as depicted in Figure 3.11. In the b_8 product ion mass spectra for the first three octapeptides, the intensity arising from the elimination of two aspartic acid residues is about 32 %, but it is nearly 52 % for the octapeptide AAAAAADD-NH₂. Additionally, the intensities corresponding to the loss of one aspartic acid residue are nearly 45 % in the b_8 ion CID mass spectra. Again, the loss of water from b_8 ion (b_8° , m/z 639) yields the strongest fragment peak in its CID mass spectrum.

The elimination intensities of A (m/z 586), 2A (m/z 515), 3A (m/z 444), D (m/z 542), 2D (m/z 427), D + A (m/z 471), D + 2A (m/z 400), and 2D + A (m/z 356) are significant whereas the peaks corresponding to the elimination of CO (a_8 , m/z 629), CO + NH₃ (a_8^* , m/z 612), 4A (m/z 373), 5A (m/z 302), D + 3A (m/z 329), D + 4A (m/z 258), 2D + 2A (m/z 285), and 2D + 3A (m/z 214) have minor intensity in b_8 ion CID mass spectra. Furthermore, A + H₂O (m/z 568), 2A + H₂O (m/z 497), 3A + H₂O (m/z 426), 4A + H₂O (m/z 355), D + H₂O (m/z 524), D + A + H₂O (m/z 453), D + 2A + H₂O (m/z 382), and D + 3A + H₂O (m/z 311) fragment ions are also observed.

In the present study, due to the existence of glutamic or aspartic acid residues in model peptides, we proposed the water elimination from the side chains of these acidic residues. As an illustration, the fragmentation mechanisms of b_8 ion (AAEEAAAA_{oxa}) of AAEEAAAA-NH₂ octapeptide are outlined in Figure 3.12 and 3.13.

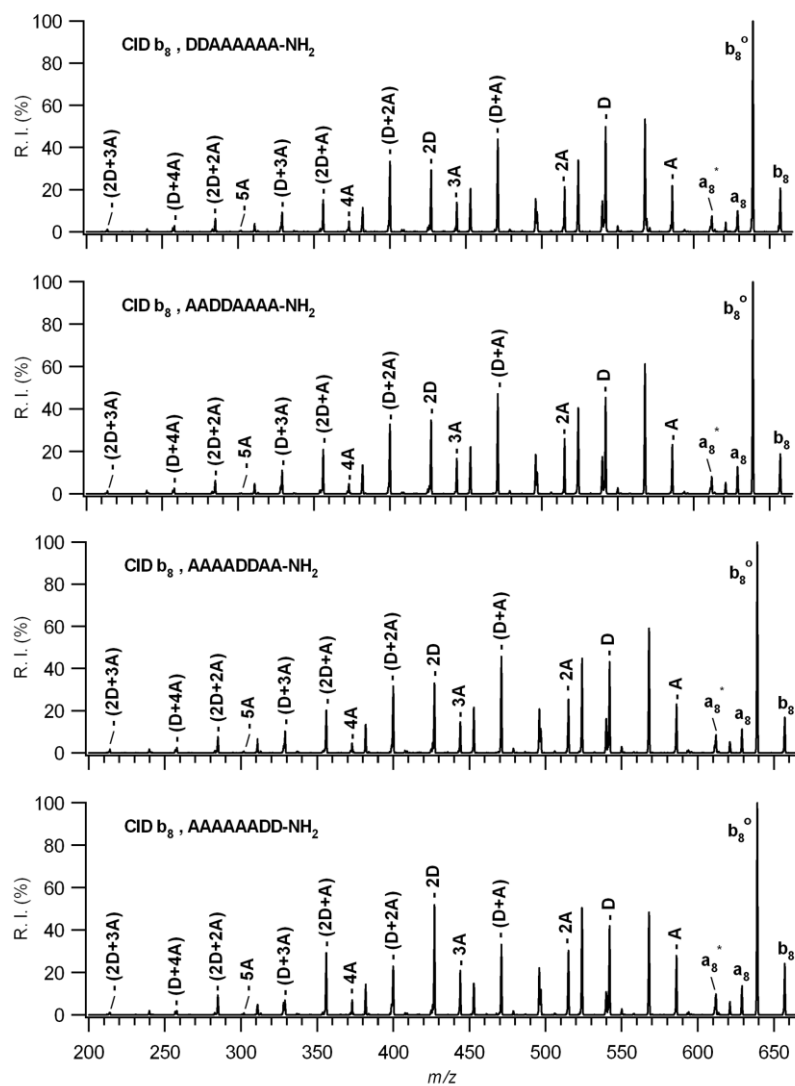


Figure 3.11. Comparison of the CID mass spectra for b_8 ions of DDAAAAA-NH₂, AADDAAAA-NH₂, AAAADDAA-NH₂, and AAAAAADD-NH₂

Briefly, the b_8 ion may follow two paths: either the elimination of water from a side chain of glutamic acid residue via path 1 (Figure 3.12), or the formation of a macrocyclic b_8 ion via path 2 (Figure 3.13). In path 1, after proton transfer (P.T.) from the oxazolone ring to the amide nitrogen of the first glutamic acid residue, water elimination can occur with the formation of an internal five-membered pyroglutamic ring, as depicted in Figure 3.12. A second water elimination can also occur through the formation of either a second internal five-membered (pyroglutamic) ring or a six-membered ring.

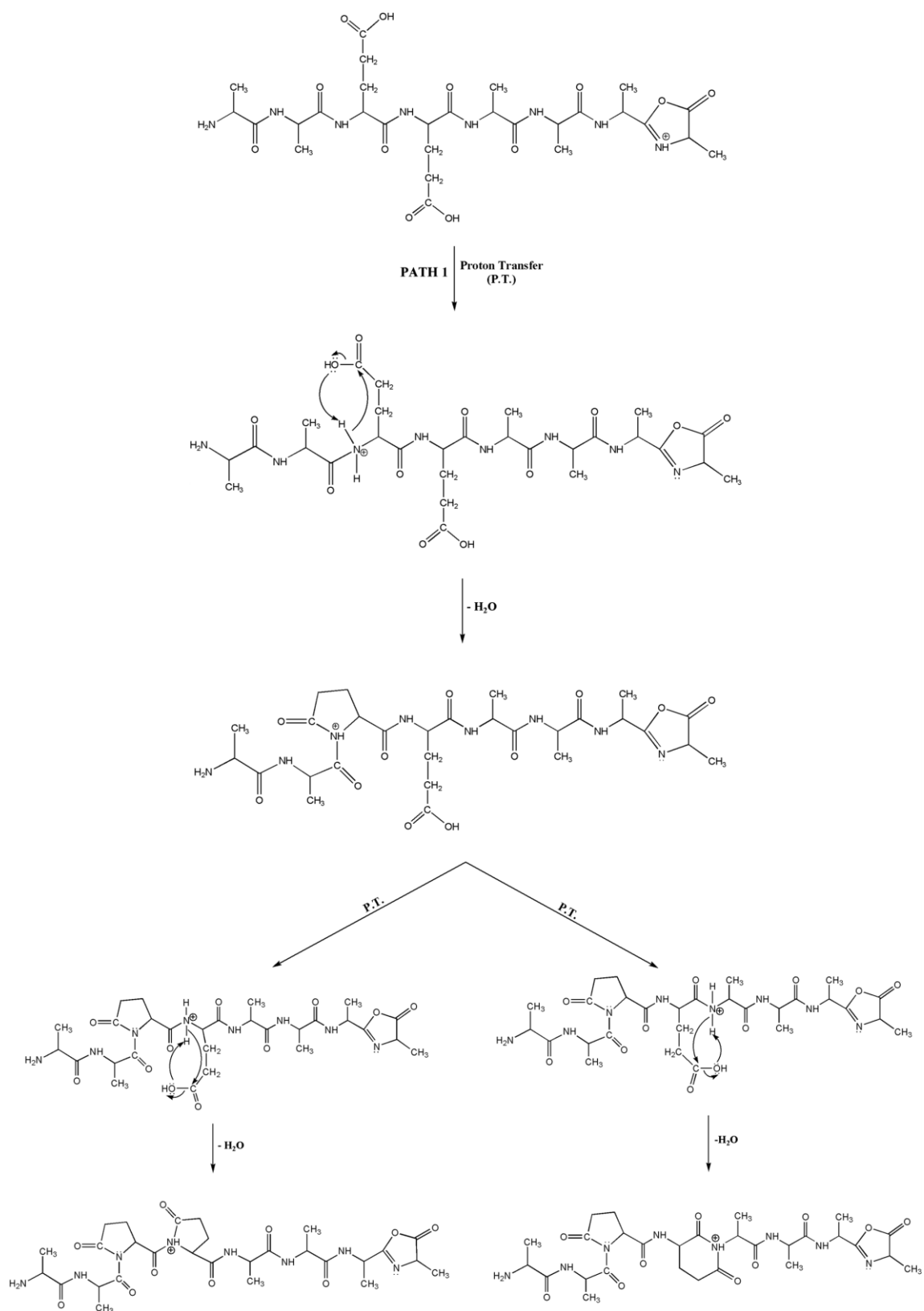


Figure 3.12. Proposed mechanisms for the elimination of water molecules from the side chains of glutamic acid residues

Consequently, these results clearly indicate that *b* ions produced from adjacent acidic residues containing model octapeptides can also undergo head-to-tail cyclization, which is the reason for the formation of the non-direct sequence ions in their CID mass spectra.

3.3.4. Effect of Acidic Residue Position in the Peptide on the Macrocyclization of b_n ($n = 7$ or 8) Ions

The potential effect of acidic, basic, or amide side chains on the formation of macrocyclic b_5 ion was studied using YAXFLG model hexapeptides series where X represents E, D, K, Q, or N residue (Molesworth et al. 2010). In their study, the authors considered only a single acidic residue (glutamic or aspartic acid), located at the third position in the peptide. However, in our study, we not only show the macrocyclization of *b* ions produced from acidic peptides, but we also investigate the dependence of macrocyclization on the position(s) of the acidic residue(s) in isomeric hepta- and octapeptides. The positions of the acidic residues in the peptides could affect the scrambling chemistry of *b* ions, in line with recent work by Bythell et al. (2010) on the effect of the histidine (H) residue on the macrocyclization. In that paper, it was shown that there is less evidence for the macrocyclization of b_5 ions derived from HA₅ and AHA₄ in their CID mass spectra; however, the formation of non-direct sequence ions is more evident due to the scrambling chemistry when the H residue is close to the C-terminus. This is why the macrocyclization cannot be generalized based on the investigation of one peptide containing a single acidic residue at the third position. In the present study, we investigated the effects of the presence of single and adjacent acidic residues in the model peptide isomers in detail. It was shown that identical CID mass spectra were obtained for hepta- and octapeptides containing single glutamic or aspartic acid residue(s) and multiple alanine residues (see Figure 3.4, 3.5, 3.10 and 3.11). Hence, it can be concluded that the macrocyclization of *b* ions does not depend on the position(s) of the acidic residue(s) in the hepta- or octapeptide series, at least for alanine containing model peptide series.

However, the scrambling chemistry of b_7 ions may change when YAGFLV model peptide series has been used. It has been clearly demonstrated that (see Figure 3.9) the macrocyclization and re-opening pathways depends on the neighboring amino

acids of the acidic residue. We can conclude that the amino acid diversity greatly affects the extent of macrocyclization of b_7 ions.

3.3.5. Collision Energy Dependence of the Preferential Cleavage of Glutamic or Aspartic Acid Residue(s) from the b_n Macrocylic Structure

Molesworth et al. (2010) reported that the selective opening of b_5 macrocyclic ions derived from the peptide YAXFLG (where X is E, D, K, Q, or N) follows the trend: $Q > K > D > N \sim E$. The authors demonstrated that aspartic acid loss is more pronounced than the glutamic acid loss from b_5 macrocyclic ion. In the current work, the preferential cleavage of glutamic or aspartic acid residue(s) from the macrocyclic structures of b_n ions ($n = 7$ or 8) is studied in order to evaluate its dependence on collision energy. The preferential cleavage of acidic residues from macrocyclic b_7 ions is shown in the left panel of Figure 3.14 (only glutamic or aspartic acid loss was considered for the purposes of comparison).

It is apparent that aspartic acid cleavage from the macrocyclic b_7 ions is favored under low-energy CID conditions rather than glutamic acid residue cleavage. However, when the collision energy is increased from 18 to 25 eV, the preferential cleavage of glutamic acid becomes more favorable than aspartic acid residue loss in the heptapeptide series. In addition, preferential aspartic acid cleavage started to decrease sharply above 20 eV, while the preferential cleavage of the glutamic acid residue also started to decrease after 25 eV.

Similarly, the preferential cleavages of acidic residue(s) from macrocyclic b_8 ions are shown in Figure 3.14 (right panel). The preferential cleavage of one aspartic acid residue from the b_8 ion decreased dramatically as the collision energy increased. However, the preferential cleavage of glutamic acid increased as the collision energy increased up to 26 eV, after which it decreased. The preferential loss of two adjacent glutamic acid residues has nearly the same profile as the preferential loss of two adjacent aspartic acid residues up to 26 eV; both show small increases in their intensities up to 26 eV. Above 26 eV, the intensity of the selective loss of two glutamic acid residues adopts a steady-state profile, while the preferential cleavage of two aspartic acid residues decreases. Based on the results discussed above, preferential

acidic residue cleavage definitely depends on the collision energy, and the order of residue cleavage preference can be changed.

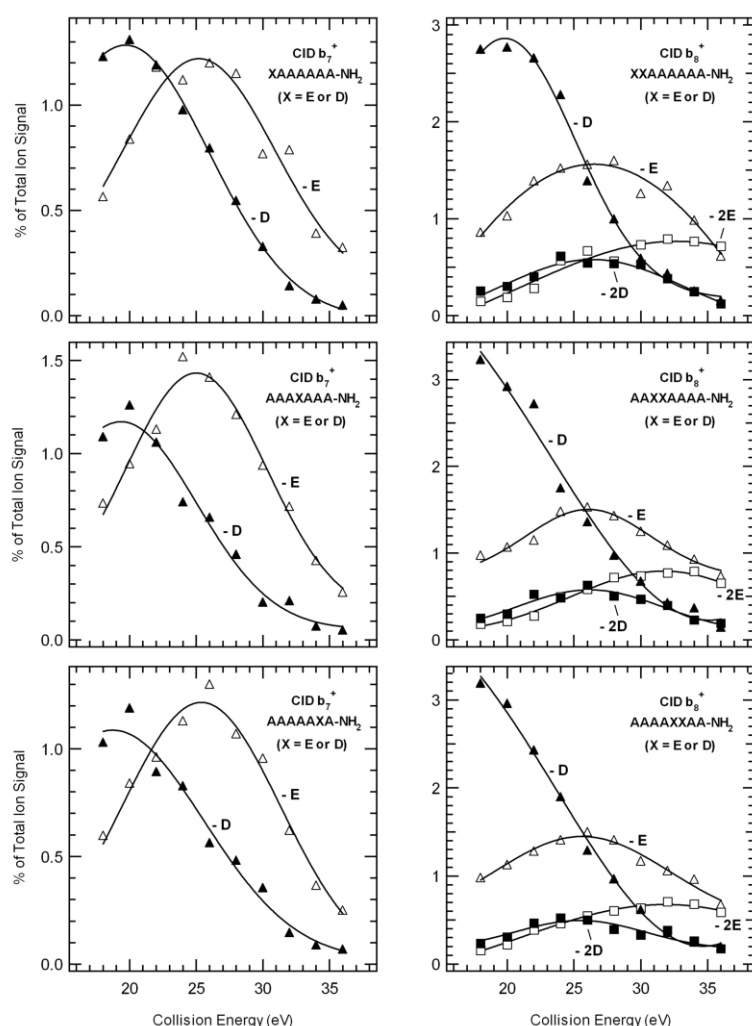


Figure 3.14. Comparison of the preferential cleavages of acidic residue(s) from macrocyclic b_7 or b_8 ions

3.3.6. Effect of Amino Acid Composition for Preferential Cleavage of Acidic Residue

The effect of amino acid composition on the preferential cleavage of glutamic or aspartic acid residue from macrocyclic b_7 ions was also explored using alanine and YAGFLV series. The study utilized the C-terminal amidated model heptapeptides XAAAAAA-NH₂, AAAXAAA-NH₂, AAAAAAX-NH₂, XYAGFLV-NH₂, YAGXFLV-NH₂, and YAGFLVX-NH₂ where X is either E or D. For the purpose of

comparison, we constructed breakdown graphs for each peptide separately (Figure 3.15).

The preferential loss of glutamic acid residue has the same profile for alanine series. Briefly, it is increased as the collision energy increased up to 25 eV, after which it decreased. Similarly, the preferential cleavage profiles are nearly same for aspartic acid and six alanine containing peptides. It is increased up to 20 eV which then decreased sharply. On the contrary, the preferential glutamic acid cleavage from YAGFLV series is favored at high collision energies (35eV) compared to the alanine series. In a similar fashion, preferential aspartic acid cleavage is favored in which the collision energy is increased up to 32 eV. Both two profiles began to decrease dramatically after they reach their maximum percent relative intensities. These results clearly show that preferential cleavage of acidic residue entirely depends on the identity of neighbor amino acids of them. In addition, the side chains of neighboring amino acid clearly affect the preferential cleavages of acidic residues.

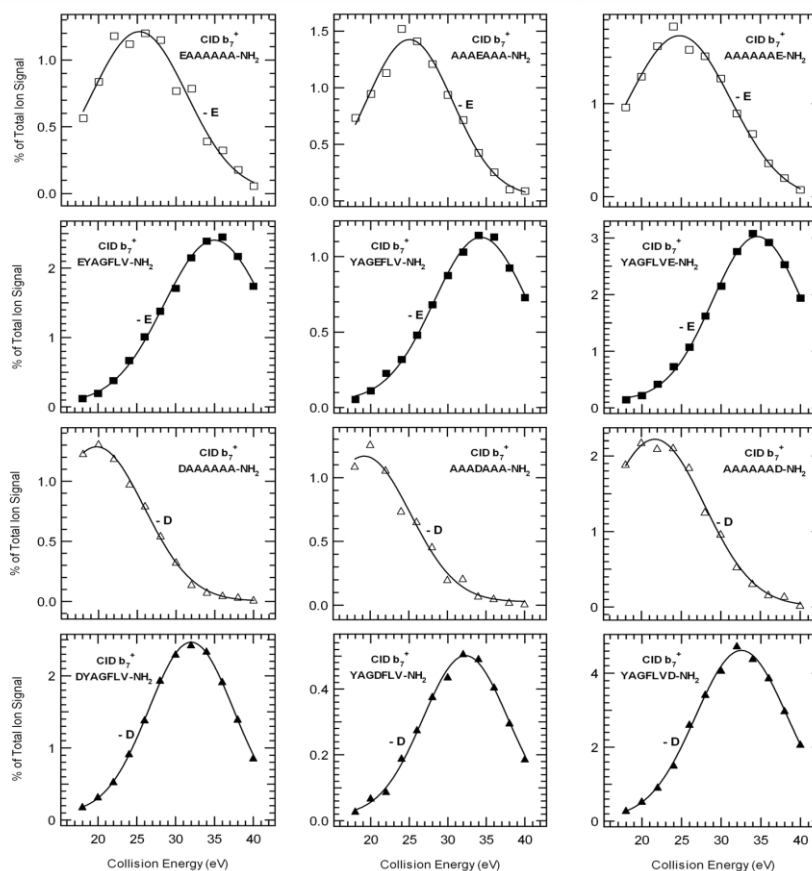


Figure 3.15. Comparison of the preferential cleavages of glutamic or aspartic acid from macrocyclic b_7 ions of alanine and YAGFLV series

CHAPTER 4

THE ROLE OF LYSINE ϵ -AMINE GROUP ON THE MACROCYCLIZATION OF *b* IONS ¹

4.1. Introduction

A detailed study on the effects of acidic amino acids (either glutamic or aspartic acid) as well as the position of the acidic group on the macrocyclization of b_7 and b_8 ions has been reported in the previous chapter. We showed that the side chain of acidic residue(s) did not prevent the sequence scrambling of *b* ions for model hepta- and octapeptides in alanine series. In addition, the dependence of preferential cleavage of acidic residue(s) on the applied collision energy was explored by plotting and evaluating breakdown graphs in model peptides (Atik and Yalcin 2011).

The macrocyclization of *b* ion is initiated by a nucleophilic attack of the free N-terminal amine (α -amine) group of the peptide on the carbonyl carbon of the C-terminal linear oxazolone structure (Harrison et al. 2006, Bleiholder et al. 2008). It was clearly shown that the macrocyclization reaction is completely blocked by acetylation of the N-terminal of peptide (Yagüe et al. 2003, Jia et al. 2007, Harrison 2009).

In early studies, it was documented that some lysine and ornithyl side chains may trigger the formation of a cyclic structure (Tang et al. 1993, Tang and Boyd 1994). In the same vein, Yalcin and Harrison (1996) proposed the formation of protonated ϵ -amino-caprolactam structure through involvement of a lysine side chain-amine group in derivatives of di- and tripeptides. Recently, Li et al. (2011) have suggested that the macrocyclization of *b* ions may take place between the lysine side chain ϵ -amine group and the C-terminal oxazolone structure. However, there is no systematic study on the side chain amine group assisted macrocyclization of *b* ions. We named this novel reaction pathway as “*side-to-tail cyclization*”.

¹ This chapter is published as: Atik, A. E.; Gorgulu, G. and Yalcin, T. “*The Role of Lysine ϵ -Amine Group on the Macrocyclization of *b* Ions*” *Int. J. Mass Spectrom.* **2012**, 316-318, 84-90.

In this current work, we carried out a systematic study to examine the potential involvement of the side chains amine groups of lysine (K), glutamine (Q), or asparagine (N) residue on the macrocyclization of *b* ions even though the N-terminals of the peptides were acetylated. The common feature of these three amino acid residues is that they contain an amine group ($-NH_2$) on their side chains (Figure 4.1). The amine group of the lysine side chain is free, whereas glutamine and asparagine have amide structures on their side chains.

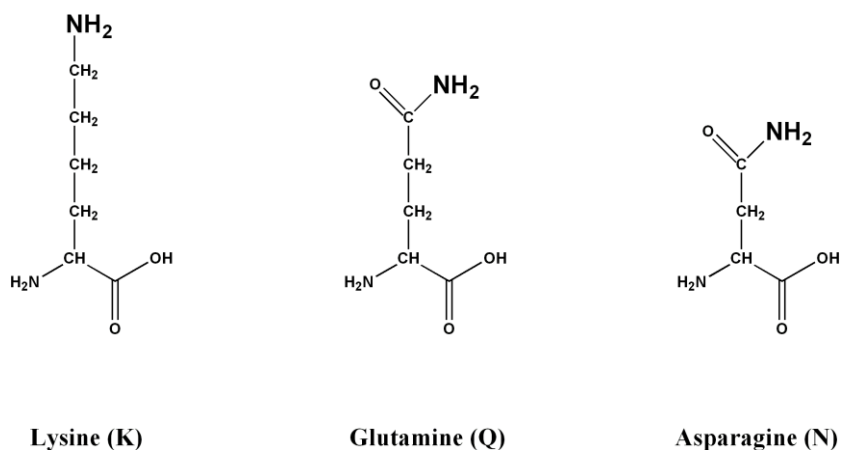


Figure 4.1. Schematic representation of lysine, glutamine, and asparagine amino acids

4.2. Experimental

All model peptides (either C-terminal amidated or free acid) were purchased from GL Biochem Ltd. (Shanghai, China) and were used as received. The peptide list composed of Ac-KYAGFLVG, Ac-QYAGFLV-NH₂, Ac-NYAGFLV-NH₂, Ac-YKAGFLVG, Ac-YAKGFLVG, Ac-YAGKFLVG, Ac-YAGFKLVG, Ac-YAGFLKVG, Ac-K_{Ac}YAGFLVG, YAGFLV-NH₂, KAGFLVG, AKGFLVG, and AGKFLVG. Approximately 2 mg of each of the solid peptide samples was dissolved to a concentration of 10^{-3} or 10^{-4} M in HPLC-grade methanol.

An LTQ XL linear ion-trap (Thermo Finnigan, San Jose, CA) equipped with an ESI source was used to acquire the MS/MS spectra of model peptides and the instrument was operated in the positive mode. The experimental conditions were the same as previously described in detail (Atik and Yalcin 2011). Briefly, 100 pmol μL^{-1} of each peptide solution was diluted in 50:50:1 (v/v/v) MeOH/H₂O/HCOOH and was

introduced into the ion source with an incorporated syringe pump at a flow rate of 5 $\mu\text{L min}^{-1}$. Other experimental parameters are as follows. The isolation width (m/z) for precursor ions was set at between 0.8 and 2.4 for MS^n stages and at least 400 scans were averaged. The normalized collision energy was varied between 20 % and 28 % (arbitrary units) where helium was used as the collision gas for CID and as a damping gas.

In order to construct the breakdown graphs, a hybrid triple quadrupole/linear ion trap instrument (4000 Q-TRAP, Applied Biosystems/MDS Sciex, Concord, Canada) equipped with a turbo ion spray source was used. The ion spray voltage was + 5.5 kV and MS/MS experiment was carried out in enhanced product ion (EPI) scan mode. The collision energy was varied from 18 to 48 eV in increments of 2 eV, and 50 cycles were averaged.

4.3. Results and Discussion

4.3.1. Effect of Lysine, Glutamine, and Asparagine Side Chain Amine Groups on the Side-to-Tail Cyclization of b_7 Ions

The CID mass spectra of b_7 ions originated from Ac-KYAGFLVG, Ac-QYAGFLV-NH₂, and Ac-NYAGFLV-NH₂ are shown in Figure 4.2. It should be mentioned that the N-terminal amine (α -amine) groups of these three heptapeptides are acetylated. The CID mass spectra of b_7 ions originated from these three peptides exhibited that the non-direct sequence ions (internal amino acid residue losses) still detected for the lysine containing peptide in spite of the N-terminal of the peptide was acetylated, but was failed to be observed for glutamine and asparagine containing peptides. However, it was reported that N-terminal acetylation blocks the macrocyclization reactions and eliminates the non-direct sequence ions in the peptide CID mass spectra (Harrison 2009).

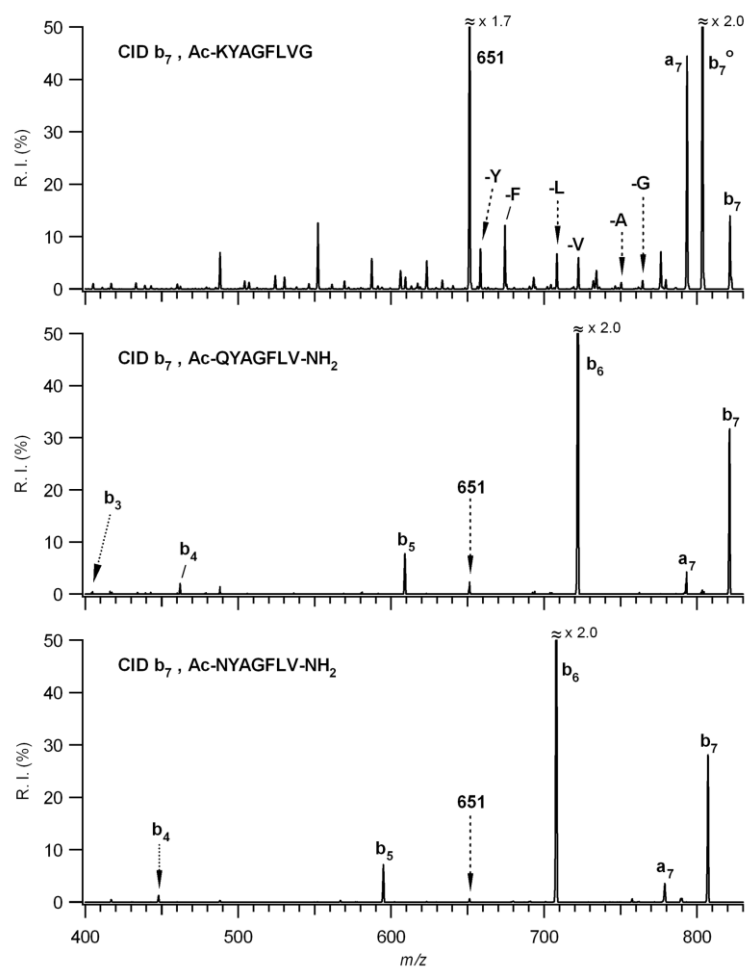


Figure 4.2. Comparison of the MS³ mass spectra of b_7 ions of protonated Ac-KYAGFLVG, Ac-QYAGFLV-NH₂, and Ac-NYAGFLV-NH₂

In the CID mass spectra of Ac-KYAGFLVG, the product ions at m/z 764, 750, 708, 674, and 658 correspond to the non-direct sequence ions which is the elimination of G (-57 Da), A (-71 Da), L (-113 Da), F (-147 Da), and Y (-163 Da), respectively. In here, it should be mentioned that the loss of V (-99 Da) is the direct sequence ion (b_6 , m/z 722) which is formed via dissociation of b_7 ion. The observed non-direct sequence ions (see upper panel of Figure 4.2) can be accepted as a major evidence of the macrocyclization of b_7 ion before fragmentation. The formation of macrocyclic structure can be explained by a nucleophilic attack of the lysine side chain ϵ -amine group to the carbonyl carbon of valine oxazolone, as depicted in Figure 4.3. This reaction differs from well-known head-to-tail cyclization; therefore we named this novel reaction mechanism as “*side-to-tail cyclization*” in which the lysine side chain assists the macrocyclization.

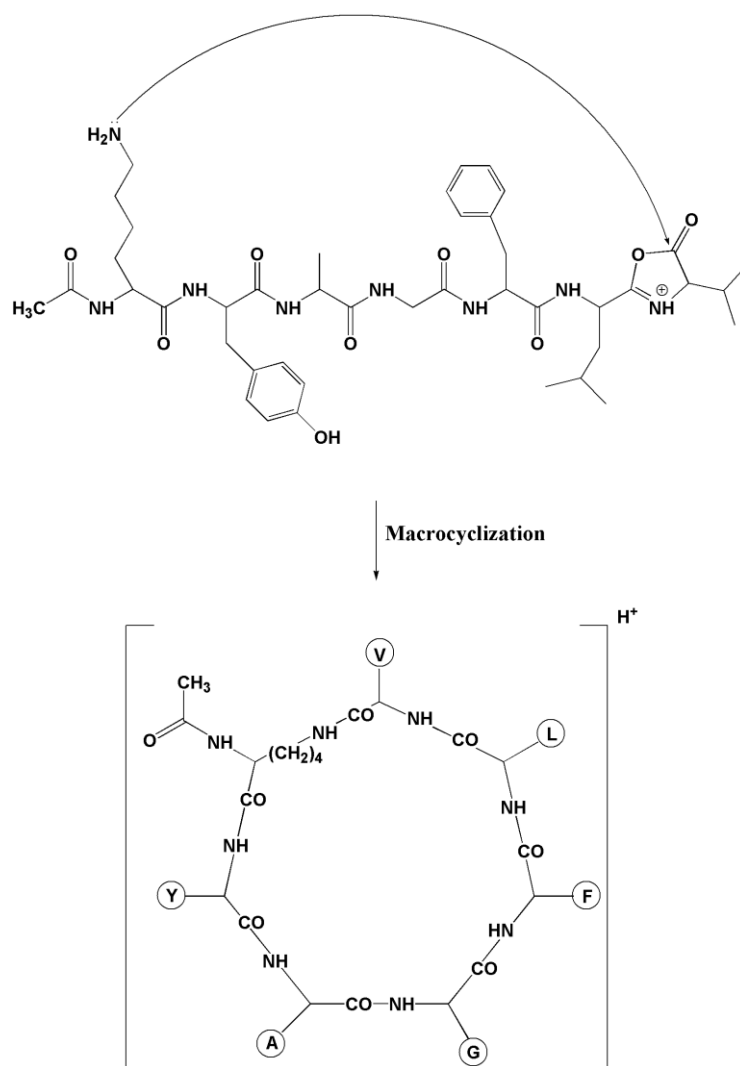


Figure 4.3. Proposed macrocyclization mechanism for b_7 ion of Ac-KYAGFLVG

The intermediate macrocyclic structure undergoes seven different ring opening pathways at various amide bonds to yield isomeric linear b oxazolones (Figure 4.4).

By contrast, non-direct sequence ions or any evidence for the macrocyclization could not be observed in the b_7 ion CID mass spectra for Ac-QYAGFLV-NH₂ and Ac-NYAGFLV-NH₂ peptides (see middle and last panels of Figure 4.2). The b_7 ion CID mass spectra derived from mentioned peptides contain only direct sequence b ions (b_6 , b_5 , b_4 , etc). This aspect can be explained by having an amide group on the side chains of glutamine and asparagine residues which makes the nucleophilic reactivity of the amine groups less compared to the lysine side chain ϵ -amine group.

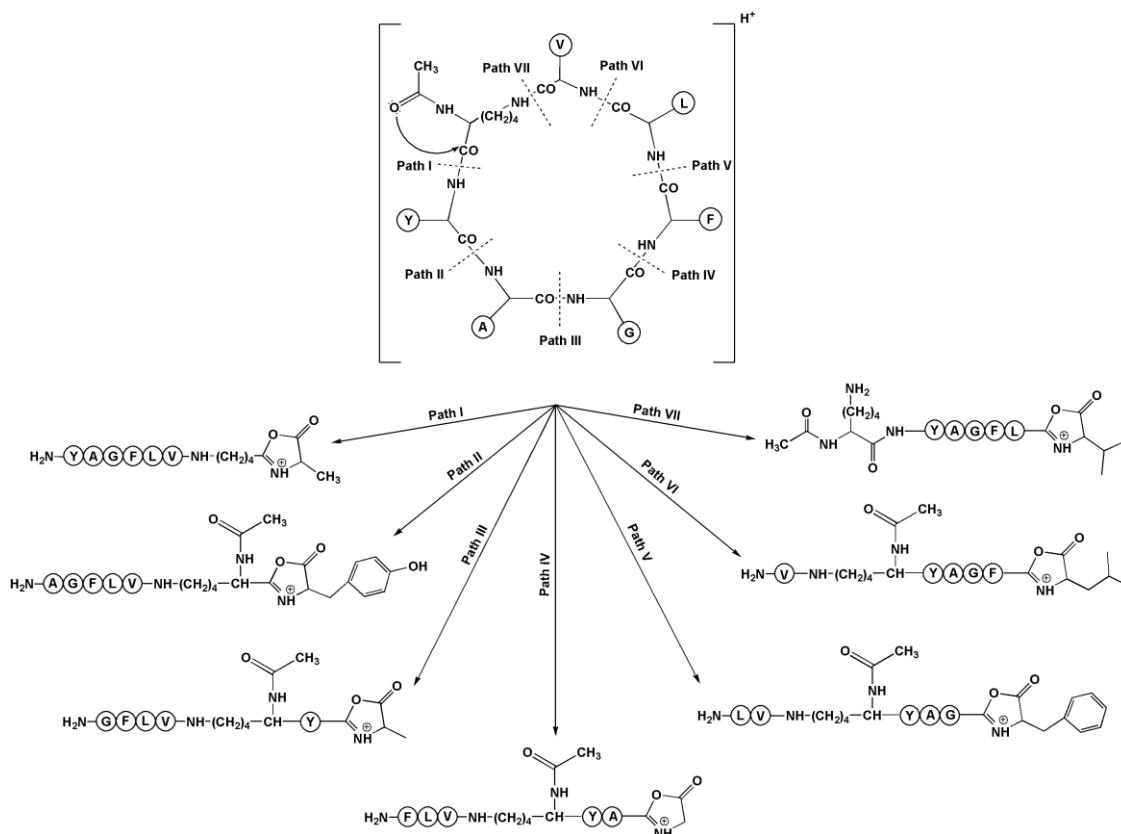


Figure 4.4. Seven possible ring opening pathways of macrocyclic b_7 ion

In order to confirm the involvement of the lysine side chain ϵ -amine group in the side-to-tail cyclization, we recorded the b_7 ion CID mass spectrum originated from Ac-K_{Ac}YAGFLVG octapeptide (acetylation of both α -amine of the peptide and ϵ -amine group of lysine residue), and Figure 4.5 displays the mass spectrum.

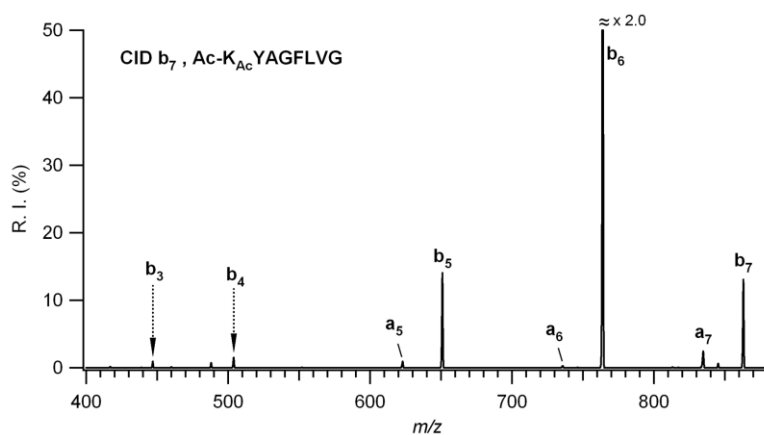


Figure 4.5. MS³ mass spectrum of b_7 ion from protonated Ac-K_{Ac}YAGFLVG

The CID mass spectrum of b_7 ion obtained from doubly acetylated peptide contains only direct sequence ions (a_7 , b_6 , a_6 , b_5 , a_5 , b_4 , and b_3). This spectrum clearly shows an evidence of the lysine ϵ -amine group involvement in the side chain assisted macrocyclization of b ion.

4.3.2. Formation and Structure of m/z 651 in the b_7 Ion CID Mass Spectra of N-Terminal Acetylated Lysine, Glutamine, and Asparagine Containing Peptides

The peak at m/z 651 is observed as a common fragment ion in all b_7 ions of Ac-KYAGFLVG, Ac-QYAGFLV-NH₂, and Ac-NYAGFLV-NH₂ peptides, as labeled in Figure 4.2. The gas-phase structure of m/z 651 ion was probed via MS⁴ ($[M + H]^+ \rightarrow b_7 \rightarrow 651$) consecutive experiments for these three peptides individually and their mass spectra are depicted in Figure 4.6.

It was shown that the fragmentation patterns of the m/z 651 ions derived from N-terminal acetylated lysine, glutamine, and asparagine containing peptides demonstrates entirely the same product ions in their CID mass spectra. It was proposed that that N-terminal acetylated lysine, glutamine, or asparagine is cleaved as a neutral from b_7 ions, leaving the YAGFLV_{oxa} as a b -type protonated oxazolone structure in the gas-phase (Figure 4.7). To support this proposed fragmentation mechanism, the model peptide YAGFLV-NH₂ was also purchased and its b_6 ion (m/z 651) CID mass spectrum was compared with the other m/z 651 ion's mass spectra, as shown in the last panel of Figure 4.6. It is obvious that the m/z 651 ions obtained from b_7 ions of N-terminal acetylated lysine, glutamine, and asparagine containing peptides and the b_6 ion obtained from YAGFLV-NH₂ have the same fragmentation pattern along with the same fragment ion intensities. Hence, we can conclude that the gas-phase structure of m/z 651 ion is YAGFLV_{oxa}.

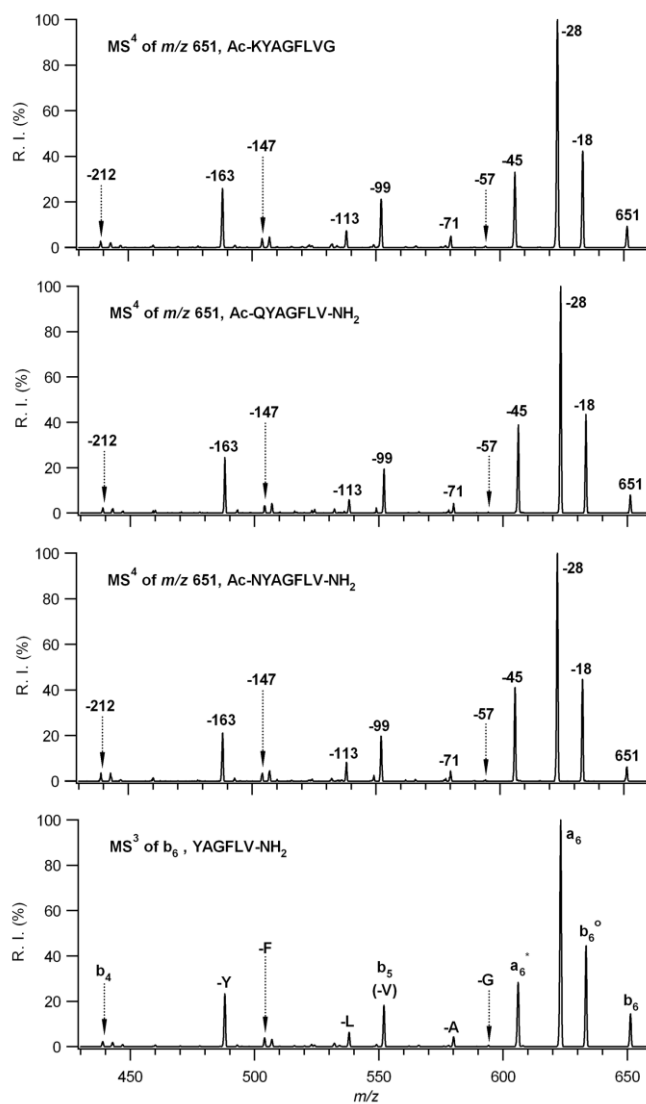


Figure 4.6. Comparison of the MS⁴ mass spectra of m/z 651 ions from protonated Ac-KYAGFLVG, Ac-QYAGFLV-NH₂, Ac-NYAGFLV-NH₂ with MS³ mass spectrum of b₆ ion derived from YAGFLV-NH₂

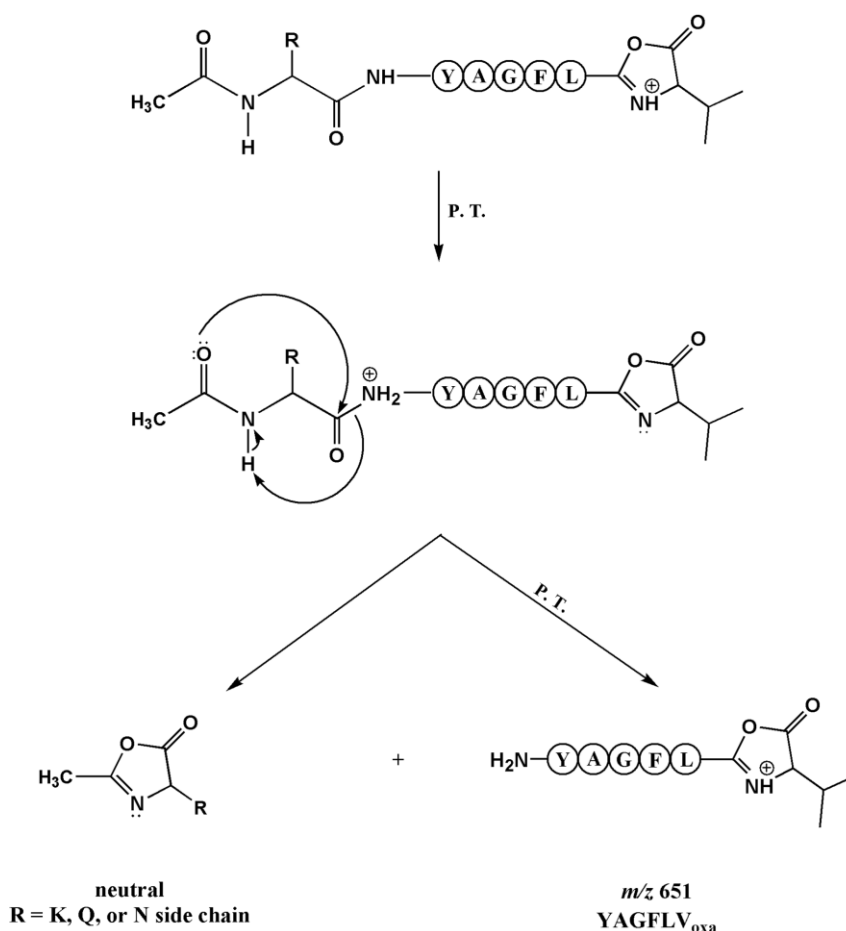


Figure 4.7. Proposed fragmentation pathway leading to the formation of neutral Ac-X (X = K, Q, or N) and protonated YAGFLV_{oxa} from Ac-KYAGFLVG, Ac-QYAGFLV-NH₂, and Ac-NYAGFLV-NH₂, respectively

4.3.3. Positional Effect of Lysine Residue on the Side-to-Tail Cyclization of *b*₇ Ions in the N-terminal Acetylated Octapeptides

In the second part of the study, a detailed analysis of six N-terminal acetylated isomeric octapeptides was performed in order to examine the positional effect of the lysine residue for the side chain assisted macrocyclization of *b* ions. This set of model peptides comprised of Ac-KYAGFLVG, Ac-YKAGFLVG, Ac-YAKGFLVG, Ac-YAGKFLVG, Ac-YAGFKLVG and Ac-YAGFLKVG where the lysine is positioned at the N-terminal position 1 through 6 in the sequence. The MS³ mass spectra of *b*₇ ions derived from each octapeptide are shown in Figure 4.8. The MS/MS spectra of [M + H]⁺ derived from each peptide were shown in the Appendix B

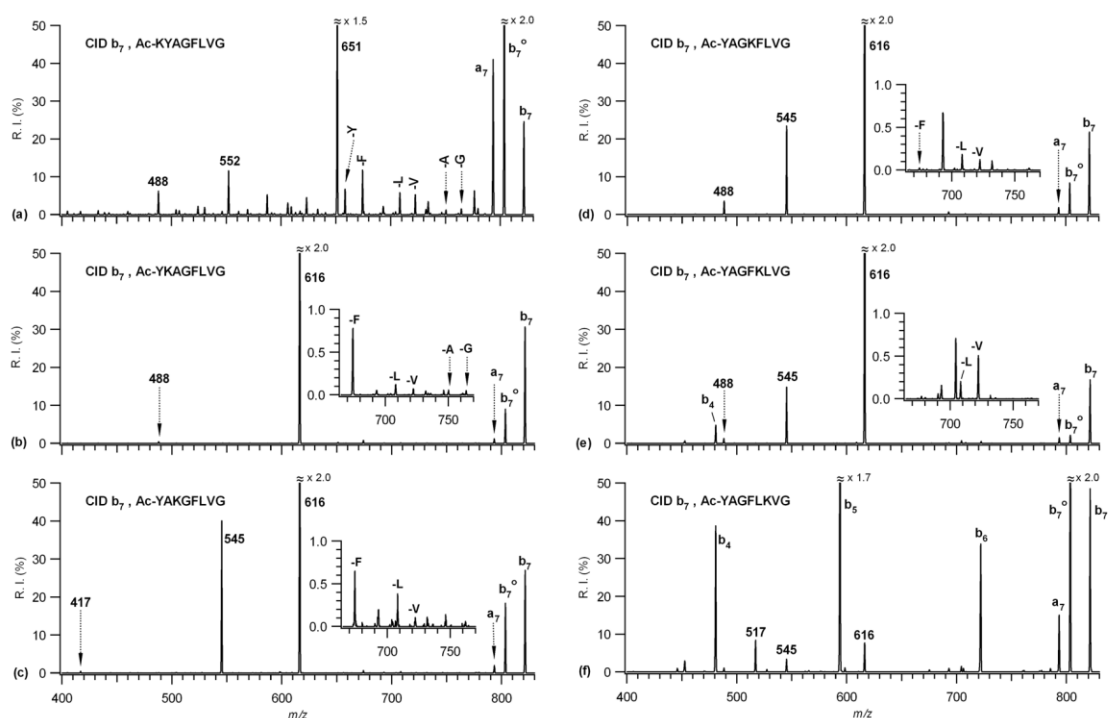


Figure 4.8. Comparison of the MS³ mass spectra of b_7 ions from protonated (a) Ac-KYAGFLVG, (b) Ac-YKAGFLVG, (c) Ac-YAKGFLVG, (d) Ac-YAGKFLVG, (e) Ac-YAGFKLVG and (f) Ac-YAGFLKVG

It is apparent that the relative intensities of the non-direct sequence ions have greatly decreased below to the 1% for the isomeric peptides where the lysine residue gets closer to the C-terminal position. This dramatic reduce in intensities of the non-direct sequence ions can explain by having a bulky group at the N-terminal side of the lysine residue whose ϵ -amine group can rationalize the side-to-tail cyclization.

For the octapeptides where the lysine residue is located at the N-terminal position 2 or any other internal position, detailed fragmentation mechanisms was proposed and the related explanations can be found in the following subsections.

4.3.3.1. Ac-KYAGFLVG

The CID mass spectrum of b_7 ion obtained from Ac-KYAGFLVG contains non-direct sequence ions as previously discussed in section 4.3.1. (Figure 4.8a). The second most abundant fragment ion is m/z 651 in the CID mass spectrum of b_7 ion and its structure was confirmed as YAGFLV_{oxa} (see Figure 4.6). We proposed that there are two fragmentation routes leading to the generation of m/z 651 ion from b_7 ion of this

peptide sequence. The first pathway involves direct cleavage of peptide bond between Ac-K and YAGFLV_{oxa}, as already described in Figure 4.7. In the second pathway, YAGFLV-Ac-K_{oxa} is formed as a result of sequence scrambling chemistry via path I which is shown in Figure 4.4 and then followed by peptide bond cleavage between the valine carbonyl moiety and the lysine ϵ -amine group (see Figure 4.9).

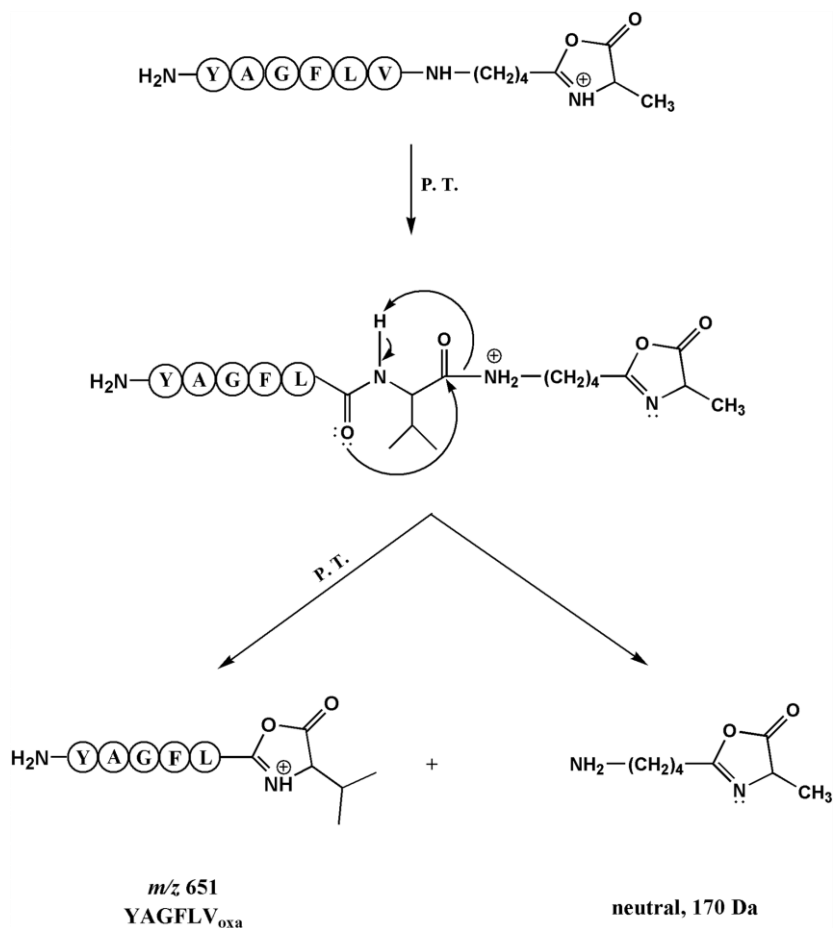


Figure 4.9. Proposed fragmentation pathway for the formation of neutral Ac-K and protonated YAGFLV_{oxa} from YAGFLV-Ac-K_{oxa} *b*₇ isomer

On the other hand, the spectrum also contains the ions at m/z 552 (valine loss, -99 Da) and m/z 488 (tyrosine loss, -163 Da) from YAGFLV_{oxa}, and their gas-phase structures were confirmed as YAGFL_{oxa} and AGFLV_{oxa}, respectively (spectra not shown).

4.3.3.2. Ac-YKAGFLVG

The CID mass spectrum of b_7 ion originating from protonated Ac-YKAGFLVG has an abundant fragment ion at m/z 616 (Figure 4.8b) which is the elimination of 205 Da from b_7 ion (m/z 821). The m/z 616 fragment ion can be formed via direct cleavage of amide bond between Ac-Y and KAGFLV_{oxa} through the dissociation of b_7 ion. (Figure 4.10).

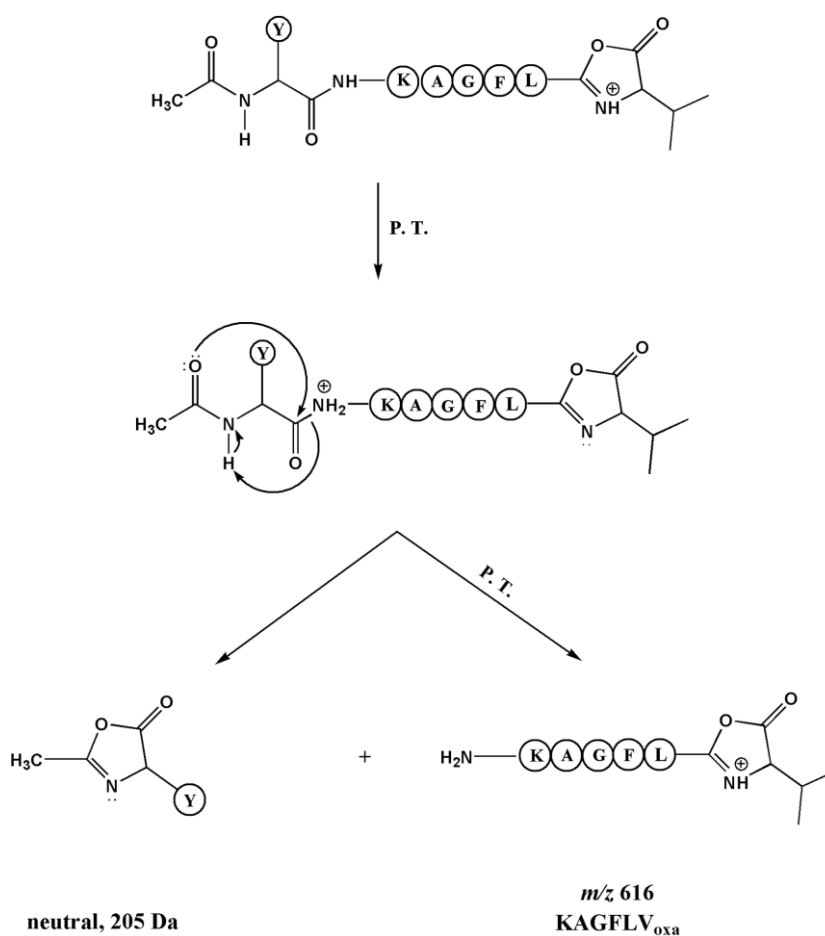


Figure 4.10. Proposed fragmentation pathways leading to neutral Ac-Y and protonated KAGFLV_{oxa} from Ac-YKAGFLVG

The protonated KAGFLV_{oxa} structure was confirmed via carrying out MS³ experiment for the b_6 ion of KAGFLVG commercial peptide and the resultant mass spectra were illustrated in Figure 4.11. The fragment ion at m/z 488 was also detected with minor intensity (Figure 4.8b) due to the low probability of bond cleavage between

Ac-YK and AGFLV_{oxa}. Additionally, the structure of m/z 488 fragment ion was confirmed as AGFLV_{oxa} (spectra not shown).

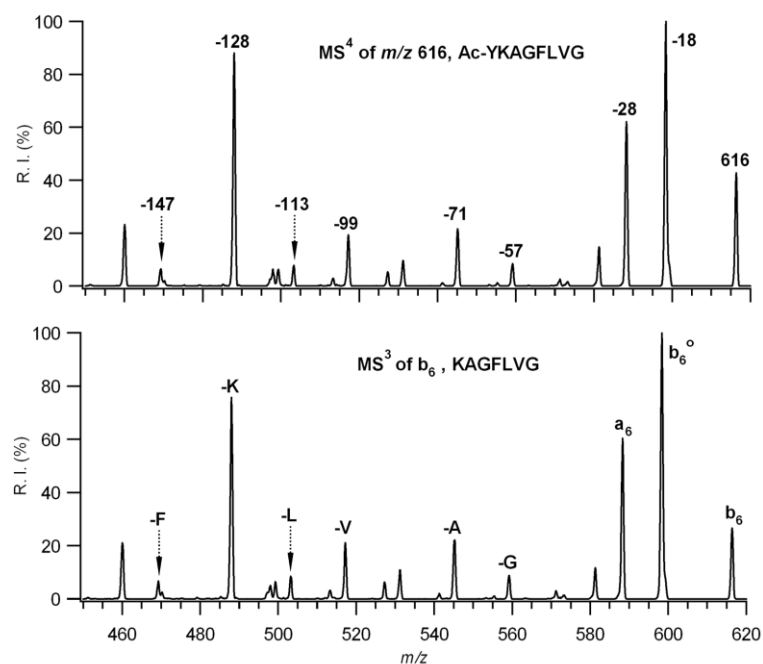


Figure 4.11. Comparison of the MS⁴ mass spectrum of m/z 616 ion from Ac-YKAGFLVG with the MS³ mass spectrum of b_6 ion of KAGFLVG

4.3.3.3. Ac-YAKGFLVG

The subsequent MS³ spectrum of the b_7 ion derived from Ac-YAKGFLVG has a major fragment ion at m/z 616 (Figure 4.8c). The fragmentation mechanism for the formation of this ion can be explained in a similar fragmentation pathway, as illustrated in Figure 4.10. In this case, the m/z 616 fragment ion has a structure of protonated AKGFLV_{oxa} by the elimination of Ac-Y as a neutral specie from b_7 ion. The gas-phase structure of AKGFLV_{oxa} was also confirmed by conducting the MS³ experiment for b_6 ion of AKGFLVG commercial peptide (Figure 4.12).

In addition, the fragment ion at m/z 545 was generated from the cleavage of peptide bond between Ac-YA and KGFLV_{oxa}. In a similar way, peptide bond cleavage between Ac-YAK and GFLV_{oxa} forms the m/z 417 ion. Two competitive fragmentation pathways were proposed for these eliminations, as depicted in Figure 4.13.

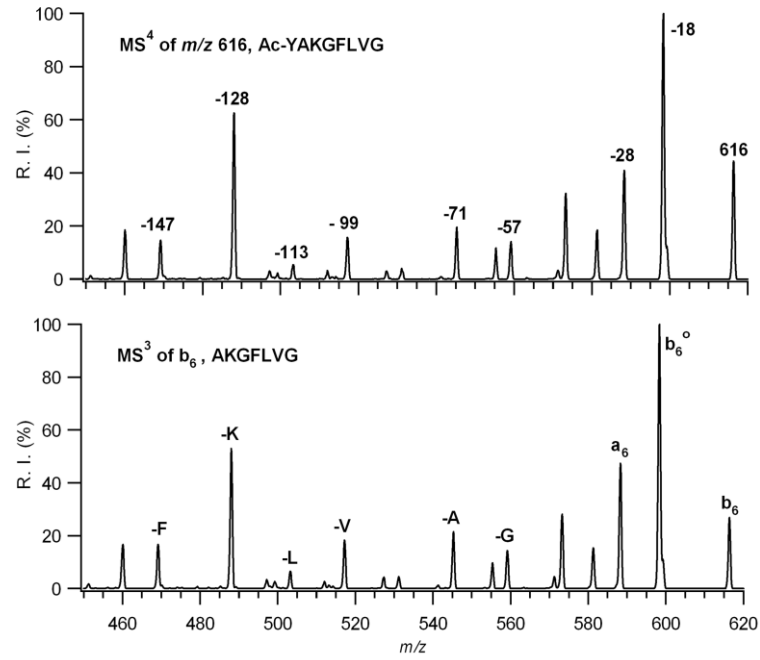


Figure 4.12. Comparison of the MS⁴ mass spectrum of *m/z* 616 ion from Ac-YAKGFLVG with the MS³ mass spectrum of *b*₆ ion of AKGFLVG

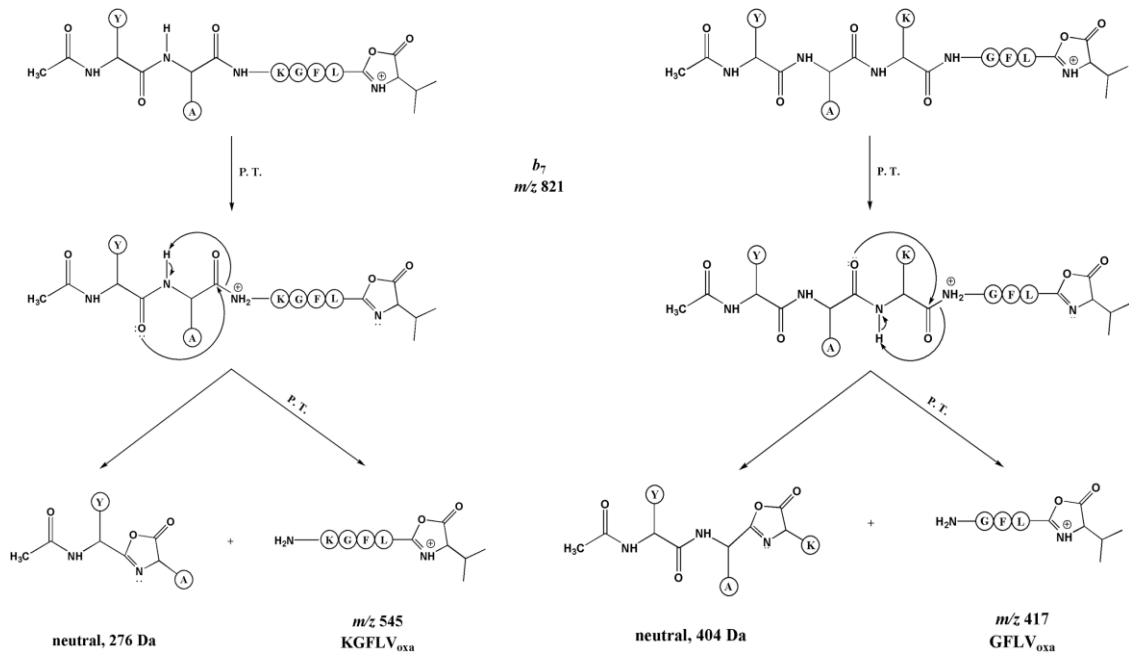


Figure 4.13. Proposed fragmentation pathway leading to formation of *m/z* 545 and *m/z* 417 ions from *b*₇ ion of Ac-YAKGFLVG

The breakdown graph was also constructed for the fragments of m/z 821 (b_7), 616, 545, and 417 ions in order to support the proposed fragmentation pathways. It is clearly shown that (see Figure 4.14) the percent total ion intensity of b_7 ion was decreased dramatically as the collision energy increased. However, the percent total ion intensities of m/z 616, 545, and 417 fragment ions were increased as the collision energy increased up to certain value, after which they decreased. The maximum percent ion intensities correspond to the loss of Ac-Y, Ac-YA, and Ac-YAK was observed at 32, 36, and 40 eV, respectively.

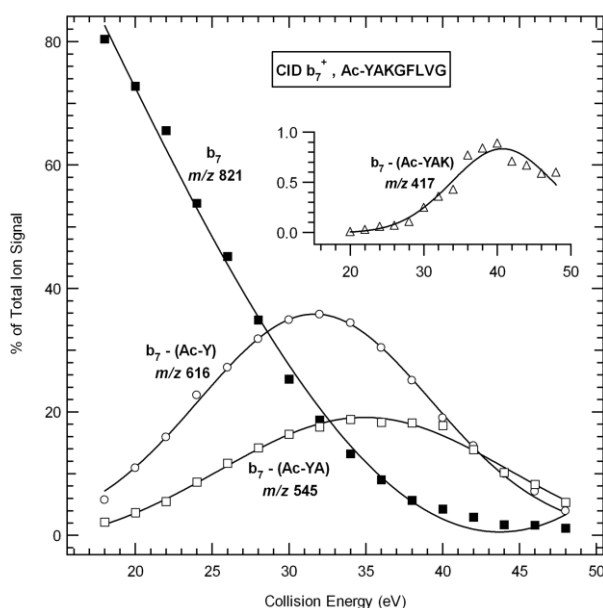


Figure 4.14. Breakdown graph of fragment ions at m/z 821, 616, 545, and 417 originated from Ac-YAKGFLVG

4.3.3.4. Ac-YAGKFLVG

The MS³ spectrum of b_7 ion derived from Ac-YAGKFLVG contains m/z 616, 545 and 488 fragment ions, as illustrated in Figure 4.8d. These fragment ions were formed via neutral loss of Ac-Y, Ac-YA, and Ac-YAG from b_7 ion, respectively, and their formation mechanisms were similar as previously proposed for other peptides (spectra and proposed mechanism not shown). The breakdown graph was constructed to evaluate the collision energy dependence of m/z 616, 545 and 488 fragment ions.

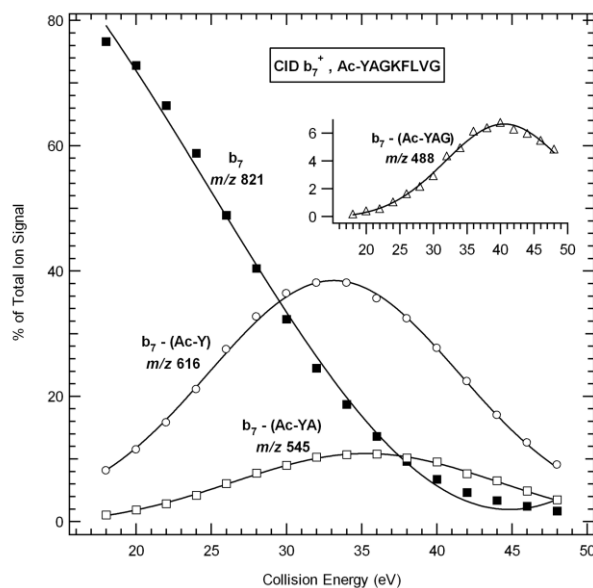


Figure 4.15. Breakdown graph of fragment ions at m/z 821, 616, 545, and 488 originated from Ac-YAGKFLVG

This plot explains that the more collision energy is required for cleavage of Ac-YA from b_7 isomer compared to the Ac-Y. Similarly, the energy needed for cleavage of Ac-YAG is higher (40 eV) than the other two fragments.

4.3.3.5. Ac-YAGFKLVG

The subsequent MS^3 spectrum of the b_7 ion derived from Ac-YAGFKLVG has fragment ions resulting from N-terminal losses. Beside to these ions, the b_4 ion is started to be appeared in the mass spectrum. This aspect is explained by inhibition of macrocyclization reaction as the lysine residue gets closer to the C-terminal end.

4.3.3.6. Ac-YAGFLKVG

For the peptide Ac-YAGFLKVG, the b_7 ion CID mass spectrum is greatly dominated by sequential direct sequence b ions (b_6 , b_5 , b_4 ...), as shown in Figure 4.4f. The intensities of the fragment ions at m/z 616 (AGFLKV_{oxa}) and 545 (GFLKV_{oxa}) are dramatically decreased due to large bulky group on the backbone of lysine residue which inhibits the macrocyclization of b_7 ion completely.

CHAPTER 5

A REARRANGMENT REACTION OF ACETYLATED LYSINE CONTAINING PEPTIDE b_n ($n = 4-7$) ION SERIES¹

5.1. Introduction

The lysine acetylation is the one of the most prominent post-translational modification (PTM) found in proteins and plays vital roles in regulation of protein activity and gene expression (Boyes et al. 1998, Glozak et al. 2005, Khan and Khan 2010). Therefore, a large number of gas-phase fragmentation reaction studies have been carried out for acetylated lysine containing peptides to find the localization of the modification in the peptide sequence (Kim et al. 2002, Zhang et al. 2004, Trelle and Jensen 2008, Fu et al. 2013). The studies have showed that the mass difference between consecutive b - and/or y - sequence ion series is 170 u which is the characteristic mass for an acetylated lysine residue.

Previous studies have showed that the m/z 143 and 126 fragments can be accepted as marker ions for peptides containing acetylated lysine residues via gas-phase fragmentation (Kim et al. 2002, Zhang et al. 2004). These ions correspond to an acetylated lysine immonium ion and loss of ammonia from the acetylated lysine immonium ion, respectively. Trelle and Jensen (2008) have proved that the m/z 126 ion has high specificity and sensitivity over the ion at m/z 143 ion in the screening of acetylated lysine. The authors also emphasized the intensities of these diagnostic marker ions are more significant when the acetylated lysine residue located at the N-terminal as compared to internal positions in peptides. Additionally, Yalcin and Harrison (1996) reported that the stable α -amino- ϵ -caprolactam structure (m/z 129) can be formed in the dissociation of lysine containing small peptides.

¹ This chapter is prepared for publication as: Atik, A. E.; Hernandez, O.; Maître, P.; Yalcin, T. “A New Rearrangement Reaction of Peptide b Ions Containing Acetylated Lysine Residue” for *J. Mass Spectrom.*

On the other hand, Kish and Wesdemiotis (2003) investigated the selective cleavage of the amide bonds at the C-terminal position of protonated and metalated peptides containing internal lysine residues. Moreover, Payne et al. (2000) reported the alteration of peptide fragmentation chemistry by acetylating the N-terminal of the peptide. Recently, the fragmentation of protonated peptides containing internal lysine and side chain acetylated lysine residues has been studied using a triple-quadrupole instrument (Fu et al. 2013). In their study, it was stated that the acetylation of the ϵ -amine group of lysine residue enhances the cleavage of K_{Ac} -XXX amide bond and allowed forming b_n ions with higher abundances in the corresponding MS/MS spectra.

In the current study, we seek novel specific ions in the dissociation of b -ion series of acetylated lysine containing peptides in addition to the previously mentioned two marker ions (m/z 143 and 126) for the $[M + H]^+$ ion mass spectra. The study utilizes model octapeptides, namely K_{Ac} YAGFLVG (acetylation of the ϵ -amine group of lysine residue), Ac-KYAGFLVG (acetylation of the α -amine group of the peptide, i.e. N-terminal), Ac- K_{Ac} YAGFLVG (acetylation of both ϵ -amine and α -amine groups), and KYAGFLV-NH₂ (no acetylation).

5.2. Experimental

All model peptides (either C-terminal amidated or free acid, purity > 95 %) were purchased from GL Biochem Ltd. (Shanghai, China), and used without any purification. The peptide list composed of Ac-KYAGFLVG, K_{Ac} YAGFLVG, Ac- K_{Ac} YAGFLVG, KYAGFLV-NH₂, Ac-YAKGFLVG, YAK K_{Ac} GFLVG, Ac-YAK K_{Ac} GFLVG, YAGFLV-NH₂, YAGFL-NH₂, GFLVYA-NH₂, YAGF-NH₂, GFLYA-NH₂, GFYA-NH₂, YAG-NH₂, GYA-NH₂, and YA-NH₂. Approximately 2 mg of each peptide was dissolved in 1:1 (v/v) mixture of HPLC-grade methanol (MeOH) and deionized water to make up stock solutions with a concentration of 10^{-3} or 10^{-4} M. All the stock solutions were stored at -20°C.

All low-energy tandem mass spectrometry (MSⁿ) experiments were performed with a LTQ XL linear ion-trap mass spectrometer (Thermo Finnigan, San Jose, CA) equipped with an electrospray ionization (ESI) source. The stock peptide solutions were diluted to a 100 μ M in 50:50 (v/v) methanol/water solvent containing 1 % formic acid and infused directly into a mass spectrometer with an incorporated syringe pump at a

flow rate of 5 $\mu\text{L min}^{-1}$. The instrument was calibrated with a Calmix solution composed of caffeine, MRFA, and Ultramark 1621 prior to experiments. The ion optics were optimized in order to provide maximum precursor ion transmission into the trap. The spray voltage was set at + 5.0 kV, and the heated capillary temperature was maintained at 275 $^{\circ}\text{C}$ with a capillary voltage of 20 V. Nitrogen was used as the sheath, sweep, and auxiliary gas with a flow rate of 10, 1, and 1 (all arbitrary units), respectively. An isolation width (m/z) of 1.2-2.0 Da was used for each MS^n acquisitions and an activation (q) of 0.250 with a 30 ms activation time was applied at each CID stage. The normalized collision energy was varied from 20 to 28 % (arbitrary units) for the dissociation of selected precursor ion. The MS^n spectra were recorded in the m/z scan range of 150–920 in the positive-ion mode and at least 400 scans were averaged. Helium was used as the collision gas for CID and also as a damping gas in the collision cell. Data acquisition was performed using XcaliburTM (version 2.0) software data system (Thermo Fisher Scientific).

5.3. Results and Discussion

5.3.1. Fragmentation Reactions of b_n ($n = 4-7$) Ions Originated from $\text{K}_{\text{Ac}}\text{YAGFLVG}$ and Ac-KYAGFLVG

The CID mass spectra of b_7 , b_6 , b_5 , and b_4 ions were recorded separately for $\text{K}_{\text{Ac}}\text{YAGFLVG}$ octapeptide upon low-energy CID- MS^3 consecutive experiments and illustrated in Figure 5.1a. It is evident that ϵ -amine group of lysine residue is acetylated and located at the N-terminal position of the peptide. Each mass spectrum comprised of both direct and non-direct sequence ions. The formation of non-direct sequence ions (internal amino acid losses) can be explained by head-to-tail cyclization and subsequent ring opening processes. In addition to these sequence ions, the fragments at m/z 668, 569, 456, and 309 were also observed in the dissociation of b_7 , b_6 , b_5 , and b_4 ion's mass spectra, respectively and these ions do not reflect any direct or non-direct sequence ions. In order to elucidate the gas-phase structures of these fragments, the multi-stage mass spectrometry (MS^4) experiments were carried out individually. The CID mass spectrum of m/z 668 fragment from b_7 ion of $\text{K}_{\text{Ac}}\text{YAGFLVG}$ is shown in Figure 5.2a.

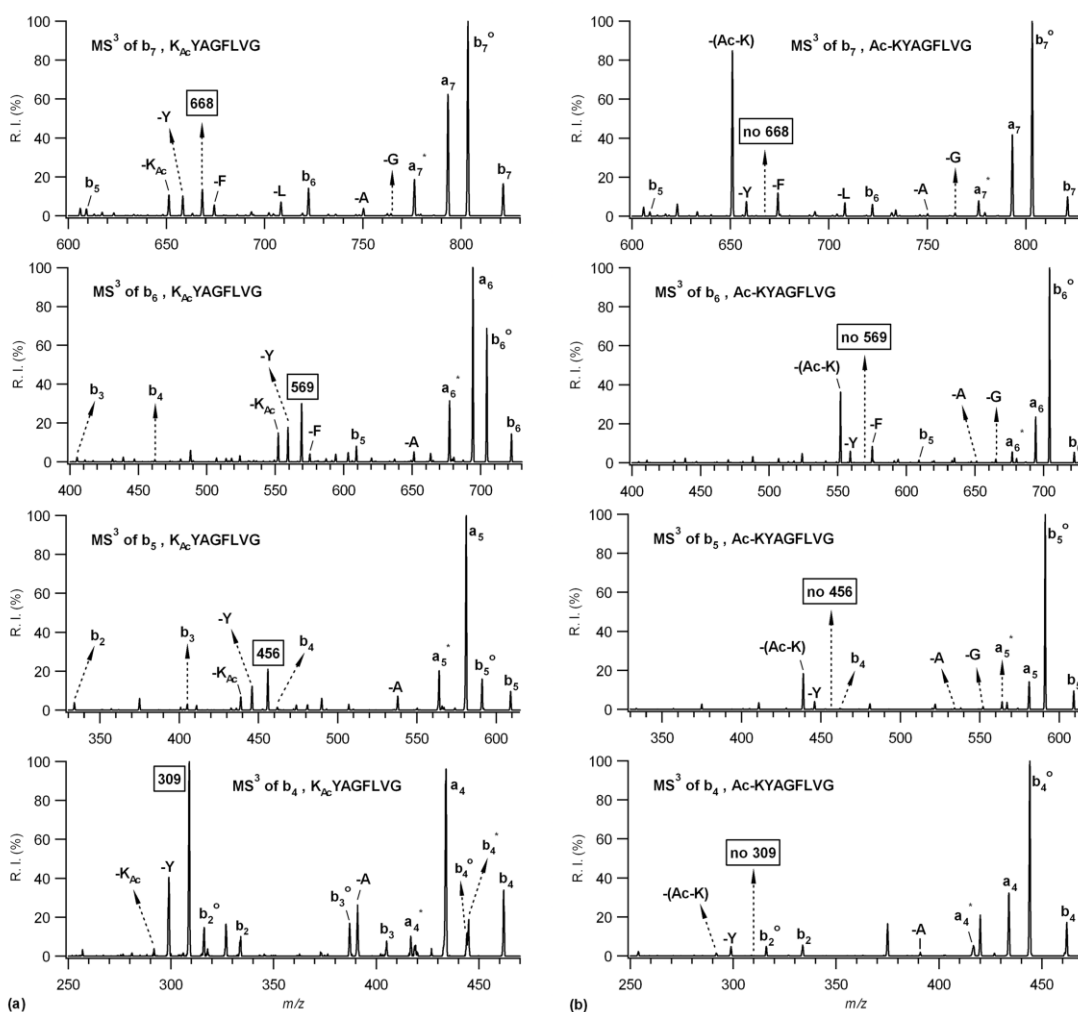


Figure 5.1. Comparison of the MS³ mass spectra of b₇, b₆, b₅, and b₄ ions originated from (a) K_{Ac}YAGFLVG and (b) Ac-KYAGFLVG, respectively

The fragmentation of m/z 668 generates m/z 651, 623, and 552 as the major product ions with weak intensities of m/z 633, 606, 524, 507, 488, 439 ions. We have recently reported the gas-phase structure of m/z 651 fragment ion as YAGFLV_{oxa} (Atik et al. 2012). In line with this work, the addition of masses of YAGFLV_{oxa} (651 u) and ammonia (17 u) together can theoretically produce the protonated m/z 668 ion's mass. In order to confirm our proposal, the MS/MS spectrum of $[M + H]^+$ ion produced from YAGFLV-NH₂ was recorded and compared with the MS⁴ spectrum of the m/z 668 fragment ion. The Figure 5.2a shows that protonated YAGFLV-NH₂ fragments to yield a product ion mass spectrum entirely identical to that of the m/z 668 from b₇ ion of K_{Ac}YAGFLVG. The resultant mass spectra reveal that the m/z 668 fragment ion has a structure of protonated YAGFLV-NH₂.

In a similar way, the m/z 569, 456, and 309 ions were isolated from b_6 , b_5 , and b_4 ions of $K_{Ac}YAGFLVG$, respectively, and allowed to dissociate under the same experimental conditions in order to obtain their gas-phase structures. The resultant mass spectra are illustrated in Figure 5.2b-d, and they entirely show completely the same fragmentation behavior (same peaks with the identical relative intensities) to that obtained for the dissociation of $[M + H]^+$ ions of commercial peptides YAGFLV-NH₂, YAGF-NH₂, and YAG-NH₂, respectively.

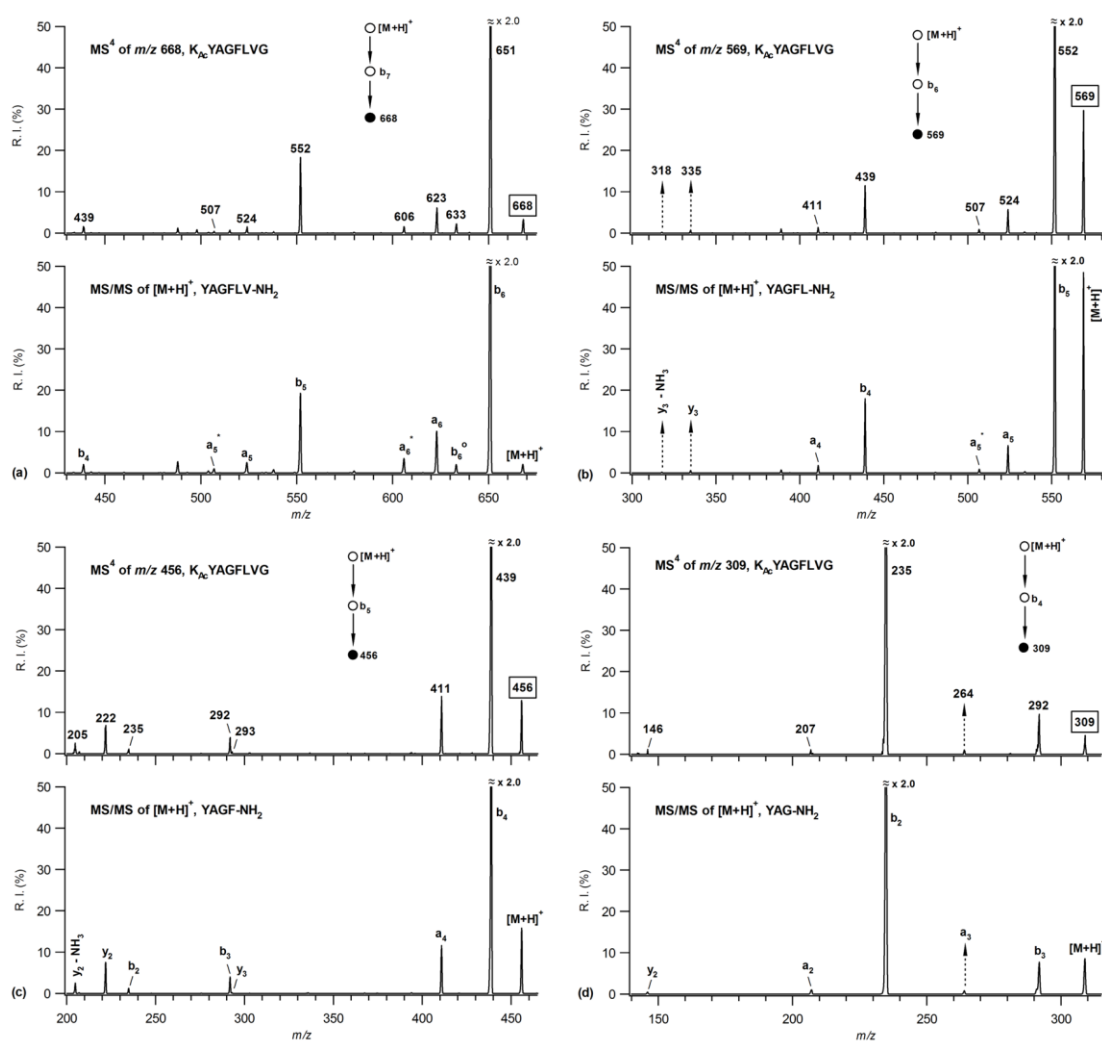


Figure 5.2. Comparison of MS⁴ mass spectrum of m/z 668, 569, 456, and 309 ions with MS/MS mass spectrum of $[M + H]^+$ ion of protonated (a) YAGFLV-NH₂, (b) YAGFL-NH₂, (c) YAGF-NH₂, and (d) YAG-NH₂, respectively

The proposed mechanism for the formation of m/z 668 fragment ion is presented in Figure 5.3. Briefly, the b_7 ion of $K_{Ac}YAGFLVG$ undergoes macrocyclization and ring-opening process to form $YAGFLVK_{Ac-oxa}$ b isomer, in which the acetylated lysine residue is positioned at the C-terminal position.

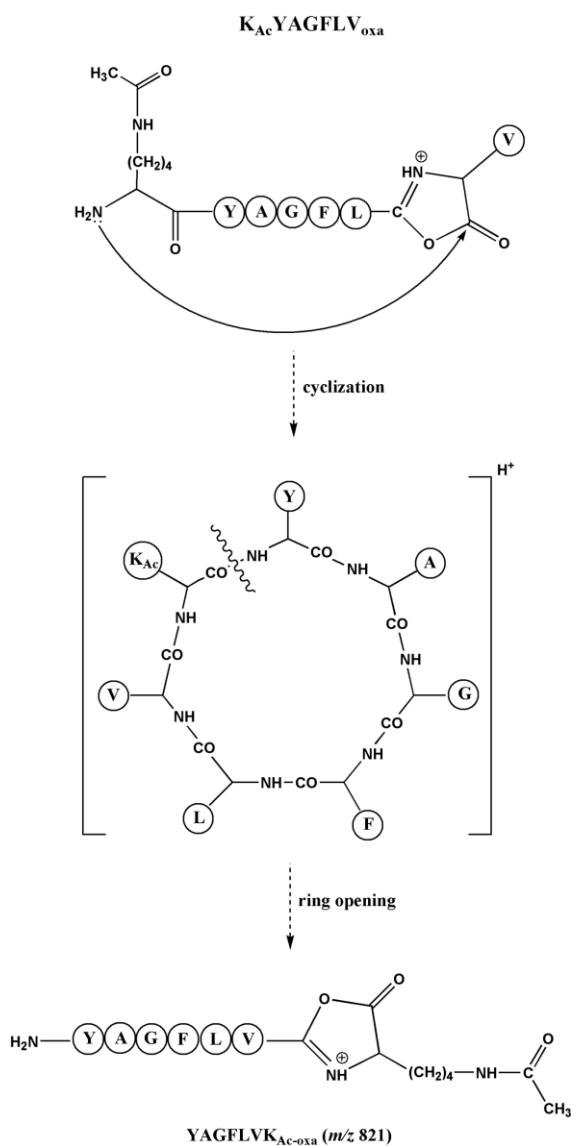


Figure 5.3. The proposed macrocyclization reaction for b_7 ion of $K_{Ac}YAGFLVG$

Then, the m/z 668 ion was cleaved as a protonated specie whereas neutral CO (28 u), C_2H_2O (42 u) and C_5H_9N (83 u) losses are believed to be formed (Figure 5.4). The formation of m/z 569, 456, and 309 fragments can be explained with the same proposed mechanism described above for m/z 668.

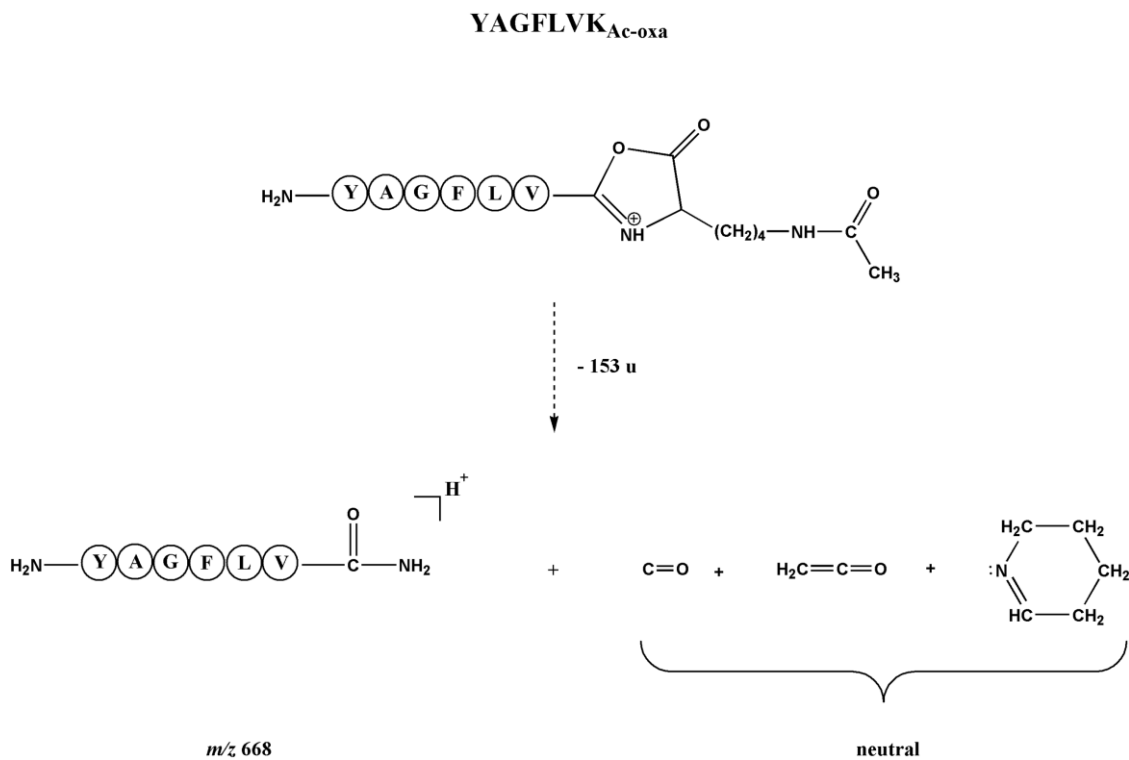


Figure 5.4. The proposed fragmentation pathway for the formation of protonated YAGFLV-NH₂ (m/z 668) from YAGFLVK_{Ac-oxa}

On the other hand, the CID mass spectrum of b_3 ion originated from K_{Ac}YAGFLVG does not show any ion signal that corresponds to rearranged fragment ion mass (Figure 5.5). This aspect can be explained by restriction of macrocyclization of b_3 ion in the gas-phase.

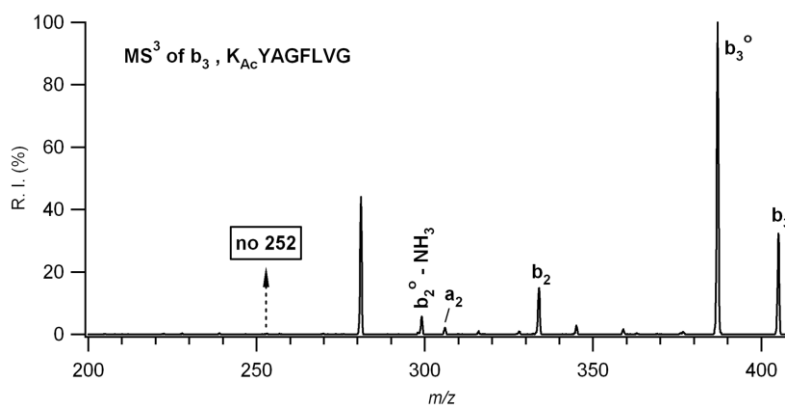


Figure 5.5. MS³ mass spectra of b_3 ion originated from K_{Ac}YAGFLVG

In the proposed mechanism, it was clearly shown that the rearranged fragment ions have C-terminal amine functionality which might come from the N-terminal amine group of the original peptide sequence. To explore the possible involvement of N-terminal amine for the formation of rearranged fragment ions, the N-terminal acetylated peptide, Ac-KYAGFLVG, was used. As illustrated in Figure 5.1b, the mentioned fragment ions were not detected in the corresponding b_n ($n = 4-7$) ions originated from N-terminal acetylated peptide. These mass spectra strongly confirm the involvement of N-terminal amine for the formation of characteristic fragment ions. The non-direct sequence ions have been also detected with different relative intensities in the dissociation of each b_7 , b_6 , b_5 , and b_4 ion mass spectra. In the previous chapter, we showed that the formation of non-direct sequence ions in detail. The macrocyclic b ion is formed by attacking of lysine ϵ -amine group to the carbonyl carbon of the oxazolone ring of b ions (side-to-tail cyclization), even if the N-terminal of the peptide was acetylated.

As a consequence of these results, the fragment ions at m/z 668, 569, 456, and 309 are only specific for side chain acetylated lysine containing peptide.

5.3.2. Fragmentation Reactions of b_n ($n = 4-7$) Ions Originated from Ac-K_{Ac}YAGFLVG and KYAGFLV-NH₂

To gain further information, we used doubly acetylated peptide (Ac-K_{Ac}YAGFLVG) in which the α -amine of the peptide and ϵ -amine of lysine residue have been both acetylated. As depicted in Figure 5.6a, the characteristic fragment ions were not detected in the corresponding b ion's mass spectra. It is apparent that the CID mass spectra of b_7 , b_6 , b_5 , and b_4 ions contain only direct sequence ions.

Similarly, we attempted to analyze the b_n ($n = 4-7$) ion's mass spectra derived from unmodified peptide sequence, KYAGFLV-NH₂, whether they contain the characteristic fragment ions or not. MS³ studies clearly show that the fragment ions at m/z 668, 569, 456, and 309 have not been encountered in the mass spectrum of b_7 , b_6 , b_5 , or b_4 ion, respectively (Figure 5.6b).

We can conclude that m/z 668, 569, 456, and 309 fragments are specific ions only for side chain acetylated lysine containing peptides. These fragment ions are not detected in the dissociation ion mass spectra of b_n ($n = 4-7$) ions derived from

Ac-KYAGFLVG, Ac-K_{Ac}YAGFLVG, or KYAGFLV-NH₂ peptide sequence. These results clearly show that the acetylation on the side chain of lysine residue can induce the generation of rearranged fragment ions.

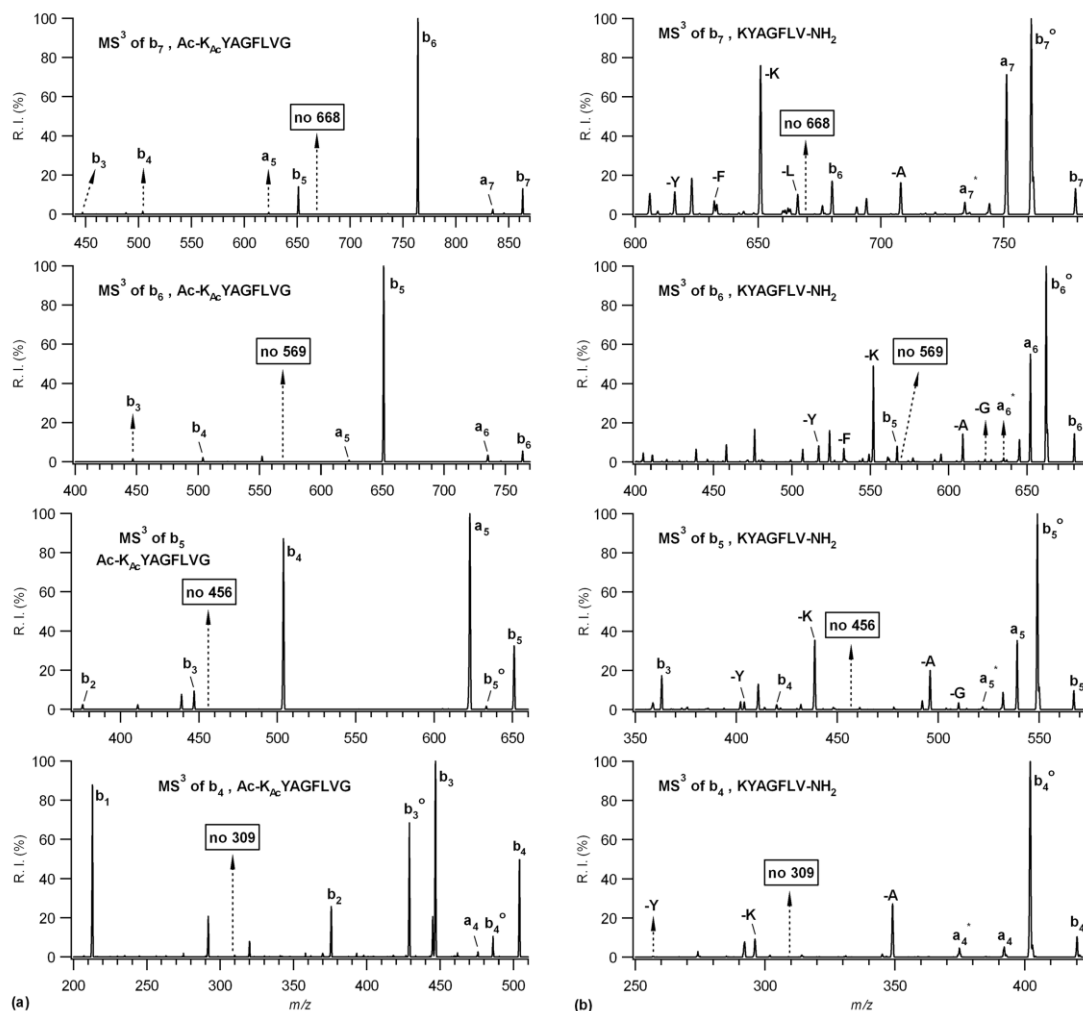


Figure 5.6. Comparison of the MS³ mass spectra of *b*₇, *b*₆, *b*₅, and *b*₄ ions originated from (a) Ac-K_{Ac}YAGFLVG and (b) KYAGFLV-NH₂ respectively

5.3.3. Positional Effect of Acetylated Lysine Residue for the Formation of Novel Fragment Ions

In the second part of the study, YAK_{Ac}GFLVG octapeptide was used in order to examine the positional effect of acetylated lysine residue for the formation of rearranged ions. In this case, the acetylated lysine residue is positioned two amino acids away from N-terminal of the peptide. Figure 5.7 displays the mass spectra of *b* ions.

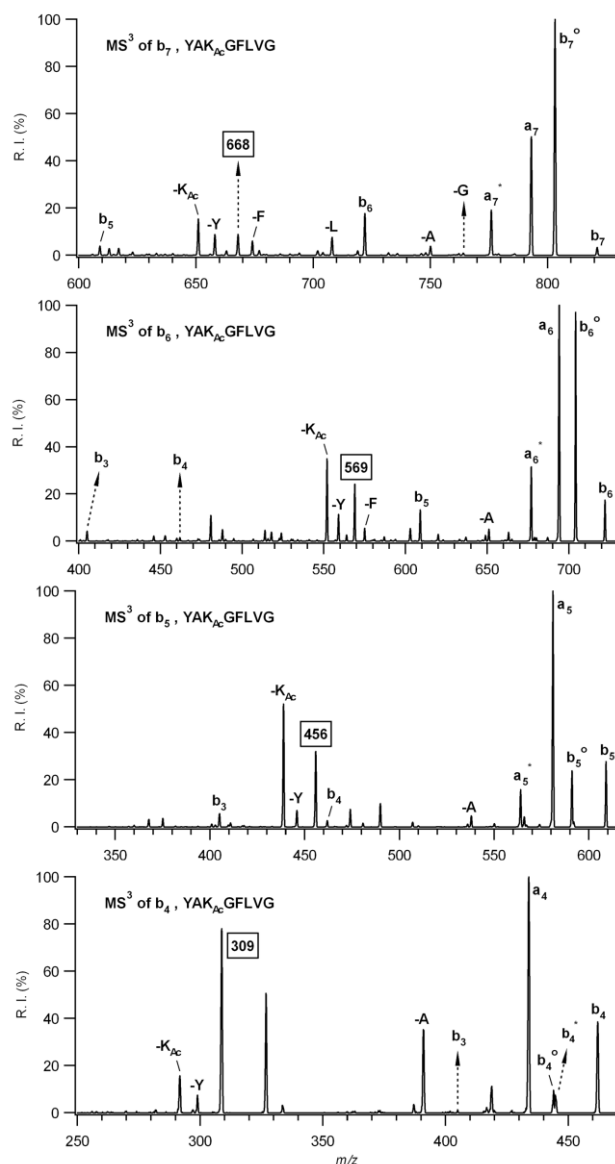


Figure 5.7. MS³ mass spectra of b_7 , b_6 , b_5 , and b_4 ions originated from YAK_{Ac}GFLVG

It was demonstrated that each mass spectrum contain both direct and non-direct sequence ions. Besides to these sequence ions, the m/z 668, 569, 456, and 309 fragment ions were also generated for this isomeric octapeptide sequence. In order to obtain the structural information of these ions, each fragment ion was subsequently isolated and then subjected to CID in ion trap mass spectrometer. As depicted in Figure 5.8a, the MS⁴ spectrum of m/z 668 fragment ion is dominated by the product ions at m/z 651, 580, and 417 with weak intensities of the ions at m/z 633, 623, 552, 463, 389, and 351. In line with the previous proposed mechanism above, the GFLVYAK_{Ac-oxa} isomer is formed via macrocyclization and ring-opening process of b_7 ion of YAK_{Ac}GFLVG. Then, this isomer can dissociate to yield the protonated GFLVYA-NH₂ (m/z 668) in the

gas-phase. In order to confirm the proposed sequence, the GFLVYA-NH₂ hexapeptide was purchased and its [M + H]⁺ ion MS/MS spectrum was recorded and compared with the MS⁴ spectrum of the *m/z* 668 fragment ion. It was clearly exhibited that the sequence of *m/z* 668 fragment ion originated from the *b*₇ ion of YAK_{Ac}GFLVG is identical to the MS/MS spectrum of protonated GFLVYA-NH₂ (see Figure 5.8a). Hence, these two ions are structurally identical in the gas-phase due to the having the same fragment ions as well as the same relative intensities.

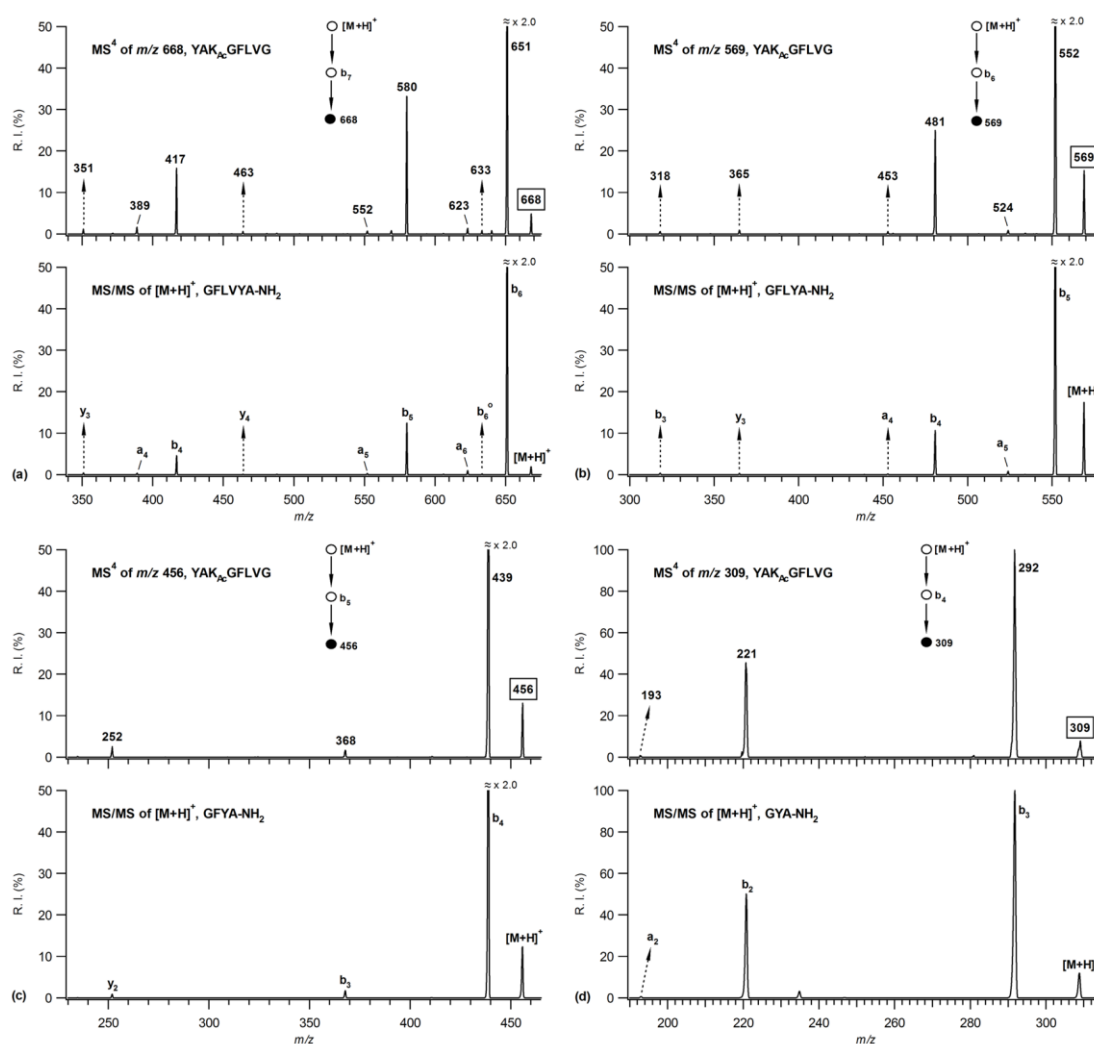


Figure 5.8. Comparison of MS⁴ mass spectrum of *m/z* 668, 569, 456, and 309 ions with MS/MS mass spectrum of [M + H]⁺ ion of protonated (a) GFLVYA-NH₂, (b) GFLYA-NH₂, (c) GFYA-NH₂, and (d) GYA-NH₂, respectively

In a similar way, the fragment ions at *m/z* 569, 456, and 309 were isolated from *b*₆, *b*₅, and *b*₄ ions, respectively, and subjected to CID for further fragmentation. The fragmentation behaviors of these ions are virtually identical compared to the

fragmentation products of $[M + H]^+$ ions obtained from GFLYA-NH₂, GFYA-NH₂, and GYA-NH₂ (see Figure 5.8b-d). The proposed mechanism leading to the formation of these ions involves the macrocyclization and subsequent ring-opening of *b*₆, *b*₅, and *b*₄ ions separately, and the acetylated lysine residue was located at the C-terminal position of the newly formed *b* isomer.

It is interesting to note that the mass spectrum of *b*₃ ion derived from YAK_{Ac}GFLVG peptide contains a fragment ion at *m/z* 252, as illustrated in Figure 5.9 which does not belong to any direct sequence ion. In this case, the acetylated lysine residue is originally positioned at the third position counting from N-terminal of the peptide.

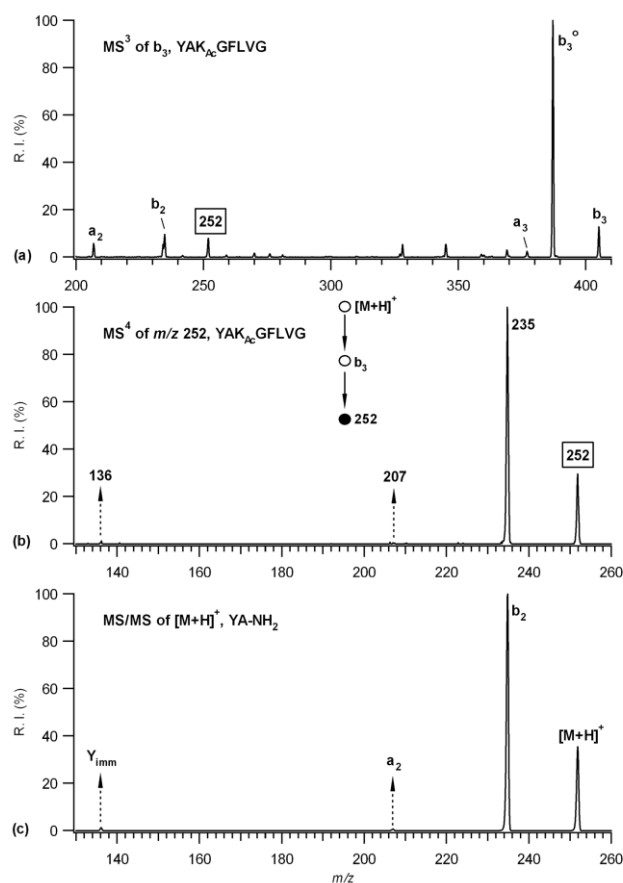


Figure 5.9. (a) MS³ mass spectrum of *b*₃ ion from protonated YAK_{Ac}GFLVG, (b) MS⁴ mass spectrum of *m/z* 252 ion from *b*₃ ion of protonated YAK_{Ac}GFLVG, (c) MS/MS mass spectrum of $[M + H]^+$ ion from protonated YA-NH₂

The *b*₃ ion, YAK_{Ac-Oxa}, underwent fragmentation to form a protonated YA-NH₂ dipeptide at *m/z* 252 and its MS⁴ mass spectrum was recorded. The C-terminal amidated

dipeptide sequence was verified by comparing the MS/MS spectrum of $[M + H]^+$ ion of commercial YA-NH₂ (see Figure 5.9c).

Furthermore, the study also utilized the Ac-YAKGFLVG (N-terminal acetylated) and Ac-YAK_{Ac}GFLVG (doubly acetylated) octapeptides in order to probe the formation of rearranged fragment ions. The MS³ studies for b_n ($n = 4-7$) ions clearly showed that the fragment ions at m/z 668, 569, 456, and 309 fragment ions were not originated from above mentioned b_n model peptides (Figure 5.10). The resultant mass spectra revealed that the formation of these characteristic fragment ions are only observed for peptides containing side chain acetylated lysine residue.

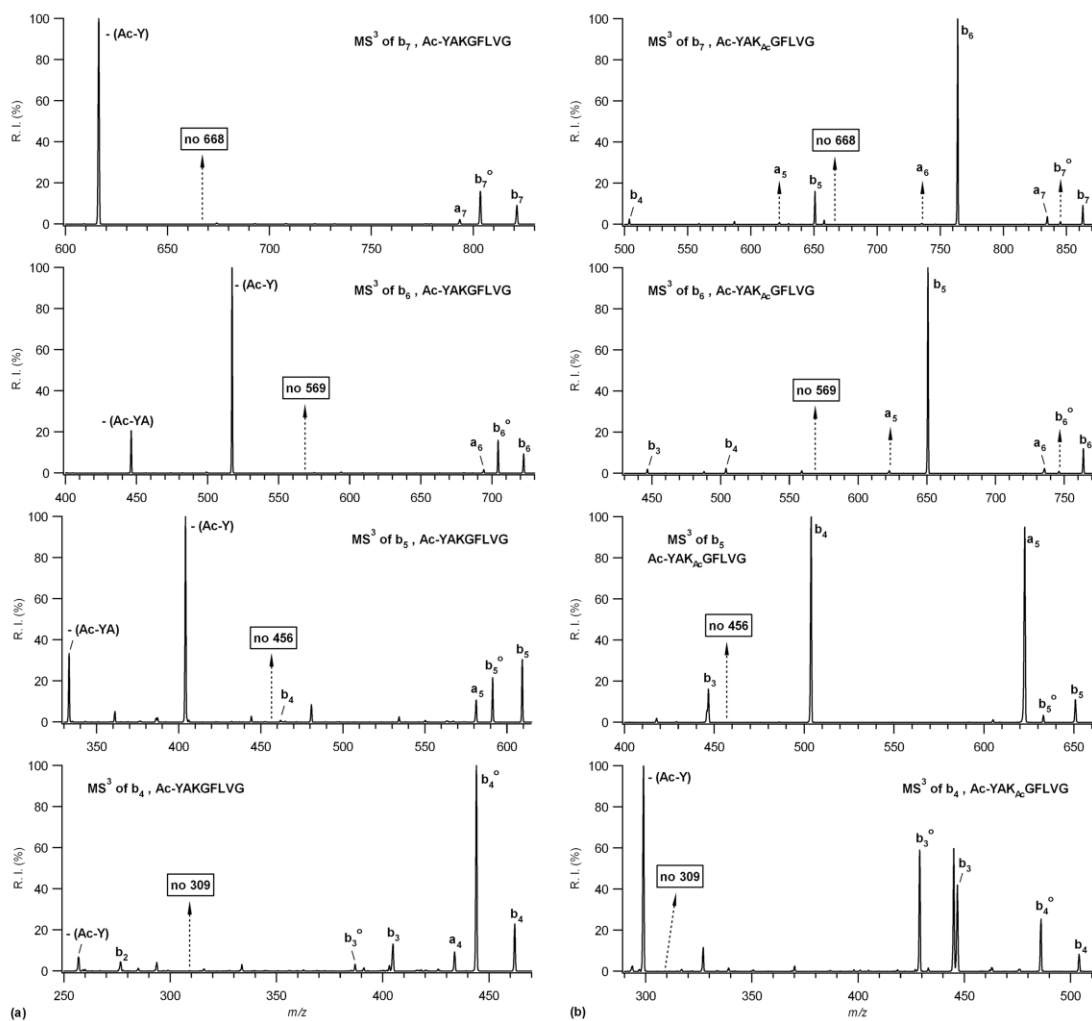


Figure 5.10. Comparison of the MS³ mass spectra of b_7 , b_6 , b_5 , and b_4 ions originated from (a) Ac-YAKGFLVG and (b) Ac-YAK_{Ac}GFLVG respectively

CHAPTER 6

PROTONATED DIPEPTIDE LOSSES FROM b_5 AND b_4 IONS OF SIDE CHAIN HYDROXYL GROUP CONTAINING PENTAPEPTIDES ¹

6.1. Introduction

The water loss from precursor ion is commonly observed fragment in the MS/MS spectra of protonated peptides. It may come from backbone amide oxygens, from the side chains of Glu, Asp, Ser and Thr amino acid residues, and from the C-terminal COOH group (Ballard and Gaskell 1993). Additionally, the neutral water molecule and protonated fragment ions may form “*ion-neutral complex*” upon low-energy CID studies.

The formation of $b_n + \text{H}_2\text{O}$ ions (where n represent the total number of residues in the peptides) have been reported over the years through gas-phase fragmentation of protonated peptides (Thorne et al. 1990, Ballard and Gaskell 1992, Gonzalez et al. 1996, Fang et al. 2000, Farrugia and O’Hair 2003, Hiserodt et al. 2007). Thorne et al. (1990) have reported for the first time the rearranged $[b_{n-1} + \text{H}_2\text{O}]$ product ions through metastable decomposition of $[\text{M} + \text{H}]^+$ ions obtained from N-terminal basic amino acid containing peptides. Additionally, Ballard and Gaskell (1992) used the ^{18}O isotopic exchange experiments to demonstrate the rearrangement reactions can generate $[b_n + \text{H}_2^{18}\text{O}]$ product ion containing labeled oxygen in the MS/MS spectra of protonated or cationized peptides. On the other hand, Fang et al. (2000) showed that the formation of novel rearranged product ions designated as $[b_{n-1} + \text{H}_2\text{O}]$ for serine- or threonine-containing bradykinin and its synthetic derivatives in MALDI-TOF post-source decay (PSD) analysis.

¹This chapter is published as: Atik, A. E. and Yalcin, T. “*Protonated Dipeptide Losses from b_5 and b_4 Ions of Side Chain Hydroxyl Group Containing Pentapeptides*” *J. Am. Soc. Mass Spectrom.* **2013**, 24, 1543-1554.

The authors demonstrated that the hydroxyl group was transferred to the neighboring residue's carbonyl group, which led to a loss of the C-terminal end of the peptide. Similarly, it has been documented that the $[b_1 + \text{H}_2\text{O}]$ product ion was formed via rearrangement reaction for the dipeptides containing lysine, arginine, and histidine residues located at the N-terminal position (Hiserodt et al. 2007). Farrugia and O'Hair (2003) have reported the importance of salt-bridge (SB) intermediate formation that yields $[b_n + \text{H}_2\text{O}]$ product ion by a charge-directed mechanism in mass spectra of protonated arginine containing dipeptides. In addition, Gonzalez et al. (1996) emphasized the effect of the position of arginine residue within a series of synthetic tetra- to heptapeptides for the formation of $[b_{n-1} + \text{H}_2\text{O}]$ product ion through C-terminal rearrangement reaction.

In this work, the gas-phase fragmentation behaviors of b_5 and b_4 ions originated from XGGFL-NH₂ and AXVYI-NH₂, where X is serine (S), threonine (T), glutamic acid (E), aspartic acid (D), or tyrosine (Y) residue, are reported. The common feature of these five amino acid residues is that they contain a hydroxyl group (–OH) on their side chains.

6.2. Experimental

The synthetic C-terminal amidated model pentapeptides, such as SGGFL-NH₂, S_{Me}GGFL-NH₂ (methylation on the side chain of serine), TGGFL-NH₂, EGGFL-NH₂, E_{OMe}GGFL-NH₂ (methylation on the side chain of glutamic acid), DGGFL-NH₂, YGGFL-NH₂, ASVYI-NH₂, ATVYINH₂, AEVYI-NH₂, ADVYI-NH₂, and AYVYI-NH₂ and free acid forms of dipeptides, such as FL-OH, LF-OH, GFOH, FG-OH, YI-OH, IY-OH, VY-OH, and YV-OH were obtained from GL Biochem Ltd. (Shanghai, China) and used without further purification. Approximately 2 mg of each solid peptide was dissolved in 1:1 (vol/vol) mixture of HPLC-grade methanol and deionized water to make stock solutions with a concentration of 10^{-3} or 10^{-4} M.

All tandem mass spectrometry (MSⁿ) experiments were conducted on a LTQ XL linear ion-trap mass spectrometer (Thermo Finnigan, San Jose, CA, USA) equipped with an electrospray ionization (ESI) source. The stock peptide samples were diluted to a 100 pmol μL^{-1} in 50:50:1 (vol/vol/vol) MeOH/H₂O/HCOOH and introduced via infusion at a flow rate of 5 $\mu\text{L min}^{-1}$ with an incorporated syringe pump. The ion optics

(multipoles, lens voltages, etc.) were optimized in order to obtain maximal precursor ion transmission into the trap. The scan range was from m/z 150 to 700 in the positive-ion mode for all MSⁿ stages, and at least 400 scans were averaged in profile mode. Spray voltage was set at + 5.0 kV, and the heated capillary (desolvation) temperature was maintained at 275 °C. Nitrogen gas was used as a sheath, a sweep, and an auxiliary gas during the experiments, whereas helium was introduced into the system for both as the collision gas and as a damping gas. The capillary voltage was kept at 20 V. The mass isolation window (m/z) was varied between 1.6 and 2.2 for MSⁿ acquisitions in order to isolate a single and the most abundant precursor ion. The activation time was set to 30 ms at each CID stage using an activation (q) of 0.250 and the normalized collision energy was varied from 18 % to 28 % for the dissociation of selected precursor ion. Data acquisition was carried out with Xcalibur (ver. 2.0) software data system.

6.3. Results and Discussion

6.3.1. The Formation of m/z 279 Fragment Ion in the b_5 Ion Mass Spectra of XGGFL-NH₂ (where X is S, T, E, D, or Y)

The CID mass spectra of the b_5 ions obtained from SGGFL-NH₂, TGGFL-NH₂, EGGFL-NH₂, DGGFL-NH₂, and YGGFL-NH₂ peptides were studied separately via low-energy CID-MS³ ($[M + H]^+ \rightarrow b_5$) consecutive experiments. The fragment ion at m/z 279 appeared in all b_5 ion mass spectra as a common peak. In Table 6.1, the relative intensities of the m/z 279 fragment ions originated from each b_5 ion are listed.

Table 6.1. Relative intensities of m/z 279 and m/z 223 fragments in the CID mass spectra of b_5 and b_4 ions from XGGFL-NH₂ model peptides, respectively

Peptide	Relative Intensity (%)	
	m/z 279	m/z 223
SGGFL-NH ₂	7.23	2.51
TGGFL-NH ₂	10.3	0.440
EGGFL-NH ₂	0.586	100
DGGFL-NH ₂	0.266	0.852
YGGFL-NH ₂	0.00659	not detected

As a representation, the CID mass spectrum of the b_5 ion derived from SGGFL-NH₂ (SGGFL_{oxa}, m/z 462) is shown in Figure 6.1a. The m/z 279 fragment ion was detected with a relative intensity of 7.23 % to the base peak of b_5 -H₂O (denoted as b_5^o).

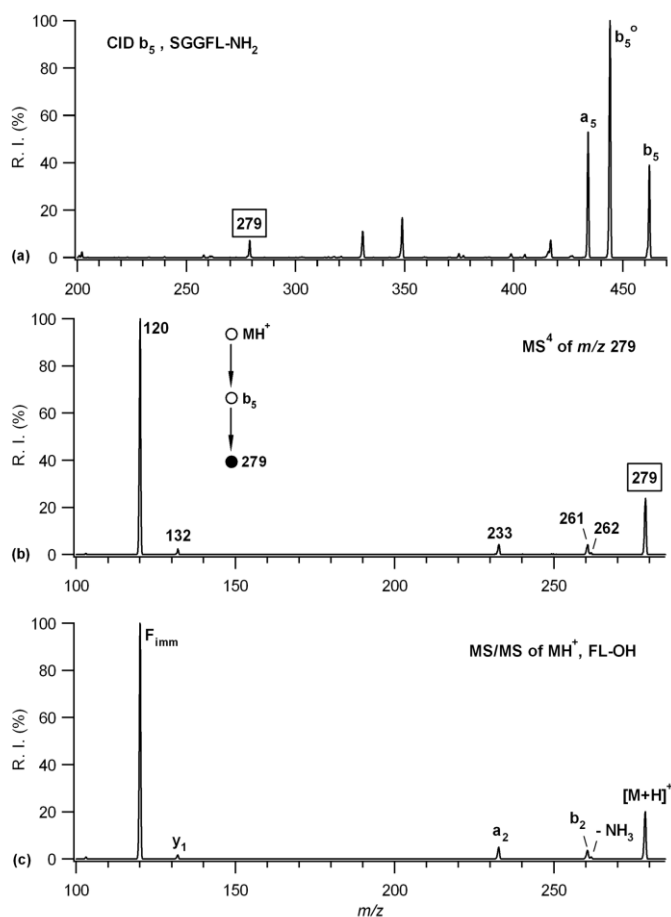


Figure 6.1. (a) MS³ mass spectrum of b_5 ion from protonated SGGFL-NH₂, (b) MS⁴ mass spectrum of m/z 279 ion from b_5 ion of protonated SGGFL-NH₂, (c) MS² mass spectrum of $[M + H]^+$ ion from protonated FL-OH

The MS⁴ ($[M + H]^+ \rightarrow b_5 \rightarrow 279$) consecutive experiments were conducted for the m/z 279 fragment ion in order to elucidate its gas-phase fragmentation pattern as well as the structure through CID. The CID-MS⁴ spectrum (see Figure 6.1b) is dominated by the product ion at m/z 120 with weak intensities of the ions at m/z 132, 233, 261, and 262. The strong m/z 120 product ion is an evidence for the presence of phenylalanine (phenylalanine immonium) within the sequence of m/z 279 ion (Ambihapathy et al. 1997) and the ion at m/z 132 could be accepted as an evidence of protonated leucine. Therefore, it could be concluded that phenylalanine (F) and leucine

(L) amino acid residues are dissociated together in the form of protonated dipeptide from b_5 ion. The source of the water molecule is thought to be the side chain of serine residue. In order to confirm our proposal, the MS/MS spectra of $[M + H]^+$ ion produced from FL-OH and LF-OH dipeptides (both of them have the same molecular mass) were recorded and compared with the MS⁴ spectrum of the m/z 279 fragment ion. Figure 6.1b and c clearly show that the MS/MS spectrum of $[M + H]^+$ ion of FL-OH yields entirely the same fragment ions with the same relative intensities to that originated from the m/z 279 fragment ion derived from b_5 ion of SGGFL-NH₂. In contrast, the fragmentation behavior of LF-OH is totally different from that of m/z 279 ion (the product ion mass spectrum of $[M + H]^+$ ion is shown in Appendix C). Therefore, the sequence of m/z 279 fragment ion is verified as a protonated FL-OH dipeptide because of the completely identical fragmentation behaviors under the same CID conditions. Additionally, the product ions at m/z 132, 233, and 261 correspond to the y_1 , a_2 , and b_2 , respectively, whereas the ion at m/z 262 was assigned as ammonia loss ($-NH_3$) from protonated FL-OH.

Each m/z 279 fragment ion was selected from b_5 ions of TGGFL-NH₂, EGGFL-NH₂, DGGFL-NH₂, and YGGFLNH₂ peptides individually and allowed to dissociate under the same experimental conditions in an ion trap mass spectrometer. As depicted in Figure 6.2, the similar fragmentation patterns were obtained in all m/z 279 ion's mass spectra which are also the same as the MS/MS spectrum of protonated FL-OH. However, the only difference in the leucine-enkephalin (YGGFL-NH₂) peptide is that the m/z 132 ion was not detected in the MS⁴ spectrum of m/z 279 fragment ion. These results clearly demonstrate that the sequence of m/z 279 ions originated from each protonated b_5 ions of XGGFL-NH₂ (where X is S, T, E, D, or Y) are protonated FL-OH.

The water losses from the side chain of hydroxyl group containing amino acid residues have been extensively investigated by several groups (Ballard and Gaskell 1993, Harrison and Yalcin 1997, O'Hair and Reid 1999, Reid et al. 2000, Serafin et al. 2004, Paizs and Suhai 2005, Neta et al. 2007, Harrison 2012). In line with these works, a possible mechanism for the formation of m/z 279 fragment ion from protonated b_5 ion of SGGFL-NH₂ is proposed (Figure 6.3). After proton transfer (P.T.) and rearrangement reaction, a water molecule can migrate to the C-terminal oxazolone ring, giving rise to form an intermediate internal complex. The complex was then dissociated to yield protonated FL-OH (m/z 279) in the gas phase. Note that the internal complex can follow

two competing dissociation paths: either charge retention on the N- or C-terminal resulting in the formation of m/z 184 or m/z 279 fragment ions.

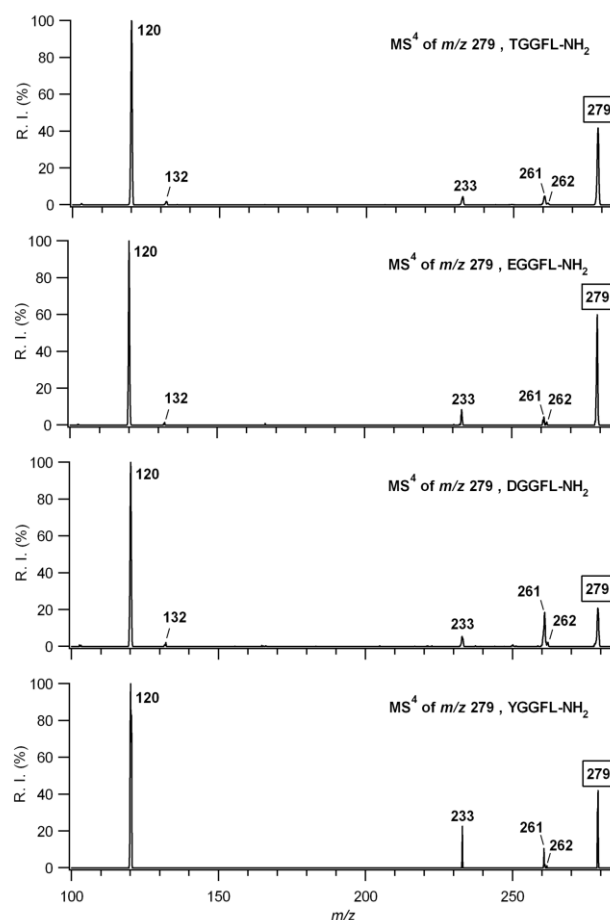


Figure 6.2. Comparison of the MS⁴ mass spectra of m/z 279 fragment ions originated from protonated TGGFL-NH₂, EGGFL-NH₂, DGGFL-NH₂, and YGGFL-NH₂, respectively

The same mechanism is also acceptable for the formation of the m/z 279 fragment ion from the b_5 ions of XGGFL-NH₂ (where X is T, E, or D) pentapeptides. It should be mentioned that the b_5 ion of YGGFL-NH₂ solely follows path 1 after dissociation of internal complex. Additionally, the possible fragmentation channel has very low contribution for the formation of m/z 279 fragment ion in the dissociation of the b_5 ion of YGGFL-NH₂ (see Table 6.1). The phenolic hydrogen is not acidic enough and this is the reason of why leu-enkephalin did not show strong protonated dipeptide elimination compare to others (Harrison and Yalcin 1997).

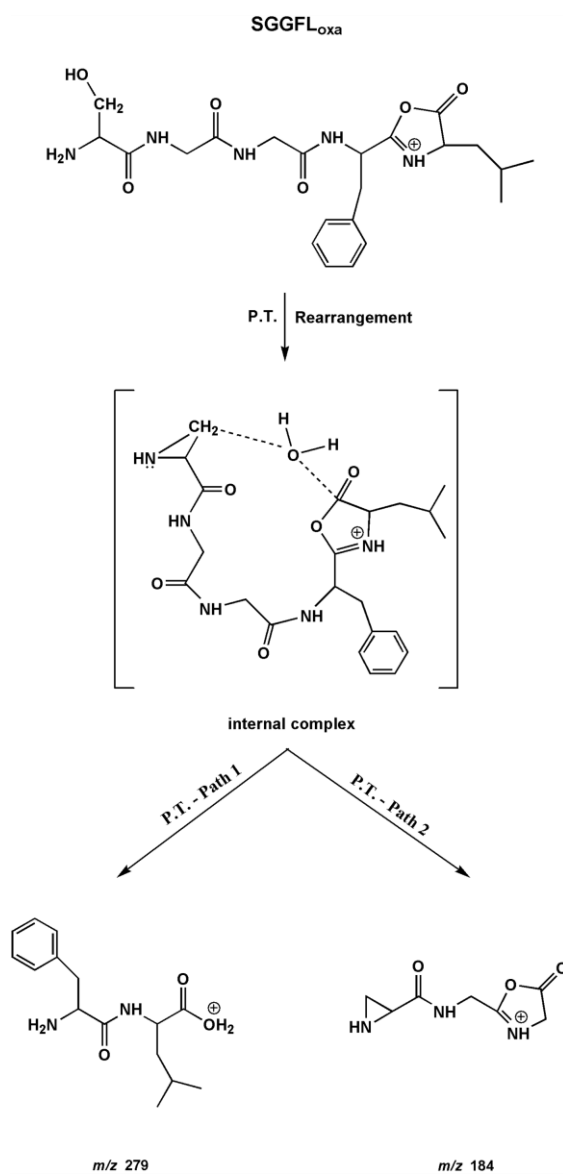


Figure 6.3. The possible mechanism for the formation of either m/z 279 or 184 fragment ions from the b_5 ion of SGGFL-NH₂

In order to emphasize the involvement of side chain hydroxyl group for the proposed mechanism, the side chain methylated serine containing pentapeptide, S_{Me}GGFL-NH₂, has been used. It is apparent that (see Figure 6.4) the m/z 279 fragment ion is not detected in the b_5 ion CID mass spectrum which is the direct evidence for migration of hydroxyl group from the side chain of serine residue to the C-terminal oxazolone ring.

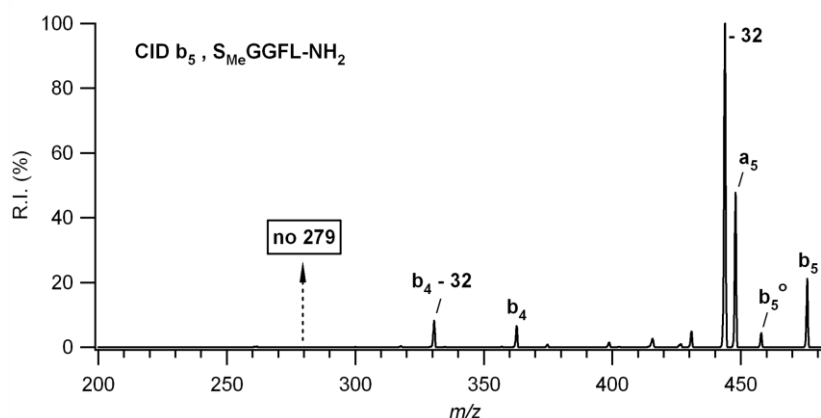


Figure 6.4. The MS³ mass spectrum of *b*₅ ion from protonated S_{Me}GGFL-NH₂

On the other hand, it has been reported that the *b*₅ ion (or even larger) undergoes head-to-tail cyclization to form a macrocyclic intermediate (Bleiholder et al 2008, Harrison 2008). This macrocyclic structure may re-open at different amide bonds to form various linear *b* isomers. In the current study, the *b*₅ ions derived from XGGFL-NH₂ (where X is S, T, E, D, Y) also form macrocyclic structures which immediately dissociate to generate internal amino acid eliminations from each *b*₅ ion (the *b*₅ ion CID mass spectra of XGGFL-NH₂ peptide case are illustrated in Appendix C). After re-opening of macrocyclic structures, LXGGF_{oxa} *b*₅ isomers may have been formed. In this case, the protonated GF dipeptide losses (*m/z* 223) are expected to be formed in the dissociation of LXGGF_{oxa} isomer via similar proposed fragmentation mechanism above. The *m/z* 223 fragment ion was detected in the dissociation of LSGGF_{oxa}, LTGGF_{oxa}, and LEGGF_{oxa} *b*₅ isomers (with very low relative intensities). Their MS⁴ mass spectra nearly show the same fragmentation pattern of [M + H]⁺ ion produced from GF-OH (spectra not shown).

6.3.2. The Formation of *m/z* 223 Fragment Ion in the *b*₄ Ion Mass Spectra of XGGFL-NH₂ (where X is S, T, E, D, or Y)

In addition to the *b*₅ ions, the *b*₄ ions from the SGGFL-NH₂, TGGFL-NH₂, EGGFL-NH₂, DGGFL-NH₂, and YGGFLNH₂ peptides were studied individually by means of low-energy CID-MS³ consecutive experiments. In this case, the ion at *m/z* 223

was observed in all b_4 ion mass spectra except the YGGFL-NH₂ (leucine-enkephalin). The relative intensities of the m/z 223 fragment ions are summarized in Table 6.1.

The CID mass spectrum of b_4 ion (EGGF_{oxa}, m/z 391) originated from EGGFL-NH₂ is shown in Figure 6.5a. It is clear to see that the m/z 223 fragment ion is the most abundant peak in the mass spectrum. In order to identify the gas-phase structure of this fragment ion, the MS⁴ ($[M + H]^+ \rightarrow b_4 \rightarrow 223$) consecutive experiments were probed in an ion trap mass spectrometer. The CID mass spectrum of m/z 223 fragment ion contains the product ions at m/z 166, 177, and 205 as the major peaks with a weak intensity of m/z 120 (Figure 6.5b). The ions at m/z 166 and 120 correspond to the masses of protonated phenylalanine residue and its immonium ion, respectively. Hence, it can be assumed that glycine (G) and phenylalanine (F) residues are dissociated together as a protonated dipeptide form from the b_4 ion.

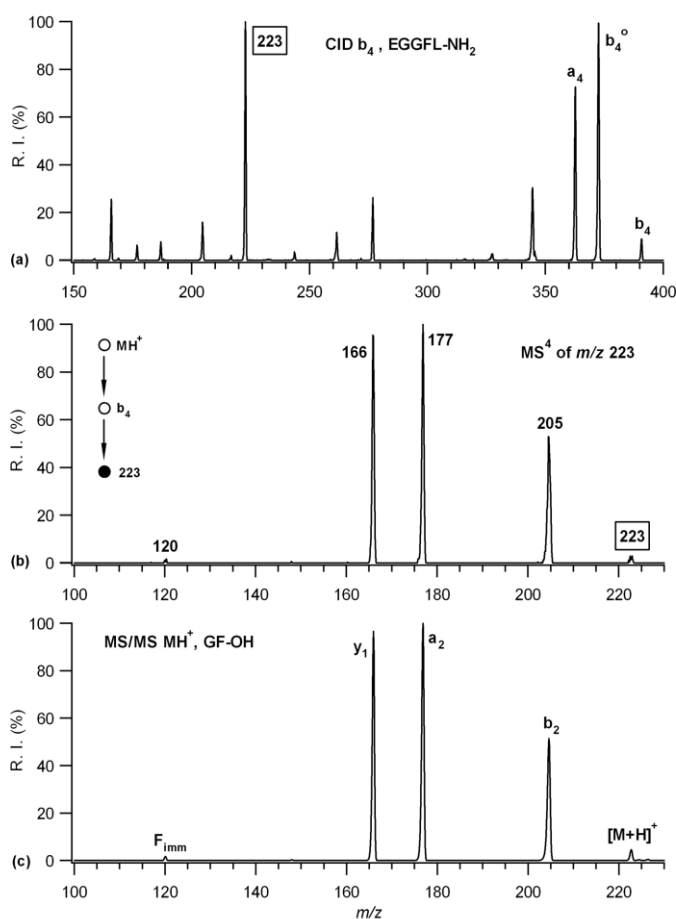


Figure 6.5. (a) MS³ mass spectrum of b_4 ion from protonated EGGFL-NH₂, (b) MS⁴ mass spectrum of m/z 223 ion from b_4 ion of protonated EGGFL-NH₂, (c) MS² mass spectrum of $[M + H]^+$ ion from protonated GF-OH

To verify the sequence of protonated m/z 223 ion, the $[M + H]^+$ ion MS/MS spectra of GF-OH and FG-OH dipeptides were recorded and the resultant MS/MS spectra were compared with the MS⁴ spectrum of the m/z 223 fragment ion. The two spectra in Figure 6.4b and c clearly exhibit that the sequence of m/z 223 fragment ion originated from the b_4 ion of EGGFL-NH₂ is identical to the MS/MS spectrum of protonated GF-OH. The products at m/z 120, 166, 177, and 205 refer to the phenylalanine immonium Fimm, y_1 , a_2 , and b_2 ions, respectively. In contrast, the fragmentation behavior of FG-OH is totally different from that of m/z 223 ion (mass spectrum is shown in Appendix C).

The m/z 223 fragment ions that originated from the b_4 ions of the SGGFL-NH₂, TGGFL-NH₂, and DGGFL-NH₂ peptides were also studied under the same fragmentation conditions. Similar fragmentation patterns (the same peaks with similar intensities) were obtained (shown in Figure 6.6) and were also comparable to the dissociation products of the protonated GF-OH. However, the relatively low intensity of m/z 120 product ion was not detected in the m/z 223 ion's MS⁴ mass spectra of TGGFL-NH₂ and DGGFL-NH₂.

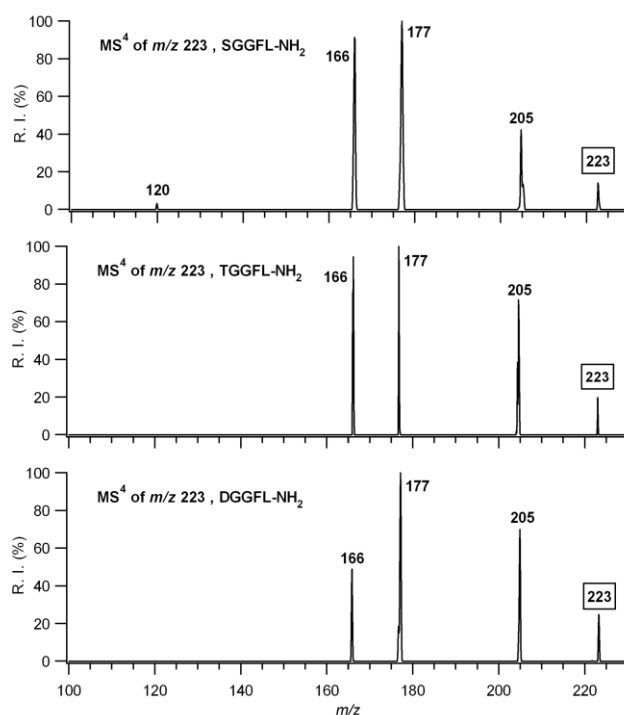


Figure 6.6. Comparison of the MS⁴ mass spectra of m/z 223 fragment ions originated from protonated SGGFL-NH₂, TGGFL-NH₂, and DGGFL-NH₂, respectively

The glutamic and aspartic acid residues have been known to lose water through gas-phase dissociation reactions because of the presence of a hydroxyl group on their side chains (Ballard and Gaskell 1993, Harrison and Yalcin 1997, Paizs and Suhai 2005). In line with these reference works, a possible mechanism for the formation of m/z 223 fragment ion from the b_4 ion of EGGFL-NH₂ is proposed (Figure 6.7).

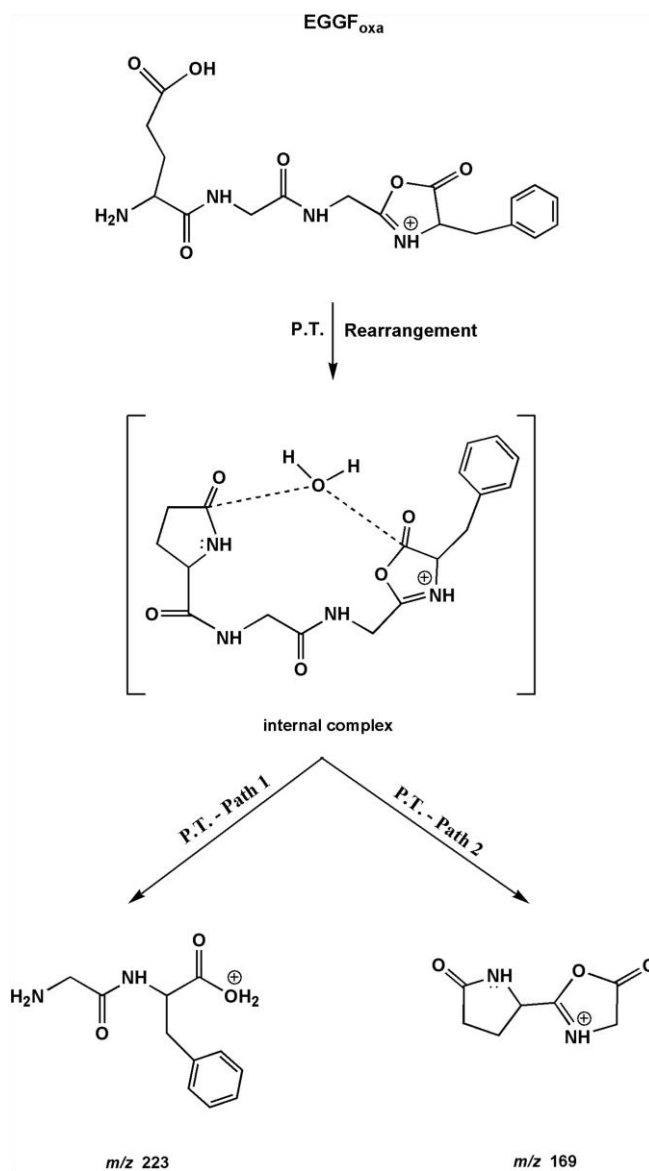


Figure 6.7. The possible mechanism for the formation of either m/z 223 or 169 fragment ions from the b_4 ion of EGGFL-NH₂

In this case, two competitive dissociation pathways of internal complex are only valid for the b_4 ion of the EGGFL-NH₂ peptide (SGGF_{oxa}, TGGF_{oxa}, and DGGF_{oxa} b_4 ions may not follow the second pathway via fragmentation of internal complex).

To gain further evidence of side chain hydroxyl group migration to the C-terminal oxazolone ring, the side chain methylated glutamic acid containing pentapeptide, E_{OMe}GGFL-NH₂, was used. The CID mass spectrum of *b*₅ ion clearly showed that the *m/z* 223 fragment ion is not observed methylated peptide (Figure 6.8).

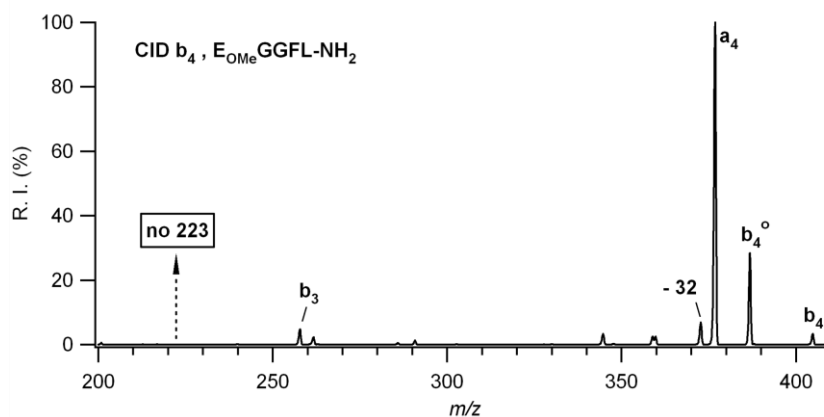


Figure 6.8. The MS³ mass spectrum of *b*₄ ion from protonated E_{OMe}GGFL-NH₂

6.3.3. The Formation of *m/z* 295 Fragment Ion in the *b*₅ Ion Mass Spectra of AXVYI-NH₂ (where X is S, T, E, D, or Y)

The *b*₅ ions that originated from ASVYI-NH₂, ATVYI-NH₂, AEVYI-NH₂, ADVYI-NH₂, and AYVYI-NH₂ were isolated via MS³ ([M + H]⁺ → *b*₅) experiments individually and allowed to dissociate under low-energy CID conditions. The fragment ion at *m/z* 295 was observed in all *b*₅ ion mass spectra as a common peak, and the relative intensities of the *m/z* 295 fragment ions are tabulated in Table 6.2.

Table 6.2. Relative intensities of *m/z* 295 and *m/z* 281 fragments in the CID mass spectra of *b*₅ and *b*₄ ions from AXVYI-NH₂ model peptides, respectively

Peptide	Relative Intensity (%)	
	<i>m/z</i> 295	<i>m/z</i> 281
ASVYI-NH ₂	2.04	0.818
ATVYI-NH ₂	0.173	1.11
AEVYI-NH ₂	0.0795	0.234
ADVYI-NH ₂	0.268	0.0658
AYVYI-NH ₂	0.0227	not detected

Figure 6.9a shows the CID mass spectrum of the b_5 ion (ASVYI_{oxa}, m/z 534) obtained from ASVYI-NH₂ pentapeptide and the relative intensity of m/z 295 fragment ion is 2.04 % compared with the base peak of b_5^0 .

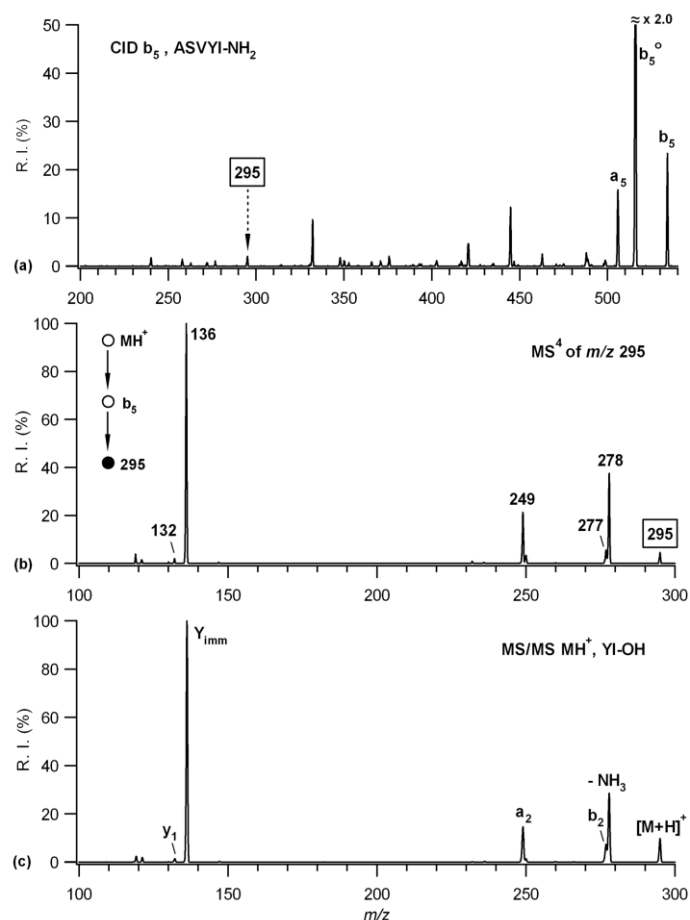


Figure 6.9. (a) MS³ mass spectrum of b_5 ion from protonated ASVYI-NH₂, (b) MS⁴ mass spectrum of m/z 295 ion from b_5 ion of protonated ASVYI-NH₂, (c) MS² mass spectrum of $[M + H]^+$ ion from protonated YI-OH

To elucidate the gas-phase structure of m/z 295, the detailed MS⁴ ($[M + H]^+ \rightarrow b_5 \rightarrow 295$) consecutive experiments were performed. As depicted in Figure 6.9b, the MS⁴ spectrum contains the product ions at m/z 132, 136, 249, 277, and 278 in which the highest relative abundance is observed for the m/z 136. It is well known that the m/z 136 represents the tyrosine immonium ion's mass and it provides evidence for the presence of tyrosine residue in the sequence of m/z 295. Additionally, the ion at m/z 132 can be accepted as a protonated isoleucine. As a similar mechanism described above, the tyrosine (Y) and isoleucine (I) amino acid residues are dissociated together in the form of protonated dipeptide from b_5 ion. Again, the source of water

comes from the side chain of serine residue. To confirm the sequence of protonated fragment ion, the $[M + H]^+$ ions of YI-OH and IY-OH dipeptides were further examined by CID MS/MS experiments. The resulting $[M + H]^+$ product ion mass spectrum of YI-OH and the MS⁴ spectrum of the m/z 295 fragment ion show entirely the same fragmentation behavior via CID (shown in Figure 6.9b and c). The mass spectra provide evidence that these ions are structurally identical in the gas phase. The products at m/z 132, 136, 249, 277, and 278 are assigned to y_1 , Y_{imm} , a_2 , b_2 , and $[M + H - NH_3]^+$ ions, respectively. On the contrary, the fragmentation behavior of IY-OH is totally different from that of m/z 295 ion (see Appendix C).

The MS⁴ consecutive experiments were also carried out separately for each m/z 295 fragment ion derived from the b_5 ions of ATVYI-NH₂, AEVYI-NH₂, ADVYI-NH₂, and AYVYI-NH₂. As Figure 6.10 displays, the obtained fragmentation patterns are remarkably alike compared with the fragmentation products of YI-OH. However, the only difference is the absence of the m/z 277 ion in the MS⁴ spectrum of the m/z 295 fragment ion derived from AYVYI-NH₂. As a consequence of identical fragmentation behaviors, it has been confirmed that the sequence of the m/z 295 fragment ions obtained from b_5 ions of AXVYI-NH₂ (where X is S, T, E, D, or Y) have a sequence of protonated dipeptide, YI-OH.

The possible fragmentation mechanism for the formation of the m/z 295 fragment ion is similar to Figure 6.3, and the two competitive dissociation pathways are valid for all b_5 ions after dissociation of internal complex (figure not shown).

Additionally, the b_5 ions originated from AXVYI-NH₂ undergo macrocyclization reaction followed by ring opening at various positions to form linear oxazolones, which generate internal amino acid losses in the product ion mass spectra (see Appendix C). Similar to the mechanism for original sequence, the m/z 203 fragment ions (IA-OH) were detected with relatively low intensities in the dissociation of permuted SVYIA_{oxa} and EVYIA_{oxa} isomers. The fragmentation patterns of m/z 203 ions and MS/MS spectrum of $[M + H]^+$ ion form IA-OH dipeptide are similar (spectra not shown).

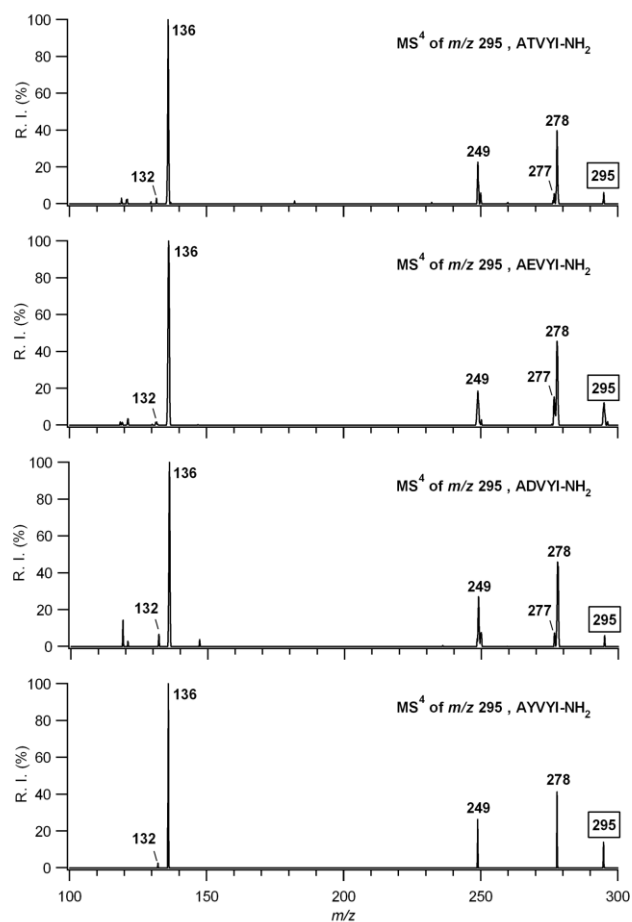


Figure 6.10. Comparison of the MS⁴ mass spectra of *m/z* 295 fragment ions originated from protonated ATVYI-NH₂, AEVYI-NH₂, ADVYI-NH₂, and AYVYI-NH₂, respectively

6.3.4. The Formation of *m/z* 281 Fragment Ion in the *b*₄ Ion Mass Spectra of AXVYI-NH₂ (where X Is S, T, E, D, or Y)

Similar to the *b*₅ ions, the *m/z* 281 fragment ion was generated in all the *b*₄ ion mass spectra of ASVYI-NH₂, ATVYI-NH₂, AEVYI-NH₂, and ADVYI-NH₂ pentapeptides with different relative intensities (Table 6.2). Figure 6.11a displays the CID mass spectrum of the *b*₄ ion (ATVY_{oxa}, *m/z* 435) originated from the ATVYI-NH₂ pentapeptide. In the mass spectrum, the *m/z* 281 fragment ion was detected with a relative intensity of 1.11 % compared with the base peak of *b*₅⁰. The MS⁴ ([M + H]⁺ → *b*₄ → 281) consecutive experiments were performed for this fragment ion to obtain its gas-phase structure under low-energy CID conditions.

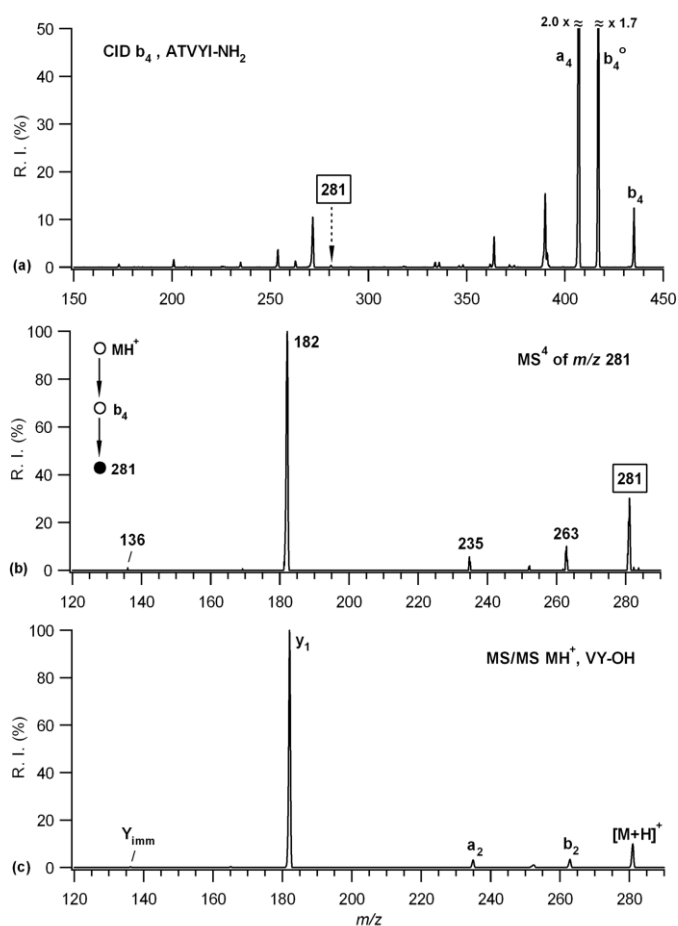


Figure 6.11. (a) MS³ mass spectrum of *b*₄ ion from protonated ATVYI-NH₂, (b) MS⁴ mass spectrum of *m/z* 281 ion from *b*₄ ion of protonated ATVYI-NH₂, (c) MS² mass spectrum of [M+H]⁺ ion from protonated VY-OH

As Figure 6.11b illustrates, the CID-MS⁴ spectrum contains an abundant product ion at *m/z* 182, whereas the *m/z* 136, 235, and 263 product ions have minor intensities in the mass spectrum. The ions at *m/z* 182 and 136 entirely reflect the masses of protonated tyrosine residue and immonium ion, respectively. Hence, the valine (V) and tyrosine (Y) residues are dissociated together as a protonated dipeptide form from the *b*₄ ion. To verify this proposal, the VY-OH and YV-OH dipeptides were used, and their [M + H]⁺ ion was selected separately and allowed to fragment in the gas phase. The MS/MS spectrum of [M + H]⁺ ion of VY-OH was identical to that obtained from the *m/z* 281 ion (Figure 6.11b and c). The comparison of these two mass spectra proves that the *m/z* 281 fragment ion has a sequence of VY-OH. The product ions at *m/z* 136, 182, 235, and 263 represent the *Y*_{imm}, *y*₁, *a*₂, and *b*₂ ions, respectively. By contrast, the product ion mass spectrum of YV-OH is totally different than the ion at *m/z* 281 and its [M + H]⁺ ion CID mass spectrum is shown in Appendix C.

Each m/z 281 fragment ion obtained from the b_4 ions of ASVYI-NH₂, AEVYI-NH₂, and ADVYI-NH₂ was isolated individually and subjected to CID for further fragmentation. The results obtained from each MS⁴ spectrum indicate that the sequence of the m/z 281 fragment ion is a protonated VY-OH (Figure 6.12). However, the relatively low intensity of Y_{imm} ion was not detected in all three mass spectra. On the other hand, the m/z 281 fragment ion could not be observed in the b_4 ion mass spectrum of AYVYI-NH₂ peptide. The possible mechanism for the formation of the m/z 281 fragment ion is similar to the other mechanisms described above. Moreover, only b_4 ions of AEVY_{oxa} and ADVY_{oxa} follow two competitive dissociation pathways after the dissociation of the internal complex (figure not shown).

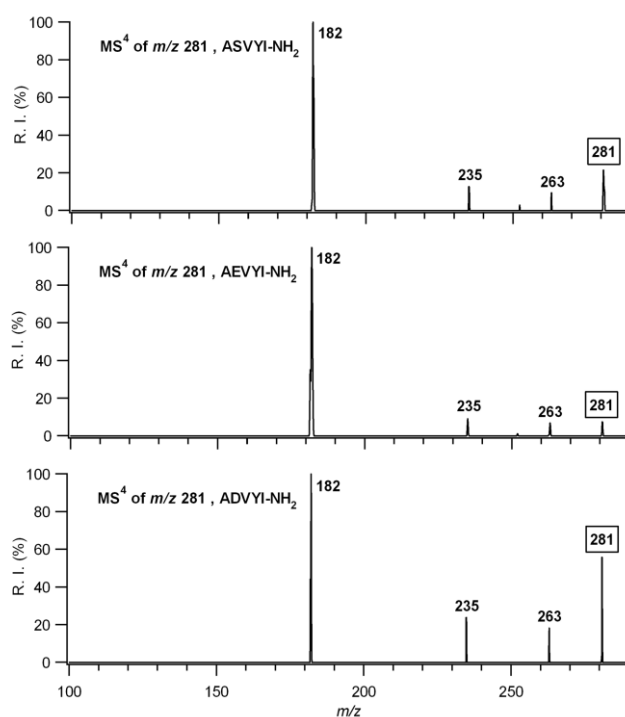


Figure 6.12. Comparison of the MS⁴ mass spectra of m/z 281 fragment ions originated from protonated ASVYI-NH₂, AEVYI-NH₂, and ADVYI-NH₂, respectively

CHAPTER 7

CONCLUSION

In the present study, the gas-phase fragmentation studies of *b* ions obtained from protonated model peptides are investigated in detail using ESI-MS. The results of this dissertation can be divided into four parts.

In Chapter 3, a systematic study is carried out to examine the effects of acidic amino acid residues, either glutamic (E) or aspartic acid (D), and the position of the acidic group on the macrocyclization of *b* ions. The CID mass spectra of *b*₇ ions produced from C-terminal amidated model heptapeptides XAAAAAA, AXAAAAA, AAXAAAA, AAAXAAA, AAAAXAA, AAAAAXA, and AAAAAAX (X is E or D) exhibits completely identical fragmentation patterns. Similarly, the fragmentation patterns of *b*₈ ions derived from C-terminal amidated model octapeptides containing adjacent acidic residues, namely XXAAAAAA, AAXXAAAA, AAAAXX, and AAAAAAXX (X is E or D), are essentially the same. These results reveal that neither the presence nor the positions of acidic residues in hepta- and octapeptides prevents *b*-type sequence scrambling, at least when these model peptides series are used. The side chains of the glutamic and aspartic acid residues do not inhibit the head-to-tail cyclization of *b* ions. In addition, the *b* ion spectra derived from the peptides become more complex as the number of acidic residues in the peptides increases.

On the other hand, the sequence scrambling chemistry of *b* ions originated from YAGFLV peptide series show differences compared to alanine series. The product ion mass spectra for *b*₇ ions of C-terminal amidated EYAGFLV and YAGFLVE heptapeptides are identical. However, the fragmentation pattern of *b*₇ obtained from YAGEFLV differs from other mass spectra. They both have non-direct sequence ions in their mass spectra but their relative intensities are different. Such difference is also recorded for aspartic acid containing peptide serie. These aspects can be explained the neighboring effect of amino acids next to acidic residues and the sequence of the studied peptide sequence.

Moreover, breakdown graphs show that non-direct sequence ions are not very abundant during the fragmentation of the $[M + H]^+$ ions derived from all of the above peptides, hence they do not complicate the $[M + H]^+$ ion mass spectra very much.

Finally, the preferential cleavage of glutamic or aspartic acid residues from macrocyclic structures of *b* ions is also investigated under various collision energy conditions. The results demonstrate that the order of acidic residue loss is changed by varying the collision energy for the hepta- and octapeptide series. To the best of our knowledge, this is the first detailed study where peptides containing acidic residue(s) have been investigated to explain the macrocyclic structures of *b* ions.

Chapter 4 demonstrates the effects of amine group ($-\text{NH}_2$) located on the side chains of lysine (K), glutamine (Q), or asparagine (N) residue on the macrocyclization of *b* ions even though the N-terminals of the peptides are acetylated. The non-direct sequence ions are still observed in the b_7 ion CID mass spectrum of Ac-KYAGFLVG. In contrast, the macrocyclization reaction is not occurred for Ac-QYAGFLV-NH₂ and Ac-NYAGFLV-NH₂ peptides. The obtained results indicate that the ϵ -amine group of a lysine residue have induced macrocyclization of *b* ion for N-terminal acetylated peptide and this novel reaction pathway is named as side-to-tail cyclization. However, the presence of amide structure on the side chains of glutamine and asparagine residues greatly reduces the nucleophilicity of amine groups; therefore the scrambled *b* ions are not detected in their b_7 ion CID mass spectra.

In addition, the positional effect of the lysine residue in the octapeptides is also studied for the side-to-tail cyclization reaction. The MS³ experiments show that the intensities of non-direct sequence ions are drastically reduced as the lysine residue is shifted into the second and any other internal positions. The extent of macrocyclic structure formation affected by a bulky group near to the lysine residue whose ϵ -amine group can rationalize the macrocyclization, that's the reason for dramatic reduce in intensities of non-direct sequence ions.

Chapter 5 discusses the fragmentation behaviors of b_n ($n = 4-7$) ions derived from side chain acetylated lysine residue containing model peptides are investigated by means of low-energy CID experiments. For K_{Ac}YAGFLVG model peptide sequence, the protonated YAGFLV-NH₂ (m/z 668), YAGFL-NH₂ (m/z 569), YAGF-NH₂ (m/z 456), and YAG-NH₂ (m/z 309) fragment ions are formed in the dissociation of b_7 , b_6 , b_5 , or b_4 ion, respectively. However, these fragments are not detected in the CID mass spectra of b_n ($n = 4-7$) ions derived from Ac-KYAGFLVG (N-terminal acetylated), Ac-K_{Ac}YAGFLVG (doubly acetylated), or KYAGFLV-NH₂ (unmodified) sequences. It is clearly demonstrated that acetylation of the lysine side chain promotes the formation of rearranged ions through dissociation of b_n ($n = 4-7$) ion series. The

mechanism for the formation of these fragments can only be achieved by macrocyclization and ring opening process of b ions followed by re-location of the acetylated lysine at the C-terminal end of the peptide. Then, the N-terminal of the peptide is cleaved to give rise a protonated C-terminal amidated peptide.

Additionally, the effect of acetylated lysine position for the formation of rearranged structure is examined using $\text{YAK}_{\text{Ac}}\text{GFLVG}$ model peptide. For this sequence, the protonated GFLVYA-NH_2 (m/z 668), GFLYA-NH_2 (m/z 569), GFYA-NH_2 (m/z 456), and GYA-NH_2 (m/z 309) fragment ions are obtained in the dissociation of b_n ($n = 4-7$) ions, respectively.

In Chapter 6, the C-terminal protonated dipeptide losses are reported in the dissociation of the b_5 and b_4 ions of pentapeptides containing side chain hydroxyl group ($-\text{OH}$) residues. The protonated FL-OH (m/z 279) and GF-OH (m/z 223) dipeptide eliminations are generated with different relative intensities in the dissociations of all the b_5 and b_4 ions (except the b_4 ion of YGGFL-NH_2), respectively, for the XGGFL-NH_2 (where X is S, T, E, D, or Y) model peptide series. Similarly, the protonated YI-OH (m/z 295) and VY-OH (m/z 281) dipeptide losses have been detected in the dissociations of all the b_5 and b_4 ions (except the b_4 ion derived from AYVYI-NH_2), respectively, derived from the AXVYI-NH_2 (where X is S, T, E, D, or Y) model peptides. The sequences of these fragment ions are verified by comparing the MS/MS fragmentation behavior of the $[\text{M} + \text{H}]^+$ ions of commercial dipeptides, namely FL-OH , GF-OH , YI-OH , and VY-OH , via low-energy CID. It should be noted that the m/z 223 and m/z 281 fragment ions are not detected in the b_4 ion mass spectra of YGGFL-NH_2 and AYVYI-NH_2 , respectively. Similarly, the relative intensities of m/z 279 and 295 fragment ions are remarkably low (below 0.03 %) in the dissociation of the b_5 ions of YGGFL-NH_2 and AYVYI-NH_2 , respectively. The reason could be explained as the phenolic hydrogen behavior. It is known that phenolic hydrogen is not acidic enough in the gas-phase and that is why tyrosine-containing peptides do not show strong protonated dipeptide elimination compared to others. These eliminations clearly demonstrate that a novel rearrangement reaction takes place through gas-phase fragmentation of the b_5 and b_4 ions from hydroxyl side chain containing pentapeptides.

To assign the correct and reliable peptide sequences, which is required for high-throughput proteomic studies, is only achieved with the knowledge of peptide fragmentation chemistry in the gas-phase. The results reported in the Chapter 3 and 4 provide better understanding of macrocyclization reaction of b ions, in terms of acidic

amino acid and N-terminal acetylated lysine containing peptides, respectively. Additionally, the novel eliminations shown in the Chapter 5 and 6 can be useful in order to deduce the sequence of peptides. Future works of this study will be gas-phase fragmentation studies of *a* ions which will positively affect correct protein identification. In addition, the negative ion fragmentation of the deprotonated peptides needs to be studied in detail.

REFERENCES

- Aebersold, R. and Goodlett, D. R. Mass Spectrometry in Proteomics. *Chem. Rev.* **2001**, *101*, 269-295.
- Alikhanov, S. G. A New Impulse Technique for Ion Mass Measurement. *J. Exp. Theor. Phys.* **1957**, *4*, 452-453.
- Ambihapathy, K.; Yalcin, T.; Leung, H.; Harrison, A. G. Pathways to Immonium Ions in the Fragmentation of Protonated Peptides. *J. Mass Spectrom.* **1997**, *32*, 209-215.
- Amini, A.; Dormady, S. J.; Riggs, L.; Regnier, F. E. The Impact of Buffers and Surfactants from Micellar Electrokinetic Chromatography on Matrix-Assisted Laser Desorption Ionization (MALDI) Mass Spectrometry of Peptides: Effect of Buffer Type and Concentration on Mass Determination by MALDI-Time-of-Flight Mass Spectrometry. *J. Chromatogr. A* **2000**, *894*, 345-355.
- Anacleto, J. F.; Pleasance, S.; Boyd, R. K. Calibration of Ion Spray Mass Spectra Using Cluster Ions. *Org. Mass Spectrom.* **1992**, *27*, 660-666.
- Anusiewicz, I.; Jasionowski, M.; Skurski, P.; Simons, J. Backbone and Side-Chain Cleavages in Electron Detachment Dissociation (EDD). *J. Phys. Chem. A* **2005**, *109*, 11332-11337.
- Ardrey, R. E. *Liquid Chromatography-Mass Spectrometry: An Introduction*, John Wiley: London, 2003.
- Arnott, D.; Kottmeir, D.; Yates, N.; Shabanowitz, J.; Hunt, D. F. *Books of Abstracts*, 42nd American Society for Mass Spectrometry Conference, Chicago, May 29 – June 3, 1994; p 470.
- Atik, A. E. and Yalcin, T. A Systematic Study of Acidic Peptides for *b*-Type Sequence Scrambling. *J. Am. Soc. Mass Spectrom.* **2011**, *22*, 38-48.
- Atik, A. E.; Gorgulu, G.; Yalcin, T. The Role of Lysine ϵ -Amine Group on the Macrocyclization of *b* Ions. *Int. J. Mass Spectrom.* **2012**, *316-318*, 84-90.
- Atik, A.E. and Yalcin, T. Protonated Dipeptide Losses from b_5 and b_4 Ions of Side Chain Hydroxyl Group Containing Pentapeptides. *J. Am. Soc. Mass Spectrom.* **2013**, *24*, 1543-1554.
- Bai, J.; Liu, Y. H.; Cain, T. C.; Lubman, D. M. Matrix-Assisted Laser Desorption/Ionization Using an Active Perfluorosulfonated Ionomer Film Substrate. *Anal. Chem.* **1994**, *60*, 3423-3430.

- Ballard, K. D. and Gaskell, S. J. Sequential Mass Spectrometry Applied to the Study of the Formation of "Internal" Fragment Ions of Protonated Peptides. *Int. J. Mass Spectrom. Ion Processes* **1991**, *111*, 173-189.
- Ballard, K. D. and Gaskell, S. J. Intramolecular [¹⁸O] Isotopic Exchange in the Gas Phase Observed During the Tandem Mass Spectrometric Analysis of Peptides. *J. Am. Chem. Soc.* **1992**, *114*, 64-71.
- Ballard, K. D. and Gaskell, S. J. Dehydration of Peptide [M+H]⁺ Ions in the Gas Phase. *J. Am. Soc. Mass Spectrom.* **1993**, *4*, 477-481.
- Barber, M.; Bordoli, R. S.; Sedgewick, R. D.; Tyler, A. N. Fast Atom Bombardment of Solids as an Ion Source in Mass Spectrometry. *Nature* **1981**, *293*, 270-275.
- Beavis, R. C. and Chait, B. T. Cinnamic Acid Derivatives as Matrices for Ultraviolet Laser Desorption Mass Spectrometry of Proteins. *Rapid Commun. Mass Spectrom.* **1989**, *3*, 432-435.
- Beavis, R. C.; Chaudhary, T.; Chait, B. T. α -Cyano-4-Hydroxycinnamic Acid as a Matrix for Matrix-Assisted Laser Desorption Mass Spectrometry. *Org. Mass Spectrom.* **1992**, *27*, 156-158.
- Beckey, H. D. Field Ionization Mass Spectrometry. *Research/Development* **1969**, *20*, 26-29.
- Biemann, K. and Scoble, H. A. Characterization by Tandem Mass Spectrometry of Structural Modifications in Proteins. *Science* **1987**, *237*, 992-998.
- Biemann, K. Contributions of Mass Spectrometry to Peptide and Protein Structure. *Biomed. Environ. Mass Spectrom.* **1988**, *16*, 99-111.
- Biemann, K. Sequencing of Peptides by Tandem Mass Spectrometry and High-Energy Collision-Induced Dissociation. *Meth. Enzymol.* **1990**, *193*, 455-479.
- Black, D. L. Protein Diversity from Alternative Splicing: A Challenge for Bioinformatic and Post-Genome Biology. *Cell* **2000**, *103*, 367-370.
- Blakley, C. R. and Vestal, M. L. Thermospray Interface for Liquid Chromatography/Mass Spectrometry. *Anal. Chem.* **1983**, *55*, 750-754.
- Bleakney, W. A New Method of Positive Ray Analysis and Its Application to the Measurement of Ionization Potentials in Mercury Vapor. *Phys. Rev.* **1929**, *34*, 157-160.
- Bleholder, C.; Osburn, S.; Williams, T. D.; Suhai, S.; Van Stipdonk, M.; Harrison, A. G.; Paizs, B. Sequence-Scrambling Pathways of Protonated Peptides. *J. Am. Chem. Soc.* **2008**, *130*, 17774-17789.

- Boyd, R. and Somogyi, Á. The Mobile Proton Hypothesis in Fragmentation of Protonated Peptides: A Perspective. *J. Am. Soc. Mass Spectrom.* **2000**, *21*, 1275-1278.
- Boyes, J.; Byfield, P.; Nakatani, Y.; Ogryzko, V. Regulation of Activity of the Transcription Factor GATA-1 by Acetylation. *Nature*, **1998**, *396*, 594-598.
- Breci, L. A.; Tabb, D. L.; Yates, J. R. 3rd; Wysocki, V. H. Cleavage N-Terminal to Proline: Analysis of a Database of Peptide Tandem Mass Spectra. *Anal. Chem.* **2003**, *75*, 1963-1971.
- Brown, R. S. and Lennon, J. J. Mass Resolution Improvement by Incorporation of Pulsed Ion Extraction in a Matrix-Assisted Laser Desorption/Ionization Linear Time-of-Flight Mass Spectrometer. *Anal. Chem.* **1995**, *67*, 1998-2003.
- Budnik, B. A.; Haselmann, K. F.; Zubarev, R. A. Electron Detachment Dissociation of Peptide Di-Anions: An Electron-Hole Recombination Phenomenon. *Chem. Phys. Lett.* **2001**, *342*, 299-302.
- Burlet, O.; Yang, C. Y.; Gaskell, S. J. Influence of Cysteine to Cysteic acid Oxidation on the Collision-Activated Decomposition of Protonated Peptides: Evidence for Intraionic Interactions. *J. Am. Soc. Mass Spectrom.* **1992**, *3*, 337-344.
- Busch, K. L.; Glish, G. L.; McLuckey, S. A. *Mass Spectrometry/Mass Spectrometry Techniques and Applications of Tandem Mass Spectrometry*, Wiley: New York, 1988.
- Bythell, B. J.; Somogyi, Á.; Paizs, B. What is the Structure of b_2 Ions Generated from Doubly Protonated Tryptic Peptides? *J. Am. Soc. Mass Spectrom.* **2009**, *20*, 618-624.
- Bythell, B. J.; Erlekam, U.; Paizs, B.; Maître, P. Infrared Spectroscopy of Fragments from Doubly Protonated Tryptic Peptides. *ChemPhysChem* **2009**, *10*, 883-885.
- Bythell, B. J.; Knapp-Mohammady, M.; Paizs, B.; Harrison, A. G. Effect of the His Residue on the Cyclization of b Ions. *J. Am. Soc. Mass Spectrom.* **2010**, *21*, 1352-1363.
- Campbell, J. M.; Collings, B. A.; Douglas, D. J. A New Linear Ion Trap Time-of-Flight System with Tandem Mass Spectrometry Capabilities. *Rapid Commun. Mass Spectrom.* **1998**, *12*, 1463-1474.
- Castaing, R. and Slodzian, G. J. Optique Corpusculaire-Premiers Essais de Microanalyse par Emission Ionique Secondaire. *Microscopie* **1962**, *1*, 395-399.
- Chait, B. T. Mass Spectrometry: Bottom-Up or Top-Down? *Science* **2006**, *314*, 65-66.
- Chapman, J. R. *Mass Spectrometry of Protein and Peptides*, Humana Press: New Jersey, 2000.

- Chen, X. and Turecek, F. Simple *b*-Ions Have Cyclic Structures. A Neutralization-Reionization Mass Spectrometric and Computational Study. *J. Am. Soc. Mass Spectrom.* **2005**, *16*, 1941-1956.
- Chowdhury, S. K.; Katta, V.; Chait, B. T. Probing Conformational Changes in Proteins by Mass Spectrometry. *J. Am. Chem. Soc.* **1990**, *112*, 9012-9013.
- Cleveland, D. W.; Fischer, S. G.; Kirschner, M. W.; Laemmli, U. K. Peptide Mapping by Limited Proteolysis in Sodiumdodecyl Sulfate and Analysis by Gel Electrophoresis. *J. Biol. Chem.* **1977**, *252*, 1102-1106.
- Cody, R. B. and Freiser, B. S. Electron-Impact Excitation of Ions from Organics-Alternative to Collision-Induced Dissociation. *Anal. Chem.* **1979**, *51*, 547-551.
- Cody, R. B.; Burnier, R. C.; Cassady, C. J.; Freiser, B. S. Consecutive Collision-Induced Dissociations in Fourier Transform Mass Spectrometry. *Anal. Chem.* **1982**, *54*, 2225-2228.
- Cody, R. B. and Freiser, B. S. Electron-Impact Excitation of Ions in Fourier Transform Mass-Spectrometry. *Anal. Chem.* **1987**, *59*, 1054-1056.
- Cole, R. B. Some Tenets Pertaining to Electrospray Ionization Mass Spectrometry. *J. Mass Spectrom.* **2000**, *35*, 763-772.
- Comisarow, M. B. and Marshall, A. G. Fourier Transform Ion Cyclotron Resonance Spectroscopy. *Chem. Phys. Lett.* **1974**, *25*, 282-283.
- Cooks, R. G.; Glish, G. L.; McLuckey, S. A.; Kaiser, R. E. Ion Trap Mass Spectrometry. *Chem. Eng. News* **1991**, *69*, 26-41.
- Cooper, H. J.; Håkansson, K.; Marshall, A. G. The Role of Electron Capture Dissociation in Biomolecular Analysis. *Mass Spectrom. Rev.* **2005**, *24*, 201-222.
- Cordero, M. M.; Houser, J. J.; Wesdemiotis, C. The Neutral Products Formed During Backbone Cleavage of Protonated Peptides in Tandem Mass Spectrometry. *Anal. Chem.* **1993**, *65*, 1594-1601.
- Cox, K. A.; Gaskell, S. J.; Morris, M.; Whiting, A. Role of the Site of Protonation in the Low-Energy Decompositions of Gas Phase Peptide Ions. *J. Am. Soc. Mass Spectrom.* **1996**, *7*, 522-531.
- Dai, Y. Q.; Whittal, R. M.; Li, L. Two-Layer Sample Preparation: An Effective Method for MALDI-MS Analysis of Complex Peptide and Protein Mixtures. *Anal. Chem.* **1999**, *71*, 1087-1091.
- Danis, P. O. and Karr, D. E. A Facile Sample Preparation for the Analysis of Synthetic Organic Polymers by Matrix-Assisted Laser Desorption/Ionization. *Org. Mass Spectrom.* **1993**, *28*, 923-925.

- de la Mora, J. F. Electrospray Ionization of Large Multiply Charged Species Proceeds via Dole's Charged Residue Mechanism. *Anal. Chim. Acta* **2000**, *406*, 93-104.
- Dehmelt, H. G. Radiofrequency Spectroscopy of Stored Ions I: Storage. *Adv. At. Mol. Phys.* **1967**, *3*, 53-72.
- Dehmelt, H. G. Radiofrequency Spectroscopy of Stored Ions II: Spectroscopy. *Adv. At. Mol. Phys.* **1969**, *5*, 109-154.
- Dempster, A. J. A New Method of Positive Ray Analysis. *Phys. Rev.* **1918**, *11*, 316-325.
- Ding, C.; Kononkov, N. V.; Douglas, D. J. Quadrupole Mass Filters with Octopole Fields. *Rapid Commun. Mass Spectrom.* **2003**, *17*, 2495-2502.
- Dobo, A. and Kaltashov, I. A. Detection of Multiple Protein Conformational Ensembles in Solution via Deconvolution of Charge-State Distributions in ESI MS. *Anal. Chem.* **2001**, *73*, 4763-4773.
- Dole, M.; Mack, L. L.; Hines, R. L. Molecular Beams of Macroions. *J. Chem. Phys.* **1968**, *49*, 2240-2249.
- Dongré, A. R.; Jones, J. L.; Somogyi, Á.; Wysocki, V. H. Influence of Peptide Composition, Gas-Phase Basicity, and Chemical Modification on Fragmentation Efficiency: Evidence for the Mobile Proton Model. *J. Am. Chem. Soc.* **1996**, *118*, 8365-8374.
- Dongré, A. R.; Somogyi, Á.; Wysocki, V. H. Surface-Induced Dissociation: An Effective Tool to Probe Structure, Energetics and Fragmentation Mechanisms of Protonated Peptides. *J. Mass Spectrom.* **1996**, *31*, 339-350.
- Douglas, D. J.; Frank, A. J.; Mao, D. Linear Ion Traps in Mass Spectrometry. *Mass Spectrom. Rev.* **2005**, *24*, 1-29.
- Dreisewerd, K. The Desorption Process in MALDI. *Chem. Rev.* **2003**, *103*, 395-425.
- Dunbar, R. C. BIRD (Blackbody Infrared Radiative Dissociation): Evolution, Principles, and Applications. *Mass Spectrom. Rev.* **2004**, *23*, 127-158.
- Edman P. Method for Determination of Amino Acid Sequence in Peptides. *Acta Chem. Scand.* **1950**, *4*, 283-293.
- Eng, J. K.; McCormack, A. L.; Yates, J. R. 3rd. An Approach to Correlate Tandem Mass Spectral Data of Peptides with Amino Acid Sequences in a Protein Database. *J. Am. Soc. Mass Spectrom.* **1994**, *5*, 976-989.
- Erlekam, U.; Bythell, B. J.; Scuderi, D.; Van Stipdonk, M.; Paizs, B.; Maître, P. Infrared Spectroscopy of Fragments of Protonated Peptides: Direct Evidence for Macrocyclic Structures of b_5 Ions. *J. Am. Chem. Soc.* **2009**, *131*, 11503-11508.

- Fang, S.; Takao, T.; Satomi, Y.; Mo, W.; Shimonishi, Y. Novel Rearranged Ions Observed for Protonated Peptides via Metastable Decomposition in Matrix-Assisted Laser Desorption/Ionization Time-of-Flight Mass Spectrometry. *J. Am. Soc. Mass Spectrom.* **2000**, *11*, 345-351.
- Farrugia, J. M.; Taverner, T.; O'Hair, R. A. J. Side Chain Involvement in the Fragmentation Reactions of Protonated Histidine and Its Peptides. *Int. J. Mass. Spectrom.* **2001**, *209*, 99-112.
- Farrugia, J. M.; O'Hair, R. A. J.; Reid, G. E. Do All b_2 Ions Have Oxazolone Structures? Results from Multistage Mass Spectrometry and *ab initio* Studies on Protonated N-Acyl Amino Acid Methyl Ester Model Systems. *Int. J. Mass. Spectrom.* **2001**, *210-211*, 71-87.
- Farrugia, J. M. and O'Hair, R. A. J. Involvement of Salt Bridges in a Novel Gas Phase Rearrangement of Protonated Arginine-Containing Dipeptides Which Precedes Fragmentation. *Int. J. Mass Spectrom.* **2003**, *222*, 229-242.
- Felitsyn, N.; Peschke, M.; Kebarle, P. Origin and Number of Charges Observed on Multiply-Protonated Native Proteins Produced by ESI. *Int. J. Mass. Spectrom.* **2002**, *219*, 39-62.
- Fenn, J. B.; Mann, M.; Meng, C. K.; Wong, S. F.; Whitehouse, C. M. Electrospray Ionization Mass Spectrometry of Large Molecules. *Science* **1989**, *246*, 64-71.
- Fenn, J. B. Ion Formation from Charged Droplets: Roles of Geometry, Energy, and Time. *J. Am. Soc. Mass Spectrom.* **1993**, *4*, 524-535.
- Fenner, N. and Daly, N. Laser Used for Mass Analysis. *Rev. Sci. Instrum.* **1966**, *37*, 1068-1070.
- Fountain, S. T.; Lee, H.; Lubman, D. M. Ion Fragmentation Activated by Matrix-Assisted Laser Desorption/Ionization in an Ion-Trap/Reflectron Time-of-Flight Device. *Rapid Commun. Mass Spectrom.* **1994**, *8*, 407-416.
- Fu, L.; Chen, T.; Xue, G.; Zu, L.; Fang, W. Selective Cleavage Enhanced by Acetylating the Side Chain of Lysine. *J. Mass Spectrom.* **2013**, *48*, 128-134.
- Gabelica, V.; De Pauw, E.; Karas, M. Influence of the Capillary Temperature and the Source Pressure on the Internal Energy Distribution of Electrosprayed Ions. *Int. J. Mass. Spectrom.* **2004**, *231*, 189-195.
- Gamero-Castaño, M. and de la Mora, J. F. Direct Measurement of Ion Evaporation Kinetics from Electrified Liquid Surfaces. *J. Chem. Phys.* **2000**, *113*, 815-832.
- Garaguso, I. and Borlak, J. Matrix layer sample preparation: an improved MALDI-MS peptide analysis method for proteomic studies. *Proteomics* **2008**, *8*, 2583-2595.

- Gauthier, J. W.; Trautman, T. R.; Jacobson, D. B. Sustained Off-Resonance Irradiation for Collision-Activated Dissociation Involving Fourier Transform Mass Spectrometry. Collision-Activated Dissociation Technique that Emulates Infrared Multiphoton Dissociation. *Anal. Chim. Acta.* **1991**, *246*, 211-225.
- Ge, Y.; Lawhorn, B. G.; ElNaggar, M.; Strauss, E.; Park, J. H.; Begley, T. P.; McLafferty F. W. Top Down Characterization of Larger Proteins (45 kDa) by Electron Capture Dissociation Mass Spectrometry. *J. Am. Chem. Soc.* **2002**, *124*, 672-678.
- Glish, G. L. and Goeringer, D. E. Tandem Quadrupole/Time-of-Flight Instrument for Mass Spectrometry/Mass Spectrometry. *Anal. Chem.* **1984**, *56*, 2291-2295.
- Glish, G. L. and Vachet, R. W. The Basics of Mass Spectrometry in the Twenty-First Century. *Nat Rev Drug Discov* **2003**, *2*, 140-150.
- Glozak, M. A.; Sengupta, N.; Zhang, X.; Seto, E. Acetylation and Deacetylation of Non-Histone Proteins. *Gene* **2005**, *363*, 15-23.
- Gobom, J.; Schuerenberg, M.; Mueller, M.; Theiss, D.; Lehrach, H.; Nordhoff, E. Alpha-Cyano-4-Hydroxycinnamic Acid Affinity Sample Preparation. A Protocol for MALDI-MS Peptide Analysis in Proteomics. *Anal. Chem.* **2001**, *73*, 434-438.
- Goeringer, D. E.; Whitten, W. B.; Ramsey, J. M.; McLuckey, S. A.; Glish, G. L. Theory of High-Resolution Mass Spectrometry Achieved via Resonance Ejection in the Quadrupole Ion Trap. *Anal. Chem.* **1992**, *64*, 1434-1439.
- Goloborodko, A. A.; Gorshkov, M. V.; Good, D. M., Zubarev, R. A. Sequence Scrambling in Shotgun Proteomics is Negligible. *J. Am. Soc. Mass Spectrom.* **2011**, *22*, 1121-1124.
- Gonzalez, J.; Besada, V.; Garay, H.; Reyes, O.; Padron, G.; Tambara, Y.; Takao, T.; Shimonishi, Y. Effect of the Position of a Basic Amino Acid on the C-Terminal Rearrangement of Protonated Peptides Upon Collision-Induced Dissociation. *J. Mass Spectrom.* **1996**, *31*, 150-158.
- Gorshkov, M. V.; Tolić, L. P.; Udseth, H. R.; Anderson, G. A.; Huang, B. M.; Bruce, J. E.; Prior, D. C.; Hofstadler, S. A.; Tang, L.; Chen, L. Z.; Willett, J. A.; Rockwood, A. L.; Sherman, M. S.; Smith, R. D. Electrospray Ionization–Fourier Transform Ion Cyclotron Resonance Mass Spectrometry at 11.5 Tesla: Instrument Design and Initial Results. *J. Am. Soc. Mass Spectrom.* **1998**, *9*, 692-700.
- Gross, M. L. Charge-Remote Fragmentations: Method, Mechanism and Applications. *Int. J. Mass Spectrom. Ion Processes* **1992**, *118-119*, 137-165.
- Gu, C.; Tsaprailis, G.; Brechi, L.; Wysocki, V. H. Selective Gas-Phase Cleavage at the Peptide Bond C-Terminal to Aspartic Acid in Fixed-Charge Derivatives of Asp-Containing Peptides. *Anal. Chem.* **2000**, *72*, 5804-5813.

- Gucinski, A. C.; Chamot-Rooke, J.; Nicol, E.; Somogyi, Á.; Wysocki, V. H. Structural Influences on Preferential Oxazolone versus Diketopiperazine b_2^+ Ion Formation for Histidine Analogue-Containing Peptides. *J. Phys. Chem. A* **2012**, *116*, 4296-4304.
- Gucinski, A. C.; Chamot-Rooke, J.; Steinmetz, V.; Somogyi, Á.; Wysocki, V. H. Influence of N-Terminal Residue Composition on the Structure of Proline-Containing b_2^+ Ions. *J. Phys. Chem. A* **2013**, *117*, 1291-1298.
- Haddon, W. F. and McLafferty, F. W. Metastable Ion Characteristics. VII. Collision-Induced Metastables. *J. Am. Chem. Soc.* **1968**, *90*, 4745-4746.
- Harrison, A. G.; Mercer, R. S.; Reiner, E. J.; Young, A. B.; Boyd, R. K.; March, R. E.; Porter, C. J. A Hybrid BEQQ Mass Spectrometer for Studies in Gaseous Ion Chemistry. *Int. J. Mass Spectrom. Ion Processes* **1986**, *74*, 13-31.
- Harrison, A. G. and Yalcin, T. Proton Mobility in Protonated Amino Acids and Peptides. *Int. J. Mass Spectrom. Ion Process* **1997**, *165/166*, 339-347.
- Harrison, A. G. and Young, A. B. Fragmentation of Protonated Oligoaliniines: Amide Bond Cleavage and Beyond. *J. Am. Soc. Mass Spectrom.* **2004**, *15*, 1810-1819.
- Harrison, A. G.; Young, A. B., Bleiholder, C.; Suhai, S.; Paizs, B. Scrambling of Sequence Information in Collision-Induced Dissociation of Peptides. *J. Am. Chem. Soc.* **2006**, *128*, 10364-10365.
- Harrison, A. G. Peptide Sequence Scrambling Through Cyclization of b_5 Ions. *J. Am. Soc. Mass Spectrom.* **2008**, *19*, 1776-1780.
- Harrison, A. G. Cyclization of Peptide b_9 Ions. *J. Am. Soc. Mass Spectrom.* **2009**, *20*, 2248-2253.
- Harrison, A. G. To b or Not to b : The Ongoing Saga of Peptide b Ions. *Mass Spectrom. Rev.* **2009**, *28*, 640-654.
- Harrison, A. G. Pathways for Water Loss from Doubly Protonated Peptides Containing Serine or Threonine. *J. Am. Soc. Mass Spectrom.* **2012**, *23*, 116-123.
- Hendrickson, C. L.; Drader, J. J.; Laude, D. A.; Guan, S. H.; Marshall, A. G. Fourier Transform Ion Cyclotron Resonance Mass Spectrometry in a 20 T Resistive Magnet. *Rapid Commun. Mass Spectrom.* **1996**, *10*, 1829-1832.
- Henzel, W. J.; Billeci, T. M.; Stults, J. T.; Wong, S. C.; Grimley, C.; Watanabe, C. Identifying Proteins from Two-Dimensional Gels by Molecular Mass Searching of Peptide Fragments in Protein Sequence Databases. *Proc. Natl. Acad. Sci. U.S.A.* **1993**, *90*, 5011-5015.
- Herzog, R. F. K. and Viehboeck, F. Ion Source for Mass Spectrography. *Phys. Rev.* **1949**, *76*, 855-856.

- Hipple, J. A.; Sommer, H.; Thomas, H. A. A Precise Method of Determining the Faraday by Magnetic Resonance. *Phys. Rev.* **1949**, *76*, 1877-1878.
- Hiserodt, R. D.; Brown, S. M.; Swijter, D. F. H.; Hawkins, N.; Mussinan, C. J. A Study of $b_1 + \text{H}_2\text{O}$ and b_1 Ions in the Product Ion Spectra of Dipeptides Containing N-Terminal Basic Amino Acid Residues. *J. Am. Soc. Mass Spectrom.* **2007**, *18*, 1414-1422.
- Hoffmann, E. and Stroobant, V. *Mass Spectrometry Principles and Applications*, 3rd ed John Wiley & Sons Ltd, 2007.
- Hogan, C. J.; Carroll, J. A.; Rohrs, H. W.; Biswas, P.; Gross, M. L. Combined Charged Residue-Field Emission Model of Macromolecular Electrospray Ionization. *Anal. Chem.* **2009**, *81*, 369-377.
- Hoyau, S.; Norrman, K.; McMahan, T. B.; Ohanessian, G. A Quantitative Basis for a Scale of Na^+ Affinities of Organic and Small Biological Molecules in the Gas Phase. *J. Am. Chem. Soc.* **1999**, *121*, 8864-8875.
- Hu, Q.; Noll, R. J.; Li, H.; Makarov, A.; Hardman, M.; Cooks, R. G. The Orbitrap: A New Mass Spectrometer. *J. Mass. Spectrom.* **2005**, *40*, 430-443.
- Hunt, D. F.; Bone, W. M.; Shabanowitz, J.; Rhodes, J.; Ballard, J. M. Sequence-Analysis of Oligopeptides by Secondary Ion/Collision Activated Dissociation Mass-Spectrometry. *Anal. Chem.* **1981**, *53*, 1704-1706.
- Hunt, D. F.; Yates, J. R. 3rd.; Shabanowitz, J.; Winston, S.; Hauer, C. R. Protein Sequencing by Tandem Mass Spectrometry. *Proc. Natl. Acad. Sci. U.S.A.* **1986**, *83*, 6233-6237.
- Iavarone, A. T.; Jurchen, J. C.; Williams, E. R. Effects of Solvent on the Maximum Charge State and Charge State Distribution of Protein Ions Produced by Electrospray Ionization. *J. Am. Soc. Mass Spectrom.* **2000**, *11*, 976-985.
- Iavarone, A. T.; Jurchen, J. C.; Williams, E. R. Supercharged Protein and Peptide Ions Formed by Electrospray Ionization. *Anal. Chem.* **2001**, *73*, 1455-1460.
- Iribarne, J. V. and Thomson, B. A. On the Evaporation of Small Ions from Charged Droplets. *J. Chem. Phys.* **1976**, *64*, 2287-2294.
- Jennings K. The Changing Impact of the Collision-Induced Decomposition of Ions on Mass Spectrometry. *Int. J. Mass Spectrom.* **2000**, *200*, 479-493.
- Jensen O. N. Modification-Specific Proteomics: Characterization of Post-Translational Modifications by Mass Spectrometry. *Curr. Opin. Chem. Biol.* **2004**, *8*, 33-41.
- Jia, C.; Qi, W.; He, Z. Cyclization Reactions of Peptide Fragment Ions During Multistage Collisionally Activated Decomposition: An Inducement to Lose Internal Amino Acid Residues. *J. Am. Soc. Mass Spectrom.* **2007**, *18*, 663-678.

- Juhasz, P.; Costello, C. E.; Biemann, K. Matrix-Assisted Laser Desorption/Ionization Mass-Spectrometry with 2-(4-Hydroxyphenylazo) Benzoic Acid Matrix. *J. Am. Soc. Mass Spectrom.* **1993**, *4*, 399-409.
- Karas, M.; Bachmann, D.; Bahr, U; Hillenkamp, F. Matrix-Assisted Ultraviolet Laser Desorption of Non-Volatile Compounds. *Int. J. Mass Spectrom. Ion Processes* **1987**, *78*, 53-68.
- Karas, M. and Hillenkamp, F. Laser Desorption Ionization of Proteins with Molecular Masses Exceeding 10,000 Da. *Anal. Chem.* **1988**, *60*, 2299-2301.
- Kebarle, P. and Tang, L. From Ions in Solution to Ions in the Gas Phase: The Mechanism of Electrospray Mass Spectrometry. *Anal. Chem.* **1993**, *65*, 972A-986A.
- Kebarle, P. and Peschke, M. On the Mechanisms by Which the Charged Droplets Produced by Electrospray Lead to Gas Phase Ions. *Anal. Chim. Acta* **2000**, *406*, 11-35.
- Kebarle, P. 2000. A Brief Overview of the Present Status of the Mechanisms Involved in Electrospray Mass Spectrometry. *J. Mass Spectrom.* **2000**, *35*, 804-817.
- Keller, B. O. and Li, L. Three-Layer Matrix/Sample Preparation Method for MALDI MS Analysis of Low Nanomolar Protein Samples. *J. Am. Soc. Mass Spectrom.* **2006**, *17*, 780-785.
- Khan, S. N.; Khan, A. U. Role of Histone Acetylation in Cell Physiology and Diseases: An Update. *Clin. Chim. Acta*, **2010**, *411*, 1401-1411.
- Kim, J. Y.; Kim, K. W.; Kwon, H. J.; Lee, D. W.; Yoo, J. S. Probing Lysine Acetylation with a Modification-Specific Marker Ion Using High Performance Liquid Chromatography/Electrospray-Mass Spectrometry with Collision-Induced Dissociation. *Anal. Chem.* **2002**, *74*, 5443-5449.
- Kingdon, K. H. A Method for the Neutralization of Electron Space Charge by Positive Ionization at Very Low Gas Pressures. *Phys. Rev.* **1923**, *21*, 408-418.
- Kish, M. M. and Wesdemiotis, C. Selective Cleavage at Internal Lysine Residues in Protonated vs. Metalated Peptides. *Int. J. Mass Spectrom.* **2003**, *227*, 191-203.
- Kjeldsen, F.; Silivra, O. A.; Ivonin, I. A.; Haselmann, K. F.; Gorshkov, M.; Zubarev, R. A. C α -C Backbone Fragmentation Dominates in Electron Detachment Dissociation of Gas-Phase Polypeptide Polyanions. *Chem. Eur. J.* **2005**, *11*, 1803-1812.
- Knochenmuss, R.; Dubois, F.; Dale, M. J.; Zenobi, R. The Matrix Suppression Effect and Ionization Mechanisms in Matrix-Assisted Laser Desorption/Ionization. *Rapid Commun. Mass Spectrom.* **1996**, *10*, 871-877.

- Knochenmuss, R.; Lehmann, E.; Zenobi, R. Polymer Cationization in Matrix-Assisted Laser Desorption/Ionization. *Eur. Mass Spectrom* **1998**, *4*, 421-426.
- Konenkov, N.; Londry, F.; Ding, C.; Douglas, D. J. Linear Quadrupoles with Added Hexapole Fields. *J. Am. Soc. Mass Spectrom.* **2006**, *17*, 1063-1073.
- Konermann, L. and Douglas, D. J. Equilibrium Unfolding of Proteins Monitored by Electrospray Ionization Mass Spectrometry: Distinguishing Two-State From Multi-State Transitions. *Rapid Commun. Mass Spectrom.* **1998**, *12*, 435-442.
- Köchling, H. J. and Biemann, K. *Books of Abstracts*, 43rd ASMS Conference on Mass Spectrometry Conference, Atlanta, GA, May 21-26 1995; p 1225.
- Kusmann, M.; Nordhoff, E.; Rahbek-Nielsen, H.; Haebel, S.; Rossel-Larsen, M.; Jakobsen, L.; Gobom, J.; Mirgorodskaya, E.; Kroll-Kristensen, A.; Palm, L.; Roepstorff, P. Matrix-Assisted Laser Desorption/Ionization Mass Spectrometry Sample Preparation Techniques Designed for Various Peptide and Protein Analytes. *J. Mass. Spectrom.* **1997**, *32*, 593-601.
- Lander, E. S.; Linton, L. M.; Birren, B.; Nusbaum, C.; Zody, M. C.; Baldwin, J.; Devon, K.; Dewar, K.; Doyle, M.; FitzHugh, W.; et al. Initial Sequencing and Analysis of the Human Genome. *Nature* **2001**, *409*, 860-921.
- Lane, C. S. Mass spectrometry-based proteomics in the life sciences. *Cell. Mol. Life Sci.* **2005**, *62*, 848-869.
- Laugesen, S. and Roepstorff, P. Combination of Two Matrices Results in Improved Performance of MALDI MS for Peptide Mass Mapping and Protein Analysis. *J. Am. Soc. Mass Spectrom.* **2003**, *14*, 992-1002.
- LeBlanc, J. C. Y.; Beuchemin, D.; Siu, K. W. M.; Guevremont, R.; Berman, S. S. Thermal Denaturation of Some Proteins and Its Effect on Their Electrospray Mass Spectra. *Org. Mass Spectrom.* **1991**, *26*, 831-839.
- Li, L.; Golding, R. E.; Whittall, R. M. Analysis of Single Mammalian Cell Lysates by Mass Spectrometry. *J. Am. Chem. Soc.* **1996**, *118*, 11662-11663.
- Li, X.; Huang, Y.; O'Connor, P. B.; Lin, C. Structural Heterogeneity of Doubly-Charged Peptide *b*-Ions, *J. Am. Soc. Mass Spectrom.* **2011**, *22*, 245-254.
- Li, Y. and Cole, R. B. Shifts in Peptide and Protein Charge State Distributions with Varying Spray Tip Orifice Diameter in Nanoelectrospray Fourier Transform Ion Cyclotron Resonance Mass Spectrometry. *Anal. Chem.* **2003**, *75*, 5739-5746.
- Lidgard, R. and Duncan, M. W. Utility of Matrix-Assisted Laser Desorption/Ionization Time-of-Flight Mass Spectrometry for the Analysis of Low Molecular Weight Compounds. *Rapid Commun. Mass Spectrom.* **1995**, *9*, 128-132.
- Liebler C. *Introduction to Proteomics Tools for the New Biology*, Humana Press: Totowa, 2002.

- Little, D. P.; Speir, J. P.; Senko, M. W.; O'Connor, P. B.; McLafferty, F. W. Infrared Multiphoton Dissociation of Large Multiply Charged Ions for Biomolecule Sequencing. *Anal. Chem.* **1994**, *66*, 2809-2815.
- Loo, J. A.; Loo, R. R. O.; Udseth, H. R.; Edmonds, C. G.; Smith, R. D. Solvent-Induced Conformational Changes of Polypeptides Probed by Electrospray-Ionization Mass Spectrometry. *Rapid Commun. Mass Spectrom.* **1991**, *5*, 101-105.
- Louris, J. N.; Brodbelt-Lustig, J. S.; Cooks, R. G.; Glish, G. L., van Berkel, G. J.; McLuckey S. A. Ion Isolation and Sequential Stages of Mass Spectrometry in a Quadrupole Ion Trap Mass Spectrometer. *Int. J. Mass Spectrom. Ion Processes* **1990**, *96*, 117-137.
- Mabud, Md. A.; Dekrey, M. J.; Cooks, G. R. Surface-Induced Dissociation of Molecular Ions. *Int. J. Mass Spectrom. Ion Processes* **1985**, *67*, 285-294.
- Macfarlane, R. D. and Torgerson, D. F. Californium-252 Plasma Desorption Mass Spectroscopy. *Science* **1976**, *191*, 920-925.
- Mack, L. L.; Kralik, P.; Rheude, A.; Dole, M. Molecular Beams of Macroions. II. *J. Chem. Phys.* **1970**, *52*, 4977-4986.
- Makarov, A. Electrostatic Axially Harmonic Orbital Trapping: A High Performance Technique of Mass Analysis. *Anal. Chem.* **2000**, *72*, 1156-1162.
- Makarov, A.; Denisov, E.; Lange, O.; Horning, S. Dynamic Range of Mass Accuracy in LTQ Orbitrap Hybrid Mass Spectrometer. *J. Am. Soc. Mass Spectrom.* **2006**, *17*, 977-982.
- Makarov, A.; Denisov, E.; Kholomeev, A.; Balschun, W.; Lange, O.; Strupat, K.; Horning, S. Performance Evaluation of a Hybrid Linear Ion Trap/Orbitrap Mass Spectrometer. *Anal. Chem.* **2006**, *78*, 2113-2120.
- Mamyrin, B. A.; Karataev, V. I.; Shmikk, D. V.; Zagualin, V. A. The Mass-Reflectron, A New Non-Magnetic Time-of-Flight Mass Spectrometer with High Resolution. *J. Exp. Theor. Phys.* **1973**, *37*, 45-48.
- Mann, M.; Meng, C. K.; Fenn, J. B. Interpreting Mass Spectra of Multiply Charged Ions. *Anal. Chem.* **1989**, *61*, 1702-1708.
- Mann, M.; Højrup, P.; Roepstorff, P. Use of Mass Spectrometric Molecular Weight Information to Identify Proteins in Sequence Databases. *Biol. Mass Spectrom.* **1993**, *22*, 338-345.
- Marshall, A. G. and Guan, S. H. Advantages of High Magnetic Field for Fourier Transform Ion Cyclotron Resonance Mass Spectrometry. *Rapid Commun. Mass Spectrom.* **1996**, *10*, 1819-1823

- McDonnell, L. A.; Giannakopoulos, A. E.; Derrick, P. J.; Tsybin, Y. O.; Hakansson, P. A Theoretical Investigation of the Kinetic Energy of Ions Trapped in a Radio-Frequency Hexapole Ion Trap. *Eur. Mass Spectrom* **2002**, *8*, 181-189.
- McKee, T. and McKee, J. R. *Biochemistry: The Molecular Basis of Life*, 3rd ed.; McGraw-Hill Companies: New York, 2003.
- McLachlan, N. *Theory and Application of Mathieu Functions*, Oxford University Press: London, 1951.
- McLafferty, F. W.; Todd, P. J.; McGilvery, D. C.; Baldwin, M. A. High-Resolution Tandem Mass Spectrometer (MS/MS) of Increased Sensitivity and Mass Range. *J. Am. Chem. Soc.* **1980**, *102*, 3360-3363.
- McLuckey, S. A. Principles of Collisional Activation in Analytical Mass Spectrometry. *J. Am. Soc. Mass Spectrom.* **1992**, *3*, 599-614.
- Medzihradszky, K. F.; Campbell, J. M.; Baldwin, M. A.; Falick, A. M.; Juhasz, P.; Vestal, M. L.; Burlingame, A. L. The Characteristics of Peptide Collision-Induced Dissociation Using a High-Performance MALDI-TOF/TOF Tandem Mass Spectrometer. *Anal. Chem.* **2000**, *72*, 552-558.
- Medzihradszky, K. F. Peptide Sequence Analysis. *Meth. Enzymol.* **2005**, *402*, 209-244.
- Miraz, U. A.; Cohen, S. L.; Chait, B. T. Heat-Induced Conformational Changes in Proteins Studied by Electrospray Ionization Mass Spectrometry. *Anal. Chem.* **1993**, *65*, 1-6.
- Mock, K. K.; Sutton, C. W.; Cottrell, J. S. Sample Immobilization Protocols for Matrix-Assisted Laser-Desorption Mass Spectrometry. *Rapid Commun. Mass Spectrom.* **1992**, *6*, 233-238.
- Molesworth, S.; Osburn, S.; Van Stipdonk, M. Influence of Size on Apparent Scrambling of Sequence during CID of *b*-Type Ions. *J. Am. Soc. Mass Spectrom.* **2009**, *20*, 2174-2181.
- Molesworth, S.; Osburn, S.; Van Stipdonk, M. Influence of Amino Acid Side Chains on Apparent Selective Opening of Cyclic *b*₅ Ions. *J. Am. Soc. Mass Spectrom.* **2010**, *21*, 1028-1036.
- Molesworth, S. and Van Stipdonk, M. Apparent Inhibition by Arginine of Macrocylic *b* Ion Formation from Singly Charged Protonated Peptides. *J. Am. Soc. Mass Spectrom.* **2010**, *21*, 1322-1328.
- Morris, H. R.; Paxton, T.; Dell, A.; Langhorne, J.; Berg, M.; Bordoli, R. S.; Hoyes, J.; Bateman, R. H. High Sensitivity Collisionally-Activated Decomposition Tandem Mass Spectrometry on a Novel Quadrupole/Orthogonal-Acceleration Time-of-Flight Mass Spectrometer. *Rapid Commun. Mass Spectrom.* **1996**, *10*, 889-896.

- Morris, H. R.; Paxton, T.; Panico, M.; McDowell, R.; Dell, A. A Novel Geometry Mass Spectrometer, The Q-TOF, for Low-Femtomole/Attomole-Range Biopolymer Sequencing. *J. Protein Chem.* **1997**, *16*, 469-479.
- Mueller, D. R.; Eckersley, M.; Richter, W. Hydrogen Transfer Reactions in the Formation of “Y+2” Sequence Ions from Protonated Peptides. *Org. Mass Spectrom.* **1988**, *23*, 217-222.
- Munson, M. S. B. and Field, F. H. Chemical Ionization Mass Spectrometry. I. General Introduction. *J. Am. Chem. Soc.* **1966**, *88*, 2621-2630.
- Neta, P.; Pu, Q. -L.; Yang, X.; Stein, S. E. Consecutive Neutral Losses of H₂O and C₂H₄O from N-Terminal Thr-Thr and Thr-Ser in Collision-Induced Dissociation of Protonated Peptides. Position Dependent Water Loss from Single Thr or Ser. *Int. J. Mass Spectrom.* **2007**, *267*, 295-301.
- Nguyen, S. and Fenn, J. B. Gas-Phase Ions of Solute Species from Charged Droplets of Solutions. *Proc. Natl. Acad. Sci. USA* **2007**, *104*, 1111-1117.
- Nielen, M. W. F. Maldi Time-of-Flight Mass Spectrometry of Synthetic Polymers. *Mass Spectrom. Rev.* **1999**, *18*, 309-344.
- Nier, A. O. A Mass Spectrometer for Isotope and Gas Analysis. *Rev. Sci. Instrum.* **1947**, *18*, 398-410.
- Niessen, W. M. A. State-of-the-Art in Liquid Chromatography–Mass Spectrometry. *J. Chromatogr. A* **1999**, *856*, 179-197.
- O’Farrell, P. H. High Resolution Two-Dimensional Electrophoresis of Proteins. *J. Biol. Chem.* **1975**, *250*, 4007-4021.
- O’Hair, R. A. J. and Reid, G. E. Does Side Chain Water Loss from Protonated Threonine Yield N-Protonated Dehydroamino-2-Butyric Acid? *Rapid Commun. Mass Spectrom.* **1999**, *12*, 999-1002.
- Paizs, B.; Lendvay, G.; Vekey, K.; Suhai, S. Formation of b_2^+ Ions from Protonated Peptides: An *ab initio* Study. *Rapid Commun. Mass Spectrom.* **1999**, *13*, 525-533.
- Paizs, B. and Suhai, S. Combined Quantum Chemical and RRKM Modeling of the Main Fragmentation Pathways of Protonated GGG. I. Cis-Trans Isomerization Around Protonated Amide Bonds. *Rapid Commun. Mass Spectrom.* **2001**, *15*, 2307-2323.
- Paizs, B. and Suhai, S. Combined Quantum Chemical and RRKM Modeling of the Main Fragmentation Pathways of Protonated GGG. II. Formation of b_2 , y_1 , and y_2 Ions. *Rapid Commun. Mass Spectrom.* **2002**, *16*, 375-389.

- Paizs, B. and Suhai, S. Towards Understanding Some Ion Intensity Relationships for the Tandem Mass Spectra of Protonated Peptides. *Rapid Commun. Mass Spectrom.* **2002**, *16*, 1699-1702.
- Paizs, B. and Suhai, S. Towards Understanding the Tandem Mass Spectra of Protonated Oligopeptides 1: Mechanism of Amide Bond Cleavage. *J. Am. Soc. Mass Spectrom.* **2004**, *15*, 103-113.
- Paizs, B. and Suhai, S. Fragmentation Pathways of Protonated Peptides. *Mass Spectrom. Rev.* **2005**, *24*, 508-548.
- Paul, W. and Steinwedel, H. Ein Neues Massenspektrometer Ohne Magnetfeld. *Z. Naturforsch. A* **1953**, *8*, 448-450.
- Paul, W. and Raether, M. Das Elektrische Massenfilter. *Z. Phys.* **1955**, *140*, 262-273.
- Payne, A. H.; Chelf, J. H.; Glish, G. L. C-Terminal Peptide Sequencing Using Acetylated Peptides with MSⁿ in a Quadrupole Ion Trap. *Analyst* **2000**, *125*, 635-640.
- Perkins, B. R.; Chamot-Rooke, J.; Yoon, S. H.; Gucinski, A. C.; Somogyi, Á.; Wysocki, V. H. Evidence of Diketopiperazine and Oxazolone Structures of HA b₂⁺ Ion. *J. Am. Chem. Soc.* **2009**, *131*, 17528-17529.
- Perkins, D. N.; Pappin, D. J. C.; Creasy, D. M.; Cottrell, J. S. Probability-Based Protein Identification by Searching Sequence Databases Using Mass Spectrometry Data. *Electrophoresis* **1999**, *20*, 3551-3567.
- Polce, M. J.; Ren, D.; Wesdemiotis, C. Dissociation of the Peptide Bond in Protonated Peptides. *J. Mass Spectrom.* **2000**, *35*, 1391-1398.
- Polfer, N. C.; Oomens, J.; Suhai, S.; Paizs, B. Spectroscopic and Theoretical Evidence for Oxazolone Ring Formation in Collision-Induced Dissociation of Peptides. *J. Am. Chem. Soc.* **2005**, *127*, 17154-17155.
- Polfer, N. C.; Oomens, J.; Suhai, S.; Paizs, B. Infrared Spectroscopy and Theoretical Studies on Gas-Phase Protonated Leu-Enkephalin and Its Fragments: Direct Experimental Evidence for the Mobile Proton. *J. Am. Chem. Soc.* **2007**, *129*, 5887-5897.
- Polfer, N. C.; Bohrer, B. C.; Plasencia, M. D.; Paizs, B.; Clemmer, D. E. On the Dynamics of Fragment Isomerization in Collision-Induced Dissociation of Peptides. *J. Phys. Chem. A* **2008**, *112*, 1286-1293.
- Price, W. D.; Schnier, P. D.; Williams, E. R. Tandem Mass Spectrometry of Large Biomolecule Ions by Blackbody Infrared Radiative Dissociation. *Anal. Chem.* **1996**, *68*, 859-866.
- Rader, H. I. and Schrepp, W. MALDI-TOF Mass Spectrometry in the Analysis of Synthetic Polymers. *Acta Polym.* **1998**, *49*, 272-293.

- Rayleigh, L. On the Equilibrium of Liquid Conducting Masses Charged with Electricity. *Philos. Mag.* **1882**, *14*, 184-186.
- Reid, G. E.; Simpson, R. J.; O'Hair, R. A. J. Probing the Fragmentation Reactions of Protonated Glycine Oligomers via Multistage Mass Spectrometry and Gas Phase Ion Molecule Hydrogen/Deuterium Exchange. *Int. J. Mass. Spectrom.* **1999**, *190/191*, 209-230.
- Reid, G. E.; Simpson, R. J.; O'Hair, R. A. J. Leaving Group and Gas Phase Neighboring Group Effects in the Side Chain Losses from Protonated Serine and Its Derivatives. *J. Am. Soc. Mass Spectrom.* **2000**, *11*, 1047-1060.
- Reid, G. E. and McLuckey, S. A. 'Top Down' Protein Characterization via Tandem Mass Spectrometry. *J. Mass Spectrom.* **2002**, *37*, 663-675.
- Riba-Garcia, I.; Giles, K.; Bateman, R. H.; Gaskell, S. J. Evidence for Structural Variants of *a*- and *b*-Type Peptide Fragment Ions Using Combined Ion Mobility/Mass Spectrometry. *J. Am. Soc. Mass Spectrom.* **2008**, *19*, 609-613.
- Rockwood, A. S.; Busman, M.; Udseth, H. R.; Smith, R. D. Thermally Induced Dissociation of Ions from Electrospray Mass Spectrometry. *Rapid Commun. Mass Spectrom.* **1991**, *5*, 582-585.
- Rodriguez, C. F.; Shoeib, T.; Chu, I. K.; Siu, K. W. M.; Hopkinson, A. C. Comparison Between Protonation, Lithiation and Argentination of 5-Oxazolones: A Study of a Key Intermediate in Gas-Phase Peptide Sequencing. *J. Phys. Chem. A* **2000**, *104*, 5335-5342.
- Rodriguez, C. F.; Cunje, A.; Shoeib, T.; Chu, I. K.; Hopkinson A. C.; Siu, K. W. M. Proton Migration and Tautomerism in Protonated Triglycine. *J. Am. Chem. Soc.* **2001**, *123*, 3006-3012.
- Roepstorff, P. and Fohlmann, J. Proposal for a Common Nomenclature for Sequence Ions in Mass Spectra of Peptides. *Biomed. Mass Spectrom.* **1984**, *11*, 601.
- Russell, D. H.; Smith, D. H.; Warmack, R. J.; Bertram, L. K. The Design and Performance Evaluation of a New High-Performance Mass-Analyzed Ion Kinetic Energy (MIKE) Spectrometer. *Int J Mass Spectrom Ion Phys* **1980**, *35*, 381-391.
- Saminathan, I. S.; Wang, X. S.; Guo, Y.; Krakovska, O.; Voisin, S.; Hopkinson, A. C.; Siu, K. W. M. The Extent and Effects of Peptide Sequence Scrambling Via Formation of Macrocyclic *b* Ions in Model Proteins. *J. Am. Soc. Mass Spectrom.* **2010**, *21*, 2085-2094.
- Schoen, A.; Amy, J. W.; Ciupek, J. D.; Cooks, R. G.; Dobberstein, P.; Jung, G. A Hybrid BEQQ Mass Spectrometer. *Int. J. Mass Spectrom. Ion Processes* **1985**, *65*, 125-140.

- Schriemer, D. C. and Li, L. Detection of High Molecular Weight Polystyrene by MALDI Mass Spectrometry. *Anal. Chem.* **1996**, *68*, 2721-2725.
- Schwartz, B. L. and Bursey, M. M. Some Proline Substituent Effect in the Tandem Mass Spectrum of Protonated Pentaalanine. *Biol. Mass Spectrom.* **1992**, *21*, 92-96.
- Senko, M. W.; Speir, J. P.; McLafferty F. W. Collisional Activation of Large Multiply Charged Ions Using Fourier Transform Mass Spectrometry. *Anal. Chem.* **1994**, *66*, 2801-2808.
- Serafin, S. V.; Zhang, K.; Aurelio, L.; Hughes, A. B.; Morton, T. H. Decomposition of Protonated Threonine, Its Stereoisomers, and Its Homologues in the Gas Phase: Evidence for Internal Backside Displacement. *Org. Lett.* **2004**, *6*, 1561-1564.
- Smith, L. L.; Hermann, K. A.; Wysocki, V. H. Investigation of Gas Phase Ion Structure for Proline-Containing b_2 Ion. *J. Am. Soc. Mass Spectrom.* **2006**, *17*, 20-28.
- Somogyi, Á.; Wysocki, V. H.; Mayer, I. The Effect of Protonation Site on Bond Strengths in Simple Peptides: Application of *ab* Initio and MNDO Bond Orders and MNDO Energy Partitioning. *J. Am. Soc. Mass Spectrom.* **1994**, *5*, 704-717.
- Stafford Jr, G. C.; Kelley, P. E.; Syka, J. E. P.; Reynolds, W. E.; Todd, J. F. J. Recent Improvements In and Analytical Applications of Advanced Ion Trap Technology. *Int. J. Mass Spectrom. Ion Processes* **1984**, *60*, 85-98.
- Stephens, W. E. A Pulsed Mass Spectrometer with Time Dispersion. *Phys. Rev.* **1946**, *69*, 691.
- Strupat, K.; Karas, M.; Hillenkamp, F. 2,5-Dihydroxybenzoic Acid: A New Matrix for Laser Desorption-Ionization Mass Spectrometry. *Int. J. Mass Spectrom. Ion Processes* **1991**, *111*, 89-102.
- Sudakov, M. and Douglas, D. J. Linear Quadrupoles with Added Octopole Fields. *Rapid Commun. Mass Spectrom.* **2003**, *17*, 2290-2294.
- Sun, S.; Yu, C.; Qiao, Y.; Lin, Y.; Dong, G.; Liu, C.; Zhang, J.; Zhang, Z.; Cai, J.; Zhang, H.; Bu, D. Deriving the Probabilities of Water Loss and Ammonia Loss for Amino Acids From Tandem Mass Spectra. *J. Proteome Res.* **2008**, *7*, 202-208.
- Syka, J. E. P.; Marto, J. A.; Bai, D. L.; Horning, S.; Senko, M. W.; Schwartz, J. C.; Ueberheide, B.; Garcia, B.; Busby, S.; Muratore, T.; Shabanowitz, J.; Hunt, D. F. Novel Linear Quadrupole Ion Trap/FT Mass Spectrometer: Performance Characterization and Use in the Comparative Analysis of Histone H3 Post-Translational Modifications. *J. Proteome Res.* **2004**, *3*, 621-626.
- Syka, J. E. P.; Coon, J. J.; Schroeder, M. J.; Shabanowitz, J.; Hunt, D. F. Peptide and Protein Sequence Analysis by Electron Transfer Dissociation Mass Spectrometry. *Proc. Natl. Acad. Sci. U.S.A.* **2004**, *101*, 9528-9533.

- Tanaka, K.; Ido, Y.; Akita, S.; Matsuda, H.; Liang, X.-T., Eds.; *Books of Abstracts, 2nd Japan-China Joint Symposium on Mass Spectrometry*, Osaka, Japan, 1987, 185-188
- Tanaka, K.; Waki, H.; Ido, Y.; Akita, S.; Yoshida, Y.; Yoshida, T.; Matsuo, T. Protein and Polymer Analyses Up to m/z 100,000 by Laser Ionization Time-of-Flight Mass Spectrometry. *Rapid Commun. Mass Spectrom.* **1988**, *2*, 151-153.
- Tang, X. J.; Thibault, P.; Boyd, R. K. Fragmentation Reactions of Multiply Protonated Peptides and Implications for Sequencing by Tandem Mass Spectrometry with Low-Energy Collision-Induced Dissociation. *Anal. Chem.* **1993**, *65*, 2824-2834.
- Tang, X. J. and Boyd, R. K. Rearrangements of Doubly-Charged Acylium Ions from Lysyl and Ornithyl Peptides. *Rapid Commun. Mass Spectrom.* **1994**, *8*, 678-686.
- Taylor, G. I. Disintegration of Water Droplets in an Electric Field. *Proc. R. Soc. A* **1964**, *280*, 383-397.
- Thomas, H.; Havlis, J.; Peychl, J.; Shevchenko, A. Dried-Droplet Probe Preparation on AnchorChip Targets for Navigating the Acquisition of Matrix-Assisted Laser Desorption/Ionization Time-of-Flight Spectra by Fluorescence of Matrix/Analyte Crystals. *Rapid Commun. Mass Spectrom.* **2004**, *18*, 923-930.
- Thomson, B. A. and Iribarne, J. V. Field Induced Ion Evaporation from Liquid Surfaces at Atmospheric Pressure. *J. Chem. Phys.* **1979**, *71*, 4451-4463.
- Thomson, B. A. Declustering and Fragmentation of Protein Ions from an Electrospray Ion Source. *J. Am. Soc. Mass Spectrom.* **1997**, *8*, 1053-1058.
- Thorne, G. C.; Ballard, K. D.; Gaskell, S. J. Metastable Decomposition of Peptide $[M + H]^+$ Ions via Rearrangement Involving Loss of the C-Terminal Amino Acid Residue. *J. Am. Soc. Mass Spectrom.* **1990**, *1*, 249-257.
- Tolic, L. P.; Anderson, G. A.; Smith, R. D.; Brothers, H. M.; Spindler, R.; Tomalia, D. A. Electrospray Ionization Fourier Transform Ion Cyclotron Resonance Mass Spectrometric Characterization of High Molecular Mass Starburst™ Dendrimers. *Int. J. Mass Spectrom. Ion Processes* **1997**, *165*, 405-418.
- Trelle, M. B. and Jensen. O. N. Utility of Immonium Ions for Assignment of ϵ -N-Acetyllysine-Containing Peptides by Tandem Mass Spectrometry. *Anal. Chem.* **2008**, *80*, 3422-3430.
- Tsprailis, G.; Somogyi, Á.; Nikolaev, E. N.; Wysocki, V. H. Refining the Model for Selective Cleavage at Acidic Residues in Arginine-Containing Protonated Peptides. *Int. J. Mass Spectrom.* **2000**, *195/196*, 467-479.
- Tsprailis, G.; Nair, H.; Zhong, W.; Kuppanan, K.; Futrell, J. H.; Wysocki, V. H. A Mechanistic Investigation of the Enhanced Cleavage at Histidine in the Gas-Phase Dissociation of Protonated Peptides. *Anal. Chem.* **2004**, *76*, 2083-2094.

- Vachet, R. W. and Glish, G. L. Effects of Heavy Gases on the Tandem Mass Spectra of Peptide Ions in the Quadrupole Ion Trap. *J. Am. Soc. Mass Spectrom.* **1996**, *7*, 1194-1202.
- Vachet, R. W.; Bishop, B. M.; Erickson, B. W.; Glish, G. L. Novel Peptide Dissociation: Gas-Phase Intermolecular Rearrangement of Internal Amino Acid Residues. *J. Am. Chem. Soc.* **1997**, *119*, 5481-5488.
- Vastola, F. and Pirone, A. Ionization of Organic Solids by Laser Irradiation. *Adv. Mass Spectrom* **1968**, *4*, 107-111.
- Venter, J. C.; Adams, M. D.; Myers, E. W.; Li, P. W.; Mural, R. J.; Sutton, G. G.; Smith, H. O.; Yandell, M.; Evans, C. A.; Holt, R. A.; et al. The Sequence of the Human Genome. *Science* **2001**, *291*, 1304-1351.
- Vestal, M. L. and Campbell, J. M. Tandem Time-of-Flight Mass Spectrometry. *Meth. Enzymol.* **2005**, *402*, 79-108.
- Vorm, O.; Roepstorff, P.; Mann, M. Improved Resolution and Very High Sensitivity in MALDI TOF of Matrix Surfaces Made by Fast Evaporation. *Anal. Chem.* **1994**, *66*, 3281-3287.
- Walsh, C. T. *Posttranslational Modifications of Proteins: Expanding Nature's Inventory*, Roberts and Company Publishers: Greenwood Village, Colorado, 2006.
- Weinberger, S. R.; Boernsen, K. O.; Finchy, J. W.; Robertson, V.; Musselman, B. D. *Books of Abstracts*, 41st American Society for Mass Spectrometry Conference, San Francisco, CA, May 31-June 4, 1993, p775a-b.
- Wells, J. M.; Gill, L. A.; Ouyang, Z.; Patterson, G. E.; Plass, W.; Badman, E. R.; Amy, J. W.; Cooks, R. G.; Schwartz, J. C.; Stafford, G. C.; Senko, M. W. *Books of Abstracts*, 46th American Society for Mass Spectrometry Conference, Orlando, 1998, p485.
- Wells, J. M. and McLuckey, S. A. Collision-Induced Dissociation (CID) of Peptides and Proteins. *Meth. Enzymol.* **2005**, *402*, 148-185.
- Whitehouse, C. M.; Dreyer, R. N.; Yamashita, M.; Fenn, J. B. Electrospray Interface for Liquid Chromatographs and Mass Spectrometers. *Anal. Chem.* **1985**, *57*, 675-679.
- Wiley, W. C. and McLaren, J. B. Time-of-Flight Mass Spectrometer with Improved Resolution. *Rev. Sci. Instrum.* **1955**, *16*, 1150-1157.
- Wilkins, M. R.; Pasquali, C.; Appel, R. D.; Ou, K.; Golaz, O.; Sanchez, J. C.; Yan, J. X.; Gooley, A. A.; Hughes, G.; Humphery-Smith, I.; Williams, K. L.; Hochstrasser, D. F. From Proteins to Proteomes: Large Scale Protein Identification by Two-Dimensional Electrophoresis and Amino Acid Analysis. *Biotechnol* **1996**, *14*, 61-65.

- Williams, E. R.; Furlong, J. J. P.; McLafferty, F. W. Efficiency of Collisionally-Activated Dissociation and 193-nm Photodissociation of Peptide Ions in Fourier Transform Mass Spectrometry. *J. Am. Soc. Mass Spectrom.* **1990**, *1*, 288-294.
- Williams, E. R.; Henry, K. D.; McLafferty, F. W.; Shabanowitz, J.; Hunt, D. F. Surface-Induced Dissociation of Peptide Ions in Fourier-Transform Mass Spectrometry. *J. Am. Soc. Mass Spectrom.* **1990**, *1*, 413-416.
- Wilm, M. and Mann, M. Analytical Properties of the Nanoelectrospray Ion Source. *Anal. Chem.* **1996**, *68*, 1-8.
- Winger, B. E.; Laue, H. -J.; Horning, S. R.; Julian, R. K.; Lammert, S. A.; Riederer, D. E.; Cooks, R. G. Hybrid BEEQ Tandem Mass Spectrometer for the Study of Ion/Surface Collision Processes. *Rev. Sci. Instrum.* **1992**, *63*, 5613-5625.
- Winger, B. E.; Light-Wahl, K. J.; Loo R. R. O.; Udseth, H. R.; Smith, R. D. Observation and Implications of High Mass-to-Charge Ratio Ions from Electrospray Ionization Mass Spectrometry. *J. Am. Soc. Mass Spectrom.* **1993**, *4*, 536-545.
- Wu, K. J.; Steding, A.; Becker, C. H. Matrix-Assisted Laser Desorption Time-of-Flight Mass Spectrometry of Oligonucleotides Using 3-Hydroxypicolinic Acid as an Ultraviolet-Sensitive Matrix. *Rapid Commun. Mass Spectrom.* **1993**, *7*, 142-146.
- Wu, K. J.; Shaler, T. A.; Becker, C. H. Time-of-Flight Mass Spectrometry of Underivatized Single-Stranded-DNA Oligomers by Matrix-Assisted Laser-Desorption. *Anal. Chem.* **1994**, *66*, 1637-1645.
- Wu, R. and McMahon, T. B. Infrared Multiple Photon Dissociation Spectroscopy as Structural Confirmation for GlyGlyGlyH⁺ and AlaAlaAlaH⁺ in the Gas Phase. Evidence for Amide Oxygen as the Protonation Site. *J. Am. Chem. Soc.* **2007**, *129*, 11312-11313.
- Wysocki, V. H.; Tsaprailis, G.; Smith, L. L.; Breci, L. A Mobile and Localized Protons: A Framework for Understanding Peptide Dissociation. *J. Mass Spectrom.* **2000**, *35*, 1399-1406.
- Xiang, F. and Beavis, R. C. Growing Protein-Doped Sinapinic Acid Crystals for Laser Desorption: An Alternative Preparation Method for Difficult Samples. *Org. Mass Spectrom.* **1993**, *28*, 1424-1429.
- Xiang, F. and Beavis, R. C. A Method to Increase Contaminant Tolerance in Protein Matrix-Assisted Laser Desorption/Ionization by the Fabrication of Thin Protein-Doped Polycrystalline Films. *Rapid Commun. Mass Spectrom.* **1994**, *8*, 199-204.
- Yagüe, J.; Paradela, A.; Ramos, M.; Ogueta, S.; Marina, A.; Barabona, F.; Lopez de Castro, J. A.; Vazquez, J. Peptide Rearrangement During Ion Trap Fragmentation: Added Complexity to MS/MS Spectra. *Anal. Chem.* **2003**, *75*, 1524-1535.

- Yalcin, T.; Khouw, C.; Csizmadia, I. G.; Peterson, M. R.; Harrison, A. G. Why Are B Ions Stable Species in Peptide Mass Spectra? *J. Am. Soc. Mass Spectrom.* **1995**, *6*, 1165-1174.
- Yalcin, T.; Csizmadia, I. G.; Peterson, M. R.; Harrison, A. G. The Structure and Fragmentation of B_n (n≥3) Ions in Peptide Spectra. *J. Am. Soc. Mass Spectrom.* **1996**, *7*, 233-242.
- Yalcin, T. and Harrison, A. G. Ion Chemistry of Protonated Lysine Derivatives. *J. Mass Spectrom.* **1996**, *31*, 1237-1243.
- Yamashita, M. and Fenn, J. B. Electrospray Ion Source. Another Variation on the Free-Jet Theme. *J. Phys. Chem.* **1984**, *88*, 4451-4459.
- Yates, J. R. 3rd.; Speicher, S.; Griffin, P. R.; Hunkapiller, T. Peptide Mass Maps-A Highly Informative Approach to Protein Identification. *Anal. Biochem.* **1993**, *214*, 397-408.
- Yost, R. A. and Enke, C. G. Selected Ion Fragmentation with a Tandem Quadrupole Mass Spectrometer. *J. Am. Chem. Soc.* **1978**, *100*, 2274-2275.
- Yost, R. A. and Enke, C. G. Triple Quadrupole Mass Spectrometry for Direct Mixture Analysis and Structure Elucidation. *Anal. Chem.* **1979**, *51*, 1251-1264.
- Yu, W.; Vath, J. E.; Huberty, M. C.; Martin, S. A. Identification of the Facile Gas-Phase Cleavage of the Asp-Pro and Asp-Xxx Peptide Bonds in Matrix-Assisted Laser Desorption Time-of-Flight Mass Spectrometry. *Anal. Chem.* **1993**, *65*, 3015-3023.
- Zenobi, R. and Knochenmuss, R. Ion Formation in MALDI Mass Spectrometry. *Mass Spectrom Rev.* **1998**, *17*, 337-366.
- Zhang, J. and Zenobi, R. Matrix-Dependent Cationization in MALDI Mass Spectrometry. *J. Mass Spectrom.* **2004**, *39*, 808-816.
- Zhang, K.; Yau, P. M.; Chandrasekhar, B.; New, R.; Kondrat, R.; Imai, B. S.; Bradbury, M. E. Differentiation Between Peptides Containing Acetylated or Tri-Methylated Lysines by Mass Spectrometry. An Application for Determining Lysine 9 Acetylation and Methylation of Histone H3. *Proteomics*, **2004**, *4*, 1-10.
- Zhang, X.; Shi, L.; Shu, S.; Wang, Y.; Zhao, K.; Xu, N.; Liu, S.; Roepstorff, P. An Improved Method of Sample Preparation on AnchorChip Targets for MALDI-MS and MS/MS and Its Application in the Liver Proteome Project. *Proteomics* **2007**, *7*, 2340-2349.
- Zhao, X. Z.; Granot, O.; Douglas, D. Quadrupole Excitation of Ions in Linear Quadrupole Ion Traps with Added Octopole Fields. *J. Am. Soc. Mass Spectrom.* **2008**, *19*, 510-519.

Zubarev, R. A.; Kelleher, N. L.; McLafferty, F. W. Electron Capture Dissociation of Multiply Charged Protein Cations. A Nonergodic Process. *J. Am. Chem. Soc.* **1998**, *120*, 3265-3266.

APPENDIX A

BREAKDOWN GRAPHS FOR $[M + H]^+$ IONS OF ACIDIC PEPTIDES

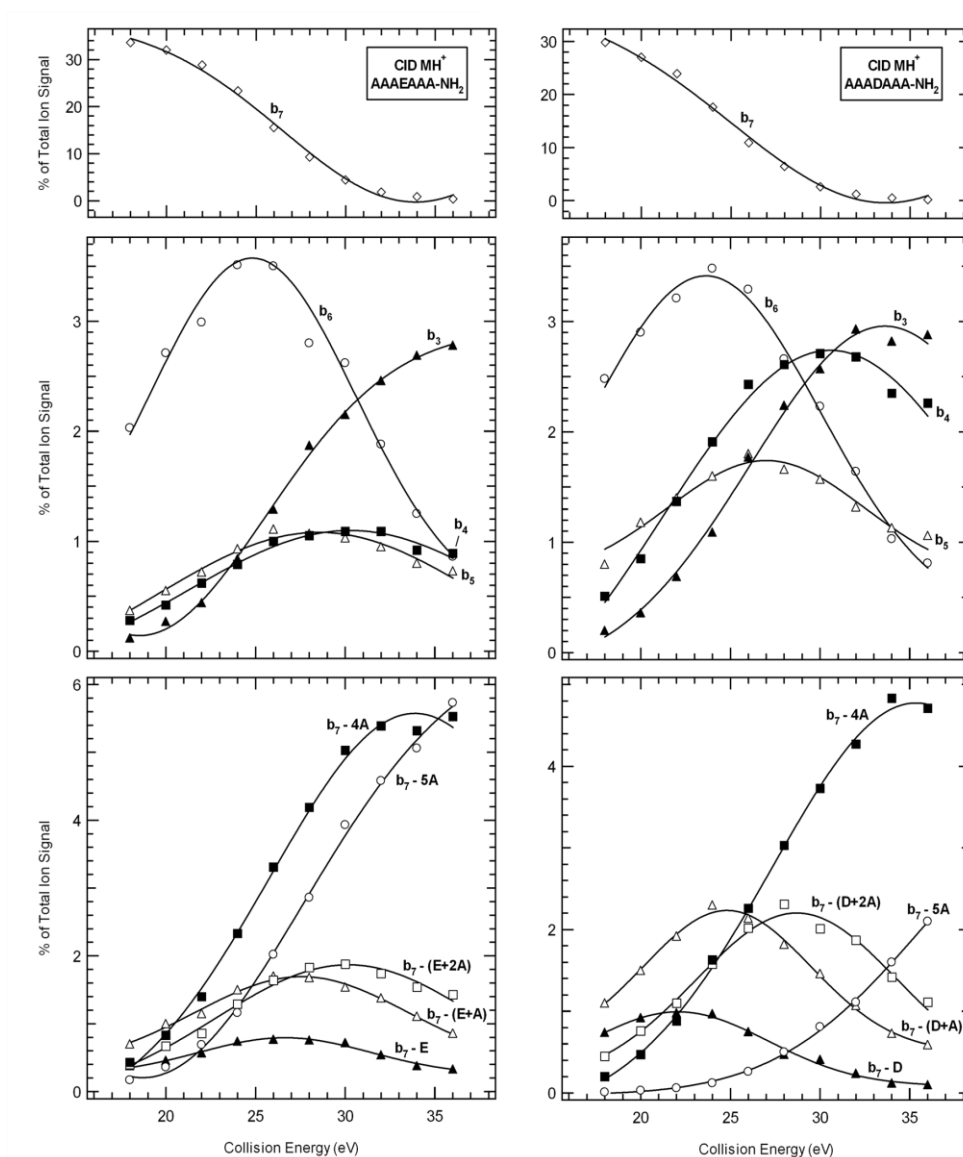


Figure A.1. Comparison of $[M + H]^+$ ion breakdown graphs of AAEEAAA-NH₂ and AAADAAA-NH₂

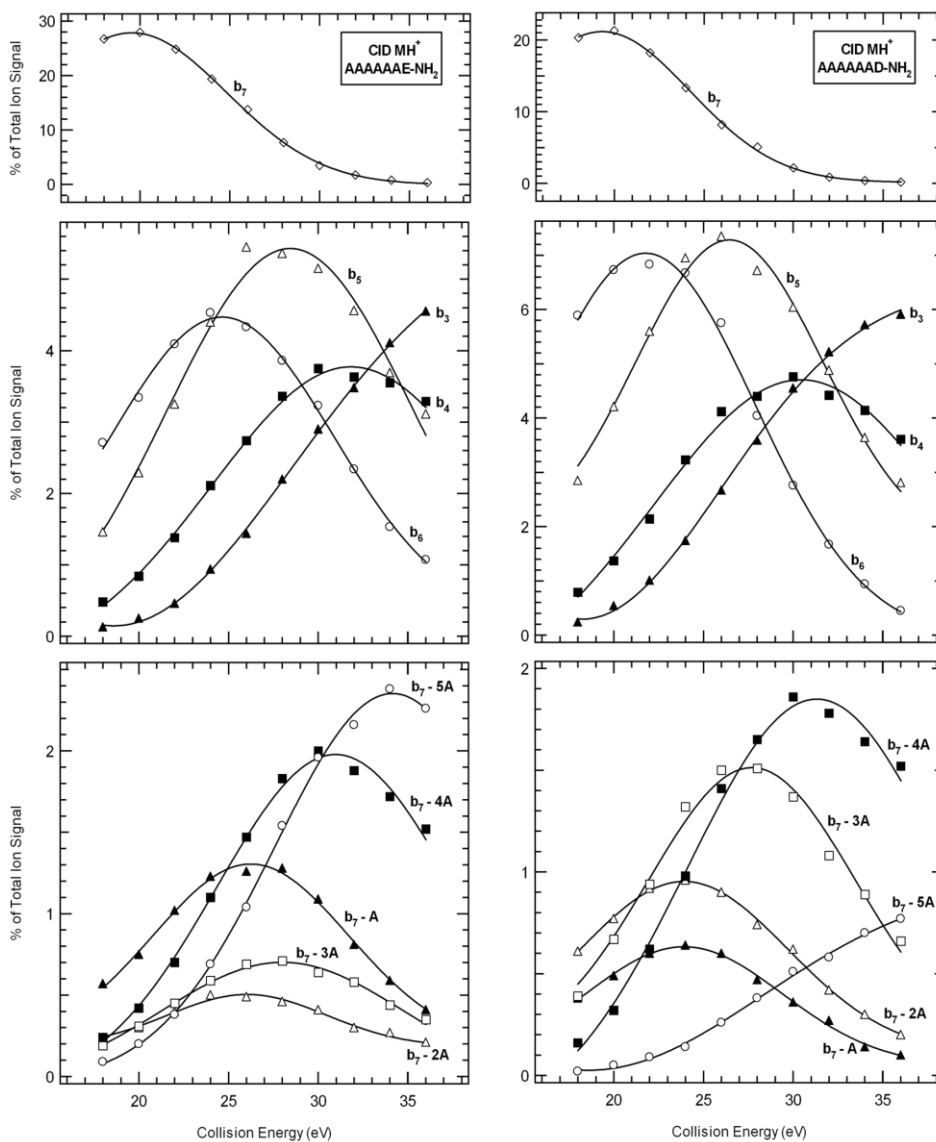


Figure A.2. Comparison of $[M + H]^+$ ion breakdown graphs of AAAAAAE-NH₂ and AAAAAAD-NH₂

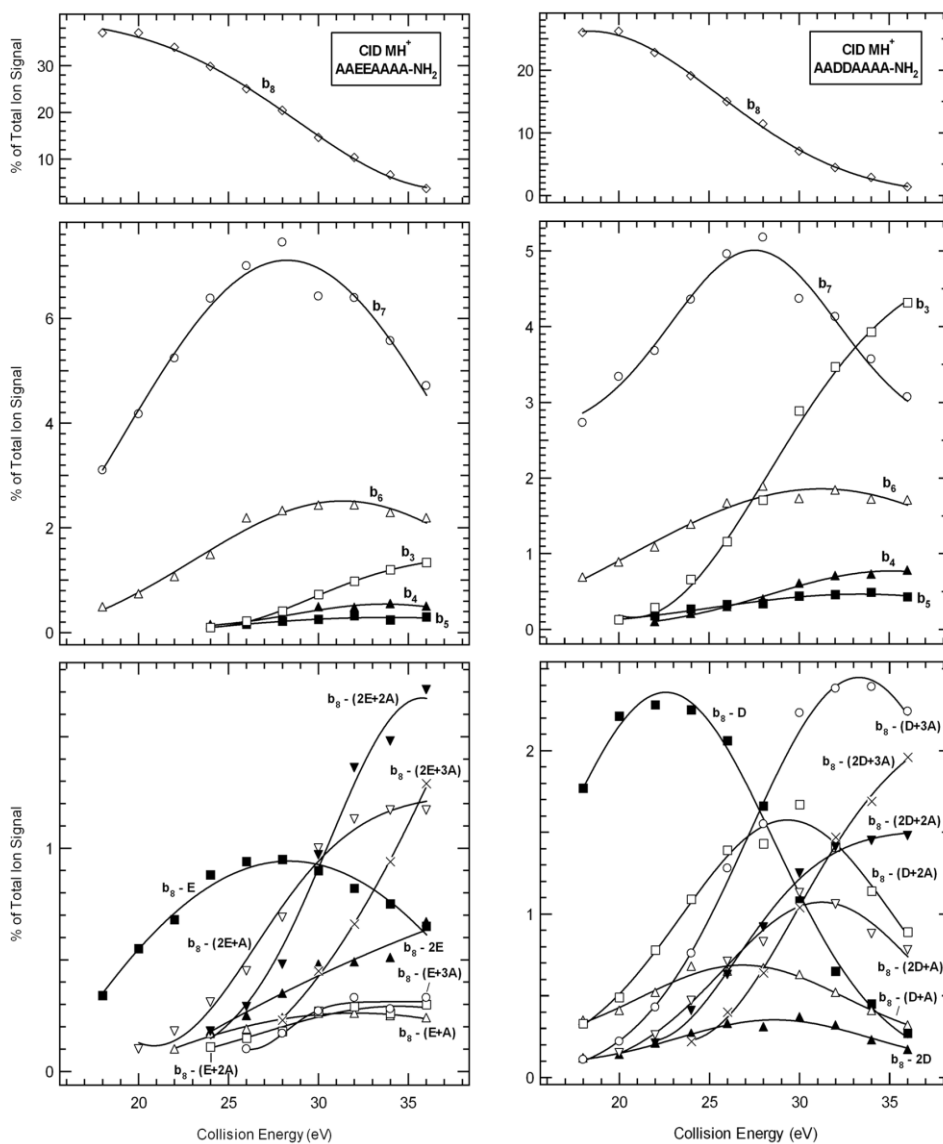


Figure A.3. Comparison of $[M + H]^+$ ion breakdown graphs of AAEEAAAA-NH₂ and AADDDAAA-NH₂

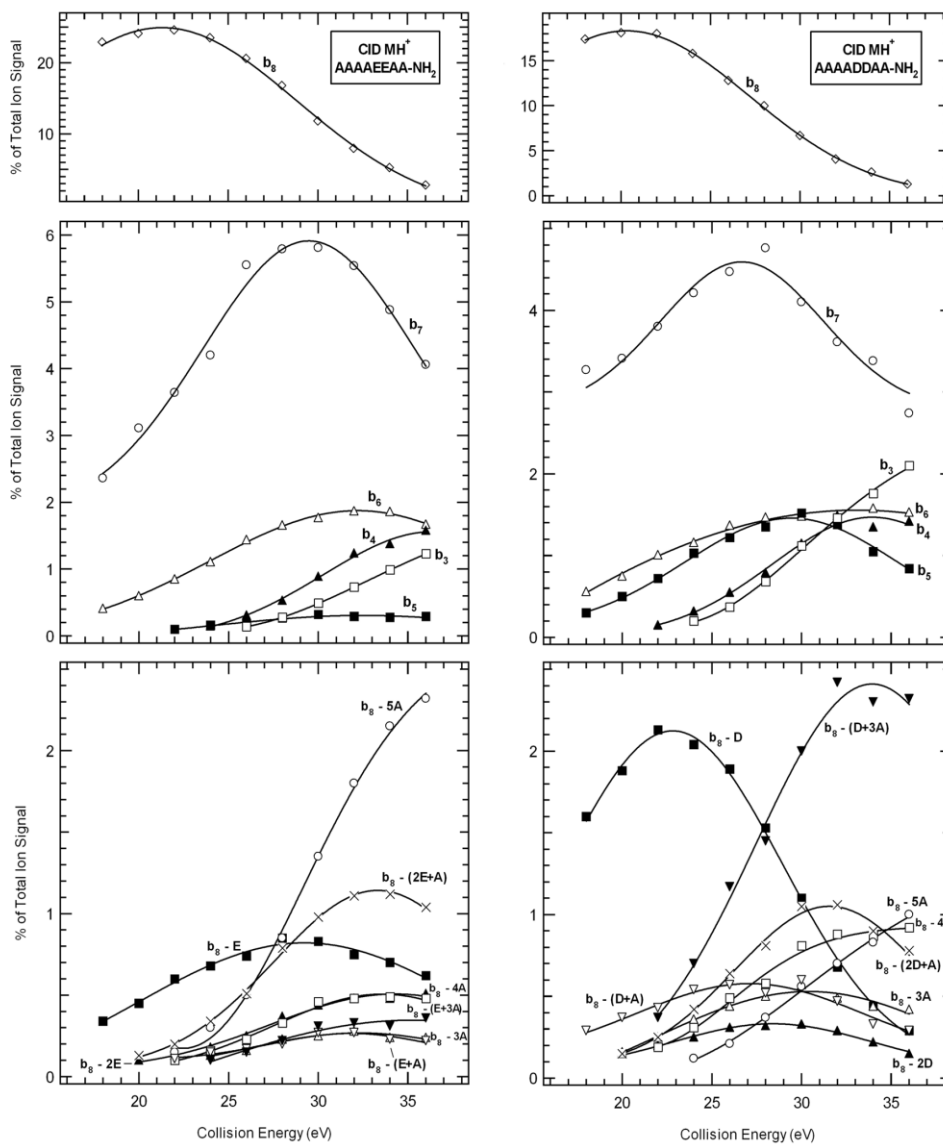


Figure A.4. Comparison of $[M + H]^+$ ion breakdown graphs of AAAAEEEA-NH₂ and AAAADDDAA-NH₂

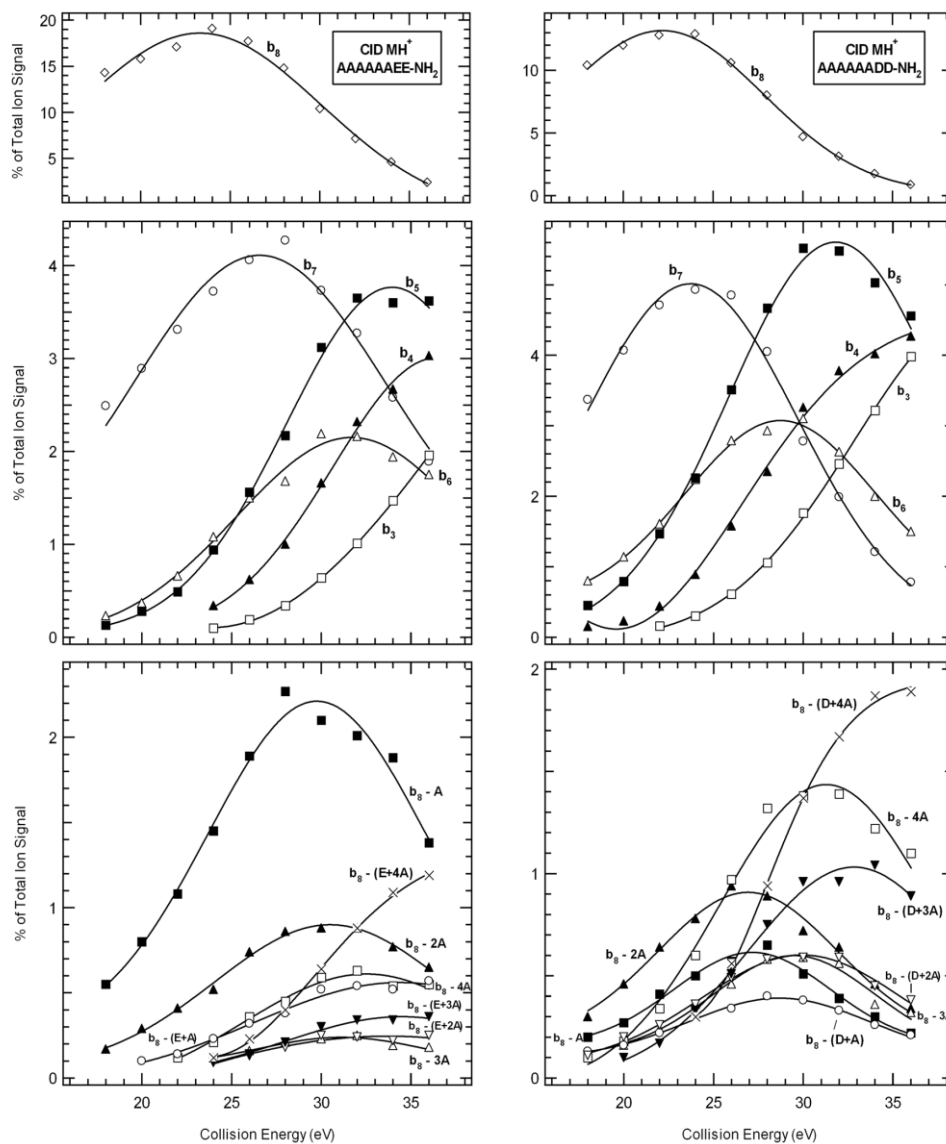


Figure A.5. Comparison of $[M + H]^+$ ion breakdown graphs of AAAAAAEE-NH₂ and AAAAAADD-NH₂

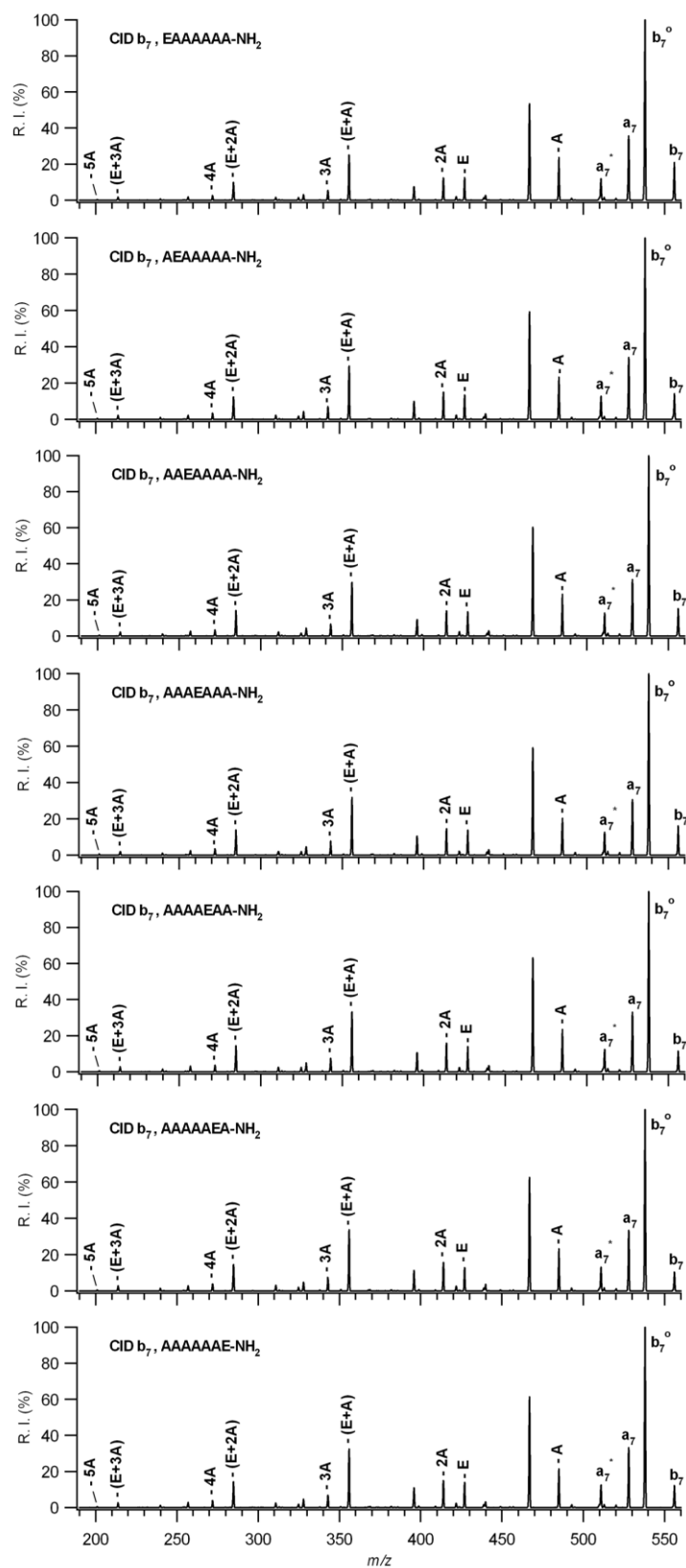


Figure A.6. Comparison of all seven CID mass spectra of b_7 ions derived from heptapeptides containing one glutamic acid and six alanine residue

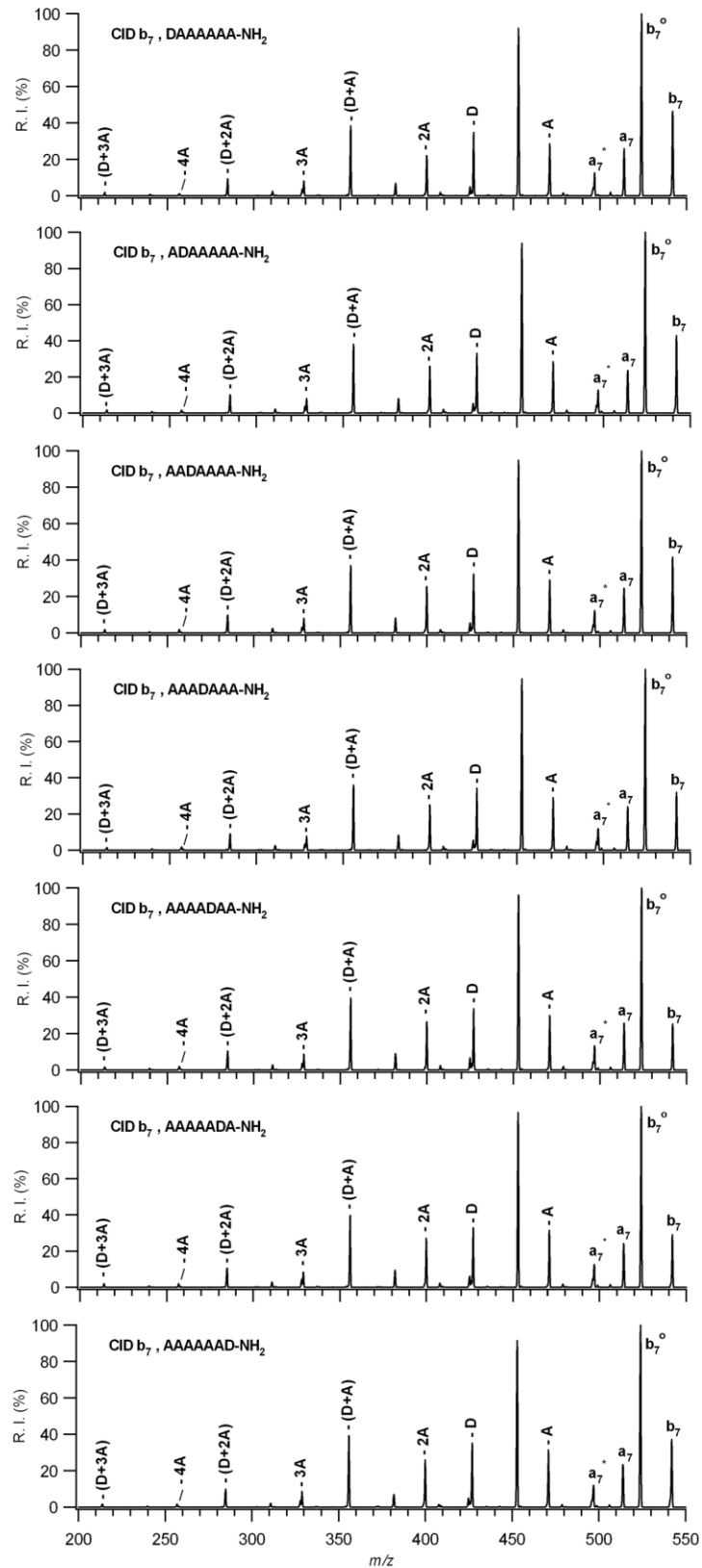


Figure A.7. Comparison of all seven CID mass spectra of b_7 ions derived from heptapeptides containing one aspartic acid and six alanine residue

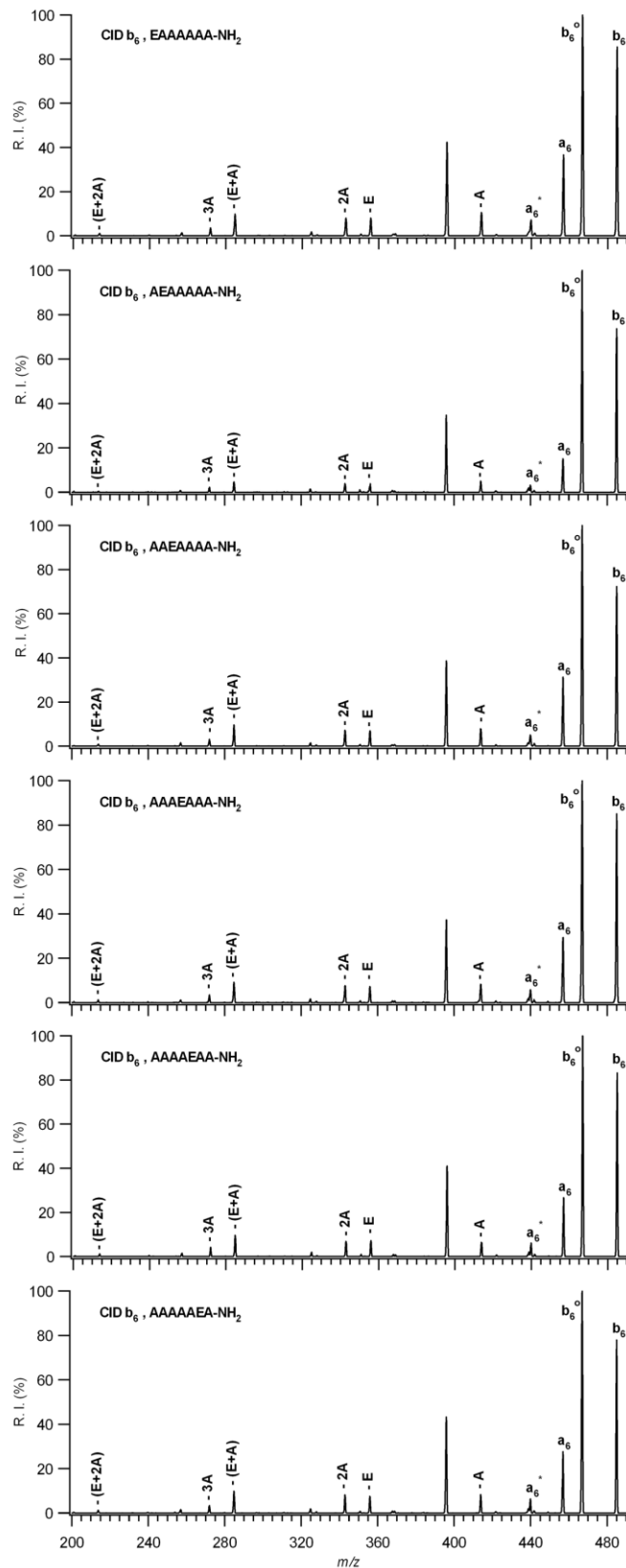


Figure A.8. Comparison of all six CID mass spectra of b_6 ions derived from heptapeptides containing one glutamic acid and six alanine residue

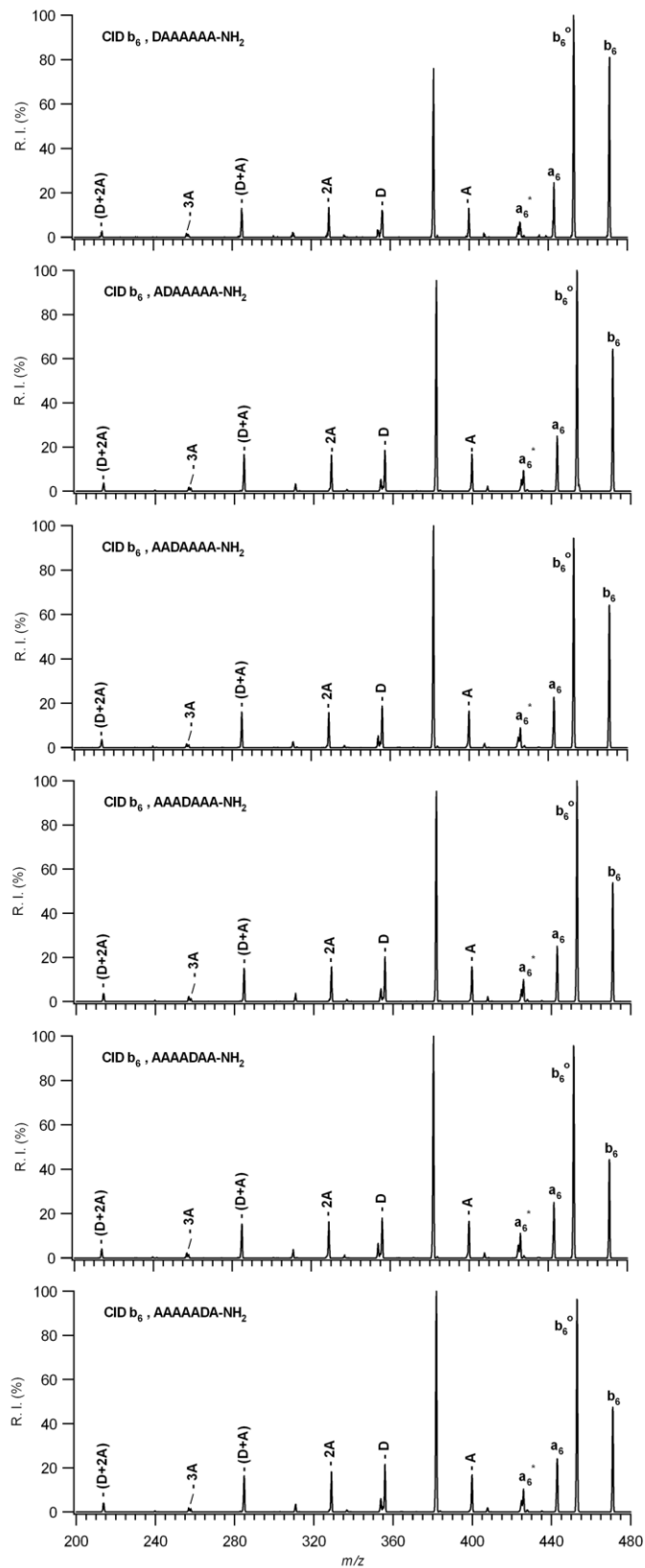


Figure A.9. Comparison of all six CID mass spectra of b_6 ions derived from heptapeptides containing one aspartic acid and six alanine residue

APPENDIX B

MS/MS SPECTRA OF $[M + H]^+$ IONS OF N-TERMINAL ACETYLATED PEPTIDES

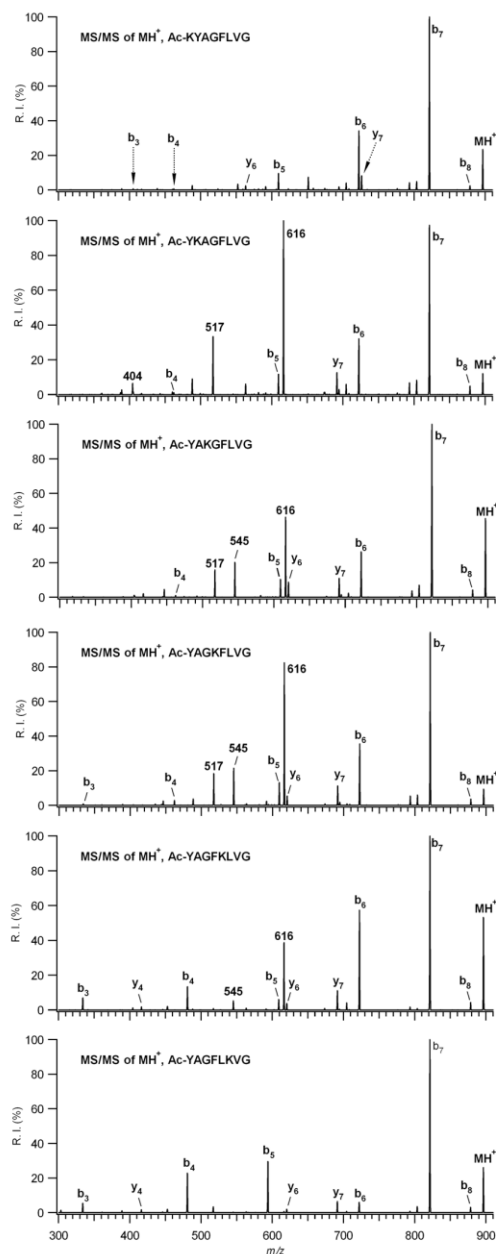


Figure B.1. The MS/MS spectra of $[M + H]^+$ of N-terminal acetylated lysine containing peptides

APPENDIX C

MS/MS SPECTRA OF $[M + H]^+$ IONS OF DIPEPTIDES AND MS^3 SPECTRA OF b_5 IONS OF XGGFL-NH₂ AND AXVYI-NH₂

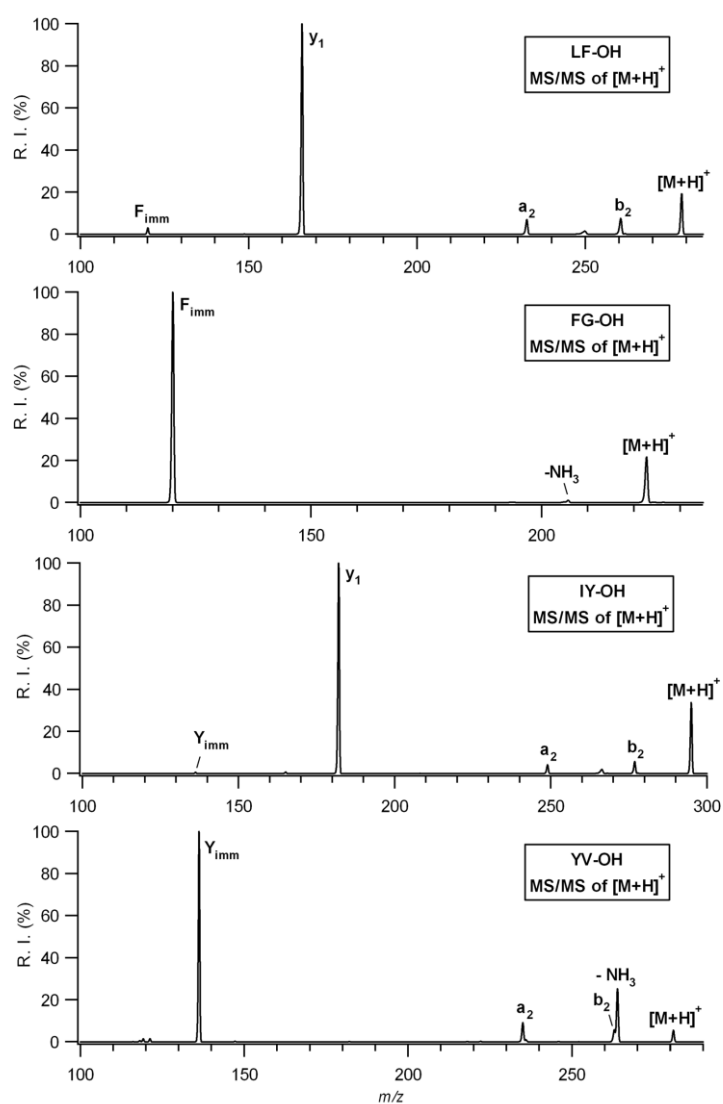


Figure C.1. The $[M + H]^+$ ion MS/MS spectra of protonated LF-OH, FG-OH, IY-OH, and YV-OH, respectively

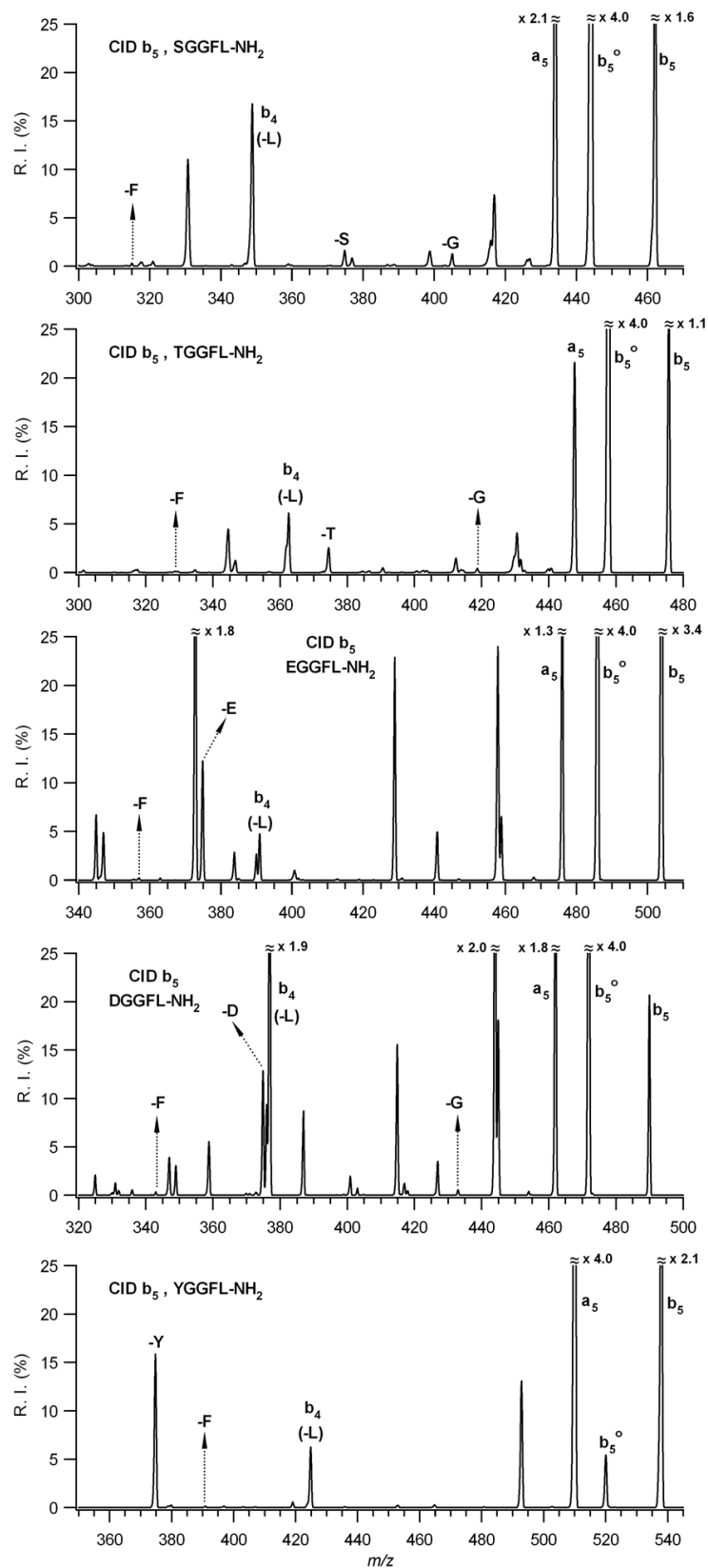


Figure C.2. MS³ mass spectra of b₅ ions from protonated XGGFL-NH₂ (X is S, T, E, D, or Y)

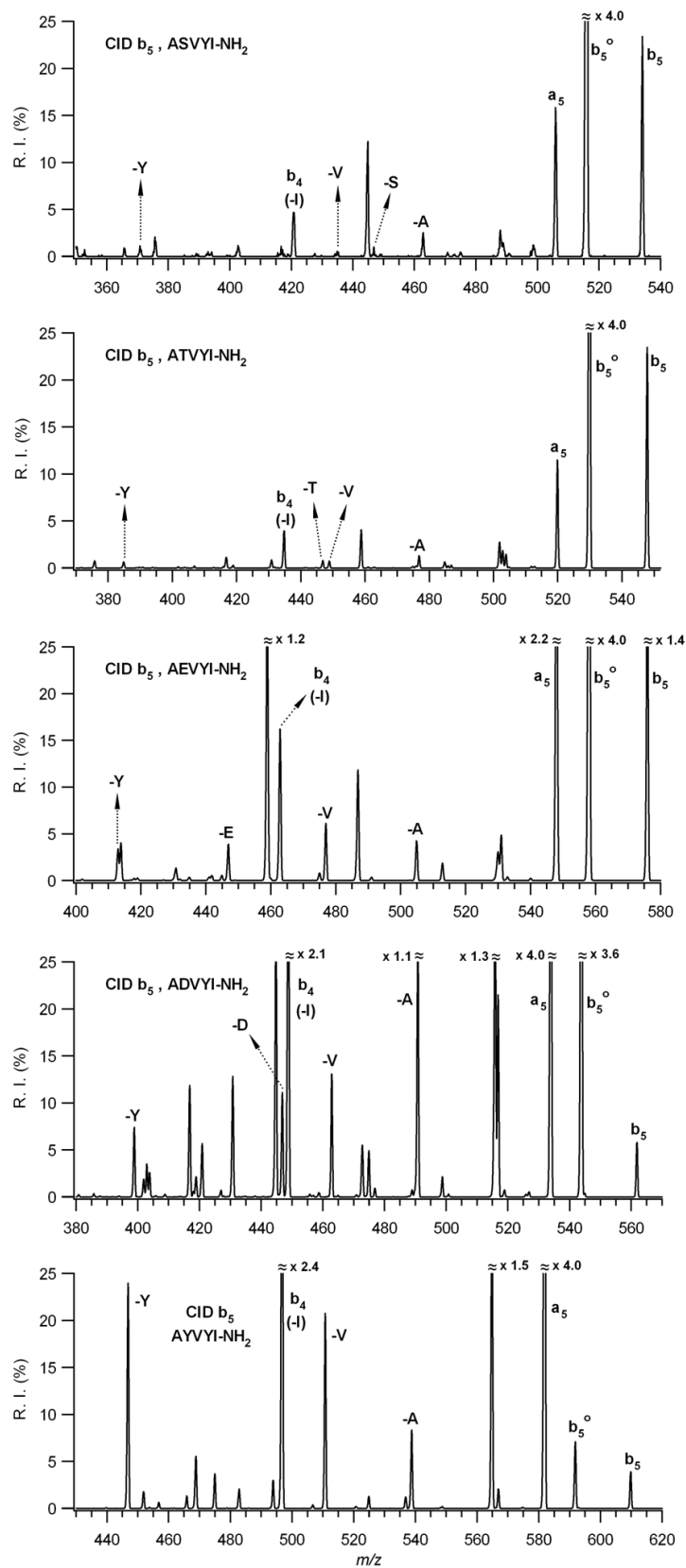


Figure C.3. MS³ mass spectra of *b*₅ ions from protonated AXVYI-NH₂ (X is S, T, E, D, or Y)

AHMET EMİN ATİK

PERSONAL INFORMATION

Date of Birth : August 26, 1981
Marital Status : Single
Nationality : Turkish
E-mail : atikaemin@gmail.com

EDUCATION

- 2007 – 2013 Doctor of Philosophy (Ph.D.)**
İzmir Institute of Technology, Department of Chemistry
Dissertation Title: Studies of Gas-Phase Fragmentation Mechanisms of Peptide *b* Ions by Mass Spectrometry - GPA: 3.79 / 4.00
Advisor: Prof. Dr. Talat Yalcin
- 2005 – 2007 Master of Science (M.Sc.)**
İzmir Institute of Technology, Department of Chemistry
Dissertation Title: A Proteomic Approach for Identifying Boron-Stress Tolerant Proteins in Barley Genotypes - GPA: 3.64 / 4.00
Advisor: Prof. Dr. Talat Yalcin
- 2001 – 2005 Bachelor of Science (B.Sc.)**
İzmir Institute of Technology, Department of Chemistry
Dissertation Title: Determination of Acrylamide in Various Fried Foods by Chromatographic Methods - GPA: 3.16 / 4.00

WORK EXPERIENCES

- **Visiting Scientist:** Université Paris-Sud XI, Laboratoire de Chimie Physique Centre Laser Infrarouge d'Orsay, France, October-November 2012.
- **Research and Teaching Assistant:** İzmir Institute of Technology, Department of Chemistry, November 2005- December 2013.

PUBLICATIONS

4. **Atik, A.E.,** Yalcin, T. Protonated Dipeptide Losses from b_5 and b_4 Ions of Side Chain Hydroxyl Group Containing Pentapeptides. *J. Am. Soc. Mass Spectrom.* 24, **2013**, 1543-1554.
3. **Atik, A.E.,** Gorgulu, G., Yalcin T. The Role of Lysine ϵ -Amine Group on the Macrocyclization of *b* Ions. *Int. J. Mass Spectrom.* 316-318, **2012**, 84-90.
2. **Atik, A.E.,** Yalcin, T. A Systematic Study of Acidic Peptides for *b*-type Sequence Scrambling. *J. Am. Soc. Mass Spectrom.* 22, **2011**, 38-48.
1. **Atik, A.E.,** Bozdog, G.O., Akinci, E., Kaya, A., Koc, A., Yalcin, T., Karakaya, H.C. Proteomic Changes during Boron Tolerance in Barley (*Hordeum vulgare*) and the Role of Vacuolar Proton-Translocating ATPase Subunit E. *Turk. J. Bot.* 35, **2011**, 379-388.